Estonian Journal of Earth Sciences

2026
75/1

ISSN 1736-4728 (print)
ISSN 1736-7557 (electronic)
Estonian Academy Publishers
www.eap.ee/earthsciences

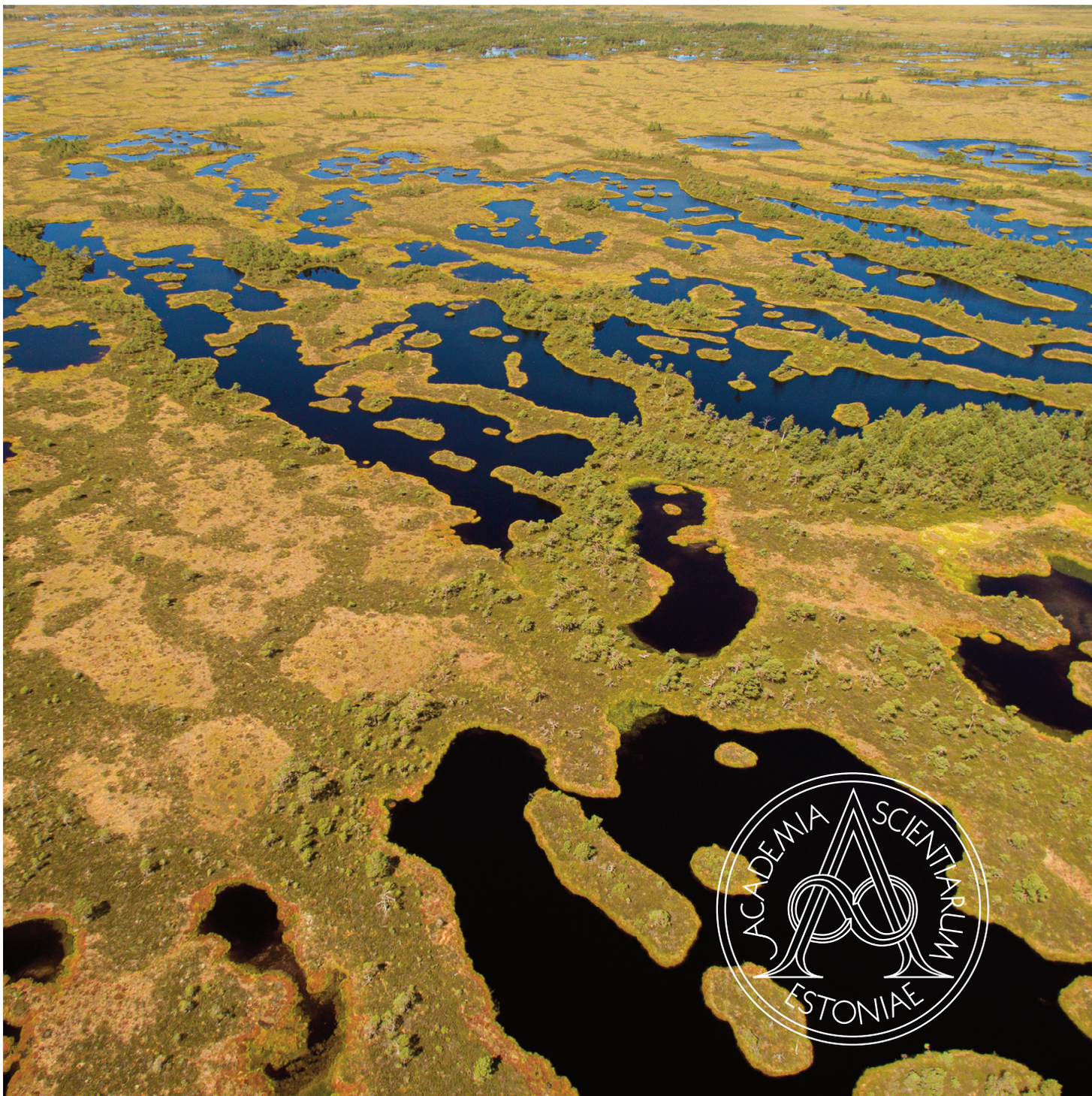

International open access scientific journal of the Estonian Academy of Sciences, published in collaboration with the Department of Geology at the University of Tartu, the Estonian University of Life Sciences, the Geological Survey of Estonia, Tallinn University, and Tallinn University of Technology

Estonian Journal of Earth Sciences

Published since 1952

Estonian Journal of Earth Sciences is published biannually

Abstracted/indexed in:
Science Citation Index Expanded™ (Web of Science), Journal Citation Reports/Science Edition, Zoological Record, Geological Abstracts, GEOBASE (Elsevier/Geo Abstracts), Chemical Abstracts, Scopus®, EBSCO, DOAJ (Directory of Open Access Journals), Gale's Academic OneFile database, WilsonWeb, ProQuest LLC, Airiti Inc., Scilit, CNKI

Editorial Office:
Kohtu 6, 10130 Tallinn, Estonia
Email: hedi.tonso@eap.ee

Front cover:
Bog pool complex in the Nätsi–Võlla Bog, SW Estonia. Photo by Marko Kohv.

Printed by Alfapress, Reti tee 8, 75312 Peetri, Estonia

Estonian Journal of Earth Sciences
2026, **75**, 1, 1–18

https://doi.org/10.3176/earth.2026.01

www.eap.ee/earthsciences
Estonian Academy Publishers

RESEARCH ARTICLE

Received 28 January 2025
Accepted 30 July 2025
Available online 14 November 2025

Keywords:
marine litter, beach litter, remote areas, islands, visual surveys

Corresponding author:
Tiia Möller-Raid
tiia.moller@ut.ee

Citation:
Möller-Raid, T., Põldma, M., Herkül, K., Torn, K., Martin, G., Kaljurand, K. et al. 2025. Marine litter pollution on uninhabited islands in Estonia, northeastern Baltic Sea. *Estonian Journal of Earth Sciences*, **75**(1), 1–18. https://doi.org/10.3176/earth.2026.01

Marine litter pollution on uninhabited islands in Estonia, northeastern Baltic Sea

Tiia Möller-Raid, Maria Põldma, Kristjan Herkül, Kaire Torn, Georg Martin, Kaire Kaljurand, Martin Teeveer, Greta Reisalu, Trude Taevere, Hanna-Eliisa Luts, Karolin Teeveer, Keili Saava, Annely Enke and Lauri London

Estonian Marine Institute, University of Tartu, Mäealuse 14, 12618 Tallinn, Estonia

ABSTRACT

This paper provides results of marine litter surveys carried out on 14 small uninhabited islands located in the coastal waters of Estonia, northeastern Baltic Sea. The islands were visited four times in total during 2019–2020. On each island, a litter survey was conducted on the beach and in terrestrial vegetation with a focus on macrolitter. Calculated over all surveys, the median value of macrolitter items per 100 m long beach section was 10.65, and the median density was 0.006 items m^{-2}. At the sub-basin level, the three islands located in the Gulf of Finland had the highest number of beach litter items per 100 m and the highest density (items m^{-2}), 38.05 and 0.017, respectively. The main litter material, representing 57.3% of all findings, was plastic; however, there were some variances across islands due to local conditions. The environmental variables most strongly correlated with differences in the composition of macrolitter were related to water movement and depth. Microlitter was found in low amounts (up to 60 items kg^{-1}) in the sediment of all studied islands. Litter items used as nest material were noted on all the islands with seabird colonies.

1. Introduction

Human-induced litter is a growing global problem (Borrelle et al. 2020). Marine litter can be found in all marine compartments (beaches, sea surface, water column, seafloor, and within biota) both close to human-populated areas and in remote areas (Galgani et al. 2013). Marine litter consists of items made or used by people that are deliberately discarded or unintentionally lost into the sea or onto beaches, including materials transported into the marine environment from land by rivers, drainage or sewage systems, or winds. Litter, especially plastic, directly affects marine ecosystems and is considered environmentally, economically, and psychologically harmful (e.g., Wyles et al. 2016; Galgani et al. 2019).

The highest densities of litter have been reported adjacent to urban centers, in enclosed seas, and on waterfronts (Barnes et al. 2009). However, distant areas, including remote islands, are also recognized as accumulation areas for marine litter, and considering the lack of human activities in those areas, the litter is transported there by water and wind (e.g., Lavers and Bond 2017; Lavers et al. 2019; Portz et al. 2022). For instance, on Henderson Island (South Pacific Ocean), which is located more than 5000 km from human habitation, the density of visible micro- and macrolitter on the beach has been reported to be as high as 671.6 items m^{-2} (Lavers and Bond 2017). Across Europe, the average presence of litter on the coastline is generally lower: in 2015–2016, the median beach macrolitter quantity was estimated at 150 items per 100 m long beach section, with different regional median values: 40 items per 100 m around the Baltic Sea; 106 items per 100 m around the Black Sea; 233 items per 100 m around the North-East Atlantic and the North Sea; and 274 items per 100 m around the Mediterranean Sea (Hanke et al. 2019). However, there is tremendous variability in litter abundance at the regional scale. For instance, in some regions of the Mediterranean Sea, visible litter can exceed 6600 items per 100 m long beach section (Vlachogianni et al. 2020).

The Baltic Sea region is currently regarded as the cleanest area in Europe in terms of beach litter (HELCOM 2018). Nevertheless, the number of litter items per 100 m

of beach section most commonly varies between 50–300. The average number of beach litter items within the Baltic Sea region has been estimated at about 280 items per 100 m of beach section on urban beaches and up to 47 items per 100 m of coastline of natural beaches (HELCOM 2018). However, the threshold for Good Environmental Status (GES) in European seas related to beach litter is set at a maximum of 20 items per 100 m of coastline, which is the target to be achieved (van Loon et al. 2020; European Commission 2022).

Marine litter has various impacts on biota (Kühn et al. 2015) and is also a specific concern for marine protected areas (e.g., Rodríguez-Rodríguez 2012; Polasek et al. 2017; Ibrahim et al. 2020). Beached litter may remain on the shore and degrade into smaller particles (GESAMP 2015). It can also move into the water environment, inland, and/or be ingested by fauna. Among the various impacts on biota, entanglement, smothering, and ingestion are the most frequently described (Kühn et al. 2015). For seabirds, plastic debris as nesting material has already become common (Votier et al. 2011). However, as the use of litter in nests depends on specific species and the availability of litter in the environment, the presence of litter in nests is not ubiquitous – marginal existence of plastic in nests has also been reported, for example in two colonies in the Bay of Biscay, Spain (Delgado et al. 2020). Evidence further shows that plastic bags in dune vegetation affect germination phenology, seedling establishment, and plant interactions via leaching. These processes can lead to changes in dune community structure (de Francesco et al. 2018; Menicagli et al. 2019).

Though the topic of marine litter has gained considerable scientific and public attention in the last decades, there are still fundamental knowledge gaps, primarily in empirical data on the distribution, composition, and amounts of litter in the marine environment. Studies addressing the marine litter problem in the Baltic Sea region have escalated since 2010; earlier work focused mostly on beach litter (e.g., Strand et al. 2015), while in the last decade, more studies have examined microlitter, floating macrolitter, and effects on biota (e.g., Canals et al. 2021; Põldma et al. 2023; Schernewski et al. 2024).

Estonia's location, encompassing several major sub-basins of the Baltic Sea, with a diverse coastline and exposure to winds from several directions, predisposes its coastal areas to the accumulation of marine litter. Thus, the litter status of small uninhabited Estonian islands reflects overall litter pollution in the Baltic Sea and its sub-basins. Numerous small and remote islands are habitats for marine birds and seals, and many endangered plant species also grow in these areas. There are over 2000 islands in Estonian coastal waters; most are located within 5 km of the mainland, and about 90% are under nature conservation (Estonian Nature Conservation Act 2004).

Before this study, no systematic research on marine litter had been conducted on remote, uninhabited islands in the northeastern Baltic Sea. Moreover, most previous studies in the Baltic Sea region have focused on a single litter type without covering related aspects. For example, in beach macrolitter survey areas, no microlitter surveys have been carried out (Press 2020), and vice versa (Urban-Malinga et al. 2020; Ershova et al. 2021; Schröder et al. 2021). This study aimed to fill the knowledge gap on the status and pathways of litter in areas with limited direct human impact in the Baltic Sea. The research provides information on the amounts, composition, and distribution of marine litter on the coasts of small, remote Estonian islands, with a focus on marine macrolitter. To cover various aspects of marine litter and provide supplementary information, we also conducted microlitter surveys and monitored the effects of macrolitter on local biota, where visible. In addition, different survey areas, such as shallow coastal waters, beaches, and terrestrial vegetation near beaches, were covered. Potential relationships between environmental conditions, human pressure, and the amount and composition of marine macrolitter were also addressed.

2. Materials and methods

2.1. Study areas

The study was carried out on small islands located in the coastal waters of Estonia, in the northeastern part of the Baltic Sea (Fig. 1; Table 1). The Baltic Sea is an enclosed, non-tidal sea with a surface area of 420 000 km^2, a catchment area of approximately 1 641 650 km^2, and about 85 million people living around it. There are over one million islands in the Baltic Sea region, the vast majority belonging to Finland and Sweden.

Estonia borders several sub-basins of the Baltic Sea: the Gulf of Finland, the Northern Baltic Proper, the Gulf of Riga, and the Eastern Gotland Basin. The total length of the Estonian coastline is about 3800 km. Of this, 1242 km belong to the mainland, while the remaining ~2550 km belong to the 2222 islands. The Estonian coastline is highly heterogeneous and variable; different coastal types can be distinguished: till (35%), silt (31%), sand (16%), gravel (11%), cliffs (5%), artificial (2%; breakwaters, protecting walls, berms), and scarps (short sections between other shore types) (Tõnisson et al. 2013).

In this study, marine litter surveys were conducted on 14 islands – 13 of which were visited four times, and one only once. The islands were selected based on the following criteria: (1) they are spatially dispersed and represent different water basins; (2) the minimum area is 0.5 km^2; (3) the island has vegetation – at least grass as primary vegetation, but preferably also shrubs and trees; (4) permanent human settlement is absent (according to the Estonian Permanently Inhabited Small Islands Act 2003). The coasts are highly heterogeneous in the northeastern part of the Baltic Sea (Łabuz 2015). Thus, coastal geomorphology (including dominant sediments) of the beaches was not included as a selection criterion. Fieldwork was carried out between June 20, 2019, and October 13, 2020, with visits in different seasons (spring, summer, and autumn). Most of the islands are prohibited from being visited between April and June (bird nesting period), which also affected the timing of fieldwork (Table S1).

2.2. Fieldwork methodology and laboratory analysis

2.2.1. Amounts and composition of macrolitter

The beach litter survey methodology was based on suggestions by the United Nations Environment Programme and

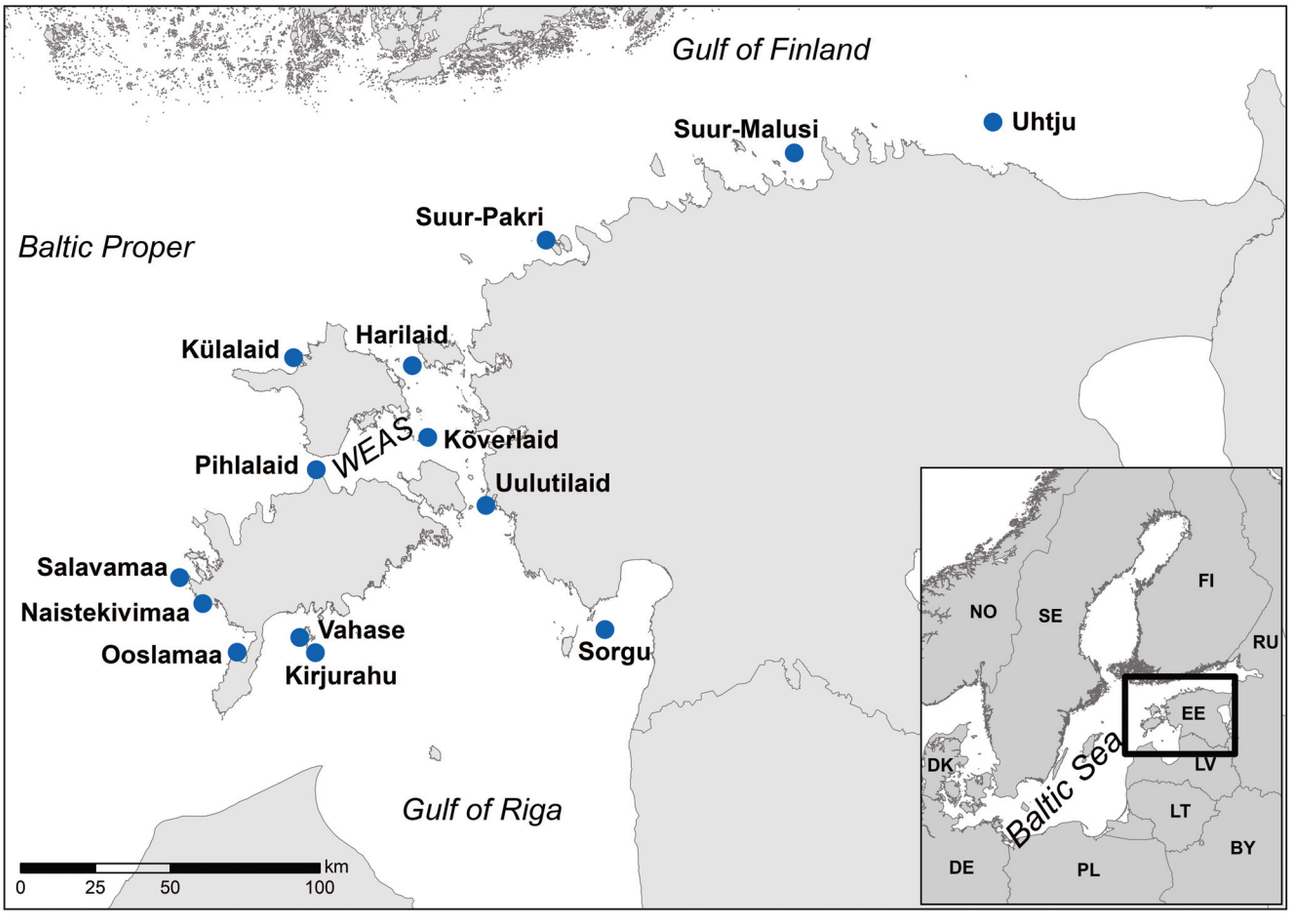

Fig. 1. Location map of the islands surveyed. WEAS – West Estonian Archipelago Sea.

Intergovernmental Oceanographic Commission (UNEP/IOC) Guidelines on Survey and Monitoring of Marine Litter (2009), MSFD (Marine Strategy Framework Directive) Technical Subgroup on Marine Litter Guidance on Monitoring of Marine Litter in European Seas (Joint Research Centre 2013), and previous beach litter research carried out in Estonia (Press 2020). On each island, litter surveys were conducted in three survey areas: shallow-water survey area, beach survey area, and vegetation survey area (Fig. 2). Shallow-water survey areas were situated in the water near the coastline at a depth of 0.5 m. Beach survey areas were located on land between the coastline and terrestrial vegetation. Beach survey areas were devoid of permanent live terrestrial vegetation. Vegetation survey areas were situated on land next to beach survey areas and were characterized by permanent live terrestrial vegetation (grasses, shrubs, or trees). All survey areas were parallel to the coastline.

According to the beach litter monitoring guidelines, litter should be monitored at least on a 100 m long beach section from the waterline to the back of the beach/start of vegetation (Joint Research Centre 2013) – this was set as a minimum in the current study. The length of the beach survey areas varied between 400–1000 m, and the width varied between 5–35 m (Table 1). Due to the often-present rough terrain and limited accessibility, the vegetation survey areas were generally shorter, and the length of the monitored area varied between 100–750 m. The main aim was to cover all the vegetation layers (primary, secondary, and tertiary) that were present on the island with the purpose of collecting the litter items that had moved inland with the highest water level (including extraordinary storms (Fig. 2). Depending on the local circumstances (i.e., the presence and dominance of either trees/shrubs or grass), the width of the vegetation survey area varied between 5–100 m (Table 1). However, there was great variation in the presence of vegetation layers among islands, e.g., some of the islands lacked shrubs or trees, and some of the islands lacked grass (Table 1). The location, length, and width of the survey areas shown in Table 1 remained constant for all the sampling campaigns.

The length of the shallow-water survey area was set to 100 m and the width to approximately 5 m. Observations in the shallow-water survey area were carried out via snorkeling or using a bathyscaphe. However, the amount of macrolitter in shallow-water areas was minimal and sporadic (only five items in total from three islands); therefore, data on macrolitter in shallow-water areas were not included in further analysis.

The classification system of litter items was based on a modified UNEP/IOC 2009 marine litter list to encompass organic waste (MARLIN 2013), resulting in UNEP/MARLIN codes for litter items found on Baltic beaches (82 categories in total; summarized, e.g., in Haaksi 2020). Accordingly, litter items were classified by material (nine categories): plastic, glass and ceramics (glass), processed wood (wood), textile,

Table 1. Overview of the islands surveyed. Sub-basins: GoF – Gulf of Finland, BP – Baltic Proper, GoR – Gulf of Riga, WEAS – West Estonian Archipelago Sea. Coordinates represent the location of each island, not the exact study area. The beach substrate and terrestrial vegetation taxa describe the dominant features of the islands. Length and width of the surveyed areas are shown separately for beaches and terrestrial vegetation. N – geographical latitude (WGS84), E – geographical longitude (WGS84). Vegetation layers are indicated as follows: [1] – primary, [2] – secondary, [3] – tertiary

Island	Abbreviation	Sub-basin	N	E	Coastline, km	Area, km^2	Beach survey area			Vegetation survey area		
							Substrate	Length, m	Width, m	Vegetation	Length, m	Width, m
Harilaid	Har	WEAS	58.9664	23.0864	3.14	1.50	Sand, stones	500	12	Grass[1]	250	20
Kirjurahu	Kir	GoR	58.0993	22.5586	2.03	0.52	Sand, stones	1000	20	Grass[1]	160	60
Kõverlaid	Kov	WEAS	58.7520	23.1802	3.16	3.05	Sand, stones	600	5	Grass[1], juniper[2], pine[3]	250	5
Külalaid	Kul	BP	58.9841	22.3953	3.34	1.62	Limestone, pebbles, boulders, sand	600	15	Grass[1], juniper[2], pine[3]	220	30
Naistekivimaa	Nai	BP	58.2382	21.9123	2.18	1.80	Limestone, pebbles	430	15	Grass[1]	370	30
Ooslamaa	Oos	BP	58.0948	22.1160	2.10	0.51	Sand, boulders	1000	12	Grass[1]	650	30
Pihlalaid	Pih	WEAS	58.6489	22.5408	1.99	0.66	Stones, pebbles, gravel	1000	12	Grass[1]	650	30
Salavamaa	Sal	BP	58.3138	21.7762	3.47	2.66	Limestone, pebbles, boulders, sand	850	15	Grass[1], juniper[2]	750	5
Sorgu	Sor	GoR	58.1766	24.2006	2.08	0.58	Sand, stones	550	15	Grass[1], juniper[2]	100	100
Suur-Malusi	Sma	GoF	59.6018	25.3288	1.55	0.62	Sand, boulders	400	20	Grass[1]	300	40
Suur-Pakri	Spa	GoF	59.3464	23.8620	22.84	12.68	Limestone, pebbles	600	25	Juniper[2]	600	25
Uhtju	Uht	GoF	59.6772	26.5122	2.28	0.96	Sand, boulders	1000	30	Grass[1]	350	50
Uulutilaid	Uul	GoR	58.5492	23.5195	4.87	3.16	Limestone pebbles, boulders, sand	620	35	Grass[1], juniper[2]	470	10
Vahase	Vah	GoR	58.1438	22.4687	6.95	0.72	Gravel, stones	750	15	Grass[1], juniper[2], pine[3]	720	10

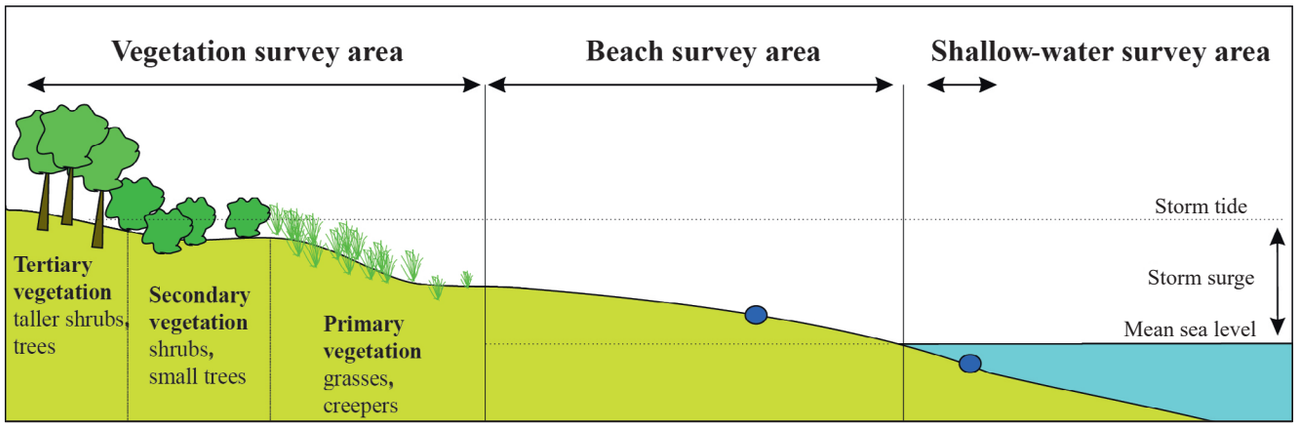

Fig. 2. General sampling scheme illustrating the locations of the survey areas for macrolitter. Blue dots indicate the microlitter sampling areas (shallow-water and beach survey areas).

paper, metal, organic, rubber, and other. The most relevant litter codes (J-codes) of the Europe-oriented marine macrolitter classification system were added for data comparability (Fleet et al. 2021); however, because the classification systems do not fully overlap and an item classified under UNEP/MARLIN may correspond to several MSFD litter codes, the original UNEP/MARLIN classification system was retained as the basis. To estimate possible sources of litter pollution, items were also assigned to source categories: agriculture-related, aquaculture-related, clothing, building and construction-related, fisheries-related, personal hygiene and care-related, medical-related, undefined use, recreation-related, smoking-related, vehicle-related, and hunting-related (based on Fleet et al. 2021).

All visible litter items were recorded in the protocol and, when possible, collected and removed from the survey areas. Most collected items were in the size class >2.5 cm (macrolitter); however, smaller items (<2.5 cm, e.g., cigarette parts, caps/lids, batteries) were included when visible. The total weight of litter from the beach and vegetation survey areas was measured. Only items that could be lifted by hand and removed easily from the environment were included in weight measurements. Large litter items that could not be removed from the location were recorded in the protocol when first observed and were not registered separately on subsequent sampling occasions.

2.2.2. Microlitter in sediment

Microlitter sample collection followed the guidelines of Hidalgo-Ruz et al. (2012). During sample collection and storage, care was taken to avoid additional contamination (Galgani et al. 2013). Several procedures were applied to reduce airborne secondary contamination and cross-contamination, including working plastic-free and including blank measurements at every step. Microlitter samples were collected from beach and shallow coastal sea sediment (top 5 cm) at 0.5 m water depth using a GEMAX sediment tube (diameter 30 mm). Three sediment samples were collected and combined into a single sample for both survey areas (shallow-water and beach survey areas; Fig. 2). Samples were placed in glass jars (previously cleaned with MilliQ water) and stored in a standard refrigerator (4 °C) until laboratory analysis. Sampling coordinates were determined by GPS (accuracy ±3 m), and subsequent island visits used the same coordinates. In total, 106 microlitter samples were collected during the study.

For laboratory analysis, each sample was homogenized by thorough mixing. Then, 100 g of the sample was weighed with a weighing scale (KERN Alt 310-4, accuracy 0.1 mg) into a glass Petri dish and covered with a glass lid. The sample was analyzed in portions on another glass Petri dish. In parallel, a second aliquot of the field sample was investigated for water content to determine the dry weight of the sediment. For this, 100 g of sample was transferred to an evaporating dish and dried at 105 °C. After drying, the subsample was cooled to room temperature in a desiccator, reweighed, and dry weight was calculated.

Microlitter was detected visually under a stereomicroscope (Olympus SZX7, magnification 126x) paired with a camera (Olympus). A semi-qualitative hot needle test was used to distinguish plastic from organic material; the hot needle melts and deforms plastic (Devriese et al. 2015; Avio et al. 2020). The lower size limit for visual inspection has been reported between 5–500 µm (summarized in Pérez-Guevara et al. 2022), with most studies using >100 µm as the lower detection limit (Primpke et al. 2020). Empty blanks were placed in the laboratory for the sample treatment/analysis period and controlled similarly under the microscope afterward to estimate sample pollution during analysis. The controls were given the same full treatment as the samples studied to assess any airborne contamination. If the blank was contaminated, microlitter items with similar characteristics (shape, color, material) were excluded from the results as proposed by Avio et al. (2020). All microlitter items were measured and classified by material, size class, shape, and color (Matiddi et al. 2021). The number of microlitter particles was expressed as items per kg of dry sediment.

2.2.3. Effect of macrolitter on biota

The effect of macrolitter on biota was estimated visually by observing mortal remains, bird nests, and bird pellets in the shallow-water, beach, and vegetation survey areas. Data are

reported on an island-based level. In total, ten bird pellets (five each from Uhtju and Sorgu islands) were collected for more detailed laboratory examination.

2.3. Data analysis

Due to topographic differences, the length of macrolitter survey areas varied between the studied islands. To bring litter counts to a standard scale, the counts were recalculated to a 100 m and 1 m^2 scale using the actual dimensions of the survey areas (see Table 1 for the lengths and widths of the survey areas). To calculate the litter counts to a 100 m scale, the counts were divided by the length of the survey areas (measured in meters) and multiplied by 100. The scaling to 1 m^2 was conducted by dividing the litter counts by the size (in square meters) of the survey areas. Two versions of spatial normalization were needed to compare our results with previous findings: normalization on a 100 m scale is predominant in gray literature while normalization on a square meter scale is preferred in scientific literature.

The Kruskal–Wallis test (Kruskal and Wallis 1952) was used to statistically test for differences in univariate variables. When the Kruskal–Wallis test showed significant differences ($p < 0.05$), Wilcoxon pairwise comparison tests (Wilcoxon 1945) were performed to reveal which factor levels differed. The Benjamini–Hochberg method (Benjamini and Hochberg 1995) was used in the Wilcoxon pairwise test for correcting *p*-values in multiple comparisons. These nonparametric rank-based tests were preferred over analysis of variance (ANOVA) because the assumption of normal distribution was not met. The Shapiro–Wilk test (Shapiro and Wilk 1965) was used to check normality.

Nonmetric multidimensional scaling (NMDS; Kruskal 1964) was used to visualize the similarity of litter structure between the islands. Relationships between the multivariate litter structure and environmental variables were studied using the BIOENV method (Clarke and Ainsworth 1993). Nine different environmental and human pressure variables (hereafter "environmental variables") were included in the analyses to elucidate potential relationships between litter and the surrounding environment (Table 2). All variables were available as georeferenced raster layer datasets. Mean values of all variables were calculated within 50, 500, 5000, and 50 000 m radii around the study sites of each island.

In the analysis of the relationships between litter and environmental variables, the study was designed to investigate spatial patterns exclusively and did not address temporal dynamics. Accordingly, datasets based on time series were represented as multi-year averages capturing the spatial patterns relevant to the analysis. The general geographical patterns of oceanographic conditions (e.g., water currents, wave exposure) have likely remained stable over recent decades, as the primary driving forces – such as coastal and seabed topography and prevailing wind directions – have not undergone significant changes. Similarly, the spatial patterns of shipping intensity are also expected to have remained consistent, given the stable locations of major ports and shipping lanes.

The R programming language, version 4.0.4 (R Core Team 2021), in the development environment RStudio (RStudio Team 2021) was used for data preparation and analysis. Potential multicollinearity among environmental variables was assessed using pairwise Pearson correlation coefficients. The highest observed correlation was 0.83 (between depth

Table 2. Environmental and human pressure variables

Variable	Short name	Source
Water depth (m)	Depth	1
Slope of seabed (°)	Slope	1
Wave exposure at sea surface based on simplified wave model (m^2 s^{-1}): based on long-term (2003–2019) mean wind speeds and directions	Wave	2
Current velocity (m s^{-1}): long-term (2005–2019) mean current velocity at seabed based on hydrodynamic model	Current	3
Orbital velocity (m s^{-1}): long-term (1989–2005) mean speed of wind-induced orbital movement of water at seabed based on hydrodynamic model	Orbital	4
Proportion of soft sediment (0…1): proportion of soft seabed sediments derived from spatial models with input from bottom grab sampling, video sampling, and scuba diving	Sediment	5
Duration of ice cover (days): long-term (2000–2016) mean duration of ice cover	Ice	6
Shipping intensity (number of ship crossings): mean shipping intensity per year in 2011–2015 measured as the number of ship crossings in a 1×1 km grid cell based on HELCOM Automatic Identification System data	Shipping	7
Baltic Sea Pressure Index (BSPI): Baltic Sea cumulative human pressure index developed by HELCOM. Higher value indicates stronger human pressure	BSPI	7

Sources:
1 – Bathymetric data by the Estonian Maritime Administration (georeferenced depth raster with 10 m pixel size)
2 – Simplified wave model based on fetch and wind data (Isæus 2004; van der Meijs and Isaeus 2020)
3 – Current speed data by the Marine Systems Institute, Tallinn University of Technology (Maljutenko and Raudsepp 2014)
4 – Orbital velocity data by the Marine Systems Institute, Tallinn University of Technology (Björkqvist et al. 2018)
5 – Databases of the Estonian Marine Institute, University of Tartu
6 – Ice data by the Marine Systems Institute, Tallinn University of Technology (Uiboupin and Pärn 2018)
7 – HELCOM Map and Data Service (https://maps.helcom.fi/website/mapservice/index.html) (HELCOM 2010)

Table 3. Macrolitter amounts in beach and vegetation survey areas, and at the island level (pooled over beach and vegetation survey areas). Sub-basins: GoF – Gulf of Finland, BP – Baltic Proper, GoR – Gulf of Riga, WEAS – West Estonian Archipelago Sea, overall – data pooled over all sub-basins. Abbreviation: SD – standard deviation

Region/ sub-basin	Survey area	No. of surveys	Mean, items 100 m^{-1}	Mean, items m^{-2}	SD, items 100 m^{-1}	SD, items m^{-2}	Median, items 100 m^{-1}	Median, items m^{-2}
Overall	Beach	53	17.39	0.009	17.63	0.0097	10.65	0.006
Overall	Vegetation	53	38.25	0.013	44.32	0.0119	21.36	0.009
Overall	Island	53	22.33	0.011	18.61	0.0088	15.19	0.008
BP	Beach	13	14.07	0.006	14.55	0.0096	8.33	0.006
BP	Vegetation	13	27.82	0.017	30.08	0.0163	19.85	0.010
BP	Island	13	19.18	0.013	14.31	0.0105	14.55	0.008
GoR	Beach	16	8.07	0.003	3.73	0.0028	8.97	0.003
GoR	Vegetation	16	38.23	0.009	50.59	0.0073	18.83	0.007
GoR	Island	16	13.28	0.006	9.64	0.0040	10.27	0.005
GoF	Beach	12	37.67	0.016	18.46	0.0082	38.05	0.017
GoF	Vegetation	12	69.56	0.017	50.87	0.0096	45.83	0.014
GoF	Island	12	45.23	0.015	14.94	0.0052	46.65	0.016
WEAS	Beach	12	13.14	0.011	16.48	0.0133	5.50	0.005
WEAS	Vegetation	12	18.25	0.009	24.18	0.0121	8.54	0.004
WEAS	Island	12	14.90	0.010	17.33	0.0115	7.15	0.005

and slope), and no variables were excluded. All combinations of environmental variables were tested in BIOENV to identify the set of variables that best explained the multivariate structure of litter. Spearman rank correlation was used in BIOENV, and a permutation test (n = 9999) was applied to calculate the statistical significance of relationships.

Environmental data at all radii (50, 500, 5000, and 50 000 m) were tested in BIOENV. Because data at the 5000 m radius resulted in the highest correlation with litter data, only results using this radius are presented in the Results section. Euclidean distance similarity matrices were used in both NMDS and BIOENV. Separate sets of NMDS and BIOENV analyses were run on litter items and litter material data. The litter material dataset was derived by summing litter item counts by material (see Table 4 and Table S2 for litter types and materials).

Separate sets of analyses were also run on data aggregated at the island level and the combined island and survey area level (beach and vegetation survey areas indicated separately). Aggregation at the island level meant that litter count data were summed across survey areas (beach, vegetation). Analysis of similarities (ANOSIM; Clarke 1993) was used to statistically test for differences in litter composition between groups of samples. Euclidean distances were used to produce dissimilarity matrices, and 9999 permutations were applied.

For NMDS and BIOENV, the litter count data in each island were summed over all sampling occasions, representing the cumulative accumulation of litter over time, and scaled to m^2. The computed litter count data were then square root-transformed to downweight the importance of litter types with very high counts. For ANOSIM, data from separate sampling occasions were not summed because intra-group replicates were required.

The R package *vegan* (Oksanen et al. 2020) was used for multivariate analyses (BIOENV, NMDS, ANOSIM). The R package *raster* (Hijmans 2020) was used for handling spatial raster data, *sf* (Pebesma 2018) for handling spatial vector data, *exactextractr* (Baston 2021) for extracting raster statistics in polygons, and *tidyverse* (Wickham et al. 2019) for tabular data manipulation and plotting.

3. Results

3.1. Amount of macrolitter

In total, 12 818 macrolitter items were recorded, and 854 kg of litter was removed from the 14 islands in 2019–2020. Overall, 6011 litter items (362 kg) were removed from the beach survey areas and 6715 items (492 kg) from the vegetation survey areas.

Across all surveys, the median value of macrolitter items was 10.65 per 100 m long beach survey area, and the respective median density for beach macrolitter was 0.006 items m^{-2}. The number of macrolitter items varied between 0–77 items 100 m^{-1} in the beach survey areas and between 0–169 items 100 m^{-1} in the vegetation survey areas. The correlation between mean and median values was strong (linear regression, $r^2 = 0.903$), and both values are presented in Table 3.

The highest median values of marine litter items and density were recorded in the sub-basin of the Gulf of Finland (Table 3). Based on data normalized per 100 m, the Gulf of Finland differed statistically significantly from all other regions (Wilcoxon pairwise test, $p < 0.001$). When normalized per m^2, the Gulf of Finland differed only from the Gulf of Riga (Wilcoxon pairwise test, $p < 0.001$).

The density of litter items per sampling occasion ranged from 0.001 to 0.053 m^{-2} (Fig. 3), with respective weights from 0.0001 to 0.0085 kg m^{-2} (Fig. S2). The density of litter did not differ statistically significantly between sampling occasions (Kruskal–Wallis test, $p > 0.05$). Vegetation survey areas had statistically significantly higher litter density than beach survey areas when data were normalized per 100 m

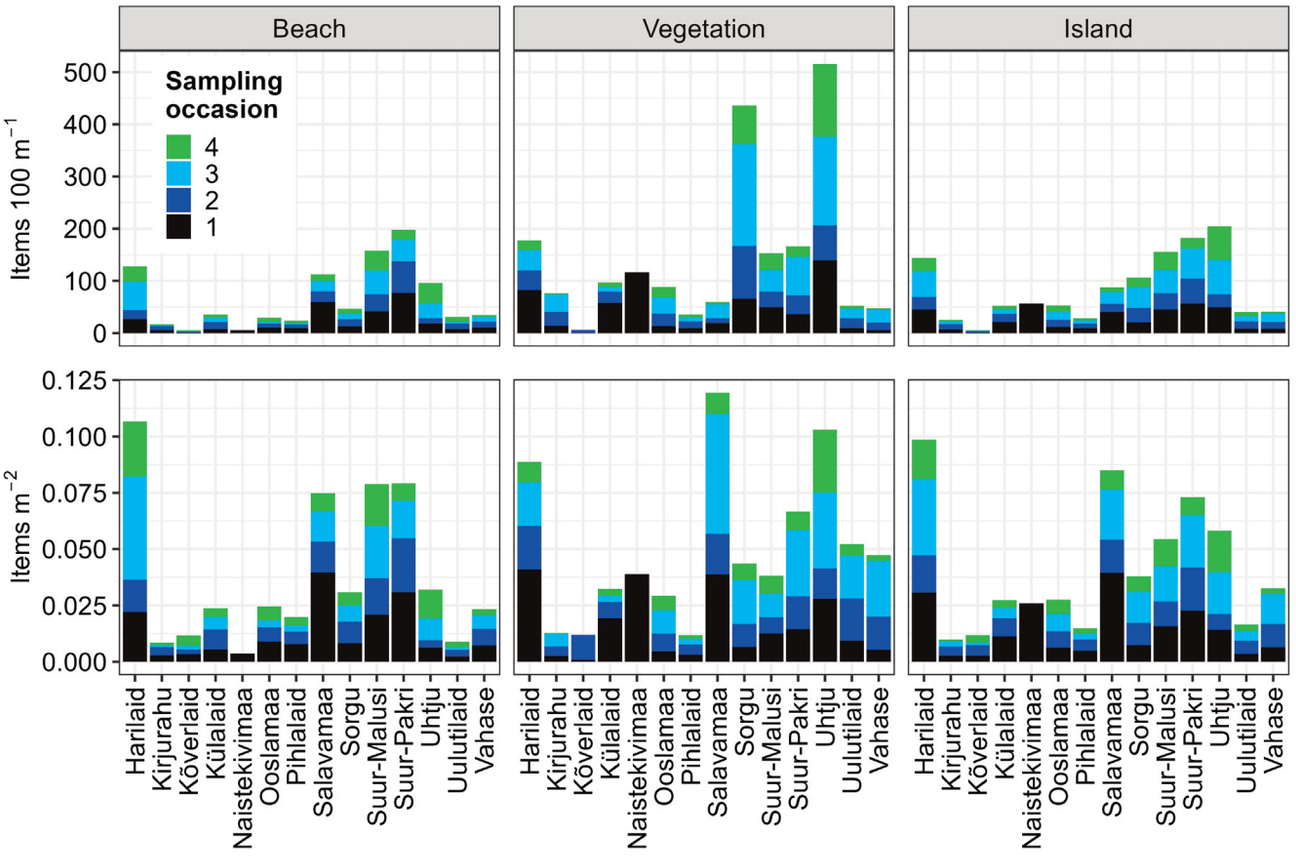

Fig. 3. The number of described litter items per 100 m long survey area and m^2 in the beach survey area, vegetation survey area, and at the island level (beach and vegetation survey areas combined).

(Kruskal–Wallis test, $p = 0.006$), but no difference was found when data were normalized per m^2 (Kruskal–Wallis test, $p = 0.13$).

3.2. Composition of macrolitter

Overall, plastic was the dominant material of litter items with 57.3%, followed by glass and ceramics at 9.2%, processed wood at 8.6%, metal at 12.7%, textile at 6.2%, rubber at 4.5%, and organic, other, and paper <1%. The lowest share of plastic materials was noted for Harilaid (30%) and Pihlalaid (42%), and the highest for Kõverlaid (88%) and Vahase (83%). For most of the islands, the share of plastic ranged between 60–70% (Fig. 4).

The distribution of litter material between the beach survey area and the vegetation survey area was mainly similar; the only difference was that organic waste and litter classified as "other" were mostly found in the beach survey area (Fig. 5). No significant change in the composition of litter material of the islands was noted over the course of sampling occasions (ANOSIM, R = –0.005, $p = 0.52$).

Out of 82 litter categories used under the UNEP/MARLIN litter classification system, 76 were present in the studied areas (Table S2). The most prevalent litter items were plastic bags, food containers, plastic fragments, and plastic bottles – these four litter types formed 44% of all litter findings (Table 4). Items categorized as single-use plastic (PL01–

Table 4. Top ten of litter items found on 14 Estonian uninhabited islands during summer 2019 – autumn 2020. The original UNEP/MARLIN macrolitter codes, together with respective J-codes and sources (Fleet et al. 2021), are presented. For the full list, see Table S1. Glass = glass and ceramics, wood = processed wood

UNEP code	J-code	Name of litter item	Material	Source/activity	Total count	%
PL07	J3	Plastic bags (opaque and clear)	Plastic	Undefined use	1831	14.28
PL06	J30	Food containers, candy wrappers	Plastic	Food consumption-related	1735	13.53
PL24	J79	Other plastic	Plastic	Undefined use	1054	8.22
PL02	J8	Bottles < 2 L	Plastic	Food consumption-related	999	7.79
WD04	J162	Processed timber and pallet crates	Wood	Undefined use	642	5.01
GC07	J208	Glass or ceramic fragments	Glass	Undefined use	569	4.44
FP04	J256	Foam (insulation and packaging)	Plastic	Building and construction-related	499	3.89
GC02	J200	Glass bottles and jars	Glass	Food consumption-related	487	3.80
PL01	J21	Bottle caps and lids	Plastic	Food consumption-related	484	3.78
WD06	J171	Other wood	Wood	Undefined use	357	2.78

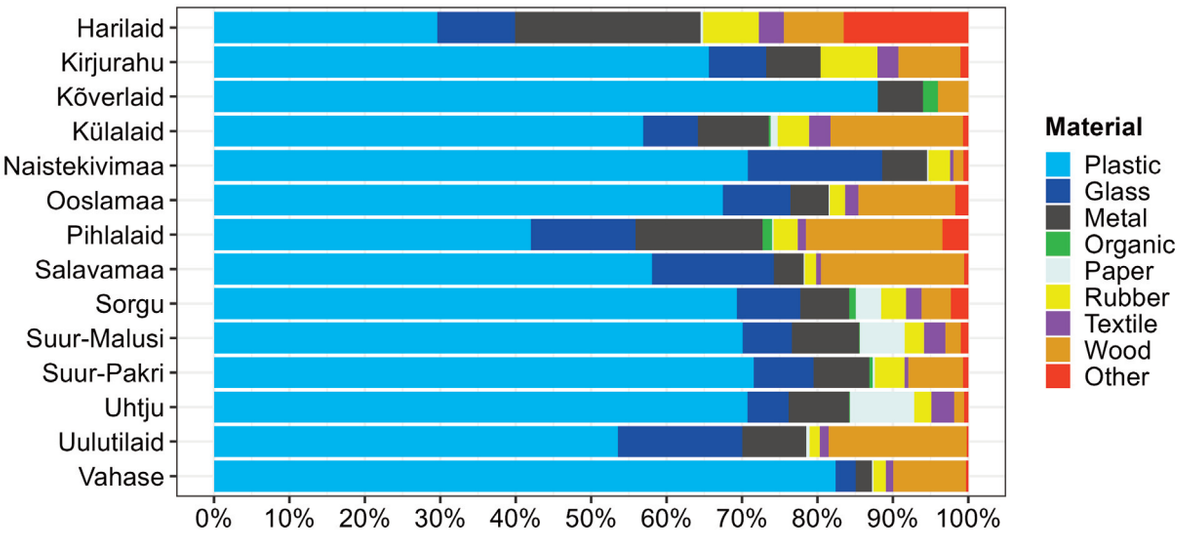

Fig. 4. Share of different macrolitter materials per island, presented over all sampling occasions (beach and vegetation survey areas, items m^{-2}). Glass = glass and ceramics, wood = processed wood.

PL07) were found 5177 times in total, accounting for 40.4% of all findings. Single-use cutlery and cigarette butts, which are both common litter items on public beaches (Addamo et al. 2017), were also found in the islands but in low abundance (34 and 25 items in total, respectively) (Table S2).

For most of the litter items (52.3%), the source could not be defined. Litter related to food consumption amounted to 35.5%, followed by building and construction-related (3.9%), fisheries-related (3%), agriculture-related (1.8%), clothing (1.5%), and recreation-related litter (1.4%). The share of smoking-related, medical-related, personal hygiene and care-related, and vehicle-related sources of litter was less than 1%. The share of different litter pollution sources varied among islands (Fig. S3).

Based on macrolitter composition, there were significant differences between islands (Fig. 6). NMDS ordination (Fig. 7) showed clear differentiation of some islands (e.g., Harilaid); differentiation at the sub-basin level was also detected by ANOSIM (litter item composition: $R = 0.27$, $p < 0.01$; litter

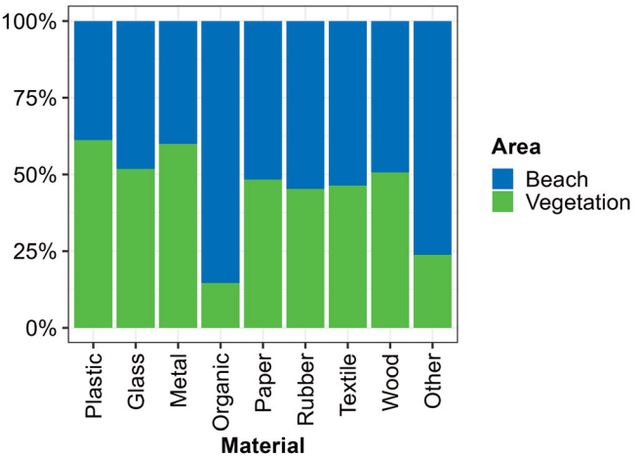

Fig. 5. Proportional distribution of litter materials between survey areas (beach and vegetation, items m^{-2}) based on pooled data from all islands and sampling occasions. Glass = glass and ceramics, wood = processed wood.

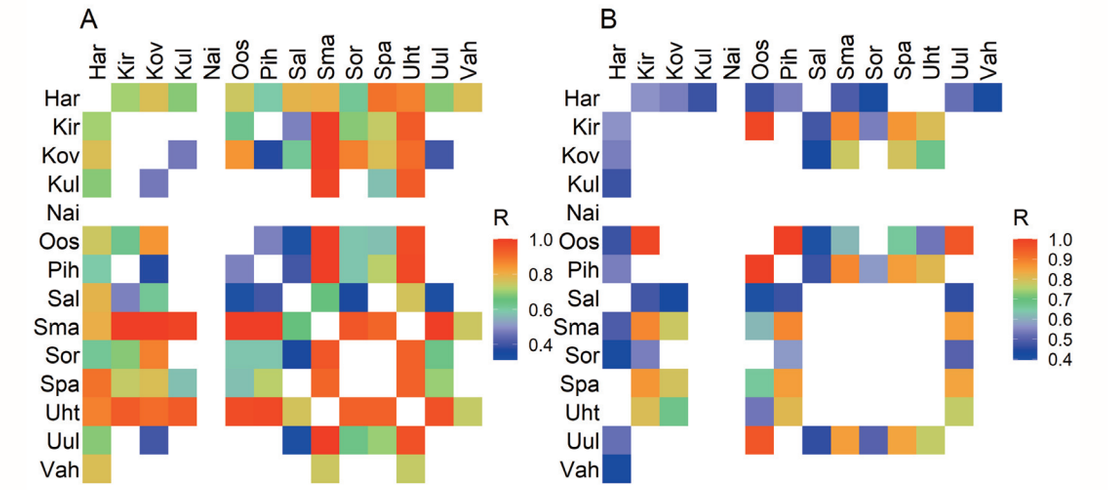

Fig. 6. Results of pairwise ANOSIM of islands' litter item (A) and material composition (B) based on litter data normalized per areal unit (m^2). The litter material dataset was derived by summing litter item counts based on material. Blank cells indicate statistically non-significant differences ($p \geq 0.05$), and all colored cells indicate statistically significant R-values ($p < 0.05$). Higher R-values indicate stronger differentiation. For the abbreviations of island names, see Table 1.

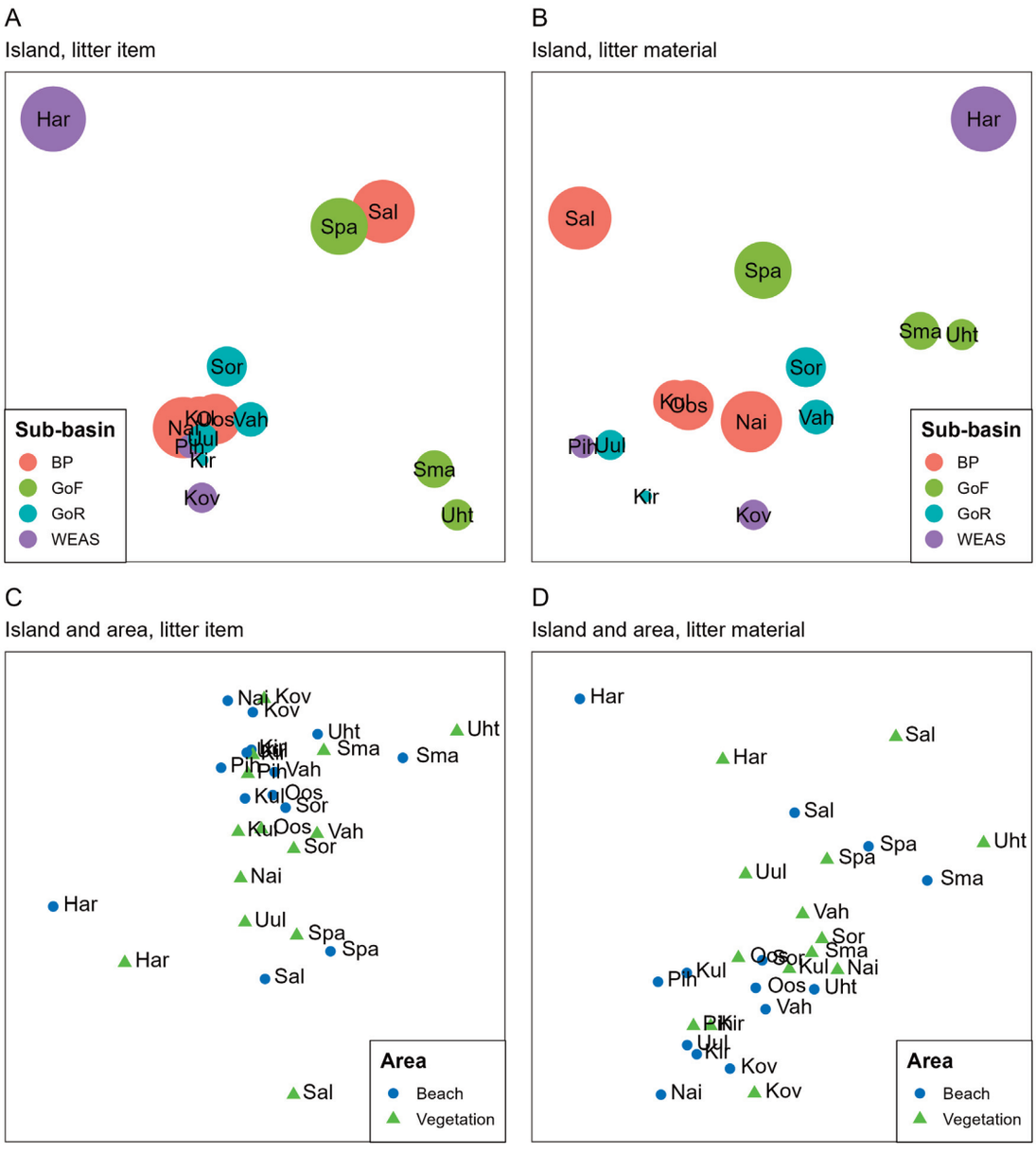

Fig. 7. NMDS ordinations of the similarity structure of litter composition (based on items m^{-2}; the litter material dataset was derived by summing litter item counts based on material). A closer distance between points reflects a higher similarity of litter composition. Plots in the upper row (A, B) represent ordinations on the island level (litter count data summed across survey areas: beach and vegetation). Plots in the lower row (C, D) represent ordinations on the island and survey areas separately (beach, vegetation). Circle sizes in the upper plots (A, B) indicate the total weight of litter. See Fig. 5 for island-level pair-wise comparisons of island differentiation and Table 1 for the abbreviations of island names.

material composition: R = 0.28, $p < 0.01$). There was no indication of a relationship between total weight and litter composition. No differentiation between the beach and vegetation survey areas was noted for litter item composition (ANOSIM, R = 0.02, $p = 0.01$) or litter material composition (ANOSIM, R = 0.02, $p = 0.05$). However, strong differentiation in litter composition between the beach and vegetation survey areas was notable for some islands (e.g., Uhtju, Naistekivimaa, Salavamaa; Fig. 7).

Based on BIOENV analysis, the set of variables that best explained the litter composition structure included current, depth, and orbital speed, with a rank correlation coefficient of 0.766 (Table 5). The BSPI was retrieved among the set of variables best explaining the litter composition only at the item level (rank correlation 0.690). Correlations were higher in the case of litter items compared to litter materials (0.766 vs. 0.627).

3.3. Microlitter in sediment

Microlitter (size >100 µm) was found in the sediment of all studied islands. However, microlitter was not present in every sampling occasion. When data from all islands and sampling episodes were pooled, a potential positive correlation was observed between macrolitter abundance (normalized beach total per m^2) and microlitter abundance in beach sediment (Pearson's $r = 0.27$), although statistical significance was slightly above the conventional threshold ($p = 0.055$). In contrast, no such relationship was found between macrolitter and microlitter abundances in the shallow coastal sea (Pearson's $r = 0.094$, $p = 0.5$).

Table 5. Results of BIOENV analyses. The top five highest correlations are shown for litter item and material (based on items m^{-2}; the litter material dataset was derived by summing litter item counts based on material)

Litter	Variables	No. of variables	Spearman rank correlation R	*p*
Item	Current, depth, orbital speed	3	0.766	< 0.001
Item	Current, depth, slope, orbital speed	4	0.739	< 0.001
Item	Current, orbital speed	2	0.737	< 0.001
Item	Current, depth, slope, orbital speed, sediment	5	0.716	< 0.001
Item	BSPI, current, depth, slope, orbital speed, sediment	6	0.690	< 0.001
Material	Current, orbital speed	2	0.627	< 0.001
Material	Current, depth, orbital speed	3	0.610	0.001
Material	Current, depth, orbital speed, sediment	4	0.580	0.001
Material	Current	1	0.550	0.001
Material	Current, depth, slope, orbital speed, sediment	5	0.545	0.003

Table 6. Microlitter amounts (number of particles kg^{-1}) in beach and shallow-water survey areas, and at the island level (pooled over beach and shallow-water survey areas). Sub-basins: GoF – Gulf of Finland, BP – Baltic Proper, GoR – Gulf of Riga, WEAS – West Estonian Archipelago Sea, overall – data pooled over all sub-basins. Abbreviation: SD – standard deviation

Region/sub-basin	Survey area	No. of surveys	Mean	SD	Median
Overall	Beach	53	8.11	10.55	0
Overall	Shallow-water	53	5.66	11.98	0
Overall	Island	53	6.89	11.09	0
BP	Beach	13	12.31	15.34	10
BP	Shallow-water	13	2.31	5.95	0
BP	Island	13	7.31	12.67	0
GoR	Beach	16	5.01	7.88	0
GoR	Shallow-water	16	4.38	7.88	0
GoR	Island	16	5.31	7.88	0
GoF	Beach	12	7.10	11.64	0
GoF	Shallow-water	12	5.83	8.26	0
GoF	Island	12	6.67	10.27	0
WEAS	Beach	12	9.17	11.87	5
WEAS	Shallow-water	12	10.83	16.05	10
WEAS	Island	12	10.00	14.14	0

Microlitter was found in 41.5% of sediment samples taken from the beach survey areas and in 34% of sediment samples taken from the shallow-water survey areas. The amount of microlitter in the sediment varied between 0–40 particles kg^{-1} for the beach and 0–60 particles kg^{-1} in the shallow coastal sea (Fig. S4) with an overall mean of 8.11 for the beach section and 5.66 for the sea section (particles kg^{-1}) (Table 6). Most of the observed microlitter particles were < 2 mm (67.5% of findings on the beach and 70% in seabed sediment). Across the islands, there were some variations in microlitter composition; however, in beach sediment, plastic fibers and glass fragments were dominant. In shallow-water sediment, plastic fibers, glass, and metal fragments were found in equal amounts (Fig. 8).

3.4. Effect of macrolitter on biota

In total, 254 mortal remains were observed on the 14 islands in 2019–2020. Of these remains, 233 belonged to birds (*Phalacrocorax carbo* on Sorgu island; otherwise *Larus* spp.; Table 7), 19 to seals (16 found on Kirjurahu, one on Sorgu, and one on Suur-Pakri), and two to terrestrial mammals (boar and deer found on Kõverlaid).

Plastic and/or ropes and strings were noted around ten bird corpses. These findings originated from common breeding areas for seabirds in the Gulf of Finland and the Gulf of Riga. However, based solely on visual observations, litter as a probable direct cause of death was noted for three birds (entanglement in a fishing net and a plastic bag entangled around the neck).

No bird nests were found on six islands (Naistekivimaa, Kõverlaid, Salavamaa, Uulutilaid, Vahase, and Külalaid). Only a few nests (< 5) were found on two islands, and those did not contain litter (Table 7). On the remaining islands, 30–60 nests were observed. Litter items were used as nest material in 83% of observed nests on Sorgu, 67% on Suur-Malusi, 20% on Uhtju, and 10% on Kirjurahu and Ooslamaa (Table 7). The litter items used as nest material were most commonly plastic bags, plastic food packaging, and ropes and strings (both plastic and textile). On a few occasions, nests had been built within plastic box remains and plastic barrels (observed on Ooslamaa and Kirjurahu). Bird pellets commonly contained fragments of plastic bags, aluminum foil, and glass. Among other items, sharp glass fragments (up to 5 cm in length) and metal clips used in food packaging were noted within bird pellets.

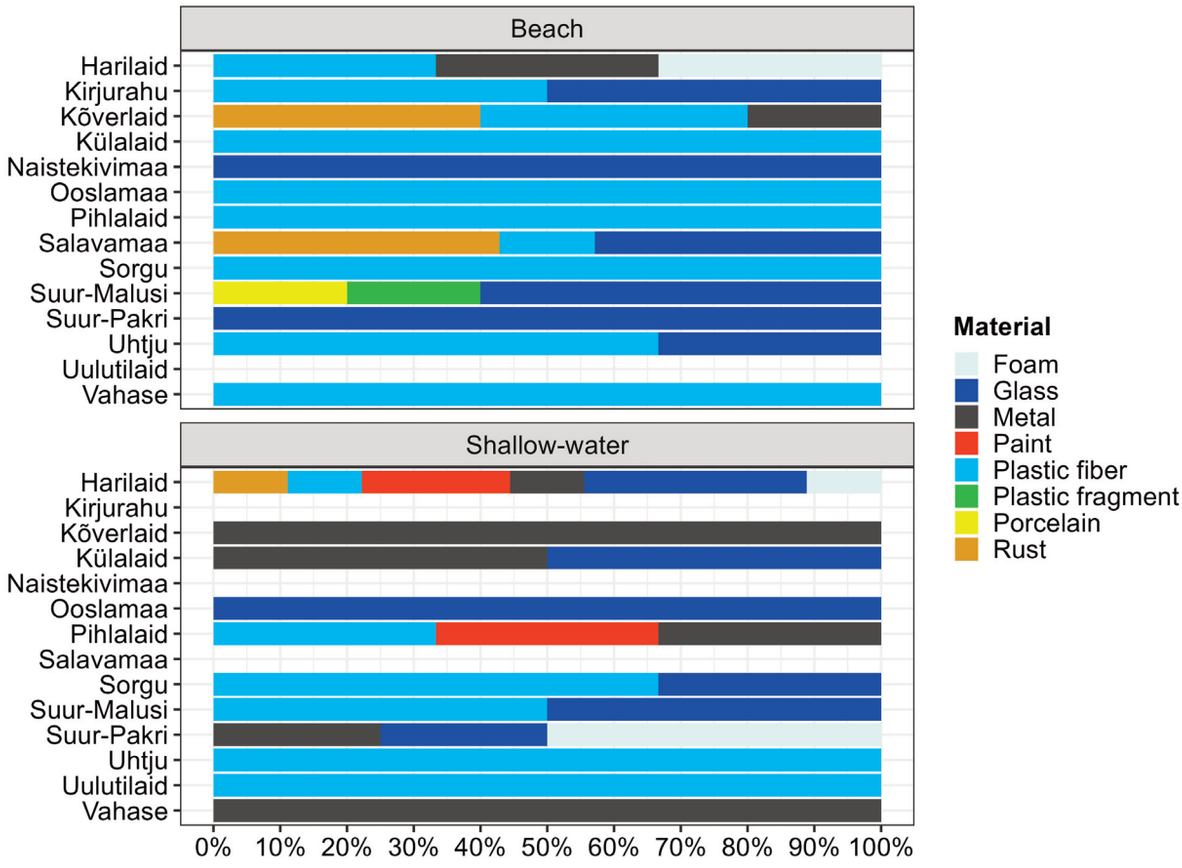

Fig. 8. Share of different microlitter materials per island presented over all sampling occasions.

Table 7. Number of observed bird corpses and nests in relation to the presence of macrolitter

Island	Corpses/deaths related to litter	Nests/nests with litter
Kirjurahu	20/0	30/3
Ooslamaa	44/0	30/3
Pihlalaid	2/0	3/0
Salavamaa	2/0	–
Sorgu	138/2	60/50
Suur-Malusi	9/0	30/20
Suur-Pakri	8/0	3/0
Uhtju	5/1	50/10
Uulutilaid	3/0	–
Vahase	2/0	–

4. Discussion

The study provides valuable insight into the quantity, composition, and distribution of marine litter in natural, uninhabited coastal regions of small islands in the northeastern Baltic Sea. However, the term "uninhabited" does not fully exclude visits from, e.g., summertime tourists, some of whom were observed picking up marine litter. Thus, considering these sporadic cleanups by visitors, the amounts of litter presented here may underestimate the actual pollution load.

4.1. Amount of macrolitter

The value of 20 litter items per 100 m of coastline was set as the threshold, reflecting the agreed value of GES in European seas for beach litter (van Loon et al. 2020; European Commission 2022). This threshold was derived from the 15th percentile of the EU litter count baseline dataset for 2015–2016 (van Loon et al. 2020). For comparison, a minimum of 40 surveys is recommended (van Loon et al. 2020). Based on our study, the median amount of litter was 10.65 items per 100 m in the beach survey areas, indicating that the natural, remote beaches in the northeastern Baltic Sea region can be considered in GES.

The number of macrolitter items in the beach survey areas remained mainly below the Baltic Sea average of 47 items per 100 m of coastline reported previously for natural beaches (HELCOM 2018). At the Baltic Sea level, the status evaluation of marine beach litter for 2016–2021 shows that 11 out of 16 sub-basins exceed the HELCOM threshold of 20 litter items per 100 m of coastline; at the sub-basin level, median values for beach litter ranged between 5–313 items

per 100 m of coastline (HELCOM 2023). Previously, the MARLIN project reported an average of 75.7 litter items per 100 m on rural beaches, and a 50% share of plastic (based on six rural beaches in Sweden, Finland, Estonia, and Latvia in 2011–2013; MARLIN 2013).

According to the HELCOM SPICE report, the mean number of beach litter items in the Baltic Sea countries varied between 33.7–354.4 items per 100 m: Finland 354.4, Germany 61.7, Denmark 99.4, Sweden 88.1, Estonia 118.4, Lithuania 222.3, Latvia 180.2, and Poland 33.7. The share of plastic varied between 53% (Latvia) and 89% (Finland). Baseline calculations for rural beaches in the Baltic Sea during 2012–2016 suggest mean and median values of 79.8 and 72.3 beach litter items per 100 m of coastline (Zalewska and Krzyminski 2017). The values presented here, calculated at the Baltic Sea sub-basin level, are below these baseline values.

The Clean Coastal Index (CCI) has been suggested as a tool for evaluating coastal cleanliness. CCI was originally based on the density of plastic items per m^2 (Alkalay et al. 2007) but has later been used as a general measure of litter density for all types of litter material (Asensio-Montesinos et al. 2021a). In our study, litter density was low – on any sampling occasion, the density of litter on an island did not exceed 0.06 items m^{-2}, and the regional (Gulf of Finland, Baltic Proper, Gulf of Riga, West Estonian Archipelago Sea) median values for density were < 0.02 items m^{-2}. Accordingly, based on CCI, all studied islands can be classified as "very clean" because the litter density was lower than one item per 10 m^2. For comparison, an average of 0.09–0.55 beach litter items m^{-2} for countries in the Baltic Sea region has been reported, reflecting generally low pollution levels when compared to other regions on a global scale (Haseler et al. 2020 and references therein). Urban beaches of the Baltic Sea region can also be regarded as clean – during the summer of 2022, CCI was estimated at 0.05–0.38 items m^{-2} on touristic urban beaches in Poland (Bigus and Jarosiewicz 2023).

The increase of litter load along the sea–inland gradient has been highlighted by, e.g., Šilc et al. (2018) and in this study. Litter pollution in vegetation survey areas was notably higher than in beach survey areas, with a median of 21.36 litter items per 100 m. Similarly, when vegetation survey areas were included, the amount of litter per sampling occasion was considerably higher on some islands, with over 200 litter items per 100 m of survey area.

The total weight of removed litter mostly remained < 5 kg per 100 m in beach survey areas and < 10 kg per 100 m in vegetation survey areas, with a maximum of 27 kg. Usually, weight is not recorded in a regular monitoring process (Hanke et al. 2019), and the presence/absence of large, heavy mega-litter can distort monitoring results by weight (Smith and Turrell 2021). Nevertheless, the numbers presented here serve as an indication for a better general understanding of marine litter pollution in the Baltic Sea region and, e.g., related manpower needs for organizing cleanups (Hidalgo-Ruz and Thiel 2015).

No clear trend in litter amount, density, or weight was observed during the two-year study period. Based on previous annual beach litter monitoring in Estonia carried out in 2012–2016, the average number of litter items per 100 m of beach section decreased from 140 to 24 (Press 2020). However, no significant change was noted in 2017–2022, when the average number of litter items per 100 m of beach section varied between 20–43 (Press 2023). In addition to the short study period, the variance in the number of litter findings could also be explained by a combination of seasonal differences (finding litter under high or low vegetation), bird activities, and coastal processes (e.g., Andriolo and Gonçalves 2022).

4.2. Composition of macrolitter

The set of environmental variables that best explained litter composition across islands included water current speed, water depth, and orbital speed at seabed. The effect of wind and storms on beach litter abundance has been shown in earlier studies (e.g., Turrell 2018; Asensio-Montesinos et al. 2021a). The BSPI, which measures the quantity and spatial distribution of potential cumulative pressures on the Baltic Sea, was also retrieved among the variables best explaining litter composition at the item level. In addition to the aforementioned environmental variables, sediment partly explained litter composition based on material. Our study included beaches with different sediments – sand, gravel, cobbles, pebbles, boulders, and rock. Given the heterogeneity and variability of sediments even on a small scale (< 1 km) in the northeastern Baltic Sea region (Łabuz 2015), it was not advisable to focus solely on sandy beaches, as beaches with hard or mixed sediment can also accumulate litter (Asensio-Montesinos et al. 2021b). The beaches of Suur-Pakri, Salavamaa, Naistekivimaa, and Külalaid were dominated by limestone and limestone pebbles; at the same time, the amounts of litter in these areas were notably high. These islands are all exposed to the Baltic Proper and intensive shipping corridors. Investigations of litter on beaches other than sandy ones are limited. However, litter burial and exhumation processes are known to occur on cobble beaches (Asensio-Montesinos et al. 2021b).

Litter composition varied between islands, and differentiation at the sub-basin level was also detected. The share of plastic ranged between 60–70% for most islands, which corresponds to general plastic pollution reported for beaches in the Baltic Sea region (Kideys et al. 2021). At the island level, the percentage of plastic litter items was highest on Kõverlaid (88%) and Vahase (83%), and lowest on Harilaid (30%) and Pihlalaid (42%). Both Kõverlaid and Vahase had overall small amounts of litter. On Vahase, the low amount of litter items and dominance of plastic items most probably reflects sporadic cleanups by summertime tourists. In the case of Kõverlaid, similar results can be explained both by its location and by the specific characteristics of the coastline. Kõverlaid, Pihlalaid, and Uulutilaid, all of which had small amounts of litter, are located within or close to the West Estonian Archipelago Sea, a relatively closed waterbody where marine traffic is mainly local (ferry lines between the largest islands, local fishermen and sailors). As (international) shipping intensity is lower here, litter pollution loads are generally lower (e.g., Čulin and Bielić 2016; this study).

Secondly, Kõverlaid has a very narrow beach section (up to 5 m wide under normal water level), and right next to the beach is a dense, wide belt (up to 50 m) of common reed (*Phragmites australis*). This reed belt acts as a substantial barrier, preventing macrolitter from moving inland. Similar effects have been shown for giant reed (*Arundo donax*) (Battisti et al. 2020) and for mangrove forests (Li et al. 2021). However, at the same time, these reed barriers may also act as litter traps, especially for meso- and microlitter (Battisti et al. 2020).

Among the islands, litter composition was most distinguishable on Harilaid, where the share of plastic was lowest. At the same time, metal, rubber, and items classified as "other" materials were more common. (The "other" category was represented mainly by fragments of asbestos cement, a common roof material in the 20th century.) These materials originate from abandoned and deteriorating facilities – berths and shipwrecks at sea, as well as houses and a lighthouse inland. Until 1992, the island and these facilities were used by the USSR Border Guard. The berth was destroyed during a powerful storm (Gudrun/Erwin) in January 2005, while the houses are facing natural deterioration (Tähiste and Mõniste 2016). Similar abandoned facilities exist on Pihlalaid, where the breakdown of wreckage and local-source pollution is reflected in the litter composition.

Overall, the most prevalent litter items were plastic bags, food containers, plastic fragments, and plastic bottles – these four litter types formed 44% of all findings. Processed wood and glass and ceramic fragments and bottles were also numerous. This pattern is similar to results reported for rural beaches in the Baltic Sea region. However, the small number of cigarette butts (25 in total during the study period) is noteworthy (Addamo et al. 2017; HELCOM 2018). The study period overlapped with the COVID-19 pandemic, which caused an increase in personal protective equipment litter (Roberts et al. 2022). This litter also made its way to the marine environment (Dybas 2021; Peng et al. 2021). During our fieldwork, however, we did not notice an increase in finding masks or rubber gloves (in total, 5 and 17 items, respectively). The masks were mainly related to construction works (dust protection, etc.). However, in the summer of 2020, a new type of litter emerged on Uhtju and Suur-Malusi islands in the Gulf of Finland – hygienic wet wipes. Although not numerous, these items had not been recorded before the pandemic at any studied location. The wet wipes could have been transported to the islands by water and birds.

For most litter items, the possible pollution source could not be defined. However, over one third of the litter items were related to food consumption, which is the dominant source of litter across the Baltic Sea (HELCOM 2018). The shares of building and construction-related, fisheries-related, agriculture-related, clothing, and recreation-related litter were small (< 5%) on most islands. Building and construction-related litter was highest on Harilaid (15%), which is associated with the deteriorating facilities mentioned above. Smoking-related, medical-related, personal hygiene and care-related, and vehicle-related sources were of minimal importance (< 1%).

4.3. Microlitter in sediment

The authors are aware of the currently suggested methodological changes related to research on microlitter in sediment. The results presented here serve as an insight into the microlitter occurrence in the study area. The amount of microlitter in the sediment was relatively low. However, it must be stressed that microlitter items were found on every island studied, and a small positive correlation between macrolitter abundance (normalized beach total per m^2) and microlitter abundance in beach sediment was noted. Our findings indicate that in regions without direct human impact, the amount of microlitter in the sediment was up to 60 items per kg. Surprisingly, these results are comparable with findings in Kiel Fjord, Western Baltic Sea, where an intensively visited beach, a beach near a sewage plant, and a beach polluted with large-size plastic debris were studied, and 1.8–4.5 microlitter particles per kg of dry sediment were counted for the first two beaches and up to 30.2 particles per kg of dry sediment were counted at the site with high litter loads (Schröder et al. 2021). The latter suggests that fragmentation of large plastic litter at the site could be a relevant source of microplastics in the sediments of the Baltic Sea region (Schröder et al. 2021). Similarly, Urban-Malinga et al. (2020) reported the findings from the Polish coast, Southern Baltic Sea, where the highest microplastic concentrations – up to 295 microlitter particles per kg of dry sediment – were reported for urban beaches. Yet, no substantial difference was noted in microplastic pollution between urban beaches and national parks without direct human impact (Urban-Malinga et al. 2020).

4.4. Effect of macrolitter on biota

With human population growth, waste production and litter pollution in the environment (including the marine environment) increase (Jambeck et al. 2015). Human-produced litter in bird nests is also an increasing trend (Votier et al. 2011; Grant et al. 2018) – when suitable litter is available, birds will use it in their nests (Grant et al. 2018). Based on our observations, litter was commonly used as nest material on the bird-breeding islands that are closer to human activities and littering related to them. Previously, human impact on the environment estimated within 100 km of a bird colony has also been significantly related to the prevalence of unnatural debris in nests (O'Hanlon et al. 2021).

On Uhtju and Suur-Malusi islands, the litter composition was most specific, comprising relatively small litter objects – mostly degrading small plastic bags and plastic, metal, and aluminum fragments related to food packaging – which were collected both from nests and vegetation. This litter composition could best be explained by the activity of birds. In the eastern Baltic Sea, birds in the Uhtju region have probably used the Kunda, Rakvere, and other nearby landfills as feeding grounds (though, e.g., the Kunda landfill was closed in

2004 and the Rakvere landfill in 2009), and based on the dominant litter items on the island, it is probable that, in addition to marine-transported litter, birds themselves transport a great deal of the litter from the mainland to the island. At the same time, misuse of food-related plastic items and their origin from ships cannot be excluded. The dominant bird species on Uhtju is seagull (*Larus* spp.), in contrast to Sorgu, where *Phalacrocorax carbo*, breeding both on the ground and in trees, prevails. Previously, it has been shown that litter is a common nest material for birds in the Baltic Sea region – over 55% of cormorant nests located on remote islands in the southern Baltic Sea region contained litter (Schernewski et al. 2018). Results presented here suggest a need for a more comprehensive study on seabirds' litter use, as comparable data are currently lacking for the northeastern Baltic Sea region (Veljo Volke, Estonian Ornithological Society, pers. comm. October 2023).

5. Conclusions

The current study was carried out as a pilot study and aimed to cover different aspects of marine litter pollution on small uninhabited islands in Estonia, in the northeastern Baltic Sea. Calculated over all conducted surveys, the median value of macrolitter items per 100 m of beach section was 10.65, and the respective median density was 0.006 items m^{-2}. Thus, regarding beach litter amounts, the studied islands can be stated to be in Good Environmental Status. However, when the litter pollution of the terrestrial vegetation survey area next to the beach was studied, the medians rose to 21.36 litter items per 100 m and 0.009 items m^{-2}. At the sub-basin level, the islands located in the Gulf of Finland had the highest number of litter items per 100 m and the highest density (items m^{-2}), 38.05 and 0.017, respectively. Litter composition varied between islands; however, the share of plastic was between 60–70% for most islands, and over one-third of the litter items were related to food consumption, which corresponds to general plastic pollution reported for beaches in the Baltic Sea region. The set of environmental variables that best explained litter composition on different islands included current, depth, and orbital speed. Microlitter was found in roughly one-third of the samples, and the amount of microlitter in the sediment was up to 60 items kg^{-1}. Macrolitter was commonly used as nest material on bird-breeding islands that are closer to human activities and littering related to them.

What is also alarming is that 11 of the visited islands are nature conservation areas, and though human access is limited, these areas are clearly affected by marine litter. A more holistic approach to marine litter research is recommended based on the fieldwork effort and the research results. Conducting both macro- and microlitter surveys and considering the possible effect on biota gives a more solid and broader view of the problems and possible solutions related to marine litter. The study also indicates the need for specifically targeted actions in nature conservation areas (irrespective of the dominant coastal sediment) that are prone to accumulate marine litter.

Data availability statement

The data are contained within the article, and the original materials are housed in the Estonian Marine Institute, Faculty of Science and Technology, University of Tartu. Data supporting this study are available upon request from the Estonian environmental monitoring database (keskkonnaportaal.ee, kese@envir.ee), project reference "ST00002774 Eesti väikesaarte mereprügi," or by direct request to the corresponding author of the article.

Acknowledgments

The research was funded by the Environmental Investment Centre, research project "Marine litter in the small islands of Estonia", 01.03.2019–10.12.2020, project No. 15425. The authors are grateful to the two anonymous reviewers for their valuable comments. The publication costs of this article were partially covered by the Estonian Academy of Sciences.

Supplementary online data

Supplementary online data to this article can be found at https://doi.org/10.3176/earth.2026.S01 and include Figures S1–S4 and Tables S1 and S2 detailing the different aspects of marine litter distribution in the Estonian coastal sea region.

References

Addamo, A. M., Laroche, P. and Hanke, G. 2017. *Top Marine Beach Litter Items in Europe: A Review and Synthesis Based on Beach Litter Data*. EUR 29249 EN. Publications Office of the European Union, Luxembourg. https://doi.org/10.2760/496717

Alkalay, R., Pasternak, G. and Zask, A. 2007. Clean-coast index – a new approach for beach cleanliness assessment. *Ocean and Coastal Management*, **50**(5–6), 352–362. https://doi.org/10.1016/j.ocecoaman.2006.10.002

Andriolo, U. and Gonçalves, G. 2022. Is coastal erosion a source of marine litter pollution? Evidence of coastal dunes being a reservoir of plastics. *Marine Pollution Bulletin*, 174, 113307. https://doi.org/10.1016/j.marpolbul.2021.113307

Asensio-Montesinos, F., Anfuso, G., Aguilar-Torrelo, M. T. and Oliva Ramírez, M. 2021a. Abundance and temporal distribution of beach litter on the coast of Ceuta (North Africa, Gibraltar Strait). *Water*, **13**(19), 2739. https://doi.org/10.3390/w13192739

Asensio-Montesinos, F., Anfuso, G., Williams, A. T. and Sanz-Lázaro, C. 2021b. Litter behaviour on Mediterranean cobble beaches, SE Spain. *Marine Pollution Bulletin*, **173**, 113106. https://doi.org/10.1016/j.marpolbul.2021.113106

Avio, C. G., Pittura, L., d'Errico, G., Abel, S., Amorello, S., Marino, G. et al. 2020. Distribution and characterization of microplastic particles and textile microfibers in Adriatic food webs: general insights for biomonitoring strategies. *Environmental Pollution*, **258**, 113766. https://doi.org/10.1016/j.envpol.2019.113766

Barnes, D. K. A., Galgani, F., Thompson, R. C. and Barlaz, M. 2009. Accumulation and fragmentation of plastic debris in global environments. *Philosophical Transactions of The Royal Society B*, **364**(1526), 1985–1998. https://doi.org/10.1098/rstb.2008.0205

Baston, D. 2021. *Exactextractr: Fast Extraction from Raster Datasets using Polygons*. R package version 0.7.2. https://CRAN.R-project.org/package=exactextractr (accessed 2023-01-12).

Battisti, C., Fanelli, G., Filpa, A. and Cerfolli, F. 2020. Giant reed (*Arundo donax*) wrack as sink for plastic beach litter: first evidence and implication. *Marine Pollution Bulletin*, **155**, 111179. https://doi.org/10.1016/j.marpolbul.2020.111179

Benjamini, Y. and Hochberg, Y. 1995. Controlling the false discovery rate: a practical and powerful approach to multiple testing. *Journal of the Royal Statistical Society: Series B (Methodological)*, **57**(1), 289–300. https://doi.org/10.1111/j.2517-6161.1995.tb02031.x

Bigus, K. and Jarosiewicz, A. 2023. Using the Coastal Clean Index to assess the impact of anthropogenic pressure on sandy beaches in Ustka, Poland. *Studia Quaternaria*, **40**(2), 67–76. https://doi.org/10.24425/sq.2023.148033

Björkqvist, J.-V., Lukas, I., Alari, V., van Vledder, G. P., Hulst, S., Pettersson, H. et al. 2018. Comparing a 41-year model hindcast with decades of wave measurements from the Baltic Sea. *Ocean Engineering*, **152**, 57–71. https://doi.org/10.1016/j.oceaneng.2018.01.048

Borrelle, S. B., Ringma, J., Law, K. L., Monnahan, C. C., Lebreton, L., McGivern, A. et al. 2020. Predicted growth in plastic waste exceeds efforts to mitigate plastic pollution. *Science*, **369**(6510), 1515–1518. https://doi.org/10.1126/SCIENCE.ABA3656

Canals, M., Pham, C. K., Bergmann, M., Gutow, L., Hanke, G., van Sebille, E. et al. 2021. The quest for seafloor macrolitter: a critical review of background knowledge, current methods and future prospects. *Environmental Research Letters*, **16**(2), 023001. https://doi.org/10.1088/1748-9326/abc6d4

Clarke, K. R. 1993. Non-parametric multivariate analysis of changes in community structure. *Australian Journal of Ecology*, **18**(1), 117–143. https://doi.org/10.1111/j.1442-9993.1993.tb00438.x

Clarke, K. R. and Ainsworth, M. 1993. A method of linking multivariate community structure to environmental variables. *Marine Ecology Progress Series*, **92**, 205–219. https://doi.org/10.3354/meps092205

Čulin, J. and Bielić, T. 2016. Plastic pollution from ships. *Pomorski zbornik*, **51**(1), 57–66. https://doi.org/10.18048/2016.51.04

Delgado, S., Zorrozua, N. and Arizaga, J. 2020. Marginal presence of plastic in nests of yellow-legged gulls (*Larus michahellis*) in the southeastern Bay of Biscay. *Animal Biodiversity and Conservation*, **43**(2), 191–195. https://doi.org/10.32800/abc.2020.43.0191

Devriese, L. I., van der Meulen, M. D., Maes, T., Bekaert, K., Paul-Pont, I., Frére, L. et al. 2015. Microplastic contamination in brown shrimp (*Crangon crangon*, Linnaeus 1758) from coastal waters of the southern North Sea and Channel area. *Marine Pollution Bulletin*, **98**(1–2), 179–187. https://doi.org/10.1016/j.marpolbul.2015.06.051

Dybas, C. L. 2021. Surgical masks on the beach: COVID-19 and marine plastic pollution. *Oceanography*, **34**(1), 12–14. https://doi.org/10.5670/oceanog.2021.105

Ershova, A. A., Eremina, T. R., Chubarenko, I. P. and Esiukova, E. E. 2021. Marine litter in the Russian Gulf of Finland and South-East Baltic: application of different methods of beach sand sampling. In *Plastics in the Aquatic Environment – Part I* (Stock, F., Reifferscheid, G., Brennholt, N. and Kostianaia, E., eds). The Handbook of Environmental Chemistry, Vol. 111. Springer, Cham. https://doi.org/10.1007/698_2021_746

Estonian Nature Conservation Act. 2004. Riigi Teataja I, **38**, 258.

Estonian Permanently Inhabited Small Islands Act. 2003. Riigi Teataja I, **23**, 141.

European Commission. 2022. MSFD CIS Guidance Document No. 19, Article 8 MSFD, May 2022. https://www.aquabiota.se/wp-content/uploads/european-commission-2022.-msfd-cis-guidance-document-no.-19-article-8-msfd-may-2022.pdf?utm_source=chatgpt.com

Fleet, D., Vlachogianni, T. and Hanke, G. 2021. *Joint List of Litter Categories for Marine Macrolitter Monitoring: Manual for the Application of the Classification System*. EUR 30348 EN. Publications Office of the European Union, Luxembourg. https://dx.doi.org/10.2760/127473

de Francesco, M. C., Carranza, M. L. and Stanisci, A. 2018. Beach litter in Mediterranean coastal dunes: an insight on the Adriatic coast (central Italy). *Rendiconti Lincei. Scienze Fisiche e Naturali*, **29**, 825–830. https://doi.org/10.1007/s12210-018-0740-5

Galgani, F., Hanke, G., Werner, S. and De Vrees, L. 2013. Marine litter within the European Marine Strategy Framework Directive. *ICES Journal of Marine Science*, **70**(6), 1055–1064. https://doi.org/10.1093/icesjms/fst122

Galgani, L., Beiras, R., Galgani, F., Panti, C. and Borja, A. 2019. Editorial: Impacts of marine litter. *Frontiers in Marine Science*, **6**, 208. https://doi.org/10.3389/fmars.2019.00208

GESAMP. 2015. *Sources, Fate and Effects of Microplastics in the Marine Environment: A Global Assessment* (Kershaw, P. J., ed.). International Maritime Organization, London.

Grant, M. L., Lavers, J. L., Stuckenbrock, S., Sharp, P. B. and Bond, A. L. 2018. The use of anthropogenic marine debris as a nesting material by brown boobies (*Sula leucogaster*). *Marine Pollution Bulletin*, **137**, 96–103. https://doi.org/10.1016/j.marpolbul.2018.10.016

Haaksi, H. 2020. *Task 2.1.1 Development of Baselines of Marine Litter - Identification of Top Litter Items in the Baltic Sea Region*. HELCOM, Helsinki. https://helcom.fi/wp-content/uploads/2020/04/Theme-2_Deliverable-2.1.1.b.pdf

Hanke, G., Walwoort, D., van Loon, W., Addamo, A. M., Brosich, A., del Mar Chaves Montero, M. et al. 2019. *EU Marine Beach Litter Baselines: Analysis of a Pan-European 2012-2016 Beach Litter Dataset*. EUR 30022 EN. Publications Office of the European Union, Luxembourg. https://doi.org/10.2760/16903

Haseler, M., Balciunas, A., Hauk, R., Sabaliauskaite, V., Chubarenko, I., Ershova, A. et al. 2020. Marine litter pollution in Baltic Sea beaches – application of the sand rake method. *Frontiers in Environmental Science*, **8**, 599978. https://doi.org/10.3389/fenvs.2020.599978

HELCOM. 2010. Towards a tool for quantifying anthropogenic pressures and potential impacts on the Baltic Sea marine environment: a background document on the method, data and testing of the Baltic Sea Pressure and Impact Indices. *Baltic Sea Environment Proceedings*, **125**. https://doi.org/10.13140/RG.2.1.2148.6961

HELCOM. 2018. State of the Baltic Sea – second HELCOM holistic assessment 2011–2016. *Baltic Sea Environment Proceedings*, **155**. https://helcom.fi/baltic-sea-trends/holistic-assessments/state-of-the-baltic-sea-2018/reports-and-materials

HELCOM. 2023. *Beach Litter.* HELCOM Core Indicator Report. https://indicators.helcom.fi/wp-content/uploads/2023/04/Beach-litter_Final_April_2023-1.pdf (accessed 2025-01-28).

Hidalgo-Ruz, V. and Thiel, M. 2015. The contribution of citizen scientists to the monitoring of marine litter. In *Marine Anthropogenic Litter* (Bergmann, M., Gutow, L. and Klages, M., eds). Springer, Cham, 429–447. https://doi.org/10.1007/978-3-319-16510-3_16

Hidalgo-Ruz, V., Gutow, L., Thompson, R. C. and Thiel, M. 2012. Microplastics in the marine environment: a review of the methods used for identification and quantification. *Environmental Science & Technology*, **46**(6), 3060–3075. https://doi.org/10.1021/es2031505

Hijmans, R. J. 2020. *Raster: Geographic Data Analysis and Modeling*. R package version 3.4-5. https://CRAN.R-project.org/package=raster (accessed 2023-01-12).

Ibrahim, E. A. A., Osman, N. A. R. and Eisa, O. A. M. 2020. Status of the beach litter in the UNESCO World Heritage Site of Dungonab and Mukkawar Island Marine National Park in Sudan, Red Sea. *International Journal of Ecology*, 6904745. https://doi.org/10.1155/2020/6904745

Isæus, M. 2004. *Factors structuring Fucus communities at open and complex coastlines in the Baltic Sea*. PhD dissertation. Stockholm University, Sweden.

Jambeck, J. R., Geyer, R., Wilcox, C., Siegler, T. R., Perryman, M., Andrady, A. et al. 2015. Plastic waste inputs from land into the ocean. *Science*, **347**(6223), 768–771. https://doi.org/10.1126/science.1260352

Joint Research Centre: Institute for Environment and Sustainability and MSFD Technical Subgroup on Marine Litter. 2013. *Guidance on Monitoring of Marine Litter in European Seas*. EUR 26113 EN. Publications Office of the European Union, Luxembourg. https://data.europa.eu/doi/10.2788/99816

Kideys, A. E., Šubelj, G. and Aydın, M. 2021. *Marine Litter and European Beaches: Learning from Citizen Science*. ETC/ICM Technical Report 1/2021. European Topic Centre on Inland, Coastal and Marine Waters, Copenhagen.

Kruskal, J. B. 1964. Nonmetric multidimensional scaling: a numerical method. *Psychometrika*, **29**, 115–129.

Kruskal, W. H. and Wallis, W. A. 1952. Use of ranks in one-criterion variance analysis. *Journal of the American Statistical Association*, **47**(260), 583–621. https://doi.org/10.2307/2280779

Kühn, S., Bravo Revolledoo, E. L., van Franeker, J. A. 2015. Deleterious effects of litter on marine life. In *Marine Anthropogenic Litter* (Bergmann, M., Gutow, L. and Klages, M., eds). Springer, Berlin, 75–116.

Łabuz, T. A. 2015. Environmental impacts – coastal erosion and coastline changes. In *Second Assessment of Climate Change for the Baltic Sea Basin, Regional Climate Studies* (The BACC II Author Team, eds). Springer, Cham, 381–396. https://doi.org/10.1007/978-3-319-16006-1_20

Lavers, J. L. and Bond, A. L. 2017. Exceptional and rapid accumulation of anthropogenic debris on one of the world's most remote and pristine islands. *PNAS*, **114**(23), 6052–6055. https://doi.org/10.1073/pnas.1619818114

Lavers, J. L., Dicks, L., Dicks, M. R. and Finger, A. 2019. Significant plastic accumulation on the Cocos (Keeling) Islands, Australia. *Scientific Reports*, **9**, 7102. https://doi.org/10.1038/s41598-019-43375-4

Li, D., Zhao, L., Guo, Z., Yang, X., Deng, W., Zhong, H. et al. 2021. Marine debris in the Beilun Estuary mangrove forest: monitoring, assessment and implications. *International Journal of Environmental Research and Public Health*, **18**(20), 10826. https://doi.org/10.3390/ijerph182010826

van Loon, W., Hanke, G., Fleet, D., Werner, S., Barry, J., Strand, J. et al. 2020. *A European Threshold Value and Assessment Method for Macro Litter on Coastlines*. EUR 30347 EN. Publications Office of the European Union, Luxembourg. https://doi.org/10.2760/54369

Maljutenko, I. and Raudsepp, U. 2014. Validation of GETM model simulated long-term salinity fields in the pathway of saltwater transport in response to the Major Baltic Inflows in the Baltic Sea. In *2014 IEEE/OES Baltic International Symposium (BALTIC), Tallinn, Estonia, 27–29 May 2014* (Carroll, J., ed.). IEEE, 23–31. https://doi.org/10.1109/BALTIC.2014.6887830

MARLIN. 2013. *Final Report of Baltic Marine Litter Project MARLIN – Litter Monitoring and Raising Awareness 2011-2013*. https://pidasaaristosiistina.fi/wp-content/uploads/2023/06/Marlin_Final_Report_2014.pdf (accessed 2025-10-01).

Matiddi, M., Pham, C. K., Anastasopoulou, A., Andresmaa, E., Avio, C. G., Bianchi, J. et al. 2021. *Monitoring Micro-Litter Ingestion in Marine Fish: A Harmonized Protocol for MSFD and RSCs Areas*. MSFD TG Marine Litter. Joint Research Centre, European Commission, Luxembourg.

van der Meijs, F., Isaeus, M. 2020. *Wave Exposure Calculations for the Gulf of Finland*. AquaBiota Water Research, AquaBiota Report, 13.

Menicagli, V., Balestri, E. and Lardicci, C. 2019. Exposure of coastal dune vegetation to plastic bag leachates: a neglected impact of plastic litter. *Science of The Total Environment*, **15**, 737–748. https://doi.org/10.1016/j.scitotenv.2019.05.245

O'Hanlon, N. J., Bond, A. L., Masden, E. A., Lavers, J. L. and James, N. A. 2021. Measuring nest incorporation of anthropogenic debris by seabirds: an opportunistic approach increases geographic scope and reduces costs. *Marine Pollution Bulletin*, **171**, 112706. https://doi.org/10.1016/j.marpolbul.2021.112706

Oksanen, J., Simpson, G. L., Blanchet, F. G., Kindt, R., Legendre, P., Minchin, P. R. et al. 2020. *Vegan: Community Ecology Package*. R package version 2.5-7. https://CRAN.R-project.org/package=vegan (accessed 2023-01-12).

Pebesma, E. 2018. Simple features for R: standardized support for spatial vector data. *The R Journal*, **10**(1), 439–446. https://doi.org/10.32614/RJ-2018-009

Peng, Y., Wu, P., Schartup, A. T., Zhang, Y. 2021. Pandemic's plastic waste is choking the seas. *Nature*, **599**, 350. https://doi.org/10.1038/d41586-021-03078-1

Pérez-Guevara, F., Roy, P. D., Kutralam-Muniasamy, G. and Shruti, V. C. 2022. Coverage of microplastic data underreporting and progress toward standardization. *Science of The Total Environment*, **829**, 154727. https://doi.org/10.1016/j.scitotenv.2022.154727

Polasek, L., Bering, J., Kim, H., Neitlich, P., Pister, B., Terwilliger, M. et al. 2017. Marine debris in five national parks in Alaska. *Marine Pollution Bulletin*, **117**(1–2), 371–379. https://doi.org/10.1016/j.marpolbul.2017.01.085

Põldma, M., Torn, K. and Saks, L. 2023. Microlitter in fish and benthic invertebrates of the NE Baltic Sea: abundance, composition and bioindicators. *International Journal of Environmental Impacts*, **6**(3), 143–153. https://doi.org/10.18280/ijei.060307

Portz, L., Manzolli, R. P., Villate-Daza, D. A. and Fontán-Bouzas, Á. 2022. Where does marine litter hide? The Provedencia and Santa Catalina Island problem, SEAFLOWER Reserve (Colombia). *Science of The Total Environment*, **813**, 151878. https://doi.org/10.1016/j.scitotenv.2021.151878

Press, M. 2020. *Merelise prügi seire Eesti rannikualadel 2019-2020*. Project report. Hoia Eesti Merd MTÜ. https://hem.ee/wp-content/uploads/2021/05/Projekti-6865_aruanne-2019-2020.pdf (accessed 2024-02-15).

Press, M. 2023. *Merelise prügi seire Eesti rannikualadel 2021-2022*. Project report. Hoia Eesti Merd MTÜ. https://hem.ee/wp-content/uploads/2023/05/Projekti-6865_aruanne_2021-2022_fin_w.pdf (accessed 2024-02-15).

Primpke, S., Christiansen, S. H., Cowger, W., De Frond, H., Deshpande, A., Fischer, M. et al. 2020. Critical assessment of analytical methods for the harmonized and cost-efficient analysis of microplastics. *Applied Spectroscopy*, **74**(9), 1012–1047. https://doi.org/10.1177/0003702820921465

R Core Team. 2021. *R: A language and Environment for Statistical Computing*. R Foundation for Statistical Computing, Vienna. https://www.R-project.org (accessed 2023-01-12).

Roberts, K. P., Phang, S. C., Williams, J. B., Hutchinson, D. J., Kolstoe, S. E., de Bie, J. et al. 2022. Increased personal protective equipment litter as a result of COVID-19 measures. *Nature Sustainability*, **5**, 272–279. https://doi.org/10.1038/s41893-021-00824-1

Rodríguez-Rodríguez, D. 2012. Littering in protected areas: a conservation and management challenge – a case study from the Autonomous Region of Madrid, Spain. *Journal of Sustainable Tourism*, **20**(7), 1011–1024. https://doi.org/10.1080/09669582.2011.651221

RStudio Team. 2021. *RStudio: Integrated Development Environment for R*. RStudio, PBC, Boston. http://www.rstudio.com (accessed 2023-01-12).

Schernewski, G., Balciunas, A., Gräwe, D., Gräwe, U., Klesse, K., Schulz, M. et al. 2018. Beach macro-litter monitoring on southern Baltic beaches: results, experiences and recommendations. *Journal of Coastal Conservation*, **22**, 5–25. https://doi.org/10.1007/s11852-016-0489-x

Schernewski, G., Escobar Sánchez, G., Felsing, S., Gatel Rebours, M., Haseler, M., Hauk, R. et al. 2024. Emission, transport and retention of floating marine macro-litter (plastics): the role of Baltic harbor and sailing festivals. *Sustainability*, **16**(3), 1220. https://doi.org/10.3390/su16031220

Schröder, K., Kossel, E. and Lenz, M. 2021. Microplastic abundance in beach sediments of the Kiel Fjord, Western Baltic Sea. *En-*

vironmental Science and Pollution Research, **28**, 26515–26528. https://doi.org/10.1007/s11356-020-12220-x

Shapiro, S. S. and Wilk, M. B. 1965. An analysis of variance test for normality (complete samples). *Biometrika*, **52**(3–4), 591–611. https://doi.org/10.1093/biomet/52.3-4.591

Šilc, U., Küzmič, F., Caković, D. and Stešević, D. 2018. Beach litter along various sand dune habitats in the southern Adriatic (E Mediterranean). *Marine Pollution Bulletin*, **128**, 353–360. https://doi.org/10.1016/j.marpolbul.2018.01.045

Smith, L. and Turrell, W. R. 2021. Monitoring plastic beach litter by number or by weight: the implications of fragmentation. *Frontiers in Marine Science*, **8**, 702570. https://doi.org/10.3389/fmars.2021.702570

Strand, J., Tairova, Z., Danielsen, J., Hansen, J. W., Magnusson, K., Naustvoll, L.-J. et al. 2015. *Marine Litter in Nordic Waters*. Nordic Council of Ministers, Copenhagen. https://doi.org/10.6027/TN2015-521

Tähiste, A. and Mõniste, M. 2016. *Merepiirivalve tehnilise vaatluse post Harilaiul Vormsi vallas Läänemaal (Technical Observation Post of Maritime Border Guard in Harilaiu, Vormsi County, Läänemaa)*. Projekti „Eesti 20. sajandi (1870–1991) sõjalise ehituspärandi kaardistamine ja analüüs" aruanne (Report of the project "Mapping and analysis of military construction heritage from 1970 to 1991 in Estonia"). https://www.mil.hiiumaa.ee/xx/Laanemaa-Vormsi-Harilaid.pdf

Tõnisson, H., Orviku, K., Lapinskis, J., Gulbinskas, S. and Žaromskis, R. 2013. The Baltic States: Estonia, Latvia and Lithuania. In *Coastal Erosion and Protection in Europe* (Pranzini, E. and Williams, A., eds). Routledge, Oxon, 47–80.

Turrell, W. R. 2018. A simple model of wind-blown tidal strandlines: how marine litter is deposited on a mid-latitude, macro-tidal shelf sea beach. *Marine Pollution Bulletin*, **137**, 315–330. https://doi.org/10.1016/j.marpolbul.2018.10.024

Uiboupin, R. and Pärn, O. 2018. *Mereala planeeringu alusuuring: jääolude analüüs ja kaartide koostamine (Marine Spatial Planning: Analysis of Ice Conditions and Production of Maps)*. TTÜ Meresüsteemide Instituut, Tallinn.

United Nations Environment Programme and Intergovernmental Oceanographic Commission 2009. *UNEP/IOC Guidelines on Survey and Monitoring of Marine Litter*. Regional Seas Reports and Studies No. 186, IOC Technical Series No. 83. https://wedocs.unep.org/20. 500.11822/13604

Urban-Malinga, B., Zalewski, M., Jakubowska, A., Wodzinowski, T., Malinga, M., Palys, B. et al. 2020. Microplastics on sandy beaches of the southern Baltic Sea. *Marine Pollution Bulletin*, **155**, 111170. https://doi.org/10.1016/j.marpolbul.2020.111170

Vlachogianni, T., Skocir, M., Constantin, P., Labbe, C., Orthodoxou, D., Pesmatzoglou, I. et al. 2020. Plastic pollution on the Mediterranean coastline: generating fit-for-purpose data to support decision-making via a participatory-science initiative. *Science of The Total Environment*, **711**, 135058. https://doi.org/10.1016/j.scitotenv.2019.135058

Votier, S. C., Archibald, K., Morgan, G. and Morgan, L. 2011. The use of plastic debris as nesting material by a colonial seabird and associated entanglement mortality. *Marine Pollution Bulletin*, **62**(1), 168–172. https://doi.org/10.1016/j.marpolbul.2010.11.009

Wickham, H., Averick, M., Bryan, J., Chang, W., D'Agostino McGowan, L., François, R. et al. 2019. Welcome to the tidyverse. *Journal of Open Source Software*, **4**(43), 1686. https://doi.org/10.21105/joss.01686

Wilcoxon, F. 1945. Individual comparisons by ranking methods. *Biometrics Bulletin*, **1**(6), 80–83. https://doi.org/10.2307/3001968

Wyles, K. J., Pahl, S., Thomas, K. and Thompson, R. C. 2016. Factors that can undermine the psychological benefits of coastal environments: exploring the effect of tidal state, presence, and type of litter. *Environment and Behavior*, **48**(9), 1095–1126. https://doi.org/10.1177/0013916515592177

Zalewska, T. and Krzymiński, W. 2017. *Task 2.1.1 Development of Baselines of Marine Litter - Report on the Analysis of Compiled Beach Litter Data and Proposals for Setting Preliminary Beach Litter Baselines in the Baltic Sea*. HELCOM, Helsinki. https://helcom.fi/wp-content/uploads/2020/04/Theme-2_Deliverable-2.1.1.a.pdf

Mereprügi levik Eesti rannikumere asustamata väikesaartel

Tiia Möller-Raid, Maria Põldma, Kristjan Herkül, Kaire Torn, Georg Martin, Kaire Kaljurand, Martin Teeveer, Greta Reisalu, Trude Taevere, Hanna-Eliisa Luts, Karolin Teeveer, Keili Saava, Annely Enke ja Lauri London

Mereprügi hulka kuuluvad kõik mittelooduslikku päritolu esemed, mida leidub mere- ja rannikukeskkonnas, ning prügi levik ja kogused peegeldavad otsest inimmõju merekeskkonnale. Artikkel annab ülevaate mereprügi uuringutest, mis teostati aastatel 2019–2020 neljateistkümnel Eesti rannikumere asustamata väikesaarel. Makroprügi (prügiesemed suurusega > 2,5 cm) esinemist hinnati nii rannal kui ka rannaga piirneval taimestikuga alal. Mereprügi arvukuse mediaanväärtus oli rannaalal 10,65 ühikut ja taimestikuga alal 21,65 ühikut 100 m pikkuse lõigu kohta. Keskmisest enam mereprügi esines Soome lahe saartel (mediaanväärtus rannaalal 38,05 ühikut ja taimestikuga alal 45,83 ühikut 100 m kohta). Peamine mereprügi materjal oli plast, mis moodustas 57,3% kõikidest leidudest. Kõigi uuritud saarte rannaala setetest leiti ka mikroprügi (prügiesemed suurusega < 0,5 cm), hinnangulised kogused olid kuni 60 eset ühe kg kuivsette kohta. Samuti täheldati lindude pesitsusaladel mereprügi kasutust pesamaterjalina. Uurimistulemused viitavad vajadusele käsitleda mereprügiga seotud probleeme ja uuringuid senisest terviklikumalt.

Estonian Journal of Earth Sciences
2026, **75**, 1, 19–34

https://doi.org/10.3176/earth.2026.02

www.eap.ee/earthsciences
Estonian Academy Publishers

RESEARCH ARTICLE

Received 28 May 2025
Accepted 9 September 2025
Available online 18 December 2025

Keywords:
Silurian, Estonia, regional stratigraphy, Baltica, biostratigraphy, lithostratigraphy, correlation chart

Corresponding author:
Peep Männik
peep.mannik@taltech.ee

Citation:
Männik, P., Meidla, T. and Hints, O. 2026. An updated correlation of the Silurian strata in Estonia. *Estonian Journal of Earth Sciences*, **75**(1), 19–34. https://doi.org/10.3176/earth.2026.02

An updated correlation of the Silurian strata in Estonia

Peep Männik[a], Tõnu Meidla[b] and Olle Hints[a]

[a] Department of Geology, Tallinn University of Technology, Ehitajate tee 5, 19086 Tallinn, Estonia

[b] Department of Geology, University of Tartu, Ravila 14A, 50114 Tartu, Estonia

ABSTRACT

The correlation of the Silurian succession of Estonia with the global standard has long been considered reliable. However, new information, particularly on the distribution of microfossils, has changed our understanding of the Silurian stratigraphy in the region. Recent palaeontological and geochemical data suggest that: the lower part of the Juuru Regional Stage (RS) is of Hirnantian age; the age of the base of the Raikküla RS in terms of global chronostratigraphy remains problematic; the Aeronian–Telychian boundary correlates with a level in the middle of the Rumba Formation (Fm); the base of the Adavere RS is of latest Aeronian age; the former Riksu Fm is considered to be the proximal, older part of the Sõrve Fm; the traditional lower boundary of the Jaagarahu RS is diachronous, and the closest biostratigraphic horizon that could be used is the first appearance datum of *Jeppssonia sagitta rhenana*; the Wenlock–Ludlow boundary correlates with a level in the upper Rootsiküla RS; the base of the Paadla RS corresponds to a level in the upper Gorstian, in the lower(?) *Phlebolepis ornata* Vertebrate Biozone; the Sauvere and Himmiste beds of the Paadla Fm are of late Gorstian age, and the Uduvere Beds are of early Ludfordian age, corresponding to part of the *Ancoradella ploeckensis* Conodont Biozone; identifying the Ludlow–Přídolí boundary in the Estonian succession is problematic, lacking reliable criteria at present. With these amendments, we present an updated regional correlation scheme drawn on a regular time scale for the first time. A problem that needs to be addressed in the future is providing better biostratigraphic definitions for the bases of regional stages.

Introduction

The study of Silurian rocks in Estonia commenced in the early 19th century (Engelhardt and Ulprecht 1830). The first stratigraphic classification of these strata was proposed by Schmidt (1858, 1881, 1892). Several of Schmidt's units (originally called *Schicht*) are close equivalents of today's regional stages, and his notation system (G, H, J, etc.) is still in use. Bekker (1922, 1925) and Luha (1930, 1933, 1946) established the formal nomenclature of the Silurian regional stages, adopting contemporary geographical names for the units.

Before the 1940s, geological studies in Estonia were based mainly on natural outcrops and small quarries. A new era of research began in the late 1940s, when extensive geological mapping, drilling, and research projects were started by the state geological survey and research institutions. The studies, based on rich core material, substantially improved knowledge of Silurian geology and stratigraphy in the region. A particularly active period of Silurian studies started in the late 1950s and 1960s. During the following decades, various aspects of the Silurian succession of Estonia were investigated, and the results were published in several monographs (e.g. Jürgenson 1966; Kaljo 1970, 1977a; Kaljo and Klaamann 1986). The most recent thorough review of Silurian geology, stratigraphy, and fossils was published in chapters of the book *Geology and Mineral Resources of Estonia* (e.g. Nestor 1997; Nestor and Einasto 1997).

During the long history of Silurian research, the regional stratigraphic scheme has been revised and updated several times. Most of the formations, members, and beds that are in use today were defined and described in the monograph *The Silurian of Estonia* (Kaljo 1970). Further amendments to the stratigraphic nomenclature and correlations with successions in adjacent areas were published in the unified regional stratigraphic schemes (Resolution… 1978; Decisions… 1987) and several other papers (e.g. Aaloe et al. 1976; Nestor and Nestor 1991, 2002; Perens 1992, 1995;

Jeppsson et al. 1994; Nestor 1995, 1997; Nestor et al. 2003; Viira and Einasto 2003; Kaljo et al. 2015).

The correlation between the Silurian regional stages and formations in Estonia and the global chronostratigraphic standard has been considered reliable and has changed little since the definition of most of these units. However, studies in recent decades have revealed several correlation problems, and the need to restudy and revise some parts of the scheme has become evident. An early version of the updated correlation scheme was published in field guidebooks (Männik 2014; Männik et al. 2024). The aim of this study is to present a revised regional correlation scheme together with comments and discussions on recent developments in the Silurian stratigraphy of Estonia. The updated scheme proposed in this paper is drawn, for the first time, on the time scale of Melchin et al. (2020). However, the calibration of the time scale is expected to change in the future, as there are only a few (eight) U–Pb dates for the Silurian, and the construction of the time scale is considered problematic by some authors (Štorch et al. 2024).

Geological background

During the Ordovician and Silurian, from the late Tremadocian to the end of the Přídolí, the territory of present-day Estonia was part of the northern flank of a shallow cratonic sea in the western part of the Baltica continent (Fig. 1). In the earlier stages of development, this sea extended from Norway to the Volga region and from Finland to the Belarussian–Mazurian Precambrian massif. During the final stages of development, the basin was restricted to the Baltic Syneclise in the East Baltic area and northern Poland (Nestor and Einasto 1997). In the Silurian, Baltica was located in equatorial latitudes and drifted gradually northwards (Melchin et al. 2004). From the Late Ordovician Katian Epoch until the end of the Silurian, the Baltic Palaeobasin was characterised by a wide range of tropical shelf environments with accumulation of carbonate deposits and the occurrence of diverse biota (Nestor and Einasto 1997; Dronov and Rozhnov 2007).

Silurian strata are exposed in western, central, and eastern Estonia; in southern Estonia, they are overlain unconformably by the uppermost Lower Devonian terrigenous rocks. As a result of the gradual infilling of the sedimentary basin from north to south and from east to west during the early Palaeozoic, the oldest Silurian rocks are found in the eastern and northern parts of the outcrop area (Fig. 1). Toward the south and southwest, progressively younger strata are exposed. The Silurian succession can be studied in several small historic quarries and several larger modern ones across central Estonia. The main natural outcrops are located along the northern and western coasts of Saaremaa Island.

Based on the distinctly expressed lateral facies changes shown by the Silurian rocks, two major facies belts have been distinguished: the Central Estonian and South Estonian facies belts (Kaljo 1977b). The Central Estonian Facies Belt is dominated by various limestones and late-diagenetic dolostones, which were originally rich in shelly faunas. These

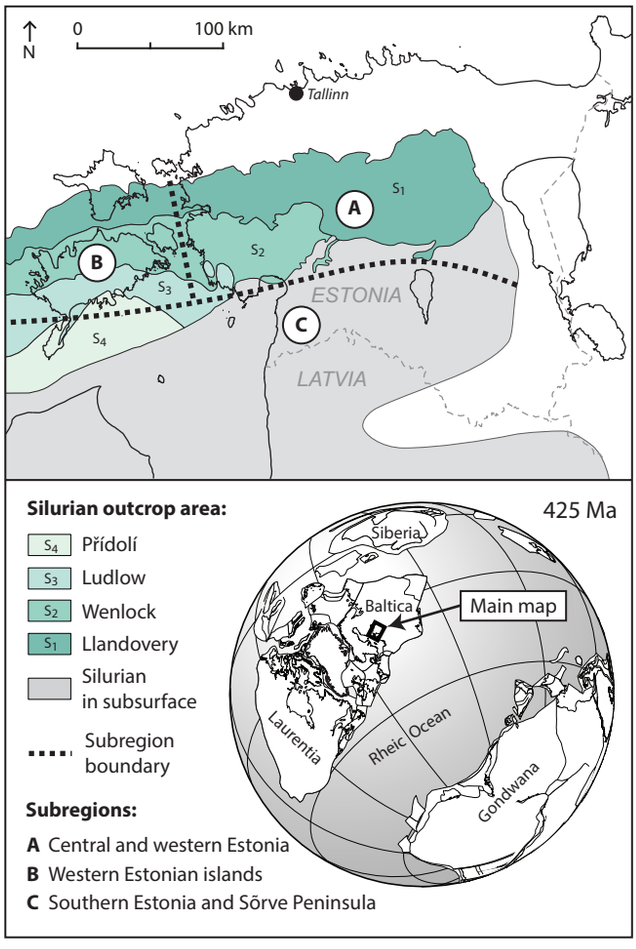

Fig. 1. Map of the distribution area of Silurian rocks in Estonia, and subregions of lithostratigraphic classification shown in Fig. 2A. Note that the boundaries between outcrop areas of series are approximate. The 425 Ma palaeogeographical reconstruction was created with BugPlates software using data from Torsvik and Cocks (2013).

rocks are widespread across the islands of the West Estonian Archipelago, as well as in the western and central parts of mainland Estonia. In general, these strata are well exposed. However, on the mainland, the Silurian succession is less complete, and its upper part has undergone extensive dolomitisation. In contrast, the South Estonian Facies Belt is characterised primarily by argillaceous carbonate rocks (marls) and siliciclastic mudstones containing deeper-water shelly faunas and, at certain levels, occasional graptolites. These rocks are unconformably overlain by the uppermost Lower Devonian siliciclastics and can be studied in drill-core sections only.

Silurian stratigraphic scheme of Estonia

Introductory remarks

The Silurian succession in Estonia is subdivided into ten regional stages (RS) (Kaljo 1970; Nestor 1997; Fig. 2). However, due to the sporadic distribution of macrofauna and limited information on microfossils, these stages were defined by a combination of palaeontological and sedimentological data, and their boundaries were based mainly on lithological criteria (see Kaljo 1970 and references therein). No boundary

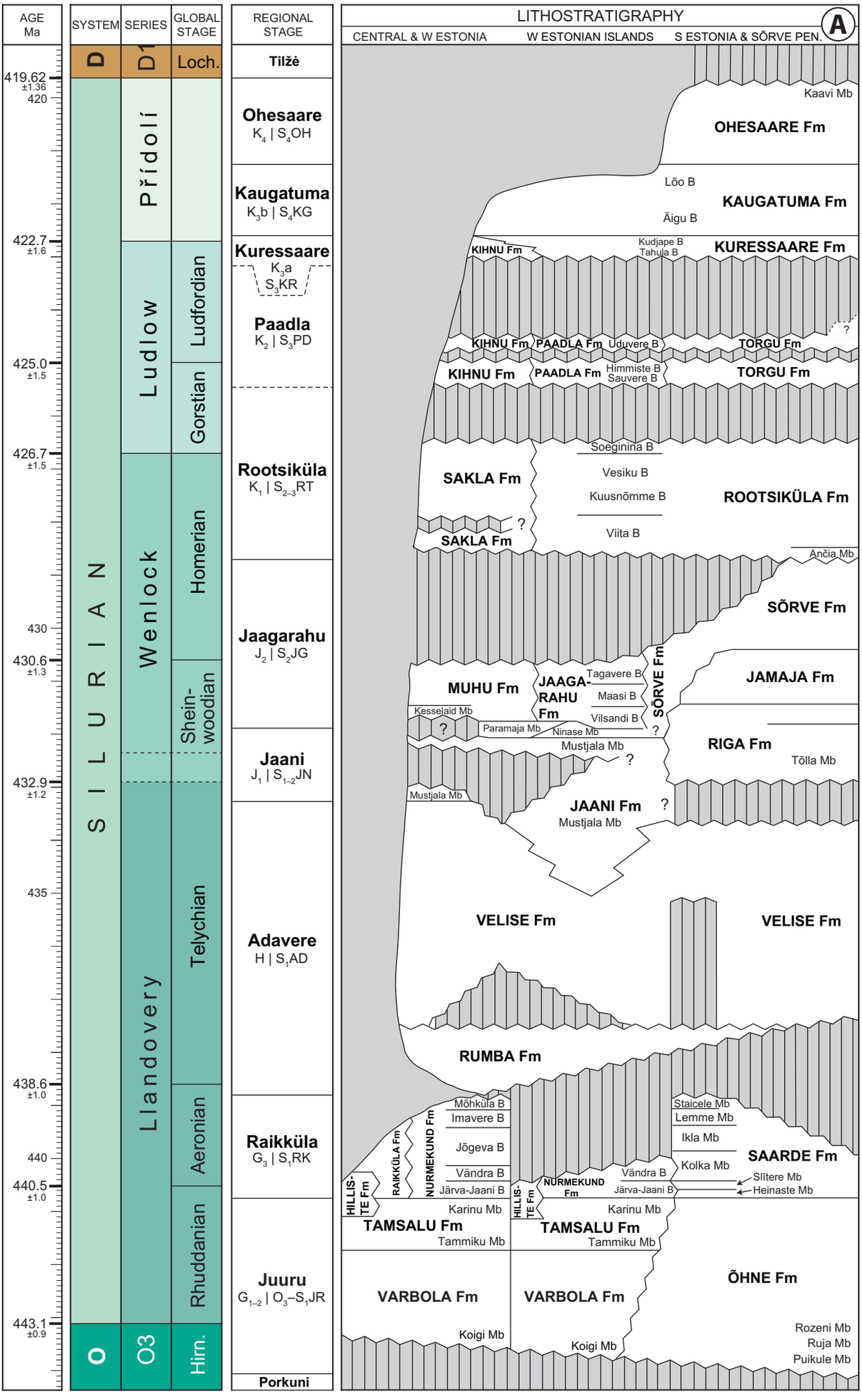
AGE Ma
SYSTEM
SERIES
GLOBAL STAGE
REGIONAL STAGE
LITHOSTRATIGRAPHY
CENTRAL & W ESTONIA
W ESTONIAN ISLANDS
S ESTONIA & SÕRVE PEN.
A
419.62 ±1.36
420
422.7 ±1.6
425.0 ±1.5
426.7 ±1.5
430
430.6 ±1.3
432.9 ±1.2
435
438.6 ±1.0
440
440.5 ±1.0
443.1 ±0.9
D
S I L U R I A N
O
D1
Přídolí
Ludlow
Wenlock
Llandovery
O3
Loch.
Ludfordian
Gorstian
Homerian
Shein-woodian
Telychian
Aeronian
Rhuddanian
Hirn.
Tilžė
Ohesaare
K4 | S4OH
Kaugatuma
K3b | S4KG
Kuressaare
K3a
S3KR
Paadla
K2 | S3PD
Rootsiküla
K1 | S2–3RT
Jaagarahu
J2 | S2JG
Jaani
J1 | S1–2JN
Adavere
H | S1AD
Raikküla
G3 | S1RK
Juuru
G1–2 | O3–S1JR
Porkuni
Kaavi Mb
OHESAARE Fm
Lõo B
KAUGATUMA Fm
Äigu B
KIHNU Fm
Kudjape B
Tahula B
KURESSAARE Fm
PAADLA Fm
Uduvere B
TORGU Fm
Himmiste B
Sauvere B
Soeginina B
SAKLA Fm
Vesiku B
Kuusnõmme B
ROOTSIKÜLA Fm
Viita B
Ančia Mb
SÕRVE Fm
MUHU Fm
JAAGA-RAHU Fm
Tagavere B
Maasi B
Vilsandi B
JAMAJA Fm
Kesselaid Mb
Paramaja Mb
Ninase Mb
Mustjala Mb
RIGA Fm
Tõlla Mb
JAANI Fm
VELISE Fm
RUMBA Fm
Möhküla B
Imavere B
Jõgeva B
Vändra B
Järva-Jaani B
Karinu Mb
Staicele Mb
Lemme Mb
Ikla Mb
Kolka Mb
SAARDE Fm
Slītere Mb
Heinaste Mb
RAIKKÜLA Fm
NURMEKUND Fm
HILLIS-TE Fm
TAMSALU Fm
Tammiku Mb
VARBOLA Fm
Koigi Mb
ÕHNE Fm
Rozeni Mb
Ruja Mb
Puikule Mb

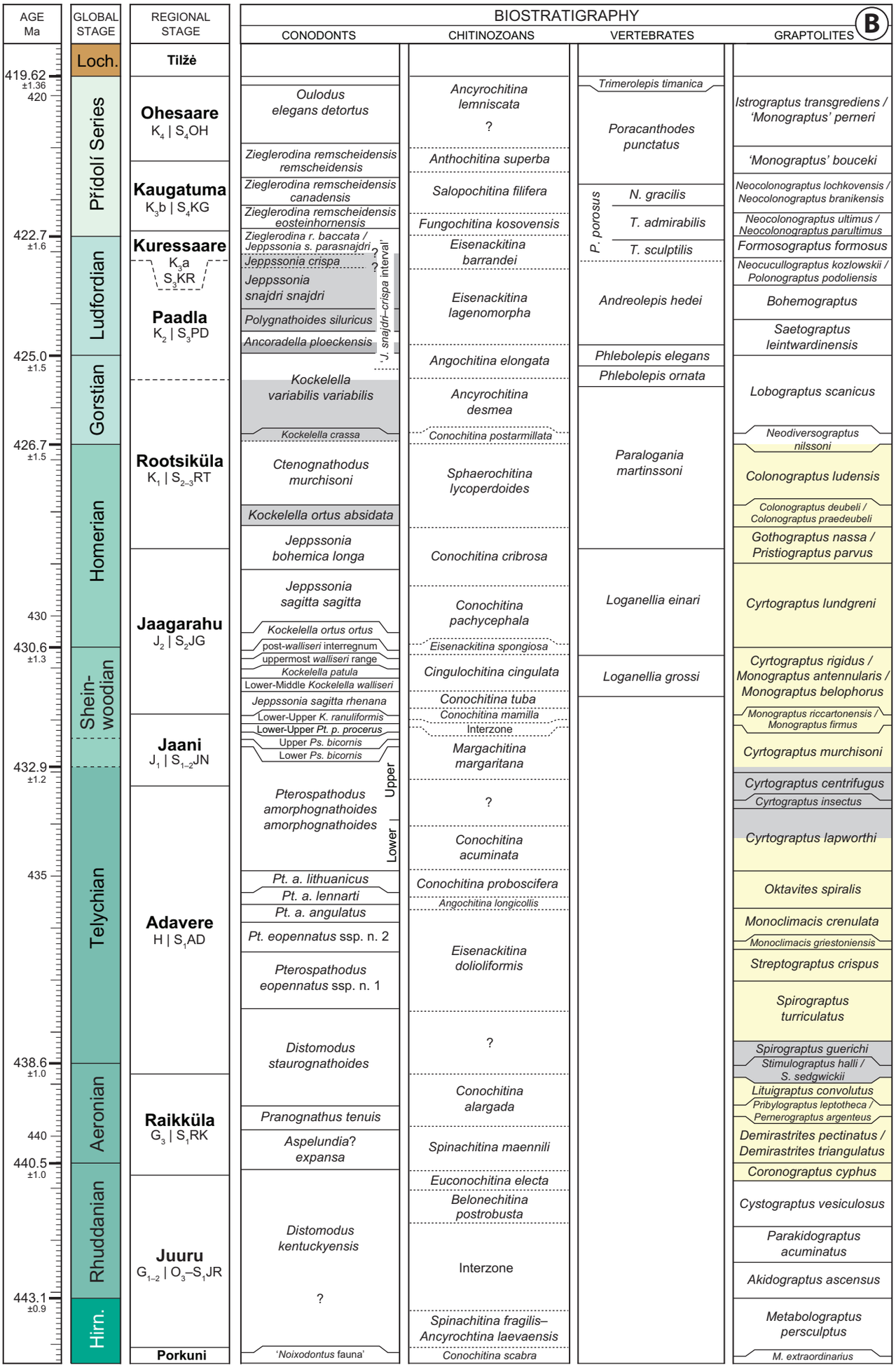
AGE Ma
GLOBAL STAGE
REGIONAL STAGE
BIOSTRATIGRAPHY
CONODONTS
CHITINOZOANS
VERTEBRATES
GRAPTOLITES
B
Loch.
Přídolí Series
Ludfordian
Gorstian
Homerian
Shein-woodian
Telychian
Aeronian
Rhuddanian
Hirn.
419.62 ±1.36
420
422.7 ±1.6
425.0 ±1.5
426.7 ±1.5
430
430.6 ±1.3
432.9 ±1.2
435
438.6 ±1.0
440
440.5 ±1.0
443.1 ±0.9
Tilžė
Ohesaare K4 | S4OH
Kaugatuma K3b | S4KG
Kuressaare K3a S3KR
Paadla K2 | S3PD
Rootsiküla K1 | S2–3RT
Jaagarahu J2 | S2JG
Jaani J1 | S1–2JN
Adavere H | S1AD
Raikküla G3 | S1RK
Juuru G1–2 | O3–S1JR
Porkuni
Oulodus elegans detortus
Zieglerodina remscheidensis remscheidensis
Zieglerodina remscheidensis canadensis
Zieglerodina remscheidensis eosteinhornensis
Zieglerodina r. baccata / Jeppssonia s. parasnajdri
Jeppssonia crispa
Jeppssonia snajdri snajdri
Polygnathoides siluricus
Ancoradella ploeckensis
J. snajdri–crispa interval
Kockelella variabilis variabilis
Kockelella crassa
Ctenognathodus murchisoni
Kockelella ortus absidata
Jeppssonia bohemica longa
Jeppssonia sagitta sagitta
Kockelella ortus ortus
post-walliseri interregnum
uppermost walliseri range
Kockelella patula
Lower-Middle Kockelella walliseri
Jeppssonia sagitta rhenana
Lower-Upper K. ranuliformis
Lower-Upper Pt. p. procerus
Upper Ps. bicornis
Lower Ps. bicornis
Pterospathodus amorphognathoides amorphognathoides
Upper
Lower
Pt. a. lithuanicus
Pt. a. lennarti
Pt. a. angulatus
Pt. eopennatus ssp. n. 2
Pterospathodus eopennatus ssp. n. 1
Distomodus staurognathoides
Pranognathus tenuis
Aspelundia? expansa
Distomodus kentuckyensis
?
'Noixodontus fauna'
Ancyrochitina lemniscata
?
Anthochitina superba
Salopochitina filifera
Fungochitina kosovensis
Eisenackitina barrandei
Eisenackitina lagenomorpha
Angochitina elongata
Ancyrochitina desmea
Conochitina postarmillata
Sphaerochitina lycoperdoides
Conochitina cribrosa
Conochitina pachycephala
Eisenackitina spongiosa
Cingulochitina cingulata
Conochitina tuba
Conochitina mamilla
Interzone
Margachitina margaritana
?
Conochitina acuminata
Conochitina proboscifera
Angochitina longicollis
Eisenackitina dolioliformis
?
Conochitina alargada
Spinachitina maennili
Euconochitina electa
Belonechitina postrobusta
Interzone
Spinachitina fragilis–Ancyrochtina laevaensis
Conochitina scabra
Trimerolepis timanica
Poracanthodes punctatus
P. porosus
N. gracilis
T. admirabilis
T. sculptilis
Andreolepis hedei
Phlebolepis elegans
Phlebolepis ornata
Paralogania martinssoni
Loganellia einari
Loganellia grossi
Istrograptus transgrediens / 'Monograptus' perneri
'Monograptus' bouceki
Neocolonograptus lochkovensis / Neocolonograptus branikensis
Neocolonograptus ultimus / Neocolonograptus parultimus
Formosograptus formosus
Neocucullograptus kozlowskii / Polonograptus podoliensis
Bohemograptus
Saetograptus leintwardinensis
Lobograptus scanicus
Neodiversograptus nilssoni
Colonograptus ludensis
Colonograptus deubeli / Colonograptus praedeubeli
Gothograptus nassa / Pristiograptus parvus
Cyrtograptus lundgreni
Cyrtograptus rigidus / Monograptus antennularis / Monograptus belophorus
Monograptus riccartonensis / Monograptus firmus
Cyrtograptus murchisoni
Cyrtograptus centrifugus
Cyrtograptus insectus
Cyrtograptus lapworthi
Oktavites spiralis
Monoclimacis crenulata
Monoclimacis griestoniensis
Streptograptus crispus
Spirograptus turriculatus
Spirograptus guerichi
Stimulograptus halli / S. sedgwickii
Lituigraptus convolutus
Pribylograptus leptotheca / Pernerograptus argenteus
Demirastrites pectinatus / Demirastrites triangulatus
Coronograptus cyphus
Cystograptus vesiculosus
Parakidograptus acuminatus
Akidograptus ascensus
Metabolograptus persculptus
M. extraordinarius

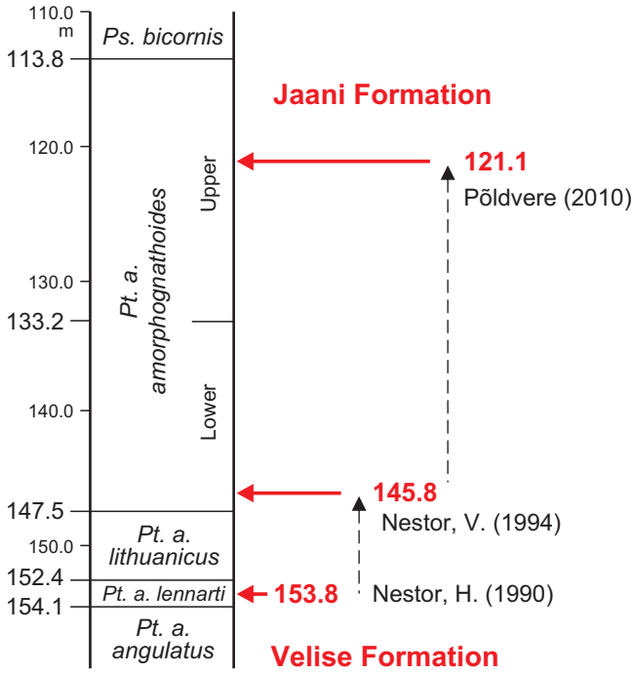

Fig. 3. Changes in interpretations of the base of the Jaani Formation in the Viki core section, after H. Nestor (1990), V. Nestor (1994), and Põldvere (2010). Abbreviations: *Ps.* – *Pseudooneotodus*, *Pt. a.* – *Pterospathodus amorphognathoides*.

stratotypes were established at the time, and although some were proposed later (e.g. Nestor 1993 and references therein), they have not gained broad acceptance or adoption. As a result, the boundaries of the RSs remain poorly constrained from a biostratigraphic perspective.

Based on lithology, the stages were subdivided into formations (Fm) within different facies belts. Before the 1990s, the rules of the Stratigraphic Code of the former Soviet Union (Stratigraphic… 1977) were followed in the region. According to that code, a formation was considered a to-postratigraphic unit, defined mainly by its specific lithological composition, while its boundaries were adjusted based on biostratigraphic data and considered to be isochronous – a feature that is evident in the earlier stratigraphic schemes from the 'box-like' appearance of the formations. Formations were also considered as subdivisions of regional stages and thus mandatorily limited to a single regional stage. The stratigraphic scheme of Nestor (1997) followed this same principle.

These rules have caused some confusion and resulted in repeated revisions of several formational boundaries from publication to publication, based on newly obtained biostratigraphic data. A good example of this is the changing position of the lower boundary of the Jaani Fm in the Viki drill core (Fig. 3). This boundary marks the base of the Jaani RS and was believed to correlate with the Llandovery–Wenlock boundary. During the initial studies, the boundary was tentatively drawn at 153.8 m based on lithological criteria (Nestor, H. 1990). Later, it was shifted upwards, considering the level of appearance of *Margachitina margaritana* (Nestor, V. 1994), and further up to the depth of 121.1 m by Põldvere (2010), where it is marked by a K-bentonite which, based on bio- and chemostratigraphic information (Männik 2007b), correlates with the bentonite at 345.8 m in the Ohesaare core section, the proposed type section of the base of the Jaani Fm and Jaani RS (Nestor, H. 1993). In comparison with the conodont succession, the proposed base of the Jaani Fm in the Viki core section has been moved from the middle *Pt. a. lennarti* Conodont Biozone (CZ; boundary in Nestor, H. 1990) into the upper part of the *Pt. a. amorphognathoides* CZ (Põldvere 2010).

Based on specific lithological characteristics, several (but not all) formations have been further subdivided into members (Mb). Additionally, as many intervals of the Silurian succession reveal apparent cyclicity, particularly within the shallow-water Central Estonian Facies Belt, cyclostratigraphic units consisting of alternating types of rocks (reflecting sea-level changes and often bounded by gaps) were distinguished. These cyclicity-based units were called 'beds' (*kihid* in Estonian, *слои* in Russian) and treated as subdivisions of formations, but sometimes also as substages.

The general lithological and palaeontological characteristics of the units presented in the Silurian stratigraphic scheme of Estonia are summarised in Nestor (1997) and references therein.

The present-day high-resolution biostratigraphy in the region, being the main tool for regional and interregional correlations, is based mainly on conodonts (Viira 1999; Männik 2007a, 2007b, 2007c) and chitinozoans (Nestor 2012 and references therein). However, the use of chitinozoan

Fig. 2. Updated Silurian stratigraphic scheme of Estonia. **A** – chronostratigraphy and lithostratigraphy; **B** – biostratigraphy. The global Silurian time scale is from Melchin et al. (2020). For the Llandovery–Wenlock boundary, two levels marking the limits of an uncertainty interval are indicated: the lower line (432.9 Ma) roughly corresponds to the base of the *Cyrtograptus murchisoni* graptolite biozone, and the upper line marks the approximate level of the base of Wenlock as defined in its stratotype at Hughley Brook, England (further comments are provided in the text). Graptolite biozonation is modified from Cramer et al. (2011). The Llandovery–Wenlock part of the conodont biozonation is based on Jeppsson (1997), Jeppsson and Calner (2003), and Männik (2007a, 2007b). The biozonation in the Ludlow interval (excluding the upper Ludfordian) is modified from Cramer et al. (2011), and the uppermost Ludfordian–Přídolí biozonation is from Viira (1999). The '*J. snajdri–crispa* interval' marks the total range interval of the closely related and difficult-to-distinguish *J. s. snajdri*, *J. crispa*, and *J. s. parasnajdri*. Due to common identification problems, all representatives of these taxa are identified as *J. snajdri* s.l. in Märss and Männik (2013). The chitinozoan biozonation is modified from Nestor (2012), and that of vertebrates and its correlation with the conodont biozonation is from Märss and Männik (2013). In the columns of regional stages, below the names of regional stages are their traditional Schmidt's notations (G, H, J, etc.), and those used in geological maps by the Geological Survey of Estonia are also indicated. Abbreviations: D – Devonian, D1 – Lower Devonian, O – Ordovician, O3 – Upper Ordovician, Hirn. – Hirnantian, Loch. – Lochkovian, Pen. – peninsula, Mb – Member, Fm – Formation, B – Beds; conodonts: *K.* – *Kockelella*, *Zieglerodina r.* – *Zieglerodina remscheidensis*, *Jeppssonia s.* – *Jeppssonia snajdri*, *Pt. a.* – *Pterospathodus amorphognathoides*, *Pt. p.* – *Pterospathodus pennatus*, *Ps.* – *Pseudooneotodus*; vertebrates: *N.* – *Nostolepis*, *P.* – *Poracanthodes*, *T.* – *Thelodus*; graptolites: *M.* – *Metabolograptus*, *S.* – *Stimulograptus*. Colours: yellow background denotes reliably correlated graptolite biozones; grey denotes missing biozones in Estonia, interpreted as gaps.

biozonation in shallow-water carbonates (limestones and dolostones) is often limited due to the sporadic occurrence of these organic-walled microfossils and some inconsistencies in their ranges. In the upper part of the succession, starting in the Wenlock, vertebrates also provide useful stratigraphic information (Märss 1986; Märss and Männik 2013).

Due to the rare occurrence of graptolites in the Silurian strata in Estonia, the correlation of several RSs with the standard graptolite succession has been – and still is – challenging. However, in the last decades, integrated biostratigraphic studies on graptolites, conodonts, and chitinozoans from core sections of southwestern Estonia and western Latvia have improved the situation considerably (Loydell et al. 1998, 2003, 2010; Loydell and Nestor 2005). The reported co-occurrences of graptolites and conodonts from Gotland, Sweden (Jeppsson and Calner 2003) have further helped to improve the correlations. As a result, most of the mid–upper Llandovery and Wenlock graptolite biozones can be reliably correlated into shallow-water settings in Estonia that do not yield graptolites. Dating of other intervals (particularly in the Rhuddanian and Přídolí; Fig. 2) has remained less precise, but combined biostratigraphic and chemostratigraphic ($\delta^{13}C$, K-bentonites) data have allowed reasonable, albeit indirect, dating of some intervals (Kiipli et al. 2012; Märss and Männik 2013; Männik 2014; Kaljo et al. 2015; Fig. 2). Few attempts have been made to apply quantitative stratigraphic methods to make use of large datasets and increase the resolution of the regional temporal framework (e.g. Sadler 2012; Hints et al. 2018 and references therein).

Changes in some conodont biozone names compared to previous ones (Fig. 2 versus e.g. Männik et al. 2024) result from the revision of the genus *Ozarkodina* and the transfer of several former taxa of this genus to the new genera *Zieglerodina* and *Jeppssonia*, introduced by Murphy et al. (2004) and Barrick et al. (2024), respectively.

Comments on selected stratigraphic units and levels

Ordovician–Silurian boundary and base of Juuru Regional Stage

The lower boundary of the Silurian System was ratified by the Silurian Subcommission of the International Union of Geological Sciences (IUGS) in 1984 (Holland 1985). It is defined by the first appearance datum (FAD) of *Akidograptus ascensus* Davies in the boundary stratotype, the Dob's Linn section in Scotland (Rong et al. 2008). Although graptolites are missing from the Ordovician–Silurian boundary interval in Estonia, the Porkuni RS has long been considered to correspond to the Hirnantian *Metabolograptus extraordinarius* and *M. persculptus* graptolite biozones (GZ). Similarly, the lower part of the Juuru RS has been correlated with the lower Rhuddanian *A. ascensus–Parakidograptus acuminatus* GZ (Kaljo et al. 2001, 2008; Brenchley et al. 2003).

The boundary between the Porkuni and Juuru RSs is marked by a sharp change in lithology resulting from a gap in Estonian sections (Meidla et al. 2014a and references therein). Correlation of the boundary interval in Estonia with the formally defined Ordovician–Silurian boundary has been based on the occurrence of Hirnantian trilobites, brachiopods, and ostracods in the Kuldiga and Saldus Fms that are considered equivalent to the Porkuni RS, as well as finds of *Stricklandia lens prima* Williams in the Varbola Fm, which was traditionally attributed to the Juuru RS (Kaljo et al. 1988; Nestor 1997). In practice, the strata immediately below and above the Porkuni–Juuru boundary often do not yield any fossils for reliable dating, and both the regional stage boundary and the system boundary are drawn at the level of a supposed major sedimentary gap in the succession (Ainsaar et al. 2015; Meidla et al. 2020 and references therein). Recent $\delta^{13}C$ studies indicate that the basal part of the Varbola Fm, the Koigi Mb, and sometimes also the lower part of the Varbola Fm above the Koigi Mb fall into an interval of declining $\delta^{13}C$ values, which most likely represents the latest part of the Hirnantian Isotope Carbon Excursion (e.g. Ainsaar et al. 2015; Gul et al. 2021). This suggests that the Varbola Fm is partly of late Hirnantian age (Meidla et al. 2020, 2023a, 2023b) and that the Ordovician–Silurian boundary in the Estonian succession correlates with a level within the Varbola Fm (Ainsaar et al. 2011, 2015; Meidla et al. 2020; Gul et al. 2021). Further to the south, the gradual decline in $\delta^{13}C$ values is observed extending over a remarkably longer interval in the Õhne Fm (e.g. in the Tartu core section; Bauert et al. 2014) and in the Stačiunai Fm in Latvia and Lithuania (Ainsaar et al. 2011; Meidla et al. 2020; Hints et al. 2023). There, the boundary level suggested by carbon isotope stratigraphy may be more than 10 m higher than the traditional position based on the distinct lithological change.

Due to the low-diversity faunas in the Varbola, Õhne, and Stačiunai Fms, finding a reliable biostratigraphic marker for the lower boundary of the Silurian in the region is complicated. One possible guidance level may be the FAD of the chitinozoan *Belonechitina postrobusta* (Nestor), although in the Estonian succession it appears in the middle part of the Varbola and Õhne Fms (Meidla et al. 2020, 2023b), probably within the *Cystograptus vesiculosus* GZ (Nestor 2012). However, this assumption should be taken with caution, as the oldest graptolite occurrences in Estonia are younger, belonging to the *Coronograptus cyphus* GZ. Elsewhere in the world, *B. postrobusta* in many cases makes its first appearance in the *ascensus–acuminatus* GZ (Butcher 2013).

Base of Raikküla Regional Stage

The Raikküla RS was originally established as lying between two distinctive units with pentamerid brachiopods: strata with *Borealis borealis* (Eichwald) below and beds rich in *Pentamerus oblongus* Sowerby above. The name 'Raikküla' was introduced for this unit by Schmidt (1881). In the second half of the 20th century, the concept of the unit evolved into a regional stage, with the lower boundary drawn at the top of the Tamsalu and Õhne Fms and considered equivalent to the base of the *Coronograptus cyphus* GZ (Nestor and Einasto 1997). The same concept of the regional stage was maintained by H. Nestor (1990, 1997), although the boundary of this zone was drawn at a lower horizon by Kaljo and Vingisaar (1969), based on the tentative record of *Pribylograptus sandersoni*

(Lapworth) and *P. incommodus* (Törnquist), co-occurring with *Rhaphidograptus toernquisti* (Elles and Wood) and *Dimorphograptus confertus* (Nicholson) in the upper 6 m of the Õhne Fm. In comparison with the updated graptolite record from the United Kingdom (Zalasiewicz et al. 2009), this assemblage cannot be taken as diagnostic of the *cyphus* GZ (equivalent to the *acinaces* and *revolutus* zones in modern British graptolite biostratigraphy; Zalasiewicz et al. 2009, fig. 2), leaving the age of the base of the Raikküla RS in terms of global chronostratigraphy open. In Fig. 2, the base of the Raikküla RS is tentatively indicated as corresponding to a level within the *C. cyphus* GZ, as indicated in Kaljo and Vingisaar (1969).

Age of Rumba Formation and Adavere Regional Stage

Dating of the Rumba Fm and the lower boundary of the Adavere RS has been problematic for a long time. Originally, based on a single find of the graptolite *Pseudoclimacograptus* (now *Metaclimacograptus*) *hughesi* (Nicholson) in the middle part of the formation in the Ikla core section (at the depth 316.6 m within cycle 5 sensu Einasto et al. 1972; see Kaljo and Vingisaar 1969), the Rumba Fm was considered to correspond to the *Stimulograptus sedgwickii* GZ (Nestor 1972). *M. hughesi*, common in the Rhuddanian and Aeronian, is known to reach the very top of the latter stage but has not been found in the Telychian (Loydell et al. 2015). This correlation of the formation has been followed in most subsequent publications and stratigraphic schemes (e.g. Nestor 1997 and references therein), but other correlations have been proposed (e.g. Nestor 2012; Männik 2014).

Based on the graptolites characteristic of the upper *Spirograptus turriculatus* GZ recorded in the sample at 964.6 m in the Aizpute-41 core section in western Latvia (Loydell et al. 2003; Walasek et al. 2018), below the Osmundsberg K-bentonite recognised at 964.4 m (Kiipli et al. 2010), the upper part of the formation is clearly of Telychian age. The Osmundsberg K-bentonite occurs in the upper half of the Rumba Fm in Estonia and serves as the boundary between cycles 8 and 9 of Einasto et al. (1972). The above data suggest that the Aeronian–Telychian boundary in Estonia should be looked for not higher than the middle of Rumba Fm and that the base of the Adavere RS correlates with a level in the uppermost Aeronian.

This correlation is further supported by chemostratigraphic data. In the $\delta^{13}C$ succession, the Rumba Fm is characterised by a distinct negative excursion, the 'Rumba low' (Kaljo and Martma 2000). In the Ikla core, the lowest $\delta^{13}C_{carb}$ and $\delta^{13}C_{org}$ values (Gouldey et al. 2010) occur together with *M. hughesi* (Kaljo and Vingisaar 1969). However, in the El Pintado section in Spain (Loydell et al. 2015) and on Cornwallis Island in Arctic Canada (Melchin and Holmden 2006), the lowest $\delta^{13}C_{org}$ values, likely corresponding to the 'Rumba low', are recorded in the lower *Sp. guerichi* GZ, indicating the earliest Telychian age of the excursion. Recently, the 'Rumba low' was recognised in the Aeronian–Telychian transition in the Sommerodde-1 core from Bornholm, Denmark, with its lowest values at a level corresponding to the lower *Sp. guerichi* GZ, just above an unfossiliferous interval (Loydell et al. 2017; Hammarlund et al. 2019). This indicates that the 'Rumba low' correlates with the Aeronian–Telychian boundary interval, being a useful chemostratigraphic marker in sections where graptolites are missing (Hammarlund et al. 2019; Loydell et al. 2025). The data above suggest that the stage boundary in the Estonian succession lies, most probably, in the middle of the Rumba Fm, within cycle 5 sensu Einasto et al. (1972).

The Rumba Fm is separated from the underlying Nurmekund Fm in central and western Estonia, and the Saarde Fm in southern Estonia and southwestern Saaremaa, by a hiatus of variable duration (Fig. 2). Its size increases to the west and southwest (Einasto et al. 1972). The most significant gap in the graptolite record is observed in the Ohesaare core, where the interval from the *Demirastrites triangulatus* GZ to the upper *Sp. turriculatus* GZ and *Pterospathodus eopennatus* ssp. n. 1 CZ is missing (Loydell et al. 1998).

Boundary between Rumba and Velise formations

At the lower boundary of the Velise Fm, just above the contact with the underlying Rumba Fm, a rich and diverse conodont fauna, including the *Pterospathodus* lineage, appears. This supports a high-resolution biostratigraphic subdivision of the main part of the Adavere RS (Männik 2003, 2007a, 2010). The distribution of the lowermost conodont biozone in this interval, the *Pt. eopennatus* ssp. n. 1 CZ, suggests diachroneity of the lower boundary of the Velise Fm. This biozone is present in the sections in the distal part of the basin (e.g. Ruhnu-500 and Viki cores; Männik 2003, 2010), but gradually becomes thinner towards the proximal part of the basin and is missing in westernmost continental Estonia, where the lower boundary of the Velise Fm lies within the *Pt. eopennatus* ssp. n. 2 CZ (e.g. Paatsalu core; Hints et al. 2006). This indicates that the gap between the Rumba and Velise Fms increases from west to east. However, further east in this region, in the vicinity of Valgu village (Männik 2008), the *Pt. eopennatus* ssp. n. 1 CZ reappears in the lowermost Velise Fm. So far, the biostratigraphically proven maximum extent of the gap occurs in southwesternmost continental Estonia, where the lower half of the Velise Fm, corresponding to the *Pt. eopennatus* ssp. n. 1 CZ up to the *Pt. amorphognathoides lithuanicus* CZ, is missing in some sections (e.g. Ristiküla-174 core; Männik, unpublished data).

Contacts between Velise and Jaani formations, Adavere and Jaani stages, and Llandovery–Wenlock boundary

Traditionally, the boundary between the Velise and Jaani Fms has been drawn to coincide with the boundary between the Adavere and Jaani stages, and the same level has been correlated with the Llandovery–Wenlock boundary (Nestor 1997 and references therein). It is now known that the Llandovery–Wenlock boundary, as defined in its type section at Hughley Brook, England, lies close to or coincides with Datum 2 of the Ireviken Event (Aldridge et al. 1993; Jeppsson 1997). This is close to the boundary between the Lower and Upper *Pseudooneotodus bicornis* CZs, within the *Cyrtograptus murchisoni* GZ (Männik 2007b; Fig. 2). The bound-

ary between the Adavere and Jaani stages is within the Upper *Pt. a. amorphognathoides* Conodont Subzone (Männik 2007a; Hints et al. 2022). However, based on data from the type section of the Mustjala Mb (Mustjala core section, at 85.8 m; Nestor 1993), the boundary between the Velise and Jaani Fms lies within the lowermost *Pt. a. lithuanicus* CZ, which corresponds to the interval from 85.85 to 82.60 m in this section (Männik, unpublished data). In the correlation chart (Fig. 2), the lower boundary of the Mustjala Mb is drawn based on published data from different sections in Estonia.

In western continental Estonia and on the islands in the Muhu Strait, the Llandovery–Wenlock boundary falls within an unconformity. In some sections, the strata corresponding to the Ireviken Event are missing entirely (Männik et al. 2014). In the distal graptolite-bearing environments, a gap corresponding to the upper *Cyrt. lapworthi*, *Cyrt. insectus* and probably *Cyrt. centrifugus* GZs was recognised (Loydell et al. 2003, 2010). If the latter hiatus is also present in proximal environments, its duration is below biostratigraphic resolution.

Jaani Regional Stage

Relationships between lithostratigraphic units traditionally included in the Jaani RS (Fig. 2) are drawn in accordance with the model of Perens (1995). This model is based on detailed lithological, geophysical, and biostratigraphic information from many core sections (mainly from Saaremaa) drilled and studied for geological mapping during the second half of the 20th century. According to that model, the lower half of the Jaani Fm is represented by marlstones of the Mustjala Mb that are replaced by the Tõlla Mb of the lower Riga Fm in the southwestern sections on the Sõrve Peninsula. Due to a regression, the shallow-water bioclastic deposits of the Ninase Mb started to accumulate on the northwestern and central parts of Saaremaa and smaller islands west of it. This formed a barrier bordering the northeastern area of Saaremaa and western continental Estonia, creating semi-restricted conditions where argillaceous sediments of the Paramaja Mb were deposited. On the Sõrve Peninsula, towards the central part of the basin, the Ninase Mb is laterally replaced by argillaceous limestones of the lower Sõrve Fm and further by marlstones of the upper Riga Fm.

The Riksu Fm was originally defined by H. Nestor (1995) as a lithologically transitional unit between the shallow shelf (upper Jaani and Jaagarahu Fms) and distal shelf to slope (upper Riga and Jamaja Fms) facies. Later, Nestor et al. (2001) reinterpreted the lower part of the Riksu Fm in the Riksu core as the Ninase and Paramaja Mbs of the Jaani Fm and correlated the lower boundary of the Riksu Fm with the traditional base of the Jaagarahu RS sensu Aaloe (1970), i.e. with the lower boundaries of the Jaagarahu and Muhu Fms. Lithologically, as stated by Nestor (1995, p. 92), the Riksu Fm is similar to the Sõrve Fm; both consist of cyclically alternating marlstones, argillaceous limestones, and nodular micritic limestones accumulated in an open shelf environment. These two units differ mainly by their age, the Riksu Fm being older than the Sõrve Fm, but otherwise they represent parts of the same lithological body, transitional between the shallow and distal shelf settings (Nestor 1997, fig. 69), with a diachronous lower boundary.

The scheme of this interval in Fig. 2 follows that of Nestor (1997), except that the Riksu Fm is abandoned and considered to be the proximal older part of the Sõrve Fm. The Paramaja Mb, indicated by Nestor (1997) as forming the uppermost part of the Jaani RS in the distalmost region, is replaced by the Riga Fm. The interval originally considered to be the lowermost part of the Riksu Fm (Nestor 1994) and later reinterpreted as representing the Ninase and Paramaja Mbs (Nestor et al. 2001) is poorly constrained and marked with a '?' in Fig. 2; further data are needed to clarify its position.

Boundary between Jaani and Jaagarahu regional stages

The boundary between the Jaani and Jaagarahu RSs has been historically based on sedimentology and drawn at a level of abrupt increase in carbonate content at the contact of the Jaani and Jaagarahu Fms in western Saaremaa, and at the contact of the Jaani and Muhu Fms in eastern Saaremaa and western continental Estonia (Nestor 1997 and references therein). The appearance of reefs has been considered to be the most characteristic feature of the lowermost Jaagarahu RS, although several authors have suggested likely diachroneity of the earliest reef units in this stratigraphic interval (Einasto and Männik 1991; Nestor 1994). The boundary has, unfortunately, been poorly constrained biostratigraphically.

In the Jaagarahu drill core (supplemental section to the old Jaagarahu quarry, the historical stratotype of both the Jaagarahu Fm and the Jaagarahu RS; Nestor 1993, 1997), *Jeppssonia sagitta rhenana* (Walliser) appears at a depth of 20.4 m, which is 1.0 m above the proposed base of the formation and regional stage at 21.4 m. It is followed by the appearance of *Ozarkodina martinssoni* Jeppsson about 15 m higher in the section (Männik, unpublished data). The same succession of appearances of these taxa is recorded in the Viki core (Männik 2010). However, there, *J. s. rhenana* appears in the Ninase Mb, which is usually attributed to the Jaani Fm (Jaani RS), whereas *Oz. martinssoni* appears in the lowermost part of the Vilsandi Beds of the Jaagarahu Fm (Jaagarahu RS).

In the chitinozoan succession, these conodonts appear in the *Conochitina mamilla* and *Con. tuba* chitinozoan biozones (ChZ), respectively (Nestor 2010). The appearance of *J. s. rhenana* has also been recorded in the Ninase Mb at Panga Cliff (in the *Con. mamilla* ChZ; Männik and Nestor 2014) and Suuriku Cliff (Meidla et al. 2014b). This indicates that the lower Jaagarahu Fm is older in northwestern Saaremaa than in the Panga section, where it correlates with the upper Jaani Fm (with the Ninase and Paramaja Mbs). Consequently, the base of the Jaagarahu Fm and the traditional base of the Jaagarahu RS are diachronous.

The gap below the Kesselaid Mb (below the basal Muhu Fm; Fig. 2) is supported by data from the Salevere section in western continental Estonia, where *J. s. rhenana* and *Oz. martinssoni* (*Ozarkodina* sp. (aff. *gulletensis*) in Einasto and Männik 1991) appear together in the lowermost part of

that member. Based on data from the Viki core section (Männik 2010), the Kesselaid Mb in Salevere correlates with the *Con. tuba* ChZ, suggesting that at least the lower *J. s. rhenana* CZ is missing in that section.

Based on chitinozoan data from the deeper part of the palaeobasin (e.g. Ohesaare and Ruhnu-500 cores), V. Nestor (1994, 2012) suggested that the lower boundary of the Jaagarahu RS corresponds to the base of the *Cingulochitina cingulata* ChZ. In the Ohesaare core, the bases of the *Cin. cingulata* ChZ (marked by the appearance of *Cin. cingulata* (Eisenack) at 299.85 m; Nestor 1994) and the Lower *K. walliseri* CZ (defined by the appearance of *K. walliseri* (Helfrich) at 301 m; Männik, unpublished data) lie very close to each other. In the Viki core section (Männik 2010; Nestor 2010), *Cin. cingulata* and *K. walliseri* also appear almost at the same level. However, this level does not fit the traditional base of the Jaagarahu RS (as shown in Nestor 1997, table 8) but corresponds instead to the boundary between the Vilsandi and Maasi beds. In the Riksu core section, *K. walliseri* appears within the Sõrve Fm (in the Middle Riksu Beds as shown by Nestor et al. 2001), in an interval corresponding to the *Cin. cingulata* ChZ. In the Riksu section, the lower boundary of the Jaagarahu RS is correlated with a level within the *Con. tuba* ChZ and *J. s. rhenana* CZ (Nestor et al. 2001). If the base of the *Cin. cingulata* ChZ is taken as the lower boundary of the Jaagarahu RS, the strata corresponding to the Vilsandi Beds of the Jaagarahu Fm (traditionally assigned to the lower Jaagarahu RS; e.g. Nestor 1997 and references therein) and their equivalents in the lower part of the Muhu Fm (Kesselaid Mb) should instead be correlated with the upper Jaani RS. This possibility was first suggested by Perens (1995).

The data above demonstrate that the lower boundary of the Jaagarahu Fm, as well as the traditional base of the Jaagarahu RS as used until now, are diachronous. However, since the lower boundary of the RS almost correlates with the FAD of *J. s. rhenana* in the Jaagarahu core (the hypostratotype of the Jaagarahu RS), we propose this biostratigraphic marker as the foremost suitable level for tracing the base of the Jaagarahu RS (Fig. 2).

Base of Paadla Regional Stage and Wenlock–Ludlow boundary

The lower boundary of the Paadla RS was initially defined based on lithological criteria: it coincides with the top of the Soeginina mottled early diagenetic (lagoonal) dolostones, which are transgressively overlain by argillaceous limestones and dolostones containing *Didymothyris didyma* (Dalman) and *Ilionia prisca* (Hisinger) (Nestor 1997). Nestor and Nestor (1991), based on chitinozoan ranges in the Ventspils (Latvia) and Ohesaare core sections, concluded that the Rootsiküla and Paadla RSs are separated by a considerable gap in the carbonate sections in Estonia, corresponding to the lower part of the Ludlow, equivalent to the *Noediversograptus nilssoni* and most of the *Lobograptus scanicus* GZs, and consequently, the base of the Paadla RS lies close to the base of the Ludfordian in Estonian successions.

Comparison of $\delta^{13}C$ data from the Priekule (Latvia) and Ohesaare cores confirmed a considerable gap below the Sauvere Beds in the latter section (Kaljo et al. 1997), although the same authors also proposed that '… transgressive parts of this long interval might be represented by some strata at the corresponding levels in the Sauvere Beds...'. The co-occurrence of *Angochitina elongata* Eisenack, *Conochitina latifrons* Eisenack, and *Phlebolepis ornata* Märss in the lower Torgu Fm (Paadla RS) in the Ohesaare core indicates that the upper part of the Gorstian (the *L. scanicus* GZ) is represented at least in southwestern Saaremaa (Viira and Aldridge 1998). Additionally, comparison of conodont data from Saaremaa and Gotland (Sweden) confirms the existence of a gap below the Paadla RS, but also suggests that the Gorstian is still partly present in the region (Jeppsson et al. 1994). The occurrence of *Ph. ornata* in the Sauvere Beds in several outcrop sections (Kandla, Kärla, Kogula) on west-central Saaremaa (Märss 1986) suggests that the upper part of the *Kockelella variabilis variabilis* CZ, comprising the upper Gorstian (Jeppsson et al. 2006; Märss and Männik 2013; Männik 2014), is preserved also in the outcrop area of the Paadla RS. The data above indicate that the base of the Paadla RS corresponds to a level within the upper Gorstian.

Conventionally, the boundary between the Rootsiküla and Paadla RSs has been correlated with the Wenlock–Ludlow boundary in Estonia (Nestor 1997 and references therein). Viira and Einasto (2003) concluded – based mainly on cyclostratigraphic reconstruction, but also on the distribution of some conodonts – that the topmost part of the Rootsiküla Fm and the Rootsiküla RS (the Soeginina Beds) are of early Ludlow age. This was previously suggested by Kaljo et al. (1997), based on correlation of $\delta^{13}C$ curves from the Ohesaare and Priekule cores, which indicated that the upper part of the Rootsiküla RS likely belongs to the Ludlow, within the *Neodiversograptus nilssoni* GZ. As the Rootsiküla RS has traditionally been considered to be of late Wenlock (Homerian) age and the Paadla RS of Ludlow age, Viira and Einasto (2003), when re-dating the uppermost Rootsiküla RS, proposed to move the Soeginina Beds from the Rootsiküla RS to the Paadla RS and, accordingly – and somewhat surprisingly – from the Rootsiküla Fm to the Paadla Fm (as indicated e.g. in Hints 2008, fig. C2). However, although the relatively poor conodont faunas in the Soeginina Beds contain some elements characteristic of the Paadla RS (e.g. *Oulodus siluricus* (Branson and Mehl; Viira and Einasto 2003; Jarochowska et al. 2017), they generally do not differ markedly from those in the underlying strata. Instead, a distinct change in the conodont succession, along with a marked increase in diversity and abundance, occurs just above the boundary between the Soeginina and Sauvere beds, in the lower part of the Paadla RS (Männik and Viira 1993; Märss and Männik 2013).

In the present paper, the traditional definition of the Rootsiküla and Paadla RSs (Nestor 1997) is followed, and the Soeginina Beds – although probably of earliest Ludlow age based on $\delta^{13}C$ data – are attributed to the uppermost part of the Rootsiküla Fm. Hence, the Wenlock–Ludlow boundary

is tentatively correlated with the boundary between the Vesiku and Soeginina beds, within the upper Rootsiküla RS (Fig. 2).

Two new units, the Anikaitse and Iide beds, have been proposed as subdivisions of the Rootsiküla Fm. The Anikaitse Beds were described on eastern Saaremaa, between the Vesiku and Soeginina beds, and dated to the latest Wenlock (Viira and Einasto 2003), but the distribution area of this proposed unit and its correlation with core sections were insufficiently addressed. Kiipli et al. (2011, p. 209) proposed the name 'Iide Beds' for microbedded limestone of the Ančia Mb in the Ohesaare core (depth interval 150.5–161.5 m), corresponding to the lowermost, transgressive part of the Rootsiküla Fm. Earlier, this interval had been assigned to the Jaagarahu RS (Einasto 1970), divided between the Jaagarahu and Rootsiküla RSs (Nestor 1997), or included entirely in the Rootsiküla RS (Kaljo et al. 1997). However, as the spatial distribution of both units is unclear or very limited in Estonia, their usefulness in regional stratigraphy remains arguable.

Paadla Formation and Paadla Regional Stage

The distribution of vertebrates and conodonts in the Sauvere Beds dates this unit to the late Gorstian. The age of the Himmiste and Uduvere beds in the middle and upper parts of the Paadla Fm is more problematic. The distribution of vertebrates – particularly the occurrence (appearance) of *Phlebolepis elegans* Pander and the lack of *Andreolepis hedei* Gross in the Himmiste Beds – suggests a correlation of these strata with the uppermost Gorstian–lowermost Ludfordian *Phl. elegans* Vertebrate Biozone (VZ). However, the lack of the lower Ludfordian *Ancoradella ploeckensis* and *Polygnathoides siluricus* CZs in the studied Estonian sections suggests that both biozones lie within a gap in the succession (Märss and Männik 2013). These CZs have been identified further south, e.g. in the Pavilosta-51 core in western Latvia, representing the distal, deeper part of the palaeobasin beyond the carbonate shelf in Estonia (Nestor and Einasto 1977). Considering these data, the Himmiste Beds overlying the Sauvere Beds in the succession correspond to the *Phl. elegans* VZ and probably also to the uppermost Gorstian (Märss and Männik 2013).

Alternatively, based on the identification of the conodont *Jeppssonia crispa* (Walliser) in several sections of the Himmiste Beds (e.g. Viira and Aldridge 1998), this unit could also be dated as late Ludfordian and correlated with the *Formosograptus formosus* GZ (Corradini and Serpagli 1999; Cramer et al. 2011). It has been shown, however, that *J. crispa* may have a considerably longer stratigraphic range in the Baltic region than elsewhere (Viira and Aldridge 1998; Viira 1999; Kaljo et al. 2015), with the oldest identifications reported from the lowermost Paadla Fm (Sauvere Beds; e.g. the Kärla section on Saaremaa; Viira and Aldridge 1998) and co-occurring with *Phlebolepis ornata* in strata of late Gorstian age. In the Riksu core, southwestern Saaremaa, *J. crispa* has been identified from below the FAD of *Phl. ornata* (identified as *Ozarkodina snajdri* s.l.; Nestor et al. 2001; Märss and Männik 2013). However, *J. crispa* belongs to closely related taxa together with *J. snajdri snajdri* (Walliser) and *J. s. parasnajdri* (Viira and Aldridge), forming the so-called *J. snajdri–crispa* lineage, which is known to appear in the upper Gorstian (Aldridge 1985; Jeppsson et al. 1994; Paškevičius et al. 1994) and extend stratigraphically upward to at least the lower Přídolí (Corradini et al. 2015). The Pa elements that are critical for the recognition of these taxa are morphologically highly variable (e.g. Viira and Aldridge 1998), which makes their reliable identification complicated and highly subjective, particularly in samples with few specimens. For example, Viira and Aldridge (1998) identified *J.* cf. *s. snajdri* in the Ohesaare core from the interval 106.25–113.35 m, *J. crispa* from 95.95–100.80 m, and *J. s. parasnajdri* from 61.20–93.40 m. C. Corradini, who restudied the collection in 2014, agreed that *J. s. parasnajdri* occurs in the interval 61.20–93.40 m but identified *J. crispa* in the interval 61.20–100.80 m and did not recognise *J. s. snajdri*. Hence, it is evident that the use of these taxa in stratigraphy should be treated with caution.

The age of the Uduvere Beds is poorly constrained. The occurrence of *Andreolepis hedei* suggests a Ludfordian age for these strata. Märss and Männik (2013) correlated the Uduvere Beds with the *J. s. snajdri* CZ. However, this interpretation disagrees with the geochemical data indicating that the strata hosting the Mid-Ludfordian (Lau) $\delta^{13}C$ excursion are missing in Estonia (Kaljo and Martma 2006). Moreover, the occurrence of *A. hedei* in the Uduvere Beds – considering that the species became extinct during the Lau Event together with *Pol. siluricus* Branson and Mehl (Eriksson et al. 2009) – indicates that they cannot be younger than early Ludfordian. Recent detailed comparison of vertebrate assemblages from Gotland and Estonia also suggests that the Uduvere Beds correlate with an interval in the lower Ludfordian, below the Mid-Ludfordian $\delta^{13}C$ excursion, and might be equivalent to part of the När Fm, Gotland, Sweden (Bremer et al. 2020).

In general, these data agree with the conclusions of Jeppsson et al. (1994) who, based on the occurrence of *Coryssognathus dubius* (Rhodes) and the lack of *Pol. siluricus* in the Uduvere Beds, correlated this unit with the youngest part of the *Ancoradella ploeckensis* CZ, an interval in which specimens of *A. ploeckensis* are very rare. Insufficient sample size may explain why this conodont has not been found in the Uduvere Beds. Based on the considerations above, the Uduvere Beds are tentatively correlated with the upper *A. ploeckensis* CZ in the updated correlation chart (Fig. 2).

Carbon isotope chemostratigraphy shows that the Mid-Ludfordian (Lau) $\delta^{13}C$ excursion, roughly corresponding to the *N. kozlowski–P. podoliensis* GZ, is missing in all studied sections in Estonia (Kaljo and Martma 2006). This indicates that most of the Mid-Ludfordian corresponds to a gap between the Paadla and Kuressaare RSs in Estonia (Fig. 2). Furthermore, identical conodont and vertebrate faunas in the Paadla and Torgu Fms (e.g. the common occurrence of *Panderodus* ex gr. *greenlandensis* Armstrong and *Pand. serratus* Rexroad in all studied collections, and the occurrence of *Phl. ornata* in the lower and *A. hedei* in the uppermost part of both formations) indicate that they are coeval in Estonia (Märss and Männik 2013). However, based on new bio- and

chemostratigraphic data, Kaljo et al. (2022) proposed that strata of mid-Ludfordian age might still be partly preserved in the distalmost sections in Estonia. Further studies are needed to confirm this and to provide reliable dating of the Kihnu Fm.

Age of Kuressaare Regional Stage and Ludlow–Přídolí boundary

The traditional boundary between the Paadla and Kuressaare RSs is lithologically sharp, marked by a bone bed in many core sections (e.g. the Sakla core) and characterised by a distinct turnover among vertebrate faunas, evidently related to a gap in the succession (Märss 1992; Märss and Männik 2013). A gap at this level was also proposed based on sedimentological evidence (Einasto 1991; Nestor and Einasto 1997).

The Kuressaare RS has been indirectly correlated with the upper part of the Ludlow, with the *Formosograptus formosus* GZ (Nestor 1997). The boundary between the Kuressaare and Kaugatuma RSs has been tentatively correlated with the Ludlow–Přídolí boundary, without strong biostratigraphic evidence. Based on the generally accepted idea, the *J. crispa* CZ is the uppermost one of the Ludlow and correlates roughly with the *F. formosus* GZ (Corradini and Serpagli 1999; Cramer et al. 2011). According to Viira (1999), in Estonia *J. crispa* appears in the upper Paadla RS, traditionally correlated with the strata older than the *F. formosus* GZ (Nestor 1997), and also occurs in the lower Kuressaare RS but not higher in succession. Considering the information above, it was proposed that at least part of the Paadla RS probably corresponds to the lower *F. formosus* GZ and that the upper part of the Kuressaare RS above the occurrence of *J. crispa* is of Přídolí age (Männik 2014).

Kaljo et al. (2015), based on a detailed analysis of available bio- and chemostratigraphic information from the Baltic region, concluded that the Kuressaare Fm (and the Kuressaare RS) is of late Ludlow age, at least in the Ohesaare core, and correlates with an interval above the Mid-Ludfordian $\delta^{13}C$ excursion. However, it is now known that the range of *J. crispa* reaches the lower Přídolí (e.g. *J. crispa* has been reported to co-occur with *Skalograptus parultimus* (Jaeger), the index taxon for the base of the Přídolí, in the Carnic Alps; Corradini et al. 2015). This is further indication that the upper Kuressaare RS, above the occurrence of *J. crispa*, is most probably of Přídolí age.

There are no reliable biostratigraphic criteria for identifying the Ludlow–Přídolí boundary in the Estonian succession. Nestor (2011, 2012), applying indirect correlations, concluded that the boundary between the East Baltic *Eisenackitina barrandei* and *Fungochitina kosovensis* ChZs approximately corresponds to the series boundary and to the contact between the Kuressaare and Kaugatuma RSs. However, considering the data above in this section, the base of the Kaugatuma RS is younger and the Ludlow–Přídolí boundary in the Estonian succession most likely corresponds to a level within the Kuressaare RS. However, further studies are required to locate its level precisely.

Conclusions

Since the beginning of Silurian research in Estonia almost two centuries ago, a vast amount of information has been accumulated on the lithologies and distribution of faunas within the succession. Based on numerous detailed studies carried out during the second half of the 20th century, a high-resolution stratigraphic framework for the Silurian succession was developed and has been widely adopted in Estonia (Nestor 1997). However, new data collected over the past 25–30 years, particularly regarding microfossils, along with the implementation of a revised international time scale (Melchin et al. 2020), have highlighted the need for an updated regional stratigraphic chart. In this paper, we present a revised version of the regional Silurian stratigraphy and discuss the main changes resulting from recent palaeontological and geochemical analyses. These include the following:

1. The lower part of the Juuru Regional Stage is of Late Ordovician (Hirnantian) age.
2. The age of the base of the Raikküla Regional Stage in terms of global chronostratigraphy remains problematic.
3. The Aeronian–Telychian boundary in Estonia should be sought no higher in the succession than the middle of the Rumba Formation.
4. The lower boundary of the Adavere Regional Stage correlates with a level in the uppermost Aeronian.
5. The former Riksu Formation is now considered to be the proximal, older part of the Sõrve Formation.
6. The lower boundary of the Jaagarahu Formation – and the Jaagarahu Regional Stage as used until now – is diachronous. Based on data from the stratotype region, the best biostratigraphic approximation for identifying the base of this stage is the first appearance datum (FAD) of *J. s. rhenana*.
7. The Wenlock–Ludlow boundary in the Estonian succession correlates with a level in the upper part of the Rootsiküla Regional Stage, tentatively placed at the boundary between the Vesiku and Soeginina beds.
8. The Sauvere and Himmiste beds of the Paadla Formation are of late Gorstian age.
9. The Uduvere Beds correspond to an interval in the lower Ludfordian, below the Mid-Ludfordian $\delta^{13}C$ excursion, and are tentatively correlated with the upper *A. ploeckensis* Conodont Zone.
10. The base of the Paadla Regional Stage corresponds to a level in the upper Gorstian, possibly within the lower *Ph. ornata* Vertebrate Zone.
11. There are no reliable biostratigraphic criteria for precisely identifying the Ludlow–Přídolí boundary in the Estonian succession; however, it most likely corresponds to a level within the Kuressaare Regional Stage.

Additionally, the duration and distribution of several gaps in the succession have been revised.

It should be emphasised, however, that the updated scheme presented here reflects the current state of knowledge and the authors' interpretation. As such, it inevitably contains less well-constrained intervals and numerous uncertainties regarding both regional and global correlations.

We have identified several areas where further improvements in regional stratigraphy are needed:

1. Improved and revised definitions of lithostratigraphic units, particularly in the context of geological mapping and applied geology.
2. Development of quantitative approaches and integration of biostratigraphic and chemostratigraphic datasets.
3. Evaluation of whether a broader and more precise application of regional stages is warranted, and whether the principles outlined in the *International Stratigraphic Guide* can be applied at the regional level.
4. The Silurian time scale adopted here for the Baltic Palaeobasin is largely based on the ages of zonal boundaries constructed by Melchin et al. (2020). Radiometric dating of additional levels to further improve the Silurian time scale and datings of the rocks from the Baltic Palaeobasin for validating this correlation are needed.

We hope that the correlation chart presented in this paper not only summarises the current state of knowledge but also represents a step forward. Undoubtedly, future research, new data, and the application of modern methods for investigating and correlating sections will continue to refine the Silurian stratigraphy of the region.

Data availability statement

The data used in this study will be made available on request.

Acknowledgements

Comments and suggestions by D. K. Loydell and S. Radzevičius helped to improve the manuscript considerably. The work was supported by the Estonian Research Council grant PRG1701. The publication costs of this article were partially covered by the Estonian Academy of Sciences.

References

Aaloe, A. 1970. Jaani Stage. Jaagarahu Stage. In *The Silurian of Estonia* (Kaljo, D., ed.). Valgus, Tallinn, 243–264.

Aaloe, A., Kaljo, D., Klaamann, E., Nestor, H. and Einasto, R. 1976. Stratigraphical classification of the Estonian Silurian. *Proceedings of the Academy of Sciences of the Estonian SSR. Chemistry, Geology*, **25**(1), 38–45.

Ainsaar, L., Truumees, J. and Meidla, T. 2011. Carbon isotope chemostratigraphy of the Ordovician/Silurian boundary beds in central Estonia: new data from drillcores in the Pandivere area. In *8th Baltic Stratigraphical Conference, Riga, Latvia, 28 August – 1 September 2011. Abstracts* (Lukševics, E., Stinkulis, G. and Vasilkova, J., eds). University of Latvia, Riga, 10.

Ainsaar, L., Truumees, J. and Meidla, T. 2015. The position of the Ordovician–Silurian boundary in Estonia tested by high-resolution $\delta^{13}C$ chemostratigraphic correlation. In *Chemostratigraphy: Concepts, Techniques, and Applications* (Ramkumar, Mu., ed.). Elsevier, 395–412.

Aldridge, R. J. 1985. Conodonts of the Silurian System from the British Isles. In *A Stratigraphical Index of Conodonts* (Higgins, A. C. and Austin, R. L., eds). Ellis Horwood, Chichester, Sussex, 68–92.

Aldridge, R. J., Jeppsson, L. and Dorning, K. J. 1993. Early Silurian oceanic episodes and events. *Journal of the Geological Society*, **150**(3), 501–513. https://doi.org/10.1144/gsjgs.150.3.0501

Barrick, J. E., Klapper, G. and Peavey, F. N. 2024. Conodont biostratigraphy of the upper member of the Henryhouse Formation (late Ludfordian–Prídolí, Silurian), southern Oklahoma, USA. *Stratigraphy*, **21**(4), 287–322. https://doi.org/10.29041/strat.21.4.02

Bauert, H., Ainsaar, L., Bauert, G., Nõlvak, J., Põldsaar, K. and Sepp, S. 2014. Integrated Ordovician $\delta^{13}C$ chemostratigraphy and chitinozoan biostratigraphy of the Tartu drillcore section, southern Estonia. In *4th Annual Meeting of IGCP 591, Tartu, Estonia, 10–19 June 2014. Abstracts and Field Guide* (Bauert, H., Hints, O., Meidla, T. and Männik, P., eds). University of Tartu, Tartu, 16.

Bekker, H. 1922. Ülevaade Eesti ordoviitsiumi ja siluri kohta käivatest uurimustest. *Loodus*, **4**, 217–224.

Bekker, H. 1925. Lühike ülevaade Eesti geoloogiast (eozoiline ja paleozoiline ladekond). In *Eesti Loodus*. Tartu Ülikooli Loodusuurijate Selts, Tartu, 31–61.

Bremer, O., Jarochowska, E. and Märss, T. 2020. Vertebrate remains and conodonts in the upper Silurian Hamra and Sundre formations of Gotland, Sweden. *GFF*, **142**(1), 52–80. https://doi.org/10.1080/11035897.2019.1655790

Brenchley, P. J., Carden, G. A., Hints, L., Kaljo, D., Marshall, J. D., Martma, T. et al. 2003. High-resolution stable isotope stratigraphy of Upper Ordovician sequences: constraints on the timing of bioevents and environmental changes associated with mass extinction and glaciation. *Geological Society of America Bulletin*, **115**(1), 89–104. https://doi.org/10.1130/0016-7606(2003)115<0089:HRSISO>2.0.CO;2

Butcher, A. 2013. Chitinozoans from the middle Rhuddanian (lower Llandovery, Silurian) 'hot' shale in the E1-NC174 core, Murzuq Basin, SW Libya. *Review of Palaeobotany and Palynology*, **198**, 62–91. http://dx.doi.org/10.1016/j.revpalbo.2012.11.009

Corradini, C. and Serpagli, E. 1999. A Silurian conodont biozonation from late Llandovery to end Přídolí in Sardinia (Italy). *Bollettino della Società Paleontologica Italiana*, **37**(2–3), 255–273.

Corradini, C., Corriga, M. G., Männik, P. and Schönlaub, H. P. 2015. Revised conodont stratigraphy of the Cellon section (Silurian, Carnic Alps). *Lethaia*, **48**(1), 56–71. https://doi.org/10.1111/let.12087

Cramer, B. D., Brett, C. E., Melchin, M. J., Männik, P., Kleffner, M. A., Mclaughlin, P. I. et al. 2011. Revised correlation of Silurian Provincial Series of North America with global and regional chronostratigraphic units and $\delta^{13}C_{carb}$ chemostratigraphy. *Lethaia*, **44**(2), 185–202. https://doi.org/10.1111/j.1502-3931.2010.00234.x

Decisions of the Interdepartmental Stratigraphic Meeting on the Ordovician and Silurian of the East European Platform in 1984 with regional stratigraphic schemes. 1987. VSEGEI, Leningrad.

Dronov, A. and Rozhnov, S. 2007. Climatic changes in the Baltoscandian basin during the Ordovician: sedimentological and palaeontological aspects. *Acta Palaeontologica Sinica*, **46**(Supplement), 108–113.

Einasto, R. 1970. Rootsiküla Stage. In *The Silurian of Estonia* (Kaljo, D., ed.). Valgus, Tallinn, 264–276.

Einasto, R. 1991. Silurian. In *Geology and Mineral Resources of Estonia: Excursion Guide* (Puura, V., Kalm, V. and Puura, I., eds). Eesti Geoloogia Selts, Tallinn, 7–9.

Einasto, R. and Männik, P. 1991. Stop 2.5: Salumägi at Salevere. In *Geology and Mineral Resources of Estonia: Excursion Guide* (Puura, V., Kalm, V. and Puura, I., eds). Eesti Geoloogia Selts, Tallinn, 51–53.

Einasto, R., Nestor, H., Kala, E. and Kajak, K. 1972. Correlation of the upper Llandoverian sections in West Estonia. *Proceedings of the Academy of Sciences of the Estonian SSR. Chemistry, Geology*, **21**, 333–343.

Engelhardt, M. and Ulprecht, E. 1830. Umriss der Felsstructures Estlands und Livlands. *Archiv für Mineralogie, Geognosie, Bergbau und Hüttenkunde (Karsten)*, **2**, 94–112.

Eriksson, M. E., Nilsson, E. K. and Jeppsson, L. 2009. Vertebrate extinctions and reorganizations during the Late Silurian Lau Event. *Geology*, **37**(8), 739–742. https://doi.org/10.1130/G25709A.1

Gouldey, J. C., Saltzman, M. R., Young, S. A. and Kaljo, D. 2010. Strontium and carbon isotope stratigraphy of the Llandovery

(Early Silurian): implications for tectonics and weathering. *Palaeogeography, Palaeoclimatology, Palaeoecology*, **296**(3–4), 264–275. https://doi.org/10.1016/j.palaeo.2010.05.035

Gul, B., Ainsaar, L. and Meidla, T. 2021. Latest Ordovician–early Silurian palaeoenvironmental changes and palaeotemperature trends indicated by stable carbon and oxygen isotopes from northern Estonia. *Estonian Journal of Earth Sciences*, **70**(4), 196–209. https://doi.org/10.3176/earth.2021.14

Hammarlund, E. U., Loydell, D. K., Nielsen, A. T. and Schovsbo, N. H. 2019. Early Silurian $\delta^{13}C_{org}$ excursions in the foreland basin of Baltica, both familiar and surprising. *Palaeogeography, Palaeoclimatology, Palaeoecology*, **526**, 126–135. https://doi.org/10.1016/j.palaeo.2019.03.035

Hints, O. 2008. The Silurian System in Estonia. In *7th Baltic Stratigraphical Conference, 15–22 May 2008, Tallinn, Estonia. Abstracts and Field Guide* (Hints, O., Ainsaar, L., Männik, P. and Meidla, T., eds). Tallinn, 113–114.

Hints, O., Killing, M., Männik, P. and Nestor, V.-K. 2006. Frequency patterns of chitinozoans, scolecodonts, and conodonts in the upper Llandovery and lower Wenlock of the Paatsalu core, western Estonia. *Proceedings of the Estonian Academy of Sciences. Geology*, **55**(2), 128–155. https://doi.org/10.3176/geol.2006.2.04

Hints, O., Antonovitš, L., Bauert, G., Nestor, V., Nõlvak, J. and Tammekänd, M. 2018. CHITDB: a database for documenting and analysing diversification of Ordovician–Silurian chitinozoans in the Baltic region. *Lethaia*, **51**(2), 218–227. https://doi.org/10.1111/let.12249

Hints, L., Pärnaste, H., Männik, P., Reich, M. and Rozhnov, S. 2022. Development of faunal diversity during the late Llandovery–early Wenlock in the easternmost part of the Baltic Palaeobasin – implications for the Ireviken Event. *Estonian Journal of Earth Sciences*, **71**(2), 89–110. https://doi.org/10.3176/earth.2022.07

Hints, O., Ainsaar, L., Lepland, A., Liiv, M., Männik, P., Meidla, T. et al. 2023. Paired carbon isotope chemostratigraphy across the Ordovician–Silurian boundary in central East Baltic: regional and global signatures. *Palaeogeography, Palaeoclimatology, Palaeoecology*, **624**, 111640. https://doi.org/10.1016/j.palaeo.2023.111640

Holland, C. H. 1985. Series and Stages of the Silurian System. *Episodes*, **8**(2), 101–103. https://doi.org/10.18814/epiiugs/1985/v8i2/005

Jarochowska, E., Viira, V., Einasto, R., Nawrot, R., Bremer, O., Männik, P. et al. 2017. Conodonts in Silurian hypersaline environments: specialized and unexpectedly diverse. *Geology* **45**(1), 3–6. https://doi.org/10.1130/G38492.1

Jeppsson, L. 1997. A new latest Telychian, Sheinwoodian and Early Homerian (Early Silurian) standard conodont zonation. *Transactions of the Royal Society of Edinburgh: Earth Sciences*, **88**(2), 91–114. https://doi.org/10.1017/S0263593300006854

Jeppsson, L. and Calner, M. 2003. The Silurian Mulde Event and a scenario for secundo–secundo events. *Transactions of the Royal Society of Edinburgh: Earth Sciences*, **93**(2), 135–154. https://doi.org/10.1017/S0263593300000377

Jeppsson, L., Viira, V. and Männik, P. 1994. Silurian conodont-based correlations between Gotland (Sweden) and Saaremaa (Estonia). *Geological Magazine*, **131**(2), 201–218. https://doi.org/10.1017/S0016756800010736

Jeppsson, L., Eriksson, M. E. and Calner, M. 2006. A latest Llandovery to latest Ludlow high-resolution biostratigraphy based on the Silurian of Gotland – a summary. *GFF*, **128**(2), 109–114. https://doi.org/10.1080/11035890601282109

Jürgenson, E. 1966. *Lithology of Llandoverian Beds in Estonia*. Academy of Sciences of the Estonian SSR, Institute of Geology, Tallinn.

Kaljo, D. (ed.) 1970. *The Silurian of Estonia.* Valgus, Tallinn.

Kaljo, D. (ed.) 1977a. *Facies and Fauna of the Baltic Silurian*. Academy of Sciences of the Estonian SSR, Institute of Geology, Tallinn.

Kaljo, D. 1977b. Structural and facial subdivisions on the East Baltic Silurian basin. In *Facies and Fauna of the Baltic Silurian* (Kaljo, D., ed.). Academy of Sciences of the Estonian SSR, Institute of Geology, Tallinn, 6–13.

Kaljo, D. and Klaamann, E. (eds) 1986. *Theory and Practice of Ecostratigraphy*. Valgus, Tallinn.

Kaljo, D. and Martma, T. 2000. Carbon isotopic composition of Llandovery rocks (East Baltic Silurian) with environmental interpretation. *Proceedings of the Estonian Academy of Sciences. Geology*, **49**(4), 267–283.

Kaljo, D. and Martma, T. 2006. Application of carbon isotope stratigraphy to dating the Baltic Silurian rocks. *GFF*, **128**(2), 123–129. https://doi.org/10.1080/11035890601282123

Kaljo, D. and Vingisaar, P. 1969. On the sequence of the Raikküla Stage in southernmost Estonia. *Proceedings of the Academy of Sciences of the Estonian SSR. Chemistry, Geology*, **18**(3), 270–277.

Kaljo, D., Nestor, H. and Põlma, L. 1988. East Baltic region. *Bulletin of the British Museum (Natural History). Geol*ogy, **43**, 85–91.

Kaljo, D., Kiipli, T. and Martma, T. 1997. Carbon isotope event markers through the Wenlock–Pridoli sequence at Ohesaare (Estonia) and Priekule (Latvia). *Palaeogeography, Palaeoclimatology, Palaeoecology*, **132**(1–4), 211–223. https://doi.org/10.1016/S0031-0182(97)00065-5

Kaljo, D., Hints, L., Martma, T. and Nõlvak, J. 2001. Carbon isotope stratigraphy in the latest Ordovician of Estonia. *Chemical Geology*, **175**(1–2), 49–59. https://doi.org/10.1016/S0009-2541(00)00363-6

Kaljo, D., Hints, L., Männik, P. and Nõlvak, J. 2008. The succession of Hirnantian events based on data from Baltica: brachiopods, chitinozoans, conodonts, and carbon isotopes. *Estonian Journal of Earth Sciences*, **57**(4), 197–218. https://doi.org/10.3176/earth.2008.4.01

Kaljo, D., Einasto, R., Martma, T., Märss, T., Nestor, V.-K. and Viira, V. 2015. A bio-chemostratigraphical test of the synchroneity of biozones in the upper Silurian of Estonia and Latvia with some implications for practical stratigraphy. *Estonian Journal of Earth Sciences*, **64**(4), 267–283. https://doi.org/10.3176/earth.2015.33

Kaljo, D., Martma, T., Märss, T., Nestor, V. and Viira, V. 2022. A bio- and chemostratigraphic search for the Mid-Ludfordian Carbon Isotope Excursion interval in the Ludlow of the Ohesaare core, Estonia. *Estonian Journal of Earth Sciences*, **71**(1), 44–60. https://doi.org/10.3176/earth.2022.04

Kiipli, T., Kallaste, T., Nestor, V. and Loydell, D. K. 2010. Integrated Telychian (Silurian) K-bentonite chemostratigraphy and biostratigraphy in Estonia and Latvia. *Lethaia*, **43**(1), 32–44. https://doi.org/10.1111/j.1502-3931.2009.00162.x

Kiipli, T., Einasto, R., Kallaste, T., Nestor, V., Perens, H. and Siir, S. 2011. Geochemistry and correlation of volcanic ash beds from the Rootsiküla Stage (Wenlock–Ludlow) in the eastern Baltic. *Estonian Journal of Earth Sciences*, **60**(4), 207–219. https://doi.org/10.3176/earth.2011.4.02

Kiipli, T., Kallaste, T. and Nestor, V. 2012. Correlation of upper Llandovery–lower Wenlock bentonites in the När (Gotland, Sweden) and Ventspils (Latvia) drill cores: role of volcanic ash clouds and shelf sea currents in determining areal distribution of bentonite. *Estonian Journal of Earth Sciences*, **61**(4), 295–306. https://doi.org/10.3176/earth.2012.4.08

Loydell, D. K. and Nestor, V. 2005. Integrated graptolite and chitinozoan biostratigraphy of the upper Telychian (Llandovery, Silurian) of the Ventspils D-3 core, Latvia. *Geological Magazine*, **142**(4), 369–376. https://doi.org/10.1017/S0016756805000531

Loydell, D. K., Kaljo, D. and Männik, P. 1998. Integrated biostratigraphy of the lower Silurian of the Ohesaare core, Saaremaa, Estonia. *Geological Magazine*, **135**(6), 769–783. https://doi.org/10.1017/S0016756898001423

Loydell, D. K., Männik, P. and Nestor, V. 2003. Integrated biostratigraphy of the lower Silurian of the Aizpute-41 core, Latvia. *Geological Magazine*, **140**(2), 205–229. https://doi.org/10.1017/S0016756802007264

Loydell, D. K., Nestor, V. and Männik, P. 2010. Integrated biostratigraphy of the lower Silurian of the Kolka-54 core, Latvia. *Geological Magazine*, **147**(2), 253–280. https://doi.org/10.1017/S0016756809990574

Loydell, D. K., Frýda, J. and Gutiérrez-Marco, J. C. 2015. The Aeronian/Telychian (Llandovery, Silurian) boundary, with particular reference to sections around the El Pintado reservoir, Seville Province, Spain. *Bulletin of Geosciences*, **90**(4), 743–794. https://doi.org/10.3140/bull.geosci.1564

Loydell, D. K., Walasek, N., Schovsbo, N. H. and Nielsen, A. T. 2017. Graptolite biostratigraphy of the lower Silurian of the Sommerodde-1 core, Bornholm, Denmark. *Bulletin of the Geological Society of Denmark*, **65**, 135–160. https://doi.org/10.37570/bgsd-2017-65-09

Loydell, D. K., Gutiérrez-Marco, J. C., Štorch, P. and Frýda, J. 2025. The replacement Global Stratotype Section and Point (GSSP) of the Telychian Stage of the Llandovery Series, Silurian System, at El Pintado (Spain). *Episodes*, **48**(2), 199–211. https://doi.org/10.18814/epiiugs/2025/025009

Luha, A. 1930. Über Ergebnisse stratigraphischer Untersuchungen im Gebiete der Saaremaa-(Ösel-)Schichten in Eesti (Unterösel und Eurypterusschichten). *Acta et Commentationes Universitatis Tartuensis*, **18**(6), 1–18.

Luha, A. 1933. Eesti geoloogiline koostis. In *Eesti Entsüklopeedia*, Vol. 2 (Kleis, R., ed.). Loodus, Tartu, 528–535.

Luha, A. 1946. *Eesti NSV maavarad. Rakendusgeoloogiline kokkuvõtlik ülevaade*. Teaduslik Kirjandus, Tartu.

Männik, P. 2003. Distribution of Ordovician and Silurian conodonts. In *Ruhnu (500) Drill Core* (Põldvere, A., ed.). *Estonian Geological Sections Bulletin*, 5. Geological Survey of Estonia, Tallinn, 17–23.

Männik, P. 2007a. An updated Telychian (Late Llandovery, Silurian) conodont zonation based on Baltic faunas. *Lethaia*, **40**(1), 45–60. https://doi.org/10.1111/j.1502-3931.2006.00005.x

Männik, P. 2007b. Some comments on the Telychian–early Sheinwoodian conodont faunas, events and stratigraphy. *Acta Palaeontologica Sinica*, **46**(Supplement), 305–310.

Männik, P. 2007c. Recent developments in the Upper Ordovician and lower Silurian conodont biostratigraphy in Estonia. *Estonian Journal of Earth Sciences*, **56**(1), 35–46. https://doi.org/10.3176/earth.2007.08

Männik, P. 2008. Conodont dating of some Telychian (Silurian) sections in Estonia. *Estonian Journal of Earth Sciences*, **57**(3), 156–169. https://doi.org/10.3176/earth.2008.3.04

Männik, P. 2010. Distribution of Upper Ordovician, Llandovery and Wenlock conodonts. In *Viki Drill Core* (Põldvere, A., ed.). *Estonian Geological Sections Bulletin*, 10. Geological Survey of Estonia, Tallinn, 21–24.

Männik P. 2014. The Silurian System in Estonia. In *4th Annual Meeting of IGCP 591, Tartu, Estonia, 10–19 June 2014. Abstracts and Field Guide* (Bauert, H., Hints, O., Meidla, T. and Männik, P., eds). University of Tartu, Tartu, 123–128.

Männik, P. and Nestor, V. 2014. Stop B5. Panga cliff. In *4th Annual Meeting of IGCP 591, Tartu, Estonia, 10–19 June 2014. Abstracts and Field Guide* (Bauert, H., Hints, O., Meidla, T. and Männik, P., eds). University of Tartu, Tartu, 185–187.

Männik, P. and Viira, V. 1993. Events in the conodont history during the Silurian in Estonia. *Proceedings of the Estonian Academy of Sciences. Geology*, **42**(2), 58–69. https://doi.org/10.3176/geol.1993.2.03

Männik, P., Põldvere, A., Nestor, V., Kallaste, T., Kiipli, T. and Martma, T. 2014. The Llandovery–Wenlock boundary interval in the west-central continental Estonia: an example from the Suigu (S-3) core section. *Estonian Journal of Earth Sciences*, **63**(1), 1–17. https://doi.org/10.3176/earth.2014.01

Männik, P., Meidla, T. and Hints, O. 2024. The Silurian System in Estonia: recent developments and challenges. In *11th Baltic Stratigraphical Conference, Tartu, Estonia, 19–21 August 2024. Abstracts and Field Guide* (Hints, O., Männik, O. and Toom, U., eds). Geological Society of Estonia, Tallinn, 60–64.

Märss, T. 1986. Silurian vertebrates of Estonia and West Latvia. *Fossilia Baltica*, **1**, 1–104.

Märss, T. 1992. Vertebrate history in the Late Silurian. *Proceedings of the Estonian Academy of Sciences. Geology*, **41**(4), 205–214. https://doi.org/10.3176/geol.1992.4.05

Märss, T. and Männik, P. 2013. Revision of Silurian vertebrate biozones and their correlation with the conodont succession. *Estonian Journal of Earth Sciences*, **62**(4), 181–204. https://doi.org/10.3176/earth.2013.15

Meidla, T., Ainsaar, L. and Hints, O. 2014a. The Ordovician System in Estonia. In *4th Annual Meeting of IGCP 591, Tartu, Estonia, 10–19 June 2014. Abstracts and Field Guide* (Bauert, H., Hints, O., Meidla, T. and Männik, P., eds). University of Tartu, Tartu, 116–122.

Meidla, T., Tinn, O., Männik, P. and Einasto, R. 2014b. Stop B7. Suuriku and Undva cliffs. In *4th Annual Meeting of IGCP 591, Tartu, Estonia, 10–19 June 2014. Abstracts and Field Guide* (Bauert, H., Hints, O., Meidla, T. and Männik, P., eds). University of Tartu, Tartu, 190–193.

Meidla, T., Truuver, K., Tinn, O. and Ainsaar, L. 2020. Ostracods of the Ordovician–Silurian boundary beds: Jūrmala core (Latvia) and its implications for Baltic stratigraphy. *Estonian Journal of Earth Sciences*, **69**(4), 233–247. https://doi.org/10.3176/earth.2020.20

Meidla, T., Hints, O. and Ainsaar, L. 2023a. Searching for the Ordovician–Silurian boundary in Estonia, Latvia and Lithuania. *Estonian Journal of Earth Sciences*, **72**(1), 70–73. https://doi.org/10.3176/earth.2023.53

Meidla, T., Ainsaar, L., Hints, O. and Radzevičius, S. 2023b. Ordovician of the Eastern Baltic palaeobasin and the Tornquist Sea margin of Baltica. In *A Global Synthesis of the Ordovician System: Part 1* (Harper, D. A. T., Lefebvre, B., Percival, I. G. and Servais, T., eds). Geological Society, London, Special Publications, 532, 317–343. https:// doi.org/10.1144/SP532-2022-141

Melchin, M. J. and Holmden, C. 2006. Carbon isotope chemostratigraphy of the Llandovery in Arctic Canada: implications for global correlation and sea-level change. *GFF*, **128**(2), 173–180. http://dx.doi.org/10.1080/11035890601282173

Melchin, M. J., Cooper, R. A. and Sadler, P. M. 2004. The Silurian period. In *A Geological Time Scale 2004* (Gradstein, F. M., Ogg, J. G. and Smith, A. G., eds). Cambridge University Press, Cambridge, 188–201.

Melchin, M. J., Sadler, P. M. and Cramer, B. D. 2020. The Silurian period. In *Geologic Time Scale 2020* (Gradstein, F. M., Ogg, J. G., Schmitz, M. and Ogg, G., eds). Elsevier, 695–732. https://doi.org/10.1016/B978-0-12-824360-2.00021-8

Murphy, M. A., Valenzuela-Ríos, J. I. and Carls, P. 2004. *On Classification of Pridoli (Silurian)–Lochkovian Spathognathodontidae (Conodonts)*. University of California, Riverside.

Nestor, H. 1972. On the stratigraphic range of the beds with *Pentamerus oblongus* and on the nature of the Late Llandoverian transgression in North Europe. *Proceedings of the Academy of Sciences of the Estonian SSR. Chemistry, Geology*, **21**(4), 344–350.

Nestor, H. 1990. Locality 9:1. Silurian sequences at Särghaua field station. In *Field Meeting, Estonia 1990. An Excursion Guidebook* (Kaljo, D. and Nestor, E., eds). Estonian Academy of Sciences, Tallinn, 184–186.

Nestor, H. 1993. *Catalogue of Silurian Stratigraphic Units and Stratotypes in Estonia and Latvia*. Estonian Academy of Sciences, Tallinn.

Nestor, H. 1995. Comments on the modernised Silurian correlation chart of Estonia and Latvia. *Geologija*, **17**, 88–95.

Nestor, H. 1997. Silurian. In *Geology and Mineral Resources of Estonia* (Raukas, A. and Teedumäe, A., eds). Estonian Academy Publishers, Tallinn, 89–106.

Nestor, H. and Einasto, R. 1977. Facies-sedimentary model of the Silurian Paleobaltic pericontinental basin. In *Facies and Fauna*

of the Baltic Silurian (Kaljo, D., ed.). Academy of Sciences of the Estonian SSR, Institute of Geology, Tallinn, 89–121.

Nestor, H. and Einasto, R. 1997. Ordovician and Silurian carbonate sedimentation basin. In *Geology and Mineral Resources of Estonia* (Raukas, A. and Teedumäe, A., eds). Estonian Academy Publishers, Tallinn, 192–204.

Nestor, H. and Nestor, V. 2002. Upper Llandovery to middle Wenlock (Silurian) lithostratigraphy and chitinozoan biostratigraphy in southwestern Estonia and northernmost Latvia. *Proceedings of the Estonian Academy of Sciences. Geology*, **51**(2), 67–87. https://doi.org/10.3176/geol.2002.2.01

Nestor, H., Einasto, R., Nestor, V.-K., Märss, T. and Viira, V. 2001. Description of the type section, cyclicity, and correlation of the Riksu Formation (Wenlock, Estonia). *Proceedings of the Estonian Academy of Sciences. Geology*, **50**(3), 149–173. https://doi.org/10.3176/geol.2001.3.02

Nestor, H., Einasto, R., Männik, P. and Nestor, V.-K. 2003. Correlation of lower–middle Llandovery reference sections in central and southern Estonia and sedimentation cycles of lime muds. *Proceedings of the Estonian Academy of Sciences. Geology*, **52**(1), 3–27. https://doi.org/10.3176/geol.2003.1.01

Nestor, V. 1994. *Early Silurian Chitinozoans of Estonia and North Latvia*. Estonian Academy Publishers, Tallinn.

Nestor, V. 2010. Distribution of Silurian chitinozoans. In *Viki Drill Core* (Põldvere, A., ed.). *Estonian Geological Sections Bulletin*, 10. Geological Survey of Estonia, Tallinn, 19–21.

Nestor, V. 2011. Chitinozoan biostratigraphy of the Přídolí Series of the East Baltic. *Estonian Journal of Earth Sciences*, **60**(4), 191–206. https://doi.org/10.3176/earth.2011.4.01

Nestor, V. 2012. A summary and revision of the East Baltic Silurian chitinozoan biozonation. *Estonian Journal of Earth Sciences*, **61**(4), 242–260. https://doi.org/10.3176/earth.2012.4.05

Nestor, V. and Nestor, H. 1991. Dating of the Wenlock carbonate sequences in Estonia and stratigraphic breaks. *Proceedings of the Estonian Academy of Sciences. Geology*, **40**(2), 50–60. https://doi.org/10.3176/geol.1991.2.03

Paškevičius, J., Lapinskas, P., Brazauskas, A., Musteikis, P. and Jacyna, J. 1994. Stratigraphic revision of the regional stages of the Upper Silurian part in the Baltic Basin. *Geologija*, **17**, 64–87.

Perens, H. 1992. Raikküla Regional Stage (Llandovery) and its lithostratigraphy in the outcrop area. *Bulletin of the Geological Survey of Estonia*, **2**(1), 27–31.

Perens, H. 1995. Transition beds of Jaani and Jaagarahu regional stages on Saaremaa Island. *Bulletin of the Geological Survey of Estonia*, **5**(1), 12–19.

Põldvere, A. (ed.) 2010. *Viki Drill Core*. *Estonian Geological Sections Bulletin*, 10. Geological Survey of Estonia, Tallinn.

Resolution of the interdepartmental regional stratigraphical conference on the elaboration of the unified stratigraphical schemes for East Baltic, 1976. 1978. Litovskij NIGRI, Leningrad.

Rong, J. Y., Melchin, M., Williams, S. H., Koren, T. N. and Verniers, J. 2008. Report of the restudy of the defined global stratotype of the base of the Silurian System. *Episodes*, **31**(3), 315–318. https://doi.org/10.18814/epiiugs/2008/v31i3/005

Sadler, P. M. 2012. Integrating carbon isotope excursions into automated stratigraphic correlation: an example from the Silurian of Baltica. *Bulletin of Geosciences*, **87**(4), 681–694. https://doi.org/10.3140/bull.geosci.1307

Schmidt, F. 1858. *Untersuchungen über die Silurische Formation von Ehstland, Nord-Livland und Oesel*. Heinrich Laakmann, Dorpat.

Schmidt, F. 1881. *Revision der ostbaltischen silurischen Trilobiten nebst geognostischer Übersicht des ostbaltischen Silurgebiets*. Abt. I. Mémoires de l'Académie impériale des sciences de St.-Pétersbourg, St. Petersburg.

Schmidt, F. 1892. Einige Bemerkungen über das baltische Obersilur in Verlassung der Arbeit des Prof. W. Dames über die Schichtenfolge der Silurbildungen Gotlands. *Bulletin de l'Académie impériale des sciences de St.-Pétersbourg*, **34**, 381–400.

Štorch, P., Loydell, D. K., Melchin, M. J. and Goldman, D. 2024. Graptolites in biostratigraphy: the primary tool for subdivision and correlation of Ordovician, Silurian, and Lower Devonian offshore marine successions. *Newsletters on Stratigraphy*. https://doi.org/10.1127/ nos/2024/0810

Stratigraphic Code of the USSR. 1977. VSEGEI, Leningrad.

Torsvik, T. H. and Cocks, L. R. M. 2013. New global palaeogeographical reconstructions for the Early Palaeozoic and their generation. In *Early Palaeozoic Biogeography and Palaeogeography* (Harper, D. A. T. and Servais, T., eds). Geological Society, London, Memoirs, 38, 5–24. https://doi.org/10.1144/M38.2

Viira, V. 1999. Late Silurian conodont biostratigraphy in the northern East Baltic. *Bollettino della Società Paleontologica Italiana*, **37**(2–3), 299–310.

Viira, V. and Aldridge, R. J. 1998. Upper Wenlock to Lower Přídolí (Silurian) conodont biostratigraphy of Saaremaa, Estonia, and a correlation with Britain. *Journal of Micropalaeontology*, **17**(1), 33–50. https://doi.org/10.1144/jm.17.1.33

Viira, V. and Einasto, R. 2003. Wenlock–Ludlow boundary beds and conodonts of Saaremaa Island, Estonia. *Proceedings of the Estonian Academy of Sciences. Geology*, **52**(4), 213–238. https://doi.org/10.3176/geol.2003.4.03

Walasek, N., Loydell, D. K., Frýda, J., Männik, P. and Loveridge, R. F. 2018. Integrated graptolite-conodont biostratigraphy and organic carbon chemostratigraphy of the Llandovery of Kallholn quarry, Dalarna, Sweden. *Palaeogeography, Palaeoclimatology, Palaeoecology*, **508**, 1–16. https://doi.org/10.1016/j.palaeo.2018.08.003

Zalasiewicz, J. A., Taylor, L., Rushton, A. W. A., Loydell, D. K., Rickards, R. B. and Williams, M. 2009. Graptolites in British stratigraphy. *Geological Magazine*, **146**(6), 785–850. https://doi.org/10.1017/S0016756809990434

Eesti Siluri kihtide uuendatud korrelatsiooniskeem

Peep Männik, Tõnu Meidla ja Olle Hints

Viimastel aastakümnetel kogutud geoloogiline informatsioon tingis vajaduse Eestis kasutusel oleva Siluri stratigraafilise skeemi täiendamiseks ja täpsustamiseks. Uue andmestiku analüüsil selgus, et (1) Juuru lademe alumised kihid on Hilis-Ordoviitsiumi Hirnanti vanusega; (2) Raikküla lademe alumise piiri vanus vajab täpsustamist; (3) Aeroni ja Telychi vaheline piir Eestis vastab tasemele Rumba kihistu keskel; (4) Adavere lademe basaalne osa on Hilis-Aeroni vanusega; (5) seni Jaagarahu lademe alumiseks piiriks loetud tase on ajas nihkuv, selle piiri määramise parimaks biostratigraafiliseks tunnuseks on praegu konodondi *J. s. rhenana* ilmumine läbilõikes; (6) Wenlocki ja Ludlow' vaheline piir Eesti läbilõikes vastab tasemele Rootsiküla lademe ülemises osas; (7) Paadla lademe alumine piir korreleerub tasemega Gorsty ülemises osas, tasemega *Ph. ornata* tsooni alumises (?) osas; (8) Paadla kihistu Sauvere ja Himmiste kihid on Hilis-Gorsty vanusega, sama kihistu Uduvere kihid vastavad intervallile Ludfordi alumises osas (osale *A. ploeckensis* konodonditsoonist); (9) Ludlow' ja Přidoli vaheline piir Eesti läbilõikes vastab tõenäoliselt tasemele Kuressaare lademe sees, kuid piiri täpse asendi määramiseks usaldusväärsed tunnused seni puuduvad.

Estonian Journal of Earth Sciences
2026, **75**, 1, 35–52

https://doi.org/10.3176/earth.2026.03

www.eap.ee/earthsciences
Estonian Academy Publishers

RESEARCH ARTICLE

Received 7 July 2025
Accepted 14 October 2025
Available online 7 January 2026

Keywords:
coastal erosion, progradation, palaeospits, palaeofires, shell dating, Holocene, Baltic Sea

Corresponding author:
Ülo Suursaar
ulo.suursaar@ut.ee

Citation:
Suursaar, Ü., Luik, K., Rosentau, A., Alexanderson, H., Rivis, R., Vaasma, T. et al. 2026. Morphostratigraphy and chronology of depositional and erosional events at the Järve scarp (Saaremaa, western Estonia) over the past 2000 years. *Estonian Journal of Earth Sciences*, **75**(1), 35–52.
https://doi.org/10.3176/earth.2026.03

Morphostratigraphy and chronology of depositional and erosional events at the Järve scarp (Saaremaa, western Estonia) over the past 2000 years

Ülo Suursaar[a,b], Katre Luik[a], Alar Rosentau[c], Helena Alexanderson[d], Reimo Rivis[a], Tiit Vaasma[a], Egert Vandel[a], Kadri Vilumaa[a], Donatas Pupienis[e] and Hannes Tõnisson[a]

[a] Institute of Ecology, School of Natural Sciences and Health, Tallinn University, Narva mnt 29, 10120 Tallinn, Estonia

[b] Estonian Marine Institute, Faculty of Science and Technology, University of Tartu, Mäealuse 14, 12618 Tallinn, Estonia

[c] Institute of Ecology and Earth Sciences, Faculty of Science and Technology, University of Tartu, J. Liivi 2, 50409 Tartu, Estonia

[d] Department of Geology, Lund University, Sölvegatan 12, 22362 Lund, Sweden

[e] Institute of Geosciences, Faculty of Chemistry and Geosciences, Vilnius University, M. K. Čiurlionio g. 21, 03101 Vilnius, Lithuania

ABSTRACT

Influenced by climate warming and sea-level rise, seacoasts in many parts of the world are undergoing regime shifts, including increased coastal erosion in the southeastern Baltic Sea. The aim of this study is to reconstruct the depositional and erosional history of the Järve coastal scarp using sediment stratigraphy, new luminescence and radiocarbon dates, ground-penetrating radar, and LiDAR data. The seaward ridge, where the 3.5-m-high sandy scarp is located, began to form around 1600 years ago, in front of a 3500–4000-year-old palaeospit system that developed through sediment accumulation and postglacial uplift. The lower section of the outcrop was deposited in the shallow nearshore zone, where underwater sandbars acted as nuclei for spit formation. Darker sediment layers and variations in lamination patterns reflect changes in sediment sources and storm activity. Above the marine-deposited sandy layers lies a thin aeolian unit, which is only weakly developed at the Järve outcrop. Dune features occur only in a few blowouts, likely associated with the Little Ice Age (~1300–1850 CE) and anthropogenic vegetation disturbance, such as logging or slash-and-burn agriculture. Over the past ~100 years, the formerly emergent system of beach ridges and spits has shifted to an erosional regime. The earlier relative sea-level fall has ceased, seasonal sea ice is diminishing, the impacts of winter storms are intensifying, and the scarp is retreating. This study demonstrates how global changes are manifested on seacoasts at a local scale and highlights methodological difficulties in using seashells for coastal stratigraphic dating.

1. Introduction

Coastal accumulation landforms, such as spits, beach ridges, and foredune plains, serve as morphological and sedimentary archives of past climatological and oceanographic conditions (Buynevich et al. 2004, 2023; Tamura 2012; Dougherty 2014; Clemmensen et al. 2015; Kalińska et al. 2024). Using various stratigraphic and chronological methods, GIS-based analysis of LiDAR elevation data, and ground-penetrating radar (GPR) surveys, it is possible to reconstruct the successive stages of the development of these landforms in response to forcing conditions and sediment availability (Rosentau et al. 2013; Muru et al. 2018; Suursaar et al. 2022; Luik et al. 2025). Deciphering signs of environmental change in coastal landscapes is especially important in the current era of rising sea levels, changing climate, and their extensive impacts on society (e.g. IPCC 2021; Costas 2022; Różyński 2023).

In many parts of the world, the coastal stretches that until recently experienced a net seaward progradation, either due to sediment accretion or uplift-driven land emergence, may now be entering a phase of coastal erosion (e.g. Morton et al. 2004;

Weisse et al. 2021). Such shifts can occur due to relative sea-level rise or a sediment deficit of variable origin. For instance, on the coasts of the southern and southeastern Baltic Sea, adverse effects of coastal erosion and dune destruction have been reported since at least the 1990s (Eberhards and Saltupe 1995; Furmanczyk and Musielak 2002; Różyński 2023; Uścinowicz et al. 2024). On the seacoasts of Estonia, the present-day isostatic postglacial uplift component (1.3–3.5 mm/a; Suursaar and Kall 2018; Vestøl et al. 2019) has so far mostly exceeded the eustatic global sea-level (GSL) rise component (~1.7 mm/a during the 20th century; IPCC 2021). However, according to recent satellite-based estimates, the GSL has accelerated to ~3.4 mm/a between 1993 and 2024 (Willis et al. 2024). Consequently, Estonia's land surface area is no longer increasing as it did throughout the Middle and Late Holocene (over the past ~7000 years). In combination with changing storminess and decreasing ice cover (Jaagus and Suursaar 2013; Suursaar et al. 2015; Tõnisson et al. 2024a), the seacoasts are becoming increasingly erosional. Such coastal systems offer a unique opportunity to study past climate events (e.g. storms) and regime shifts by juxtaposing relict accretional landforms with recent erosional evidence (e.g. Buynevich et al. 2023).

The Järve coast in southern Saaremaa (Fig. 1) is an illustrious example of such shifts, where a system of palaeospits emerged from the sea ~3500 years ago. Over time, the barrier gradually grew and fused with the main part of Saaremaa due to postglacial uplift and sediment accretion, eventually becoming erosional on its southern side. This transition likely occurred by the 1940s–1950s, as the local relative sea level began to rise at Järve and the duration of seasonal ice cover significantly decreased (Luik et al. 2024a; Tõnisson et al. 2024a; Suursaar et al. 2025). A photo (fig. 10B in Luik et al. 2025) shows the 4-m-high Järve scarp streaked with several near-horizontal dark layers, which could hypothetically reflect shifts in the formation of the palaeospit, and possibly past storm events. However, the age, origin, and lithological characteristics of these streaks were not analysed in detail in that otherwise extensive study. Based on previous dating from the Järve interior (Luik et al. 2025), it was suggested that the age of landforms that run along the present day coastline is ~2000 years at Järve (Fig. 1). However, there was at least a 1500-year-long gap in dating due to a more recent transition from accretion to coastal erosion.

To fill the gap revealed by previous studies (Orviku 2006; Luik et al. 2025), additional fieldwork was conducted in

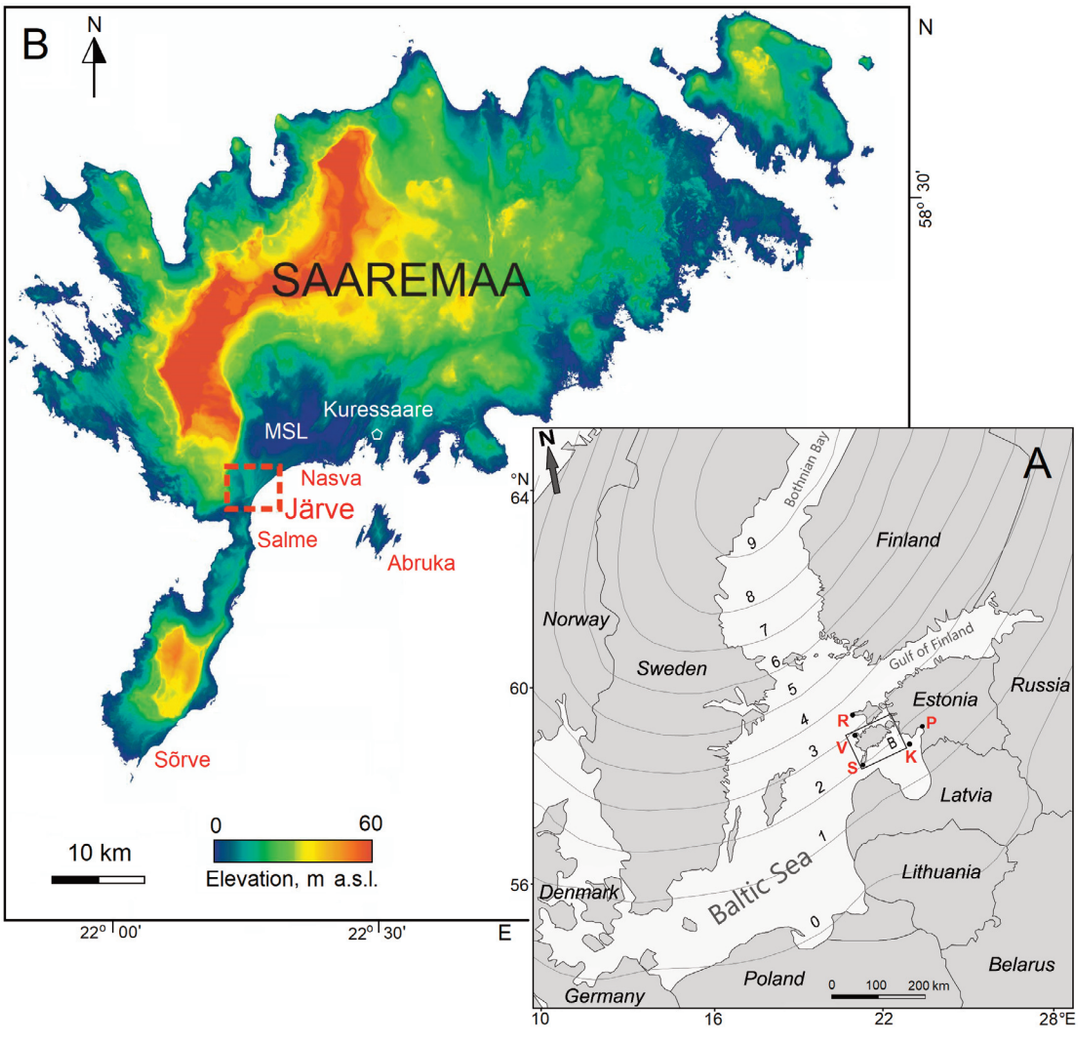

Fig. 1. Location of Saaremaa Island in the Baltic Sea with the present-day isobases (mm/a) according to the NKG2016LU_lev land uplift model (Vestøl et al. 2019). Coastal hydrometeorological stations (A): R – Ristna, V – Vilsandi, S – Sõrve, K – Kihnu, P – Pärnu. LiDAR-based elevation map of Saaremaa (B) with the Järve area (see Fig. 2) marked with a rectangle. MSL – Mullutu-Suurlaht Lagoon.

December 2024 to further investigate the geomorphic history revealed by the Järve outcrop. The aims of this study are: (1) to reconstruct the depositional and erosional events of the Järve palaeospit based on new optically stimulated luminescence (OSL) and radiocarbon (^{14}C) dates, as well as a lithological description of the outcrop; (2) to interpret the occurrences of different layers (streaks) in the outcrop in relation to possible climatic and oceanographic shifts or extreme events; and (3) to discuss the processes related to the transition from coastal progradation/accretion to erosion, which is expected to occur at an accelerating pace in many areas around the world.

2. Materials and methods

2.1. Geological and climatological setting of the study area

The study area, located along the Järve coast in Saaremaa, Estonia, is a dynamic coastal system that has been shaped by postglacial land emergence, coastal progradation, and sedimentary processes over the past 4000 years (i.e. roughly the Limnea Sea stage of the Baltic Sea; e.g. Hang et al. 2020). Saaremaa, the fourth largest island in the Baltic Sea, is part of the West Estonian Archipelago and currently covers an area of ~2673 km^2. Geologically, Saaremaa lies at the edge of the Fennoscandian Shield, where the crystalline basement consists mainly of metamorphic rocks and granite (Kalm 2006). This basement is covered by Silurian limestone and a relatively thin Quaternary sediment layer. The area's subsequent geological evolution was closely related to the development stages of the Baltic Sea basin following the Late Weichselian glaciation and subsequent shoreline changes driven by eustatic sea-level fluctuations, postglacial rebound, and alteration between oceanic and dammed-up limnic conditions (Kalm 2006; Rosentau et al. 2009, 2020; Andrén et al. 2011). In the study area, falls in water level were interrupted by the Lake Ancylus and Littorina Sea transgressions (~10 700–10 200 and ~8500–7300 years ago, respectively; Saarse et al. 2009; Hang et al. 2020; Harff et al. 2020). Filling a buried ancient valley, the Quaternary cover below the Järve area is relatively thick (20–40 m). Serving as a local depot for sandy sediment, it is overlain by more recent moraine and laminated Littorina sediment (Suuroja et al. 2020). Subsequently, this sedimentary complex has been raised by glacio-isostatic uplift to the zone of active coastal processes and ultimately above sea level.

Throughout the Middle and Late Holocene, the surface area of Saaremaa has been increasing, with smaller islands and shoals gradually emerging from the sea and merging with one another. The retreating ice sheet left behind extensive deposits of morainic and glaciofluvial sediments, which were subsequently reshaped by wave action, currents, and wind, giving rise to various accretional landforms (Raukas 2000). The Järve region (Fig. 1) is characterised by a sequence of elevated accretional palaeospits (Fig. 2), primarily composed

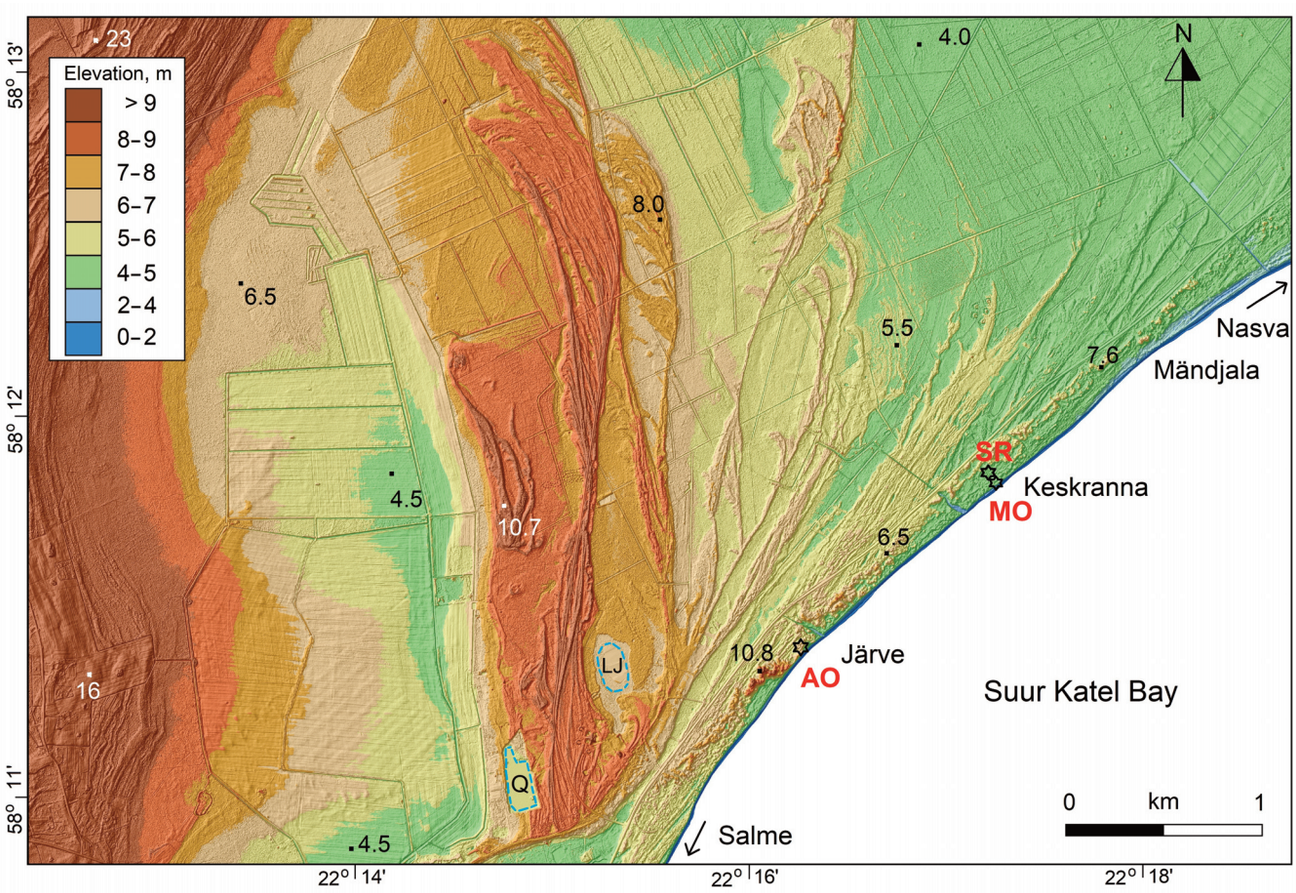

Fig. 2. LiDAR-based digital elevation model of the Järve study area (a few elevation marks are added). Locations of fieldwork: MO – master outcrop, SR – scarp rim, AO – additional outcrop; GPR profiles run between the MO and SR. LJ – Lake Järve, Q – quarry. Elevation at the main blowout near the AO is 10.8 m relative to the EH2000 datum. Arrows point towards the Salme and Nasva locations.

of marine sands interspersed with thin gravel layers, reaching heights of 10–11 m above present sea level (Luik et al. 2025). The Järve study area, located ~10–15 km west-southwest of Kuressaare, the island's largest town, borders a shallow bay in the Gulf of Riga known as Suur Katel. Coastal waters here are relatively shallow, with depths of less than 5 m extending 2–3 km from the shoreline. The area features a sandy beach, ~20–30 m wide, backed by sandy ridges and foredunes stretching ~8 km in length. The seaward ridge is predominantly 4–5 m high, with its highest point reaching 10.8 m above sea level at a blowout (Fig. 2). At Järve, wave action has eroded a scarp into earlier coastal sediments.

Although south-westerly and westerly winds dominate in Estonia, with an average wind speed in Saaremaa of ~6 m/s (Tarand et al. 2013), the Järve coast is currently predominantly influenced by winds and waves approaching from the south, and to a lesser degree from the southwest or southeast. Winds from the west–northwest–north–northeast sector, which is sheltered by land, practically do not excite waves at Järve. Due to the shallowness of the Suur Katel Bay and relatively short fetch distances (50 km to the south; the potentially up to 150 km fetch to the southeast is considerably hindered by Abruka Island), the long-term mean significant wave height near Järve is less than 0.4 m, and the maximum is up to 1 m (Najafzadeh et al. 2024). Hence, the Järve coast is a relatively well-sheltered, tideless, low-energy coast, where storm surges can occasionally reach heights of up to 1.6 m during extreme winter storms, such as the cyclone Gudrun on 9–10 January 2005 (Suursaar et al. 2006). The long-term annual mean temperature at the meteorological station in Sõrve (Fig. 1) is 7.5 °C, and it has increased by 0.037 degrees per year between 1951 and 2020 (Tõnisson et al. 2024a). The long-term average annual precipitation is ~590 mm, which slightly exceeds potential evaporation. Consequently, the foredunes and beach ridges become vegetated relatively fast, which is also favoured by relatively modest amounts of shifting sands. Due to the warming climate, the duration of both snow and ice cover has considerably declined in the area over the past seventy years. One consequence of this is that, particularly in winter, wave and hydrodynamic loads on the coastal zone have increased (Najafzadeh and Soomere 2024; Suursaar et al. 2025). Secondly, coastal sediment tends to persist for a shorter period in a frozen and more solid state (Tõnisson et al. 2024a).

The development of the Järve shoal, which soon evolved into an island, began ~4000 years ago. As the sea level fell, sediments from the emerging sea floor were reworked by waves from various directions into beach ridges and spits (Luik et al. 2025). About 3000 years ago, the expanding spit system had connected with Saaremaa. The gradual emergence of the Sõrve Peninsula and the ultimate closure of the Salme Strait (Nirgi et al. 2022) sheltered the Järve area from westerly wind and wave forcing. Sediment accumulation gradually shifted eastward, infilling shallow marine areas at Mändjala and extending the coastal barrier, which contributed to the isolation of the Mullutu-Suurlaht Lagoon by ~1600 CE (Suursaar et al. 2024). At the same time, intensification of dune formation occurred, likely influenced by the Little Ice Age (LIA; usually considered to be between 1300 and 1850 CE) and anthropogenic factors such as deforestation (Jackson et al. 2019; Tõnisson et al. 2020; Luik et al. 2025). However, since the end of the LIA, rising air temperatures, reduced seasonal ice cover, and accelerating global sea-level rise have increasingly affected coastal processes (Tõnisson et al. 2024a). Although the Järve area is still undergoing postglacial isostatic rebound, with current geocentric uplift rates estimated at 2–2.3 mm/a (Suursaar and Kall 2018; Vestøl et al. 2019), this is compensated for, and even exceeded by, the ongoing sea-level rise (Luik et al. 2024a). Local relative sea-level (RSL) rise has caused a shift towards sediment deficit at Järve, as there is insufficient sediment being supplied from the nearshore sea bottom. However, during extreme storms, such as those in 1990, 1999, 2005, and 2007, the scarp erodes at rates of ~1–5 m per event, and the released sediment is transported eastward towards Mändjala and Nasva Port (Tõnisson et al. 2008; Suuroja et al. 2020; Luik et al. 2025). For a while, the cleaned-up scarp reveals some darker, gravelly streaks. Afterwards, the sandy scarp usually becomes levelled until the next erosion event forces it to steepen and migrate landward again (Tõnisson et al. 2024a).

2.2. Fieldwork, sedimentological analysis and chronology

This study builds upon fieldwork conducted between the 1990s and 2024, the results of which were partially presented in an earlier publication (Luik et al. 2025) and a data repository (Luik et al. 2024b). In this study, we present new results specifically focused on describing the Järve scarp, including new luminescence and radiocarbon dates obtained in December 2024 (Fig. 3). Another main aim was to document the apparent streaks in the scarp (Fig. 4) and to relate them to the development stages of the Järve coast and to varying forcings.

Fieldwork at the study site (Figs 2 and 3; 58° 11′ 53″ N, 22° 17′ 14″ E) was conducted on 4–5 December 2024. During excavation, the scarp talus was cleared of debris, and a near-vertical outcrop was exposed at elevations ranging from ~0.8 m to 3.6 m (in the EH2000 height system, relative to the Normaal Amsterdams Peil). The outcrop's lithology was described visually on-site, with sediment structure and grain size determined according to the Udden–Wentworth grade scale. The stratigraphic sequence was documented by measuring the thickness of each layer and recording the absolute elevation of stratigraphic boundaries and surfaces using a Leica GS09 RTK-GPS.

A total of 16 sand samples were collected for subsequent granulometric analysis in the laboratory using a Fritsch Analysette 3 PRO sieving apparatus. Before processing, the samples were dried at 60 °C. A set of standard mesh sizes (2000, 1000, 500, 250, 125, 63, and 36 μm) was used for fraction separation. After weighing and calculating the weight percentages of each fraction, statistical grain-size parameters were determined using the arithmetic method of moments in the GRADISTAT 8.0 software (Blott and Pye 2001).

An additional outcrop (AO in Fig. 2; 58° 11′ 25″ N, 22° 16′ 16″ E), located ~1.2 km southwest of the master

Fig. 3. Setting of the master outcrop (the sea-facing profile, marked with a red dashed line, is partly obscured); GPR instrument shown on the left. Fallen trees in the background indicate recent scarp erosion. Photo by Ü. Suursaar, 4 December 2024.

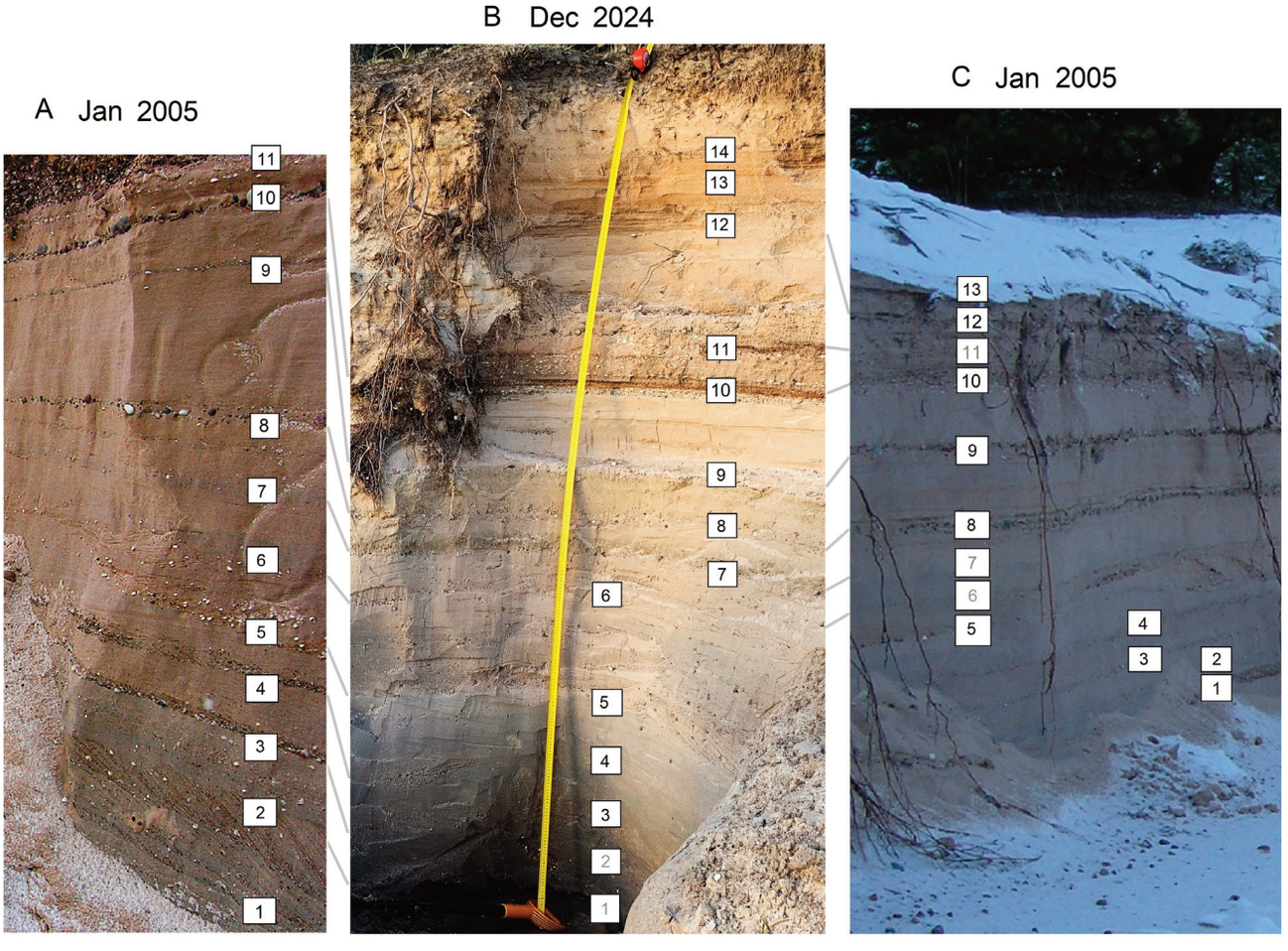

Fig. 4. Correlation of the storm or regime shift streaks (interbeds) on photos taken on 25 January 2005 (A, C; two different locations near the master outcrop, exact locations unknown) and on 4 December 2024 (B). Photos by K. Orviku (A), Ü. Suursaar (B), and H. Tõnisson (C).

Table 1. Radiocarbon (^{14}C) and luminescence (OSL) samples taken at the Järve scarp area. SE – sample elevations in the EH2000 system. Short codes R1* and L1* correspond to R1 and L1 in Luik et al. (2025)

Type	Code	Lab code	SE, m	Material	Reference
MO – master outcrop (58°11'53" N, 22°17'14" E)					
^{14}C	C1	FTMC-XK54-1	0.80	Shells	This study
^{14}C	C2	FTMC-XK54-2	1.69	Shells	This study
^{14}C	C3	FTMC-XK54-3	2.05	Shells	This study
^{14}C	C4	FTMC-XK54-4	2.45	Shells	This study
^{14}C	C5	FTMC-XK54-5	2.90	Shells	This study
OSL	L1	25003Q	1.78	Sand	This study
OSL	L2	25004Q	2.31	Sand	This study
SR – master outcrop scarp rim (58°11'56" N, 22°17'11" E)					
^{14}C	R1*	Poz-114329	4.01	Charcoal	Luik et al. (2025)
OSL	L1*	SJ15-OSL1	3.01	Sand	Luik et al. (2025)
AO – additional outcrop (58°11'25" N, 22°16'16" E)					
^{14}C	C6	FTMC-HC21-2	5.35	Charcoal	This study
OSL	L3	25001Q	5.13	Sand	This study
OSL	L4	25002Q	5.57	Sand	This study

outcrop (MO), was partially cleaned and examined. From this secondary exposure, one radiocarbon and two OSL samples were collected. In total, four samples for luminescence dating were collected from sand deposits at the two outcrops (Table 1) using opaque PVC tubes (30 cm in length, 5 cm in diameter), which were inserted horizontally into the outcrop. Sampling depths were chosen to capture the point at which sand grains were likely no longer exposed to direct sunlight. Once extracted, the tube ends were sealed with duct tape and stored in darkness until analysis.

The luminescence analyses were conducted at the Lund Luminescence Laboratory, Lund University, Sweden. Sample preparation included sieving, treatment with 10% HCl, 10% H_2O_2, 10% and 40% HF, and density separation at 2.62 and 2.58 g/cm^3 (LST Fastfloat; Murray et al. 2021). Small (2 mm) single aliquots of quartz and K-feldspar grains were analysed in Risø TL/OSL readers, model DA-20, using single aliquot regeneration (SAR) protocols. Post-IR blue stimulation with 220 °C pre-heat and 180 °C cut-heat temperatures was used for quartz (Murray and Wintle 2000, 2003; Roberts and Wintle 2001), and a post-$IR_{50}IR_{225}$ protocol was used for K-feldspar (Buylaert et al. 2009). Doses were calculated using the Risø Analyst 4.57 software with exponential curve fitting; the first 0.48 s of the signal were integrated for the peak, and the last 4 s for background. Aliquots with a recycling ratio within 10% of unity, a test dose error <10%, and a relative dose error <30% were accepted. Sediment dose rates were determined with a dual α/β scintillator μDose instrument (Tudyka et al. 2018), and total environmental dose rates and ages were calculated using the DRAC online calculator v1.2 (Durcan et al. 2015). Average water content was assumed to be similar to or slightly higher than that at the time of sampling. Ages were calculated based on the mean dose and the central age model (CAM; Galbraith et al. 1999) using the function calc_CentralDose v.1.4.1 (Kreutzer et al. 2025).

For comparison and verification of the dates, five seashell samples were taken from the MO and one charcoal sample from the AO (see Fig. 5A; Table 1) for radiocarbon dating. The analyses were conducted at the Vilnius Radiocarbon Laboratory, Lithuania, using a single-stage accelerator mass spectrometer (SSAMS; NEC, USA) and automated graphitisation equipment AGE-3 (Ionplus AG, Switzerland). Following chemical preparation, the samples were treated with phosphoric acid and subsequently graphitised. Reference materials IAEA C2, SIRI K, and NIST-OXII were used throughout the process. The calculated ^{14}C ages were calibrated into calendar years using the IntCal20 calibration curve (Reimer et al. 2020) in the OxCal v.4 online software, and presented alongside with their 68.3% probability limits. Table 1 also includes two earlier samples taken from the scarp rim (SR in Fig. 2), located a few dozen metres inland from the MO, previously presented by Luik et al. (2025).

Providing additional data on layering in the deposits, two GPR profiles were taken along a 50 m transect across the scarp, ~10 m west of the outcrop, and parallel to the scarp on top of its rim. The two GPR profiles cross each other ~15 m northwest from the outcrop (roughly between the MO and SR; Fig. 2) at 58° 11′ 53″ N, 22° 17′ 13″ E. An ImpulseRadar (model CO730) was used with transceivers operating at 70 and 300 MHz, featuring ranges up to 400 ns and a trace spacing of 0.02 m (for details, see Muru et al. 2018). The digital GPR data were post-processed and visualised using GPR-SLICE software.

To assess heavy mineral concentration (HMC) in sand sediments, vertical profiles of low-field magnetic susceptibility (MS) were determined using two devices. Twenty-nine samples were collected across the entire profile at 10 cm intervals and later analysed in the laboratory for MS using a Bartington MS3 meter with MS2K surface scanning sensor (Pupienis et al. 2017). The measurements were performed at constant room air temperature; each sample was measured three times, and the final MS value represents the average of three readings. After every nine measurements, the instrument was reset and calibrated using a calibration sample provided

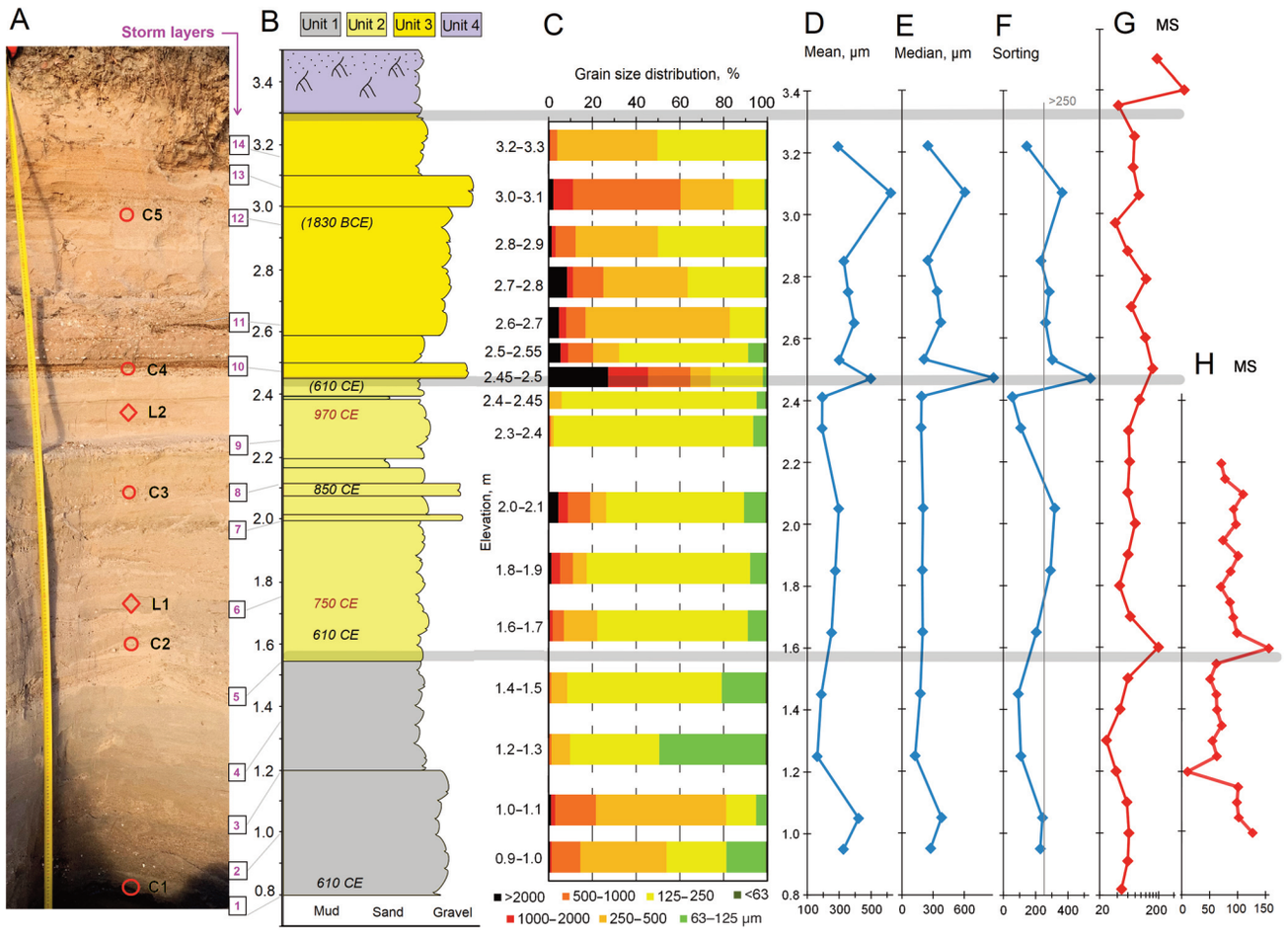

Fig. 5. Photo of the Järve outcrop (A) showing the locations of radiocarbon (C1–C5) and OSL (L1, L2) dates, as well as enumerated interbeds or storm layers (1–14; see also Fig. 4). Note that the vertical scale varies slightly in the slant photo (A). Sediment stratigraphy (B) and granulometry (C–F) of the Järve scarp are based on sand sample analyses. The boundaries of the sedimentary units (1–4) are marked with thick grey lines. The obtained dates are shown in B; the radiocarbon ages C4–C5 are not reliable (see Discussion) and therefore appear in parentheses. Magnetic susceptibility (MS, values in 10^{-6} SI units) is presented in G and H (log scale in G). Photo by Ü. Suursaar, 4 December 2024.

by the manufacturer (Dearing 1999). Bulk MS serves as a reliable indicator of allochthonous mineral matter in sediments and thus probable storm layers (Pupienis et al. 2017; Buynevich et al. 2023). Measurements were also taken on-site using a magnetic susceptibility meter SM-30 (ZH instruments, Czech Republic). Readings were taken every 5 cm in the lower half of the pit, at elevations ranging from 1 to 2.2 m (in EH2000).

2.3. Auxiliary elevation and forcing data

The general evolution of the study area has been previously analysed in our recent article (Luik et al. 2025). In the present study, we narrow our focus to the development of the Järve scarp along the current erosional section, which spans ~2–3 km along the shore. To establish the background setting, a digital elevation model (DEM) was constructed utilising LiDAR elevation data provided by the Estonian Land Board (ELB 2025b; Fig. 2). The elevations are given in the EH2000 system. Through cartographic analysis using GIS, we examined the present-day landforms – such as individual beach ridges and spits, erosional scarps, and the beach face – and evaluated changes in the coastline linked to various forcing factors.

Historical maps (ELB 2025c) and field photos taken at various times (1990, 2004, 2005, and 2024; ELB 2025d) were compared. In discussing our results, we considered data partially presented in the data repository (Luik et al. 2024b), as well as findings from our previous studies on Late Holocene relative sea-level changes (Nirgi et al. 2022; Suursaar et al. 2024), potential shifts in wind and storm regimes (Suursaar et al. 2015; Suursaar 2023; Tõnisson et al. 2024a), ice conditions (Suursaar et al. 2025), and sediment dynamics over recent decades (Orviku 2006; Suuroja et al. 2020; Luik et al. 2025).

3. Results and interpretation

3.1. Lithological description of the sediments in the Järve outcrop

During the fieldwork, the water line was ~10 m seaward from the exposed outcrop. The base of the outcrop was at an elevation of 0.8 m, and its cleaned-up top reached 3.6 m in the EH2000 system. No long-term sea-level measurements exist for Järve, but based on interpolated statistics from nearby coastal stations (mainly Pärnu and Ristna; Fig. 1A), the current mean sea-level height in this area is around zero in the (old) BK77 system, or 0.2 m in the EH2000 system

(Tõnisson et al. 2024a). As a result of southerly winds (5–8 m/s), the sea level varied between 0.2 and 0.4 m on 4–5 December 2024 (EWS 2025). Several fallen tree trunks in the surrounding area indicated erosion events during previous winter storms (Fig. 3). At the scarp, the groundwater table was recorded at 0.8 m.

The visual assessment of the outcrop revealed that the deposits consisted predominantly of sand with some gravel and very little silt. There were some darker layers (interbeds) consisting of coarser sand fractions and seashells (Figs 4 and 5). When juxtaposing the outcrop photo with older photos taken roughly from the same location, the patterns of interbeds appeared partly similar. We identified and correlated 14 interbeds (Fig. 4), which were provisionally called 'storm layers'. Although layers 1–14 should be the same in all photos, the darkness and thickness varied somewhat, probably due to differences in moisture conditions and the natural variability of the layers. Some were darker layers with coarser material (e.g. 10 and 11 in Fig. 4), whereas others appeared as erosional surfaces between cross-bedded and laminated layers; these layer indicators were drawn just above the erosional surface (e.g. 2 and 5 in Fig. 4).

According to granulometric analysis (Fig. 5C–F), the sediment was sandy in all layers. It was mostly moderately or poorly sorted, as the threshold for well-sorted sediment was approximately <90–110 µm, and >230–360 µm for poorly sorted sediment (Fig. 5F). Seashell fragments occasionally occurred throughout most of the outcrop and were sometimes abundant, e.g. between layers 10 and 11 (Fig. 4). Based on lithological and structural characteristics, the entire sequence can be divided into four main sedimentary units (Fig. 5B). In general, longshore transport prevailed in units 1 and 2, cross-shore transport in unit 3, and aeolian input in unit 4.

Unit 1 (elevation from 0.8 to 1.55 m, ~75 cm thick; Fig. 5) consisted of greyish-beige medium- to fine-sand beds (layers), for which four granulometric analyses were performed. The two lowermost beds were cross-laminated (with shore-parallel dip), composed primarily of poorly to moderately sorted medium sand with interlaced dark mineral laminae, occasional shells, and gravel grains. Mean grain size reached 422 µm and median 359 µm in the 1.0–1.1 m sample (Fig. 5C–E). The two upper beds in this interval were horizontally laminated, consisting of well-sorted very fine to fine sands with occasional shell fragments. The lowest mean (163 µm) and median (126 µm) grain-size values of the entire profile were found there. The lower boundaries of these beds were sharply marked by ~10 cm thick layers of coarser sand and gravelly sand, possibly representing storm deposits.

Unit 2 (1.55–2.45 m, 90 cm thick; Fig. 5) consisted of beige medium- to fine-sand beds, from which five granulometric samples were collected. Moderately to poorly sorted fine sands dominated. The two lowermost beds in this unit were high-angle cross-laminated (up to 29° towards east–northeast, i.e. shore-parallel) fine to medium sands. In the middle (2.0–2.1 m), a poorly sorted fine-sand layer with a multimodal distribution consisting of 10.2% coarse sand was found. The three upper beds were horizontally laminated, composed of fine sand, with organic laminae present at 2.2 and 2.4 m. The lower boundaries of these beds were also defined by coarser deposits (6–10 cm thick), forming an erosional base and interpreted as storm deposits.

Unit 3 (2.45–3.3 m, 85 cm thick; Figs 5 and 6A) comprised subhorizontally laminated sand beds that contained five sandy–gravelly sub-layers, interpreted as storm deposits. The beds consisted of fine to medium sand that was reddish brown to beige and subhorizontally laminated. The lower boundaries of these beds were marked by layers of coarse sand and gravelly sand deposits (1–5 cm thick). Four to five shell layers between 2.4 and 2.6 m (Fig. 5) were present in the basal part. Shells were exceptionally well preserved and occurred in distinct, continuous layers. Seven granulometric samples were analysed. In general, the samples contained larger proportions of coarse fractions and were poorly sorted. The sample immediately above the lower unit (at ~2.5 m) was poorly sorted very coarse sand with a trimodal, skewed distribution, with a mean of 499 µm and a median of 846 µm. It included 19.4% of coarse sand. On top of this layer, several strata of poorly sorted fine to medium sands occurred, with occasional shells.

Unit 4 (3.30–3.50 m, ~20 cm thick; Fig. 5) comprised massive fine- to medium-grained light brown humus-rich sand with roots and pebbles. The sand in this unit was likely modified by aeolian and paedogenic processes. Aeolian influence was weak at this location, but the thickness of the

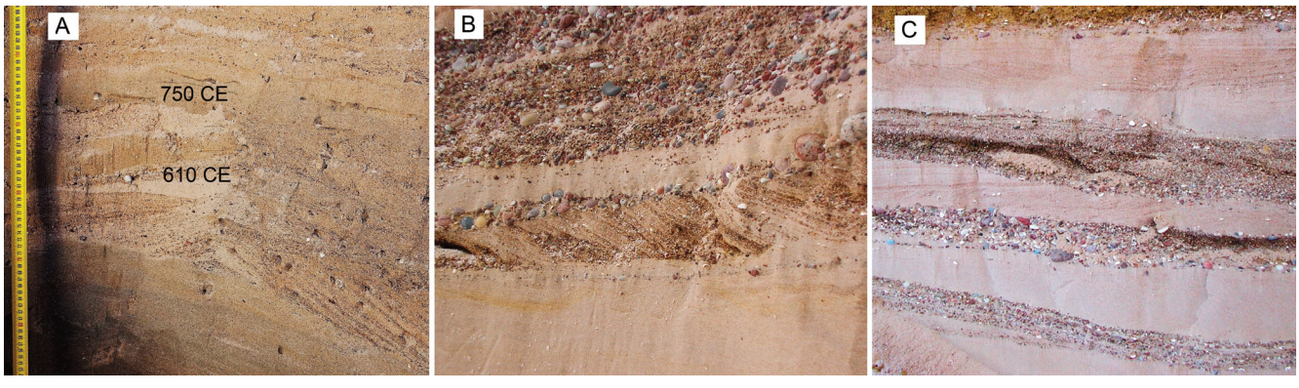

Fig. 6. Close-up views of cross-bedding at the Järve scarp from 4 December 2024 (A; elevation ~1.4–2.0 m) and from 25 January 2005 (B, C; close to the land surface at ~3.5–4 m, although the exact elevation, scale, and location are unknown). Dates were available for A (see Fig. 5) but not for B and C. Photos by Ü. Suursaar (A) and K. Orviku (B, C).

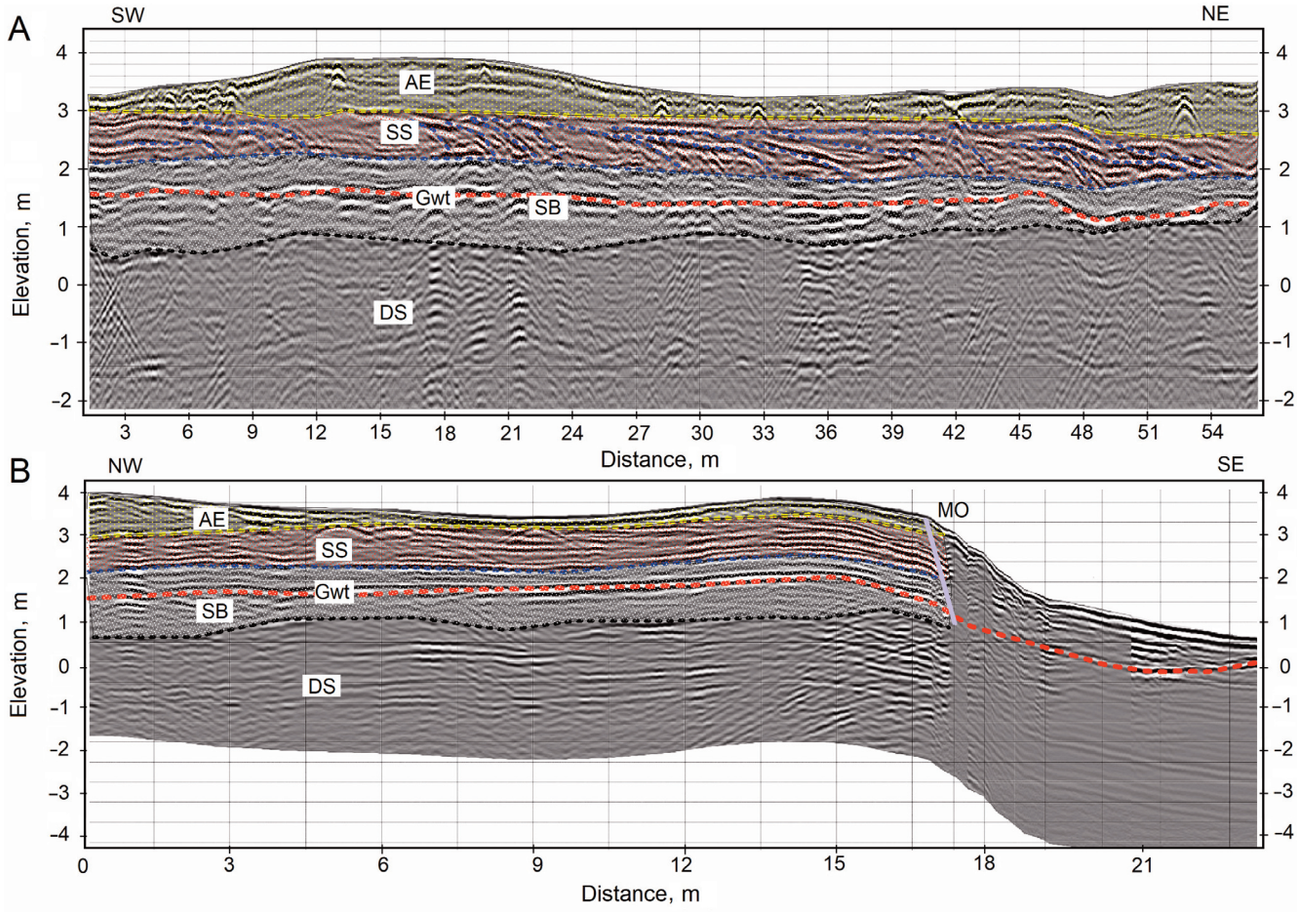

Fig. 7. GPR profile fragments taken alongshore (A) and cross-shore (B) in December 2024. Note that layering is unreadable in the steep outcrop section (B). AE – aeolian facies (sand); SS – spit sediment (sand with gravel and pebbles, wave-transported, longshore-dipping increments); SB – underwater nearshore sandbar (cross-bedded); DS – deeper sea/glaciofluvial sediment (reworked from submerged glaciofluvial sand and clayey moraine deposits); Gwt – groundwater table (red dashed line); MO – master outcrop, the cleaned scarp. Parabolic features visible at elevations ~3 m (horizontal distance 3–9 m in A) are artefacts. The profiles cross each other at ~20 m (A) and ~2 m (B).

aeolian layer varied between 0–1 m in the very proximity of the outcrop and reached up to ~5 m (at the 10.8 m absolute elevation mark; Fig. 2) at the blowout site 1.5 km to the southwest.

The MS values (Fig. 5G, H) showed higher values in the lower part of the pit (0.8–1.0 m), at the lower boundary of unit 2 (around 1.6 and 2.5 m), and in the upper zone affected by paedogenic processes (unit 4). Smaller maxima were also found at around 2.0, 2.8, and 3.1 m (note the logarithmic scale in Fig. 5G). Most of these maxima coincided with the enumerated (1–14) storm (or regime-shift) layers, though not universally because some interbeds included only some strata of coarser fractions without erosional surfaces.

The GPR profiles obtained at the MO location also showed some distinct layering (Fig. 7). In general, facies of sub-horizontally layered sea-bottom sediment (DS), marine-built underwater sandbar (SB) and spit sediment (SS), and aeolian deposits (AE) can be identified (Fig. 7). The slant layers in the SS facies indicated spit elongation, where each stronger storm or stormy season likely resulted in a new tongue-like increment. These longshore-dipping reflectors (visible in Fig. 7A) were not well differentiated on the cross-shore profile (Fig. 7B). Due to the inherent vertical resolution (~20 cm) of the GPR imagery, the sub-parallel streaks (between 2–4 m in Fig. 7B) cannot be individually correlated with the streaks visible in Fig. 4. Moreover, some of the streaks in Fig. 4 showed only insignificant granulometric differences and therefore did not necessarily create a reflector on the GPR image. Several reflectors occurred in the DSs around –1.5 m (Fig. 7A), likely originating from gravelly sub-layers or lenses within the older buried valley. Some appeared only as discontinuous or short reflectors. This glaciofluvial-type sediment is also observed, for example, in the Quaternary cover maps (ELB 2025a) and in the quarry near Lake Järve (Fig. 2). The groundwater table undulated around 1.5 m in the interior of the spit; it descended steeply in the scarp area (0.8 m) and reached zero near the shoreline. In general, the layers were undulated (by up to 1 m) in height, which also explains the variations and differences in layers visible in Fig. 4. It is also important to note that over the past 19 years, the scarp has receded by ~5 m at that location (Luik et al. 2024a), hence the layers cannot lie in exactly the same positions as in Fig. 4A and B. Nevertheless, the layered, varying nature of the outcrop is obvious (Figs 4, 5 and 7).

3.2. OSL and ^{14}C dates

Though the luminescence signal from the quartz was relatively weak, it had a strong or dominant fast component, and

the excellent dose-recovery ratio (1.00 ± 0.04, n = 19) showed that the analytical protocols can accurately recover a given dose. Only a few aliquots of K-feldspar were measured, and due to relatively high residual doses (0.4–7.6 Gy) compared with the equivalent doses (1.9–8.8 Gy), as well as fading, the quartz ages (Table 2) were preferred for age determination. Additional information on quartz and feldspar analyses (not used in the article) is provided in the Supplementary material (Tables S1–S3).

The ages obtained from the middle part of the MO, 53 cm apart, differed by ~220 years (970 CE and 750 CE; Table 2). In the AO, near the blowout, although samples L3 and L4 were vertically only 44 cm apart (depths of ~1.1 and 0.7 m from the outcrop rim; Fig. 8), their ages differed considerably. As in the MO, the lower dating clearly corresponded to the original landward ridge, built entirely by the sea. The upper sample was probably formed at a later stage by a combination of aeolian and marine processes, when the ridge gained height and lateral width. The dark palaeosoil streak between these two samples marked a significant regime shift. The uppermost aeolian-facies age (1630 ± 310 CE; Table 2) corresponded to our earlier dates for the Järve dune. According to Luik et al. (2025), the radiocarbon sample R1* (Table 1) gave an age of 1460 ± 30 CE for the dune facies just behind the MO scarp, and an OSL sample (code L2b in Luik et al. 2025) yielded both U-pIRIR and pIRIR dates at ~1400 ± 100 CE.

In Table 3, calibrated years based on the IntCal20 curve are presented in three different versions. The first one (*R(0)*), which is valid for the charcoal sample C6, is not appropriate for the seashell samples C1–C5. It is well known that radiocarbon dating of seashells can be compromised by the so-called marine reservoir effect (e.g. Long et al. 2012). This effect is highly variable, and its exact values are not known for the Gulf of Riga. As an assumption, we rely on fig. 6 in Lougheed et al. (2013), which indicates that the effect may vary from about 400 radiocarbon years at the Danish Straits to 25–50 years at the bottom of the Bothnian Bay. The study did not provide estimates for the interior of the Gulf of Riga, but the regression-based estimate for the Baltic Proper, near the West Estonian Archipelago, was 200–250 years. Decreasing alongside salinity from the open sea to the bay, this effect can be tentatively estimated at about 200 ^{14}C years in our study area. Therefore, for the second set of dates (*R(200)* in Table 3), 200 years were subtracted from the ^{14}C ages before calibration with IntCal20. In addition, the coastal sea south of Saaremaa is marked as a hard-water-prone area in Lougheed et al. (2013), which can add more than 500 ^{14}C years to the correction (*R(t)*). Silurian limestone is widespread on Saaremaa and occasionally outcrops along coasts and streams. The hard-water correction was determined empirically by comparing OSL ages with ^{14}C dates (Tables 2 and 3). Consequently, the third set of dates is presented in Table 3, with the total correction applied (200 + 500 = 700 years).

Fig. 8. Locations and ages of two luminescence dates (L3, L4; grey sampling tube ends visible in the outcrop) and one ^{14}C date (C6) near the blowout (AO in Fig. 2; Table 2). Photo by Ü. Suursaar, 5 December 2024.

Table 2. Luminescence (quartz) dates from the master outcrop (L1, L2; Table 1; Fig. 5) and the additional outcrop (L3, L4; Fig. 8). SE – sample elevation; WC – sample water content; CAM – Central Age Model (weighted mean) age (ka = 1000 years); MD – mean dose; n – number of aliquots

Code	Lab code Lund	SE, m	WC, %	CAM age, ka	MD, Gy	n, accepted/total	Dose rate, Gy/ka	**Age, CE**
L1	25003	1.78	12	1.28 ± 0.07	2.54 ± 0.07	27/48	1.98 ± 0.10	**750 ± 70**
L2	25004	2.31	8	1.06 ± 0.08	2.23 ± 0.11	23/39	2.06 ± 0.12	**970 ± 80**
L3	25001	5.13	8	1.44 ± 0.12	2.65 ± 0.16	17/24	1.86 ± 0.10	**590 ± 120**
L4	25002	5.57	8	0.39 ± 0.31	0.69 ± 0.05	21/48	1.78 ± 0.10	**1630 ± 310**

Table 3. Radiocarbon dates (^{14}C, years BP), calibrated years (min and max at the 68.3% probability level), and median values (Med), expressed in CE (–CE = BCE). Results are presented in three different versions using IntCal20: no correction (*R(0)*), marine reservoir effect correction (*R(200)*; Lougheed et al. 2013), and empirical reservoir + hard-water correction (*R(700)*). SE – sample elevation

				R(0)			*R(200)*			*R(700)*		
Code	SE	^{14}C	Lab code	Min	Max	Med	Min	Max	Med	Min	Max	Med
C1	0.80	2165 ± 29	FTMC-XK54-1	–360	–160	–210	10	120	60	580	640	610
C2	1.69	2162 ± 30	FTMC-XK54-2	–360	–150	–200	20	120	60	580	650	610
C3	2.05	1883 ± 30	FTMC-XK54-3	120	210	160	260	420	380	880	890	850
C4	2.45	2155 ± 30	FTMC-XK54-4	–350	–110	–190	20	120	70	590	650	610
C5	2.90	4215 ± 33	FTMC-XK54-5	–2900	–2700	–2790	–2580	–2470	–2530	–1900	–1770	–1830
C6	5.35	740 ± 28	FTMC-HC21-2	1260	1290	1270						

4. Discussion

4.1. Mismatch between OSL and ^{14}C dates; marine reservoir and hard-water effect

In comparison with the OSL samples, the radiocarbon samples, except for C6, appear to be offset to varying degrees (Tables 2 and 3). The uppermost two dates in the MO (C4 and C5) are older than those below (C1–C3) and are therefore highly questionable, but even the lower samples (C1–C3) remain problematic. In the non-corrected version (Table 3: *R(0)*), the offset from the OSL dates is ~900–1200 years. After applying the reservoir effect correction (Table 3: *R(200)*), the offset decreases to ~700–900 years. Finally, when applying both the reservoir and hard-water corrections (*R(700)*), the C1–C3 dates become comparable with the OSL ages (Table 4). By contrast, the charcoal sample (C6 from the AO), taken between OSL samples L3 and L4 (Table 3; Fig. 8), does not require any correction and aligns well with the OSL results (Table 4).

Unfortunately, the proper quantification of these effects is not well established, which considerably reduces the reliability of seashell-based dates. The marine reservoir effect arises because terrestrial organisms obtain ^{14}C directly from the atmosphere, whereas marine organisms, such as molluscs and fish, may incorporate older carbon from seawater (e.g. Long et al. 2012). As a result, radiocarbon ages are typically (i.e. globally) offset by ~400 years, but the magnitude of this effect is highly variable in space and time (Ascough et al. 2005; Alves et al. 2018). Several estimates exist for the Baltic Sea region. For example, Hedenström and Possnert (2001) reported variations ranging from ~750 years to near zero within a single sedimentary sequence from Lake Lilla Harsjön (an isostatically isolated basin in Sweden) spanning about 7000 years. In this study, the correction *R(200)* was adopted from fig. 6 in Lougheed et al. (2013). That study also indicated that the so-called hard-water effect can add more than 500 years to radiocarbon ages in areas underlain by limestone. The empirically estimated correction used here (Table 3) roughly corresponds to this suggestion by Lougheed et al. (2013). However, these corrections remain tentative and are not yet supported by direct on-site measurements.

A third effect is the possible relocation of seashells, meaning that they may not have died and been buried at their present location. This process can be even more variable than the effects mentioned above. It may occur on a relatively small scale through the displacement of shells during deposition in the coastal marine environment. For instance, a 200–250-year discrepancy in ages can arise from merely 50 cm vertical misplacement of shells. Freshly dead and unmineralised seashells contain voids and organic matter, making them less dense (~1 g/cm^3 or even less) than the surrounding sand (~2.7 g/cm^3). When sifted back and forth by waves on the shallow seabed near the coast, seashells can remain on the sediment surface for longer, while grains of sand settle downward. Storm waves can also toss clams and seashells onto the beach, forming so-called shell ridges. When buried under the sand, these shells are apparently 'older' than the surrounding sediment indicates. For example, if the shell ridges occur up to a metre above the usual waterline, this would mean a potential age difference of up to 450 years at 2.2 mm/a uplift.

However, for the upper two samples in the MO (C4 and C5), the obtained ages are ~1000–3500 years older than expected. The most plausible explanation is the reworking and relocation of previously buried material that was later eroded and redeposited. It is well established that the Järve palaeospit developed through sediment accretion and postglacial uplift over ~4000 years (Luik et al. 2025). After the closure of the Salme Strait, the alongshore supply of new sediment from the west diminished, and the Järve coast was increasingly subjected to erosion for various reasons.

It was not possible to determine the precise provenance of the shells in samples C4 and C5. Unlike luminescence samples, which are reset with each episode of bleaching and redeposition, radiocarbon ages reflect the time of death of the organism and not the location of redeposition. Consequently, the radiocarbon ages of C4 and C5 likely do not provide reliable information in the stratigraphic context of this study. Regrettably, shells were the only datable organic material available at the Järve MO.

It can be concluded that, unlike the charcoal-rich humic layer (the dark layer dated to 1270 CE in Fig. 8), seashells cannot be considered reliable dating material in coastal stratigraphic studies at accretional–erosional seacoasts (see also e.g. Long et al. 2012). Seashells are subject to reservoir and hard-water effects and may also be displaced by waves, deposited and eroded multiple times, transported alongshore, and ultimately redeposited in new locations. All these effects may be present at the Järve study site, but their separate roles cannot yet be estimated. To accurately determine these effects in the Gulf of Riga, further localised studies are necessary. These would require either paired terrestrial and marine samples from the same context or the parallel use of different dating methods.

Table 4. Vertical sequence (from lower to higher elevation) of luminescence and radiocarbon dates from the main outcrop (MO), additional outcrop (AO), and scarp rim (SR, codes R1* and L1*; Luik et al. 2025; Fig. 5A; Tables 1–3). The strongly offset age of the probably relocated sample C5 is discarded here; C4 is also questionable. SE – sample elevation; age includes reservoir and hard-water effect corrections in C1–C4); FE – formation elevation of deposits, calculated considering the present-day elevations (SE), the 2.2 mm/a uplift rate, and corrected ages

Location	Code	SE, m	Age, CE	FE, m
AO	L4	5.57	1630	4.7
AO	C6	5.35	1270	3.7
AO	L3	5.13	590	2.0
SR	R1*	4.01	1522	3.1
SR	L1*	3.01	620	0.0
MO	C4	2.45	610	–0.7
MO	L2	2.31	970	0.0
MO	C3	2.05	850	–0.5
MO	L1	1.78	750	–1.0
MO	C2	1.69	610	–1.5
MO	C1	0.80	610	–2.4

4.2. Possible provenance of the sub-layers in the outcrop

According to the stratigraphic and granulometric analyses (Figs 5 and 7) and the obtained or estimated dates (Table 4), the lowermost unit 1 was deposited in a shallow (–2.5…–1.5 m) nearshore sea ~1300–1500 years ago. The sediment consisted mostly of sub-horizontally laminated marine (Limnea Sea) sand (Suuroja et al. 2020; Tõnisson et al. 2022) and included a few strata of slightly coarser material, seashells, and cross-bedding. As a rule, sets of underwater sandbars developed along sandy shores in Estonia (e.g. Tõnisson et al. 2024a, 2024b, 2024c). Such sub-parallel ridges are also visible on aerophotos along the Järve–Mändjala coast, especially closer to Nasva Harbour (ELB 2025d; Luik et al. 2025). The relative height of underwater bars is ~0.5 m, and those situated closer to shoreline sometimes appear above the water surface in low sea-level conditions. The sediment in the lowermost part of the studied outcrop is not necessarily from the crest of the bar, but more likely from the trough (Fig. 7). However, the layers vary spatially and appear at slightly different elevations as the scarp retreats. On emerging coasts, underwater bars quite often (but not necessarily always) form a core for future beach or foredune ridges.

Unit 2, between present-day elevations of 1.55 and 2.45 m, is also of marine origin and likely formed just below or close to the water surface (–1.0…0.0 m; Table 4) ~1300–1100 years ago, whereas unit 3 (the layer between 2.45 and 3.3 m), judging by its elevation and internal layered structure (Fig. 7A), formed above the sea surface. The ridges grew both lengthwise and sideways, subsequently merging into larger spits. The lengthwise elongation of the spit is also traceable on the GPR image (Fig. 7A). Unit 2 includes several cross-bedded zones that indicate storms arriving from different directions (i.e. basically either southwest or southeast) and varying hydrodynamic regimes. Sediments of units 2 and 3 (Figs 5 and 6) also exhibit distinct layers of coarser material (due to combined cross-shore and longshore transport), which must have been eroded by storm waves from the nearby sea bottom and tossed onto the shoreface. Since the Salme palaeostrait between Saaremaa and Sõrve (Figs 1B and 2) must have been practically closed by that time (Nirgi et al. 2022), no additional material from the hydrodynamically more energetic Baltic Proper side (Najafzadeh et al. 2024) could have entered the Suur Katel Bay from the west.

Unfortunately, the sediments of the layers of units 3 and 4 in the MO remain without direct dating results so far. Still, considering the stratigraphy and granulometry (sub-layers of coarse sand; some cobbles and seashells; Fig. 5), the sediments of unit 3 were likely formed by a combination of marine and aeolian processes and deposited before the onset of dominant aeolian activity (unit 4) during the LIA. Considering the 2.2 mm/a uplift rate, unit 3 (2.45–3.3 m layer in the MO) is probably 700–1000 years old. On top of that, the aeolian layer (unit 4) is very thin and intertwined with paedogenic processes. Considering the present-day elevation, the material cannot be younger than the dune (1400–1600 CE; Luik et al. 2025). A previously obtained radiocarbon age from approximately the same location, but 20–25 m inland and closer to the land surface, was ~1450 CE (Luik et al. 2025). This indicates that, before the recent erosion stage began, beach ridges (spits) gradually grew seaward, with older ones located inland and younger ones closer to the sea. Due to the relatively humid climate and moderate wind conditions, foredunes and beach ridges normally become fixed by vegetation relatively fast in Estonia (e.g. Ratas et al. 2011; Vilumaa et al. 2017; Suursaar et al. 2022). However, the younger marine-built ridges are now missing (eroded away) on the seaside, which makes it impossible to obtain the corresponding dates in the scarp. Although the dune part is also missing in the upper part of the present-day outcrop, the 0.2–1.0 m thick (and 400–600 years old) aeolian cover reappears the score of metres inland (Fig. 7B) and also occurs in the AO (Fig. 8; Table 4).

The sporadic aeolian layer is essentially composed of reworked spit sand that has been reblown from its initial elevation of 2–4 to 6–10 m. After the dune formed, it began to roll landward, gradually feeding on itself. Today, only the younger part of this dune has survived, as material from the 'older' (original) part of the dune has either been blown landward or eroded away from the seaward side.

4.3. Development stages, shifts, and storm layers over the past 2000 years

Currently, the most seaward part of the Järve palaeospit, where the studied scarp is located, likely emerged from the sea ~1400–1600 years ago (Luik et al. 2025). It grew in height and volume through both sediment accretion and post-glacial uplift (amounting to ~3.5 m in height over the past 1600 years). As revealed by the granulometric–stratigraphic analysis, the lower part (nowadays 0.8–1.4 m) of the examined outcrop was formed by accumulation on the shallow nearshore sea bottom, possibly on top of the underwater bar (Fig. 9A). The shore-parallel, cross-bedded laminae indicate rapid spit growth both in width and length towards Mändjala (Fig. 9B). Several darker (coarser) streaks and variations between different lamination regimes indicate changes in forcing conditions (i.e. storminess) and sediment provenance.

The 14 identified streaks (interbeds or storm layers; Fig. 4) occur between 0.8 and 3.2 m and correspond to ages from 610 CE (Table 4) to ~1300 CE, yielding on average a period of ~50 years per stripe. The distances between the streaks are uneven. Between C1 and L2 (Table 4), for instance, there are nine streaks covering ages between 610 and 970 CE. A roughly 50-year periodicity suggests that the interbeds formed during exceptionally strong storms (e.g. storms such as those in 1967 and 2005), which were capable of accreting material that differed from routinely accumulated material – either coarser fractions or darker material with higher heavy-mineral content and MS values (Buynevich et al. 2023, 2024). In that sense, interbed 10 (Fig. 5) prominently features both in granulometry and MS values. Its formation time was ~1000–1100 CE (Table 4). The interface between units 1 and 2 (events between 610 and 790 CE) and the layer around interbeds 2 and 3 in the lower part of

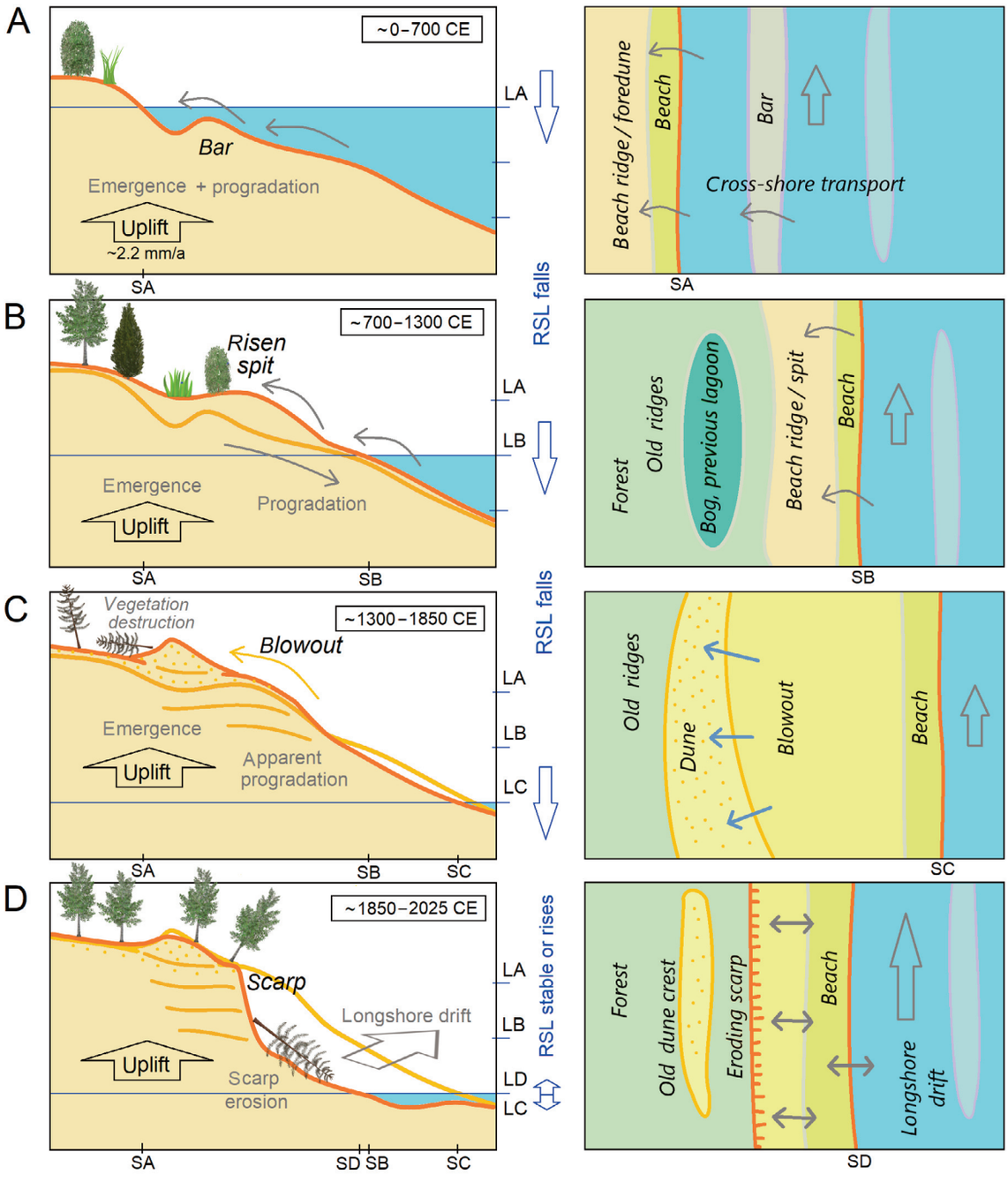

Fig. 9. Conceptual model illustrating the developmental phases of the Järve coast over the past ~2000 years, shown as cross-sections (left panel) and views from above (right panel). Emergence of a spit due to uplift and initial beach ridge accumulation followed by stabilisation by vegetation (A–B); activation of aeolian processes due to vegetation destruction and/or the colder climate of the LIA (C); and activation of coastal erosion due to relative sea-level stabilisation or rise, cessation of fresh marine sediment accumulation at Järve, and increasing storm impacts during ice-free winter conditions (D). SA–SD denote shoreline positions in stages A–D, and LA–LD denote sea levels in stages A–D. In the left panel, the orange line represents an incremental change compared to the yellow line representing the previous stage. A few storm layers are indicated (in C and D).

unit 1 (610 CE) are also more distinct. Some interbeds were probably not exactly accretional storm layers but erosional surfaces between cross-bedded and laminated layers (i.e. evidence of storm erosion) or just marked particular periods in the gradual accumulation process under varying sedimentary conditions. Because these former underwater formations – although buried – are now elevated above sea level, we can study storminess shifts in the Järve scarp through these formations. This is rarely feasible elsewhere, as comparable work typically requires underwater sampling.

An obvious shift in the development of the raised Järve coast was the onset of LIA dune formation (Fig. 9C). This process has been noted in many locations along the Estonian coast (Tõnisson et al. 2020), as well as in other areas in Europe (Clemmensen et al. 2015; Jackson et al. 2019). A sharp charcoal-rich humic layer, dating to ~1270 CE, separates sandy layers dating to 590 and 1630 CE (Fig. 8). It indicates that, at least at the AO site, a forest fire may have destroyed vegetation and facilitated the development of the aeolian layer sometime between 1270 and 1630 CE. Quite possibly, the

blowout visible in the background of Fig. 8 occurred later. However, the extent and wider impact of the event marked by the charcoal date at ~1270 CE remain unknown. Forest fires of this kind likely occurred repeatedly during the Late Holocene (e.g. Kuosmanen et al. 2018). An earlier aeolian sand influx (ASI)-based storminess reconstruction from a bog near Lake Järve (Fig. 2) showed higher ASI values around 200 BCE–50 CE, 900–1000 CE, 1100–1300 CE, and during the last 500 years (Vandel et al. 2019; Vaasma et al. 2025). Although it is difficult to directly compare studies conducted using different methods and resolutions, the periods of increased storminess around 1000–1300 CE and during the LIA appear to align.

It has been widely discussed that the LIA resulted in large-scale transgressive coastal dune behaviour and manifested in a relocation of sand in coastal zone throughout Europe (Jackson et al. 2019). Several mechanisms may have been intertwined, including those of climatic and anthropogenic background. Specifically, in the Baltic Sea area, the large dune ridge on the Curonian Spit (Lithuania) formed only from the 16th century onwards, largely due to destructive human practices and forest fires (Dobrotin et al. 2013). Quite similarly, the removal of some vegetation from the frontal dunes at Skagen Peninsula (Denmark) by local inhabitants during the early and middle part of the LIA made the dunes vulnerable to remobilisation. It is also known that King Christian III of Denmark promulgated a law in 1539 CE forbidding the removal of vegetation from the dunes, implying that dune vegetation may have been partly destroyed during the LIA (Clemmensen et al. 2015).

In Estonia, it has been suggested that anthropogenic deforestation in the Järve area, driven by population growth, the construction of the nearby Kuressaare Episcopal Castle (~1380 CE), and increased marine transport, may have contributed to dune formation (Luik et al. 2025). The need for additional firewood to cope with the cooling climate could have further accelerated forest cutting. In addition, slash-and-burn agriculture, which frequently resulted in widespread forest fires, was a common technique in medieval Europe, including Estonia (Jääts et al. 2010). Rapid deforestation is evidenced, for instance, by a 1297 law prohibiting coastal forest cutting near Tallinn (Etverk 1997). Fire cultivation and extensive forest cutting only declined considerably in Estonia by the 19th century (Jääts et al. 2010).

As previously discussed, although the ridges along the Järve coast are sandy, wind-blown dunes are practically missing at the Järve outcrop (MO) location. Aeolian contributions to the landscape are sporadic. Despite traditional names found in the area – Järve dunes (*Järve luited* in Estonian) or Mändjala dunes (*Mändjala luited*) – the landform is predominantly not of aeolian origin. The Järve spit (or coastal barrier) system is mainly marine-built. The difference between the gently bending palaeospits shaped by marine processes and the 'rougher' aeolian landforms is noticeable on the digital elevation model (Fig. 2). The aeolian layer is relatively thin, and the impression of dunes occurs only in a few reblown locations near the current coastline, where (marine) sand has been reworked and blown upwards (on top of a 4–5-m high marine ridge), reaching 10.8 m above mean sea level. Another blowout at Mändjala (7.6 m elevation; Fig. 1) contributed 2–3 m in thickness.

Finally, the past ~100–150 years (Fig. 9D) have been characterised by a growing sediment deficit at the Järve site (Luik et al. 2025). The Järve barrier, now mostly 4–5 m high, is eroding along its seaward side (Orviku 2006; Tõnisson et al. 2024a). The eroded material has been transported northeast towards Mändjala and Nasva (Fig. 2). A similar longshore sediment transport pattern, generally directed from southwest to northeast by prevailing winds, waves, and coastline configuration, can also be observed on the Latvian side of the Gulf of Riga (Soomere et al. 2025). It is difficult to assess the total recession (i.e. the extent of land loss), but in total it may reach ~100–200 m at Järve. Aerial photos document up to 75 m of shoreline recession between 1956 and 2023, and 20 m of scarp recession (Luik et al. 2025). The erosion-prone, scarped coastal section is currently 2–3 km long at Järve, but it is expected to lengthen as relative sea level rises and the duration of protective seasonal sea-ice cover continues to diminish.

5. Conclusions

1. The seaward section of the Järve palaeospit, where the studied scarp is located, began to emerge approximately 1600 years ago in front of the older spit system dating back 3500–4000 years. It has grown in height and volume due to both sediment accretion and postglacial uplift, which alone has raised it by ~3.5 m over the past 1600 years.
2. A comparison of OSL and radiocarbon (^{14}C) dates from the scarp revealed that seashells are not reliable for dating in coastal stratigraphic studies, particularly on shores with prevailing longshore sediment transport. Shells may be displaced by storm waves and reworked through cycles of deposition and erosion. In addition, the obtained ages can be influenced by the marine reservoir effect and the hard-water effect. These influences may act simultaneously at the Järve site and point to a more general issue. Further site-specific studies are needed to better quantify these effects or to avoid seashell-based dating altogether.
3. Stratigraphic and granulometric analyses showed that the lower part of the examined outcrop (now at 0.8–1.4 m elevation) was formed by sediment accumulation in a shallow (1–3-m deep) nearshore seabed, possibly atop an underwater bar. Cross-bedded laminae indicated fluctuating energy conditions and a rapid expansion of the spit in both width and length, extending towards Mändjala. The elongation of the raised sandy spit is also visible in the GPR imagery. Darker or coarser material streaks and variations in lamination patterns point to changes in sediment provenance and environmental forcing, including storm activity. Above the marine-deposited spit layers, a thin aeolian layer is present, though it is intermixed with paedogenic processes at the Järve site. Owing to the raised-beach setting, it was possible to detect changes in forcing conditions even within the underwater formations at Järve.

4. The activation of aeolian processes and sand redistribution during the Little Ice Age (~1300–1850 CE), a phenomenon observed along many European coasts, had only a limited impact at Järve. Despite traditional place names such as Järve dunes and Mändjala dunes, the coastal landforms are predominantly of marine origin. The Järve coastal barrier system was primarily built by marine processes, whereas the upper aeolian layer is thin and patchy, with dune-like features appearing only in a few isolated blowout areas. In one such location, marine sand was reblown into a dune reaching a height of 5 m (10.8 m above sea level). These blowouts were attributed to the colder climate of the Little Ice Age and anthropogenic disturbances to vegetation, such as logging or slash-and-burn agriculture.
5. Over the past 100–150 years, the Järve coast has experienced an increasing sediment deficit. The emergent barrier system – composed of older beach ridges and spits, some up to 10 m high – has become erosional. Apparent sea-level lowering has ceased, and both the duration and extent of seasonal sea ice have declined. While it is difficult to quantify the total extent of coastal recession (i.e. the amount of 'lost' land), it may have reached several hundred metres at Järve. The eroded sediments have been transported northeast towards Mändjala and Nasva, where the coastline continues to advance due to ongoing accretion.
6. In addition to the methodological insights regarding seashell-based dating, the broader significance of the study is that it demonstrates how global environmental changes are manifested at a local scale on seacoasts.

Data availability statement

Data not already included in the paper or its supplementary material will be made available upon request. Some of the data related to this article are included in the DataDOI repository at https://doi.org/10.23673/re-484.

Acknowledgements

The study was supported by the Estonian Research Council grant PRG1471. We are grateful to the Estonian Land Board for the elevation data and to the Estonian Weather Service for providing sea-level and meteorological data. We also thank Dr. Žilvinas Ežerinskis of the Vilnius Radiocarbon Laboratory for the dating analyses. The luminescence analyses were conducted within the ArchLab (National Infrastructure for Archaeological Science, Sweden) and Lu^2D^2 (Lund Luminescence Centre for Dating and Dosimetry) infrastructures. The publication costs of this article were partially covered by the Estonian Academy of Sciences.

Supplementary online data

Supplementary online data to this article can be found at https://doi.org/10.3176/earth.2026.S03 and include Tables S1–S3.

References

Alves, E. Q., Macario, K., Ascough, P. and Bronk Ramsey, C. 2018. The worldwide marine radiocarbon reservoir effect: definitions, mechanisms, and prospects. *Reviews of Geophysics*, **56**(1), 278–305. https://doi.org/10.1002/2017RG000588

Andrén, T., Björck, S., Andrén, E., Conley, D., Zillén, L. and Anjar, J. 2011. The development of the Baltic Sea basin during the last 130 ka. In *The Baltic Sea Basin* (Harff, J., Björck, S. and Hoth, P., eds). Springer, Berlin, Heidelberg, 75–97. https://doi.org/10.1007/978-3-642-17220-5_4

Ascough, P. L., Cook, G. T. and Dugmore, A. 2005. Methodological approaches to determining the marine radiocarbon reservoir effect. *Progress in Physical Geography*, **29**(4), 532–547. http://eprints.gla.ac.uk/5017

Blott, S. J. and Pye, K. 2001. Gradistat: a grain size distribution and statistics package for the analysis of unconsolidated sediments. *Earth Surface Processes and Landforms*, **26**(11), 1237–1248. https://doi.org/10.1002/esp.261

Buylaert, J. P., Murray, A. S., Thomsen, K. J. and Jain, M. 2009. Testing the potential of an elevated temperature IRSL signal from K-feldspar. *Radiation Measurements*, **44**(5–6), 560–565. https://doi.org/10.1016/j.radmeas.2009.02.007

Buynevich, I. V., FitzGerald, D. M. and van Heteren, S. 2004. Sedimentary records of intense storms in Holocene barrier sequences, Maine, USA. *Maine Geology*, **210**(1–4), 135–148. https://doi.org/10.1016/j.margeo.2004.05.007

Buynevich, I. V., Tõnisson, H., Suursaar, Ü., Pupienis, D., Davydov, O. V., Kont, A. et al. 2023. Diverse erosional indicators along a rapidly retreating Holocene strandplain margin, leeward Hiiumaa Island, Estonia. *Baltica*, **36**(1), 79–88. https://doi.org/10.5200/baltica.2023.1.7

Buynevich, I. V., Tõnisson, H., Pupienis, D., Rosentau, A., Bitinas, A., Jarmalavičius, D. et al. 2024. High-resolution sampling and rapid image-based assessment of dark opaque fractions in coastal sands. *Journal of Coastal Research*, **113**(SP1), 778–782. https://doi.org/10.2112/JCR-SI113-153.1

Clemmensen, L. B., Glad, A. C., Hansen, K. W. T. and Murray, A. S. 2015. Episodes of aeolian sand movement on a large spit system (Skagen Odde, Denmark) and North Atlantic storminess during the Little Ice Age. *Bulletin of the Geological Society of Denmark*, **63**, 17–28. https://doi.org/10.37570/bgsd-2015-63-03

Costas, S. 2022. Evolutionary trajectories of coastal sand barriers along the West Portuguese coast during the Holocene. *Journal of Marine Science and Engineering*, **10**(12), 1894. https://doi.org/10.3390/jmse10121894

Dearing, J. A. 1999. *Environmental Magnetic Susceptibility: Using the Bartington MS2 System*. 2nd ed. Chi Publishers, Kenilworth.

Dobrotin, N., Bitinas, A., Michelevičius, D., Damušyte, A. and Mažeika, J. 2013. Reconstruction of the Dead (Grey) Dune evolution along the Curonian Spit, southeastern Baltic. *Bulletin of the Geological Society of Finland*, **85**, 53–64. https://doi.org/10.17741/bgsf/85.1.004

Dougherty, A. J. 2014. Extracting a record of Holocene storm erosion and deposition preserved in the morphostratigraphy of a prograded coastal barrier. *Continental Shelf Research*, **86**, 116–131. https://doi.org/10.1016/j.csr.2013.10.014

Durcan, J. A., King, G. E. and Duller, G. A. T. 2015. DRAC: Dose Rate and Age Calculator for trapped charge dating. *Quaternary Geochronololgy*, **28**, 54–61. https://doi.org/10.1016/j.quageo.2015.03.012

Eberhards, G. and Saltupe, B. 1995. Accelerated coastal erosion – implications for Latvia. *Baltica*, **9**, 16–28.

ELB (Estonian Land Board). 2025a. *Geological data*. https://xgis.maaamet.ee/xgis2/page/app/geoloogia400k (accessed 2025-04-01).

ELB (Estonian Land Board). 2025b. *Elevation data*. http://geoportaal.maaamet.ee/eng/Maps-and-Data/Topographicdata/Elevation-data-p308.html (accessed 2025-04-01).

ELB (Estonian Land Board). 2025c. *Historic maps*. https://xgis.maaamet.ee/xgis2/page/app/ajalooline (accessed 2025-04-01).

ELB (Estonian Land Board). 2025d. *Photo storage*. https://fotoladu.maaamet.ee (accessed 2025-04-01).

Etverk, I. 1997. Lisamõtteid Anno Domini 1297 juurde (Additional thoughts on 'Anno Domini 1297'). *Eesti Mets*, **2**, 10–11.

EWS (Estonian Weather Service). 2025. *Coastline stations*. https://www.ilmateenistus.ee/meri/vaatlusandmed/kogu-rannik/kaart/?lang=en (accessed 2025-04-01).

Furmanczyk, K. and Musielak, S. 2002. Important features of coastline dynamics in Poland: "nodal points" and "gates". In *Baltic Coastal Ecosystems. Central and Eastern European Development Studies* (Schernewski, G. and Schiewer, U., eds). Springer, Berlin, Heidelberg, 141–147. https://doi.org/10.1007/978-3-662-04769-9_10

Galbraith, R. F., Roberts, R. G., Laslett, G. M., Yoshida, H. and Olley, J. M. 1999. Optical dating of single and multiple grains of quartz from Jinmium rock shelter, northern Australia: part I, experimental design and statistical models. *Archaeometry*, **41**(2), 339–364. https://doi.org/10.1111/j.1475-4754.1999.tb00987.x

Hang, T., Veski, S., Vassiljev, J., Poska, A., Kriiska, A. and Heinsalu, A. 2020. A new formal subdivision of the Holocene Series/Epoch in Estonia. *Estonian Journal of Earth Sciences*, **69**(4), 269–280. https://doi.org/10.3176/earth.2020.15

Harff, J., Jöns, H. and Rosentau, A. 2020. Geological, paleoclimatological, and archaeological history of the Baltic Sea region since the last glaciation. In *Oxford Research Encyclopedia of Climate Science*. Oxford University Press, Oxford, 1–50. https://doi.org/10.1093/acrefore/9780190228620.013.621

Hedenström, A. and Possnert, G. 2001. Reservoir ages in Baltic Sea sediment – a case study of an isolation sequence from the Litorina Sea stage. *Quaternary Science Reviews*, **20**(18), 1779–1785. https://doi.org/10.1016/S0277-3791(01)00069-5

IPCC. 2021. *AR6 Climate Change 2021: The Physical Science Basis*. https://www.ipcc.ch/report/ar6/wg1 (accessed 2025-04-01).

Jaagus, J. and Suursaar, Ü. 2013. Long-term storminess and sea level variations on the Estonian coast of the Baltic Sea in relation to large-scale atmospheric circulation. *Estonian Journal of Earth Sciences*, **62**(2), 73–92. https://doi.org/10.3176/earth.2013.07

Jääts, L., Kihno, K., Tomson, P. and Konsa, M. 2010. Tracing fire cultivation in Estonia. *Forestry Studies*, **53**, 53–65. https://doi.org/10.2478/v10132-011-0089-3

Jackson, D. W. T., Costas, S. and Guisado-Pintado, E. 2019. Large-scale transgressive coastal dune behaviour in Europe during the Little Ice Age. *Global and Planetary Change*, **175**, 82–91. https://doi.org/10.1016/j.gloplacha.2019.02.003

Kalińska, E., Weckwerth, P., Lamsters, K., Alexanderson, H., Martewicz, J. and Rosentau, A. 2024. Paleostorm redeposition and post-glacial coastal chronology in the eastern Baltic Sea, Latvia. *Geomorphology*, **467**, 109456. https://doi.org/10.1016/j.geomorph.2024.109456

Kalm, V. 2006. Pleistocene chronostratigraphy in Estonia, southeastern sector of the Scandinavian glaciation. *Quaternary Science Reviews*, **25**(9–10), 960–975. https://doi.org/10.1016/j.quascirev.2005.08.005

Kreutzer, S., Burow, C., Dietze, M., Fuchs, M. C., Schmidt, C., Fischer, M. et al. 2025. Luminescence: Comprehensive Luminescence Dating Data Analysis. R package version 1.1.0. https://CRAN.R-project.org/package=Luminescence (accessed 2025-04-01).

Kuosmanen, N., Marquer, L., Tallavaara, M., Molinari, C., Zhang, Y., Alenius, T. et al. 2018. The role of climate, forest fires and human population size in Holocene vegetation dynamics in Fennoscandia. *Journal of Vegetation Science*, **29**(3), 382–392. https://doi.org/10.1111/jvs.12601

Long, A. J., Strzelecki, M. C., Lloyd, J. M. and Bryant, C. L. 2012. Dating High Arctic Holocene relative sea level changes using juvenile articulated marine shells in raised beaches. *Quaternary Science Reviews*, **48**, 61–66. https://doi.org/10.1016/j.quascirev.2012.06.009

Lougheed, B. C., Filipsson, H. L. and Snowball, I. 2013. Large spatial variations in coastal ^{14}C reservoir age – a case study from the Baltic Sea. *Climate of the Past*, **9**(3), 1015–1028. https://doi.org/10.5194/cp-9-1015-2013

Luik, K., Suursaar, Ü., Tõnisson, H., Rivis, R., Suuroja, S. and Vilumaa, K. 2024a. Millennia-long progradation turned into coastal erosion at Järve coast of the Baltic Sea. *Journal of Coastal Research*, **113**(SP1), 235–239. https://doi.org/10.2112/JCR-SI113-047.1

Luik, K., Tõnisson, H., Rivis, R., Vilumaa, K., Vaasma, T., Vandel, E. et al. 2024b. *Geomorphology of the Järve coast (Saaremaa Island, Estonia)*. Dataset. https://doi.org/10.23673/re-484

Luik, K., Tõnisson, H., Rivis, R., Vilumaa, K., Vaasma, T., Vandel, E. et al. 2025. Development shifts on the emerging Järve coast (Estonia) in Late Holocene. *Marine Geology*, **481**, 107478. https://doi.org/10.1016/j.margeo.2025.107478

Morton, R. A., Miller, T. L. and Moore, L. J. 2004. *National Assessment Of Shoreline Change: Part 1, Historical Shoreline Changes and Associated Coastal Land Loss Along the U.S. Gulf of Mexico*. https://pubs.usgs.gov/publication/ofr20041043

Murray, A. S. and Wintle, A. G. 2000. Luminescence dating of quartz using an improved single-aliquot regenerative-dose protocol. *Radiation Measurements*, **32**(1), 57–73. https://doi.org/10.1016/S1350-4487(99)00253-X

Murray, A. S. and Wintle, A. G. 2003. The single aliquot regenerative dose protocol: potential for improvements in reliability. *Radiation Measurements*, **37**(4–5), 377–381. https://doi.org/10.1016/S1350-4487(03)00053-2

Murray, A., Arnold, L. J., Buylaert, J.-P., Guérin, G., Qin, J., Singhvi, A. K. et al. 2021. Optically stimulated luminescence dating using quartz. *Nature Reviews Methods Primers*, **1**, 72. https://doi.org/10.1038/s43586-021-00068-5

Muru, M., Rosentau, A., Preusser, F., Plado, J., Sibul, I., Jõeleht, A. et al. 2018. Reconstructing Holocene shore displacement and Stone Age palaeogeography from a foredune sequence on Ruhnu Island, Gulf of Riga, Baltic Sea. *Geomorphology*, **303**, 434–445. https://doi.org/10.1016/j.geomorph.2017.12.016

Najafzadeh, F. and Soomere, T. 2024. Impact of changes in sea ice cover on the wave climate of semi-enclosed, seasonally ice-covered water bodies at temperate latitudes: a case study in the Gulf of Riga. *Estonian Journal of Earth Sciences*, **73**(1), 26–36. https://doi.org/10.3176/earth.2024.03

Najafzadeh, F., Jankowski, M. Z., Giudici, A., Männikus, R., Suursaar, Ü., Viška, M. et al. 2024. Spatiotemporal variability of wave climate in the Gulf of Riga. *Oceanologia*, **66**(1), 56–77. https://doi.org/10.1016/j.oceano.2023.11.001

Nirgi, T., Grudzinska, I., Kalińska, E., Konsa, M., Jõeleht, A., Alexanderson, H. et al. 2022. Late-Holocene relative sea-level changes and palaeoenvironment of the Pre-Viking Age ship burials in Salme, Saaremaa Island, eastern Baltic Sea. *The Holocene*, **32**(4), 237–253. https://doi.org/10.1177/09596836211066596

Orviku, K. 2006. Development ties between Järve-Mändjala beach and Nasva harbour. *Proceedings of the Estonian Maritime Academy*, **3**, 7–18.

Pupienis, D., Buynevich, I., Ryabchuk, D., Jarmalavičius, D., Žilinskas, G., Fedorovič, J. et al. 2017. Spatial patterns in heavy-mineral concentrations along the Curonian Spit coast, southeastern Baltic Sea. *Estuarine, Coastal and Shelf Science*, **195**, 41–50. https://doi.org/10.1016/j.ecss.2016.08.008

Ratas, U., Rivis, R., Truus, L., Vilumaa, K., Multer, R. and Anderson, A. 2011. The aeolian coastal ecosystems of Estonia and their changes. *Journal of Coastal Research*, **64**(SI), 430–434.

Raukas, A. 2000. Rapid changes of the Estonian coast during the late glacial and Holocene. *Marine Geology*, **170**(1–2), 169–175. https://doi.org/10.1016/S0025-3227(00)00072-4

Reimer, P. J., Austin, W. E. N., Bard, E., Bayliss, A., Blackwell, P. G., Bronk Ramsey, C. et al. 2020. The IntCal20 Northern Hemisphere radiocarbon age calibration curve (0–55 cal kBP). *Radiocarbon*, **62**(4), 725–757. https://doi.org/10.1017/RDC.2020.41

Roberts, H. M. and Wintle, A. G. 2001. Equivalent dose determinations for polymineralic fine-grains using the SAR protocol: application to a Holocene sequence of the Chinese Loess Plateau. *Quaternary Science Reviews*, **20**(5–9), 859–863. https://doi.org/10.1016/S0277-3791(00)00051-2

Rosentau, A., Vassiljev, J., Hang, T., Saarse, L. and Kalm, V. 2009. Development of the Baltic Ice Lake in the eastern Baltic. *Quaternary International*, **206**(1–2), 16–23. https://doi.org/10.1016/j.quaint.2008.10.005

Rosentau, A., Jõeleht, A., Plado, J., Aunap, R., Muru, M. and Eskola, K. O. 2013. Development of the Holocene foredune plain in the Narva-Jõesuu area, eastern Gulf of Finland. *Geological Quarterly*, **57**(1), 89–100.

Rosentau, A., Nirgi, T., Muru, M., Bjursäter, S., Hang, T., Preusser, F. et al. 2020. Holocene relative shore level changes and Stone Age hunter-gatherers in Hiiumaa Island, eastern Baltic Sea. *Boreas*, **49**(4), 783–798. https://doi.org/10.1111/bor.12452

Różyński, G. 2023. Coastal protection challenges after heavy storms on the Polish coast. *Continental Shelf Research*, **266**, 105080. https://doi.org/10.1016/j.csr.2023.105080

Saarse, L., Vassiljev, J. and Rosentau, A. 2009. Ancylus Lake and Litorina Sea transition on the Island of Saaremaa, Estonia: a pilot study. *Baltica*, **22**(1), 51–62.

Soomere, T., Jankowski, M. Z., Eelsalu, M., Parnell, K. E. and Viška, M. 2025. Alongshore sediment transport analysis for a semi-enclosed basin: a case study of the Gulf of Riga, the Baltic Sea. *Ocean Science*, **21**(2), 619–641. https://doi.org/10.5194/os-21-619-2025

Suuroja, S., Veski, A., Liira, M., Tuuling, I. and Ausmeel, M. 2020. *2019.–2020. aasta mererannikute seire tööd (Coastal monitoring work in 2019–2020)*. Aruanne. Eesti Geoloogiateenistus, Rakvere. https://kese.envir.ee/kese/downloadReportFile.action?fileUid=20443975&monitoringWorkUid=17723750 (accessed 2025-04-01).

Suursaar, Ü. 2023. Variations in wind velocity components and average air flow properties at Estonian coastal stations in 1966–2021; Sõrve Peninsula case study. *Estonian Journal of Earth Sciences*, **72**(2), 197–210. https://doi.org/10.3176/earth.2023.85

Suursaar, Ü. and Kall, T. 2018. Decomposition of relative sea level variations at tide gauges using results from four Estonian precise levelings and uplift models. *IEEE Journal of Selected Topics in Applied Earth Observations and Remote Sensing*, **11**(6), 1966–1974. https://doi.org/10.1109/JSTARS.2018.2805833

Suursaar, Ü., Kullas, T., Otsmann, M., Saaremäe, I., Kuik, J. and Merilain, M. 2006. Cyclone Gudrun in January 2005 and modelling its hydrodynamic consequences in the Estonian coastal waters. *Boreal Environment Research*, **11**, 143–159. https://www.borenv.net/BER/archive/pdfs/ber11/ber11-143.pdf

Suursaar, Ü., Jaagus, J. and Tõnisson, H. 2015. How to quantify long-term changes in coastal sea storminess? *Estuarine, Coastal and Shelf Science*, **156**, 31–41. https://doi.org/10.1016/j.ecss.2014.08.001

Suursaar, Ü., Rosentau, A., Hang, T., Tõnisson, H., Tamura, T., Vaasma, T. et al. 2022. Climatically induced cyclicity recorded in the morphology of uplifting Tihu coastal ridgeplain, Hiiumaa Island, eastern Baltic Sea. *Geomorphology*, **404**, 108187. https://doi.org/10.1016/j.geomorph.2022.108187

Suursaar, Ü., Torn, K., Mäemets, H. and Rosentau, A. 2024. Overview and evolutionary path of Estonian coastal lagoons. *Estuarine Coastal and Shelf Science*, **303**, 108811. https://doi.org/10.1016/j.ecss.2024.108811

Suursaar, Ü., Luik, K., Mäll, M., Jaagus, J. and Tõnisson, H. 2025. Long-term variations in sea ice extent can influence trends in maximum sea level in the northeastern Baltic Sea. *Continental Shelf Research*, **289**, 105451. https://doi.org/10.1016/j.csr.2025.105451

Tamura, T. 2012. Beach ridges and prograded beach deposits as palaeoenvironment records. *Earth-Science Reviews*, **114**(3–4), 279–297. https://doi.org/10.1016/j.earscirev.2012.06.004

Tarand, A., Jaagus, J. and Kallis, A. 2013. *Eesti kliima minevikus ja tänapäeval* (*Estonian Climate, Past and Present*). University of Tartu Press, Tartu.

Tõnisson, H., Orviku, K., Jaagus, J., Suursaar, Ü., Kont, A. and Rivis, R. 2008. Coastal damages on Saaremaa Island, Estonia, caused by the extreme storm and flooding on January 9, 2005. *Journal of Coastal Research*, **24**(3), 602–614. https://doi.org/10.2112/06-0631.1

Tõnisson, H., Suursaar, Ü., Rivis, R., Tamura, T., Aarna, T., Vilumaa, K. et al. 2020. Characteristics and formation of a solitary dune belt encountered along the coast of Estonia. *Journal of Coastal Research*, **95**(SP1), 689–694. https://doi.org/10.2112/SI95-134.1

Tõnisson, H., Männikus, R., Vaasma, T. and Rohumägi, K. 2022. *Nasva sadama tuuliku mõju setete liikumisele ja heljumi levik süvendamisel (The effect of the Nasva harbour windmill on sediment transport and turbidity dispersion during dredging)*. Report. Tallinn University, Institute of Ecology, Tallinn.

Tõnisson, H., Kont, A., Suursaar, Ü., Jaagus, J., Rivis, R. and Buynevich, I. 2024a. Morphosedimentary evolution of Estonian coastline: role of climatic and hydrodynamic forcing over the past decades. *Boreal Environment Research*, **29**(1–6), 103–125. https://www.borenv.net/BER/archive/pdfs/ber29/ber29-103-125.pdf

Tõnisson, H., Luik, K., Suursaar, Ü., Buynevich, I., Kont, A., Männikus, R. et al. 2024b. Rapidly transforming Holocene strandplain, affected by port jetty and hydroclimatic shifts – natural laboratory of past and future shoreline behavior. *Journal of Coastal Research*, **113**(SP1), 715–719. https://doi.org/10.2112/JCR-SI113-141.1

Tõnisson, H., Männikus, R., Kont, A., Palginõmm, V., Alari, V., Suuroja, S. et al. 2024c. Application of shore sediments accumulated in navigation channel for restoration of sandy beaches around Pärnu city, SW Estonia, Baltic Sea. *Journal of Marine Science and Engineering*, **12**(3), 394. https://doi.org/10.3390/jmse12030394

Tudyka, K., Miłosz, S., Adamiec, G., Bluszcz, A., Poręba, G., Paszkowski, Ł. et al. 2018. µDose: a compact system for environmental radioactivity and dose rate measurement. *Radiation Measurements*, **118**, 8–13.

Uścinowicz, G., Uścinowicz, S., Szarafin, T., Maszloch, E. and Wirkus, K. 2024. Rapid coastal erosion, its dynamics and cause – an erosional hot spot on the southern Baltic Sea coast. *Oceanologia*, **66**(2), 250–266. https://doi.org/10.1016/j.oceano.2023.12.002

Vaasma, T., Vandel, E., Sugita, S., Tõnisson, H., Suursaar, Ü., Kont, A. et al. 2025. Storminess reconstruction in the northeastern Baltic Sea region over the past 7600 years based on aeolian sand influx into coastal bogs. *The Holocene*, **35**(1), 61–74. https://doi.org/10.1177/09596836241285783

Vandel, E., Vaasma, T., Sugita, S., Tõnisson, H., Jaagus, J., Vilumaa, K. et al. 2019. Reconstruction of past storminess: evaluation of an indicator approach using aeolian mineral grains buried in peat deposits, Estonia. *Quaternary Science Reviews*, **218**, 215–227. https://doi.org/10.1016/j.quascirev.2019.06.026

Vestøl, O., Ågren, J., Steffen, H., Kierulf, H. and Tarasov, L. 2019. NKG2016LU: a new land uplift model for Fennoscandia and the Baltic Region. *Journal of Geodesy*, **93**, 1759–1779. https://doi.org/10.1007/s00190-019-01280-8

Vilumaa, K., Ratas, U., Tõnisson, H., Kont, A. and Pajula, R. 2017. Multidisciplinary approach to studying the formation and development of beach-ridge systems on non-tidal uplifting

coasts in Estonia. *Boreal Environment Research*, **22**, 67–81. https://www.borenv.net/BER/archive/pdfs/ber22/ber22-067-081-Vilumaa.pdf

Weisse, R., Dailidienė, I., Hünicke, B., Kahma, K., Madsen, K., Omstedt, A. et al. 2021. Sea level dynamics and coastal erosion in the Baltic Sea region. *Earth System Dynamics*, **12**(3), 871–898. https://doi.org/10.5194/esd-12-871-2021

Willis, J., Hamlington, B. and Fournier, S. 2024. *Global Mean Sea Level, Trajectory and Extrapolation*. https://doi.org/10.5281/zenodo.7702314 (accessed 2025-04-01).

Akumulatsiooni- ja erosioonisündmuste morfostratigraafia ning kronoloogia Järve rannajärsakul (Saaremaal, Lääne-Eestis) viimase 2000 aasta jooksul

Ülo Suursaar, Katre Luik, Alar Rosentau, Helena Alexanderson, Reimo Rivis, Tiit Vaasma, Egert Vandel, Kadri Vilumaa, Donatas Pupienis ja Hannes Tõnisson

Kliimamuutuse ja meretaseme tõusu koosmõjul toimuvad paljudes maailma paikades mererannikutel režiiminihked, näiteks Läänemere lõuna- ja kaguosas on suurenenud rannikuerosioon. Uuring rekonstrueerib Järve rannajärsaku setete ladestumise ja erosiooni ajaloo, kasutades uusi luminestsents- ja radiosüsiniku vanusemääranguid, georadari ja LiDARi kõrgusandmeid ning paljandi litoloogilist kirjeldust. Merepoolne rannavall, kus praegu asub uuritud 3,5 meetri kõrgune liivadesse tekkinud järsak, hakkas kujunema jääajajärgse maakerke ja setete kuhjumise tulemusena 3500–4000 aasta vanuse maasääre ette umbes 1600 aastat tagasi. Paljandi alumine osa settis madalas rannavööndis rannabarridele. Tumedamad settekihid ja litoloogilise koostise varieerumine peegeldavad muutusi settimistingimustes ja tormide aktiivsuses. Mereliste protsesside tagajärjel kuhjunud liivakihtide ülaosas asub õhuke eoolne kiht, mis on konkreetses paljandis nõrgalt arenenud. Luitelised pinnavormid esinevad Järve–Mändajala piirkonnas vaid mõnes üksikus nn ümberpuhutud kohas, mis on tõenäoliselt seotud väikese jääaja (~1300–1850 AD) külmema kliima ja inimtekkelise taimestiku kahjustamisega, nagu metsaraie või alepõllundus. Viimase ~100 aasta jooksul on varem kerkinud ja laienenud rannavallide ja maasäärte süsteem muutunud erosiooniliseks. Varasem suhtelise meretaseme langus on peatunud, talvist merejääd on üha vähem ning seetõttu on talvetormide mõju tugevam ja järsak taandub. Uuring demonstreerib, kuidas globaalsed muutused avalduvad mererannikul kohalikul tasandil, tuues ühtlasi esile merekarpide kasutamisega seotud metodoloogilised raskused rannikualade stratigraafilisel dateerimisel.

Estonian Journal of Earth Sciences
2026, **75**, 1, 53–66

https://doi.org/10.3176/earth.2026.04

www.eap.ee/earthsciences
Estonian Academy Publishers

RESEARCH ARTICLE

Received 3 September 2025
Accepted 25 February 2026
Available online 6 April 2026

Keywords:
Ordovician, stratigraphy, sedimentology, facies, sequences, Baltic, Estonia

Corresponding author:
Mark T. Harris
mtharris@uwm.edu

Citation:
Harris, M. T., Ainsaar, L., Hints, L., Männik, P., Meidla, T., Nõlvak, J. et al. 2026. The Upper Ordovician of Estonia: facies, sequences, and basin development. *Estonian Journal of Earth Sciences*, **75**(1), 53–66. https://doi.org/10.3176/earth.2026.04

The Upper Ordovician of Estonia: facies, sequences, and basin development

Mark T. Harris[a], Leho Ainsaar[b], Linda Hints[c], Peep Männik[c], Tõnu Meidla[b], Jaak Nõlvak[c], Tory Schultz[a] and Peter M. Sheehan[d]

[a] Department of Geosciences, University of Wisconsin-Milwaukee, Milwaukee, WI 53201, USA

[b] Department of Geology, Institute of Ecology and Earth Sciences, University of Tartu, Ravila 14a, 50411 Tartu, Estonia

[c] Department of Geology, Tallinn University of Technology, Ehitajate tee 5, 19086 Tallinn, Estonia

[d] Milwaukee Public Museum, 800 W. Wells Street, Milwaukee, WI 53233, USA

ABSTRACT

Sequence stratigraphic analysis of the Nabala–Porkuni regional stages (RSs; upper Katian–Hirnantian) of Estonia clarifies the Late Ordovician evolution of the Estonian Shelf–Livonian Basin. The integration of depositional facies, biostratigraphy, carbon isotope chemostratigraphy, karst surfaces, and hiatuses indicates seven sequences: (1) Nabala (Paekna and Saunja Formations (Fms)); (2) Vormsi (Kõrgessaare, Tudulinna, and Fjäcka Fms); (3) Lower Pirgu (Moe and Jonstorp Fms); (4) Middle Pirgu (most of the Adila and Halliku Fms, and Jelgava and Parovėja Fms); (5) Upper Pirgu (Kabala Member (Mb), part of the Halliku Fm); (6) Lower Porkuni Sequence (most of the Ärina Fm); and (7) part of the Upper Porkuni–Juuru Sequence (Kamariku Mb and Saldus Fm). A lowstand systems tract is only identified in the uppermost sequence. Transgressive units are marked by onlapping depositional packages. Highstands consist of one or more shallowing-upward shelf packages (notably in the Vormsi, Lower Pirgu, and Middle Pirgu sequences). The sequences record the progradation of shallow-to-middle ramp facies as sediment infilled the northern edge of the Livonian Basin, leading to an open shelf (Porkuni RS). Eustasy was the major factor in sequence boundary formation with larger amplitude sea level oscillations associated with Hirnantian (Porkuni) glaciations. A shift to more strongly differentiated ramp facies at the Nabala–Vormsi transition coincides with the initial collision of Baltica and Avalonia.

Introduction

This study describes the depositional facies and stratigraphic sequences of the upper Katian–Hirnantian (Upper Ordovician) strata of Estonia, and interprets the evolution of the Estonian Shelf of the East Baltic region. Sequence stratigraphy provides a method for interpreting facies patterns and stratigraphic relations within a chronostratigraphic framework. A sequence-by-sequence facies analysis can reveal the detailed history of relative sea level changes and basin-scale depositional patterns that can clarify tectonic history. This report builds on our prior study of western Estonia (Harris et al. 2004) in three ways. First, it uses additional core data to extend the stratigraphic analysis to include mainland Estonia. Second, the integration of core coverage with recent biostratigraphic and chemostratigraphic studies clarifies the position and temporal resolution of facies changes, stratigraphic hiatuses, and stratal relationships at a systems tract level. Third, the expanded geographical coverage reveals the evolution of the Estonian Shelf from a carbonate ramp to an open shelf at the end of the Ordovician, and subtle tectonic influences on depositional patterns.

Geological setting and stratigraphy

The study area lies along the north flank of an epicontinental basin on the paleocontinent of Baltica that formed during the late Precambrian and that was influenced by the collision with the Avalon microcontinent during the Late Ordovician (Torsvik and Rehnström 2003; Cocks and Torsvik 2005). It straddles the transition between the Estonian Shelf and the Livonian Basin, an embayment of the Scandinavian Basin

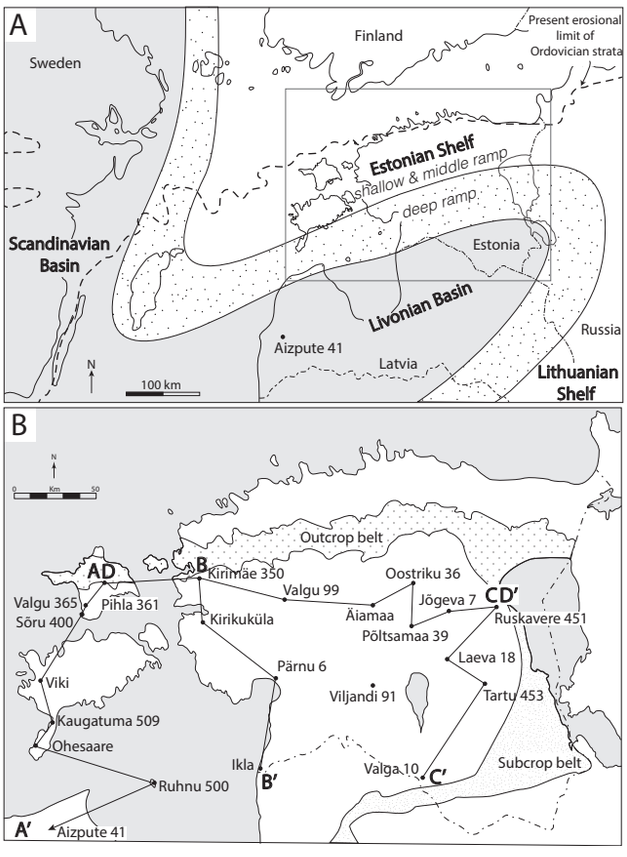

Fig. 1. Location map of the study area. **A** – major paleogeographic features of the Baltic region during the late Katian (Vormsi–Pirgu RSs). The location of the Aizpute core in northwestern Latvia is shown. The boxed area indicates the location of B. Modified from Ainsaar and Meidla (2001). **B** – locations of studied cores and the lines of cross sections A–A′ to D–D′ used in Figs 4–7.

(Jaanusson 1973, 1976; Bassett et al. 1989; Kaljo 1990; Raukas and Teedumäe 1997; Fig. 1A). The northern Estonian outcrop belt nearly parallels depositional strike and exposes a section of shallow-ramp and middle-ramp carbonates (Fig. 1B). The section deepens southward across the central Estonian deep-ramp zone into deep-water shales of the Livonian Basin in southern Estonia, western Latvia, and northwestern Lithuania. The Lithuanian Shelf forms the southeastern edge of the Livonian Basin in eastern Latvia, southeastern Lithuania, and northwestern Belarus.

The stratigraphic nomenclature of the study area is complex, reflecting the location along an environmental gradient and resulting in the use of different formation names for shallow and deep sections (Fig. 2). Within the East Baltic, regional stages provide a consistent framework (Bassett et al. 1989; Männil 1990; Männil and Meidla 1994; Raukas and Teedumäe 1997 and references therein) based on biostratigraphic work on conodonts (Männik and Viira 1990), chitinozoans (Nõlvak and Grahn 1993; Nõlvak 1999), ostracodes (Meidla and Sarv 1990; Meidla 1996), graptolites (Männil 1976; Männil and Meidla 1994), brachiopods (Hints 1990), bentonite correlations (Kiipli et al. 2004), and, most recently, carbon isotope chemostratigraphy (Ainsaar et al. 2010, 2015; Meidla et al. 2020; Hints et al. 2023). These stratigraphic studies are also the basis for correlations of the Baltic regional stages with global stages (Hints et al. 1994; Goldman et al. 2023; Meidla et al. 2024). This study addresses the upper Nabala, Vormsi, Pirgu, and Porkuni regional stages (RSs), and is equivalent to the upper Katian and most of the Hirnantian Global Stages. This study's lithostratigraphic nomenclature follows general usage with more recent updates (Raukas and Teedumäe 1997; Hints et al. 2005; Meidla et al. 2024; Fig. 2).

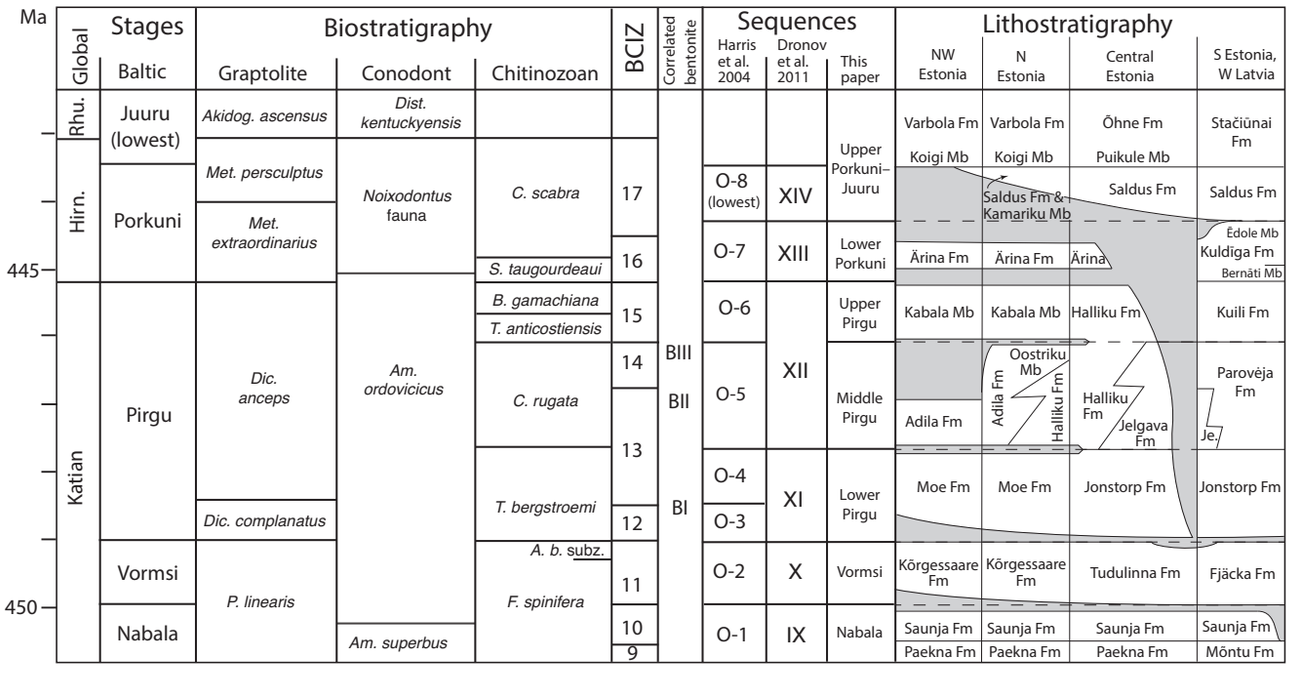

Fig. 2. Late Ordovician (Nabala to basal Juuru RSs) stratigraphy. Abbreviations: Hirn. – Hirnantian, Rhu. – Rhuddanian, BCIZ – Baltic carbon isotope zones (Ainsaar et al. 2010), *Akidog.* – *Akidograptus*, *Met.* – *Metabolograptus*, *Dic.* – *Dicellograptus*, *P.* – *Pleurograptus*, *Dist.* – *Distomodus*, *Am.* – *Amorphognathus*, *C.* – *Conochitina*, *S.* – *Spinachitina*, *B.* – *Belonechitina*, *T.* – *Tanuchitina*, *A. b.* subz. – *Acanthochitina barbata* subzone, *F.* – *Fungochitina*, Fm – formation, Mb – member, Je. – Jelgava. The Kamariku Mb is part of the Ärina Fm (see text for discussion). The time scale is from Goldman et al. (2020, 2023) and Meidla et al. (2024).

This paper uses the absolute time scale currently in use by the Estonian Geological Survey (Goldman et al. 2020, 2023; Meidla et al. 2024), pending consideration of ongoing research (Zhang et al. 2025).

Materials and methods

This study is based on a detailed, centimeter-scale description of 23 cores distributed from the Estonian Shelf to the Livonian Basin (Fig. 1B). The cores were described on sedimentological logs at a 1:50 scale that summarized depositional texture, sedimentary structures, grain size, ichnofabric index, clay content, color, and fossil content. The cores are held at the core storage facilities of the Geological Survey of Estonia and the Department of Geology of Tallinn University of Technology. Twenty-two of the cores were drilled in Estonia, and one in Latvia. Most cores penetrated the entire study section (upper Nabala through Porkuni RSs). The cores do not include the type sections of the stratigraphic units studied because most formations were defined in outcrop sections, and others are in cores that we did not examine. Our major criteria were to select cores that are relatively complete, provide coverage across the facies belts, and include useful biostratigraphic and chemostratigraphic data. We have also made use of stage-level thickness maps that incorporate data from numerous additional wells (Raukas and Teedumäe 1997).

A critical factor in the analysis of these sections is the identification of stratigraphic hiatuses using biostratigraphy, bentonite correlations, and carbon isotope chemostratigraphy. The study spans eight Baltic carbon isotope zones (BCIZ), seven chitinozoan zones, and five graptolite zones. Four conodont zones occur within the studied section, with the *Amorphognathus ordovicicus* Zone dominating the lower three-quarters. Three key bentonite beds correlated by phenocryst chemistry provide additional chronostratigraphic horizons in the Pirgu RS (Kiipli et al. 2004; Hints et al. 2005). Multiple studies of the BCIZ and chitinozoan zones in key cores have clarified the age relationships among these chronostratigraphically useful horizons (Bauert et al. 2014; Hints et al. 2014; Ainsaar et al. 2015; Meidla et al. 2020; Hints et al. 2023), resulting in an integrated chronostratigraphic framework (Fig. 2).

Depositional facies

The studied cores extend from the Estonian Shelf to the northern edge of the Livonian Basin, and are characterized by five interfingering facies. These facies shifted north and south across the profile, reflecting transgressions and regressions (Jaanusson 1973, 1976; Einasto 1986, 1995; Bassett et al. 1989; Nestor 1990a, 1990b; Nestor and Einasto 1997; Harris et al. 2004; Dronov et al. 2011).

Grain-supported facies

The grain-supported facies consists of packstones and grainstones with a diverse marine fauna and common sedimentary structures indicative of wave and current activity. Four subfacies occur: (1) Packstones containing physical structures (ripples, wavy and cross laminations) overprinted by burrowing and bioturbation indicate depositional conditions at or above fairweather wavebase. These are widespread in updip Vormsi, Pirgu, and Porkuni RSs. (2) Ooid grainstone with crossbeds and wavy, flat, and cross lamination styles is restricted to the Porkuni RS. (3) Algal grainstone beds adjacent to lower Pirgu algal mounds are dominated by the calcareous algae *Palaeoporella*. (4) Intraclastic floatstone beds (1–3 m thick) occur at the base of some channel fills in the Porkuni RS (Jõgeva and Oostriku cores).

The grain-supported facies is interpreted as a shallow-water deposit that accumulated above fairweather wavebase. In the Vormsi and Pirgu RSs, it typically occurs at the top of shallowing-upward facies successions in updip locations. In the Porkuni RS, the grain-supported facies occurs across the shelf and includes ooid grainstones. Quartz sand is widespread in Porkuni RS strata, reaching up to 40% in the basal parts of the Saldus Formation (Fm) in some cores. In the most basinward core (Aizpute, northwestern Latvia), a 3-m bed of rippled ooids and quartz sand occurs.

Mixed facies

The mixed facies primarily consists of two subfacies: (1) the interbedded packstone and wackestone subfacies that are marked by abundant burrows, a diverse marine biota, and a high level of bioturbation, and (2) the argillaceous wackestone subfacies with a higher clay content that occurs as thin beds within this subfacies. The absence of physical sedimentary structures and the interlayering of grain-rich and argillaceous deposits suggest deposition at intermediate depths between fairweather and storm wavebase.

The mixed facies occurs in middle ramp settings throughout the Vormsi and Pirgu RSs, and in the most updip facies preserved in the upper Nabala RS (Saunja Fm).

Mud-supported facies

The mud-supported facies includes several subfacies differentiated based on faunal and clay content; all are well burrowed. (1) The main part of the Saunja Fm consists of the mudstone subfacies with echinoids, bryozoans, gastropods, ostracodes, and other fossil fragments with marly interbeds. (2) The fossiliferous wackestone subfacies contains a diverse marine fauna (echinoderms, tabulate corals, rugose corals, brachiopods, calcareous algae, etc.) with argillaceous and/or mudstone interbeds. It predominates in deep-ramp zone areas of the Vormsi (Tudulinna Fm) and Pirgu RSs (Halliku and Jonstorp Fms) and also occurs in the lagoon in northern Estonia (Pirgu RS). (3) The argillaceous mudstone-marl subfacies contains up to 40–45% clay and fine fossil fragments. It occurs in the Tudulinna Fm (Vormsi RS) in the deep-ramp zone and in the Pirgu RS along the edge of the Livonian Basin.

These subfacies all record quiet-water deposition. The mudstone subfacies is limited to the Saunja Fm, whereas the wackestone subfacies accumulated widely during the Vormsi–Pirgu time. The argillaceous mudstone-marl subfacies records the increased clay influx that characterizes the Vormsi RS.

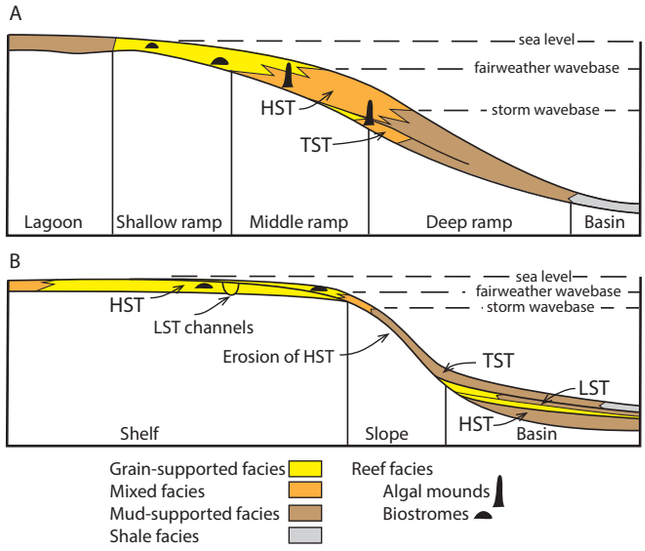

Fig. 3. Facies models with systems tracts. **A** – ramp facies model for the Nabala, Vormsi, and Pirgu RSs. **B** – open-shelf facies model for the Porkuni RS. Abbreviations: HST – highstand systems tract, TST – transgressive systems tract, LST – lowstand systems tract.

Shale facies

Basinal sections of the Vormsi RS consist of laminated to bioturbated black, dark gray, and green shales with horizontal burrows. The sparse fauna predominantly consists of graptolites. These shales are assigned to the Fjäcka Fm, a unit that occurs throughout the central Livonian and Scandinavian basins.

Mud mound facies

Two mud mounds occur in the studied cores in the lower Pirgu RS. (1) The Moe Fm in the Kaugatuma core contains a 5.7 m-thick unit of the stromatactis subfacies. The mound is red to pink in color and consists of four 1–2.6 m-thick stromatactis beds interbedded with 20-cm-thick beds of skeletal packstone. It is overlain by a 90-cm-thick bed of skeletal packstone. (2) The Jõgeva core penetrated a 25.3 m-thick algal mound dominated by *Palaeoporella* algae (Perens 1995). This subfacies contains abundant algae, crinoid clasts, and vugs; it is highly dolomitized. Both mounds initially formed in middle-ramp settings; the Jõgeva mound was more updip and persisted into shallow-ramp conditions.

Mud mounds consisting of stromatactis, *Palaeoporella*, or a combination of both subfacies are widespread in Pirgu sections of the East Baltic (Kröger et al. 2017). The thickest (52 m) mud mound occurs in the Võhma core, 24 km west of Põltsamaa, and includes both subfacies (Kröger et al. 2017).

Although not encountered in the described cores, patch reefs and biostromes are reported from the Pirgu and Porkuni RSs in shallow-ramp sections. These are up to 3 m thick and consist of a core with abundant stromatoporoids and tabulate corals flanked by pelmatozoan grainstone (Kröger et al. 2017).

Facies model

The Nabala to Pirgu strata were deposited on a broad homoclinal ramp; the depositional facies reflect an energy gradient related to fairweather and storm wavebase (Read 1983; Burchette and Wright 1992; Fig. 3A). The grain-supported, mixed, and mud-supported facies belts represent progressively deeper and lower-energy settings of shallow, middle, and deep ramp environments, respectively. The distribution of the shale facies is limited to the deep basin. Within the middle ramp settings, the *Palaeoporella* bioherms and stromatactis mud mounds form local shoals and patch reefs. Pirgu sequences include a zone of updip mud-supported facies that represents a lagoon landward of the shallow ramp shoal and patch reef environments. Thicker shallow- and middle-ramp facies accumulations resulted in shallowing and progradation of the facies succession.

Porkuni age facies are similar but are interpreted as representing an open shelf setting with shallow shelf and basin facies separated by an erosional/bypassing slope (James et al. 2010; Fig. 3B). Grain-supported facies delineate an extensive zone of shallow-water deposition; basinal marls and mudstones are interbedded with grain-supported beds with abundant quartz, small lithoclasts, and redeposited ooids. The intervening stratigraphic gap between these facies and the deposits in the Livonian Basin is interpreted as due to slumps, slides, and erosion associated with a major hiatus in a slope setting.

Stratigraphic hiatuses

Well-documented stratigraphic hiatuses occurring within the studied Estonian Shelf sections are marked by missing biostratigraphic and/or carbon isotope zones (Einasto 1995; Nestor and Einasto 1997; Ainsaar et al. 2010; Meidla et al. 2024). These occur at the top of the Nabala RS, at the top of the Vormsi RS, in the middle of the Pirgu RS (at the top of the Moe and Jonstorp Fms), in the upper Pirgu RS (at the base of the Kabala Member (Mb)), at the top of the Pirgu RS, and in the middle of the Porkuni RS (below the Kamariku Mb of the Ärina Fm and the Saldus Fm; Fig. 2). In updip cores, hiatuses are marked by missing biozones and the absence of transgressive beds (found in more basinward cores).

The most extensive hiatuses occur in two specific positions in the profile. At the outer edge of the Porkuni shelf, erosion along the shelf margin and slope locally removed all or most of the Pirgu RS, probably augmented by sliding and slumping as the ramp prograded and built an open-shelf platform with a steepened outer slope (Figs 4–6). Shallow open-shelf sections are marked by local erosional channels cut into deposits of the Pirgu and Porkuni RSs (Fig. 7).

Sequences

Placing the facies distribution into a sequence stratigraphic framework reveals the three-dimensional facies architecture and depositional history of the Estonian Shelf (Figs 4–8). The NNE–SSW orientation of the Livonian Basin results in facies trends slightly oblique to the outcrop belt, resulting in a transition into slightly deeper environments to the east (Figs 1 and 7).

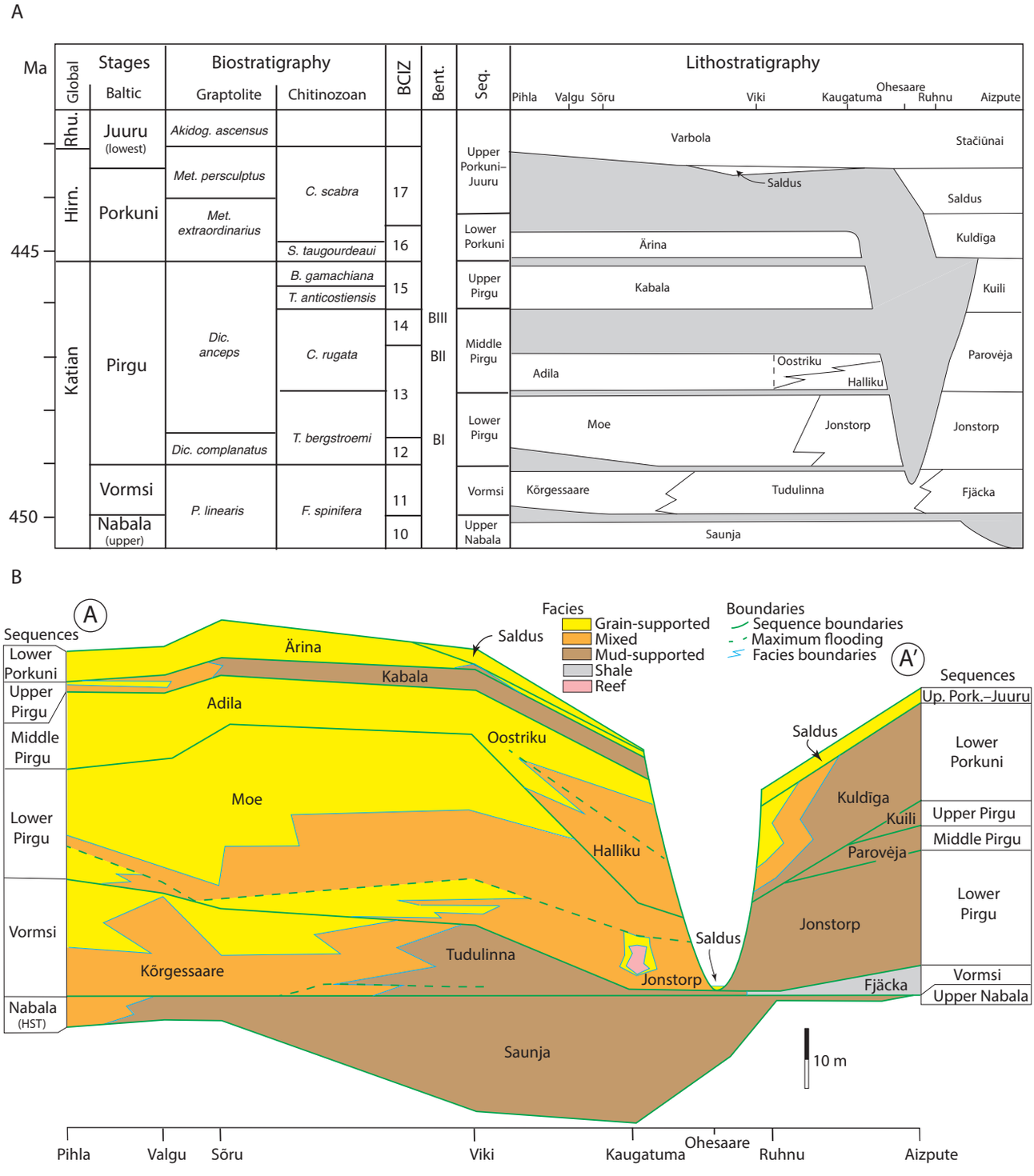

Fig. 4. Section A–A′ (Fig. 1B). The Aizpute core is located in northwestern Latvia (Fig. 1A). **A** – chronostratigraphy; **B** – facies relations and sequence interpretations. Note that the Saldus Fm is recognized in the Viki and Kaugatuma cores (unlike in Harris et al. 2004), following Hints et al. (2014). Abbreviations: Bent. – bentonite, Seq. – sequences, Up. Pork. – Upper Porkuni; for other abbreviations, see Fig. 2.

The facies patterns, erosional features, and stratigraphic gaps provide the basis for dividing the studied section into five complete sequences and two partial sequences. Ideally, sequences consist of onlapping transgressive systems tracts (TST) overlain by a maximum flooding surface, which is the base of a shallowing-upward highstand systems tract (HST) capped by an exposure surface (Fig. 3). In practice, some transgressive units cannot be resolved (in downdip sections) or are missing (in updip sections), and some highstands are eroded. A lowstand systems tract (LST) is only clearly resolvable in the Upper Porkuni–Juuru Sequence.

Nabala Sequence

The Nabala Sequence consists of the laterally equivalent Paekna and Mõntu Fms, and the overlying Saunja Fm. They are within the *Fungochitina spinifera* chitinozoan biozone; the lower

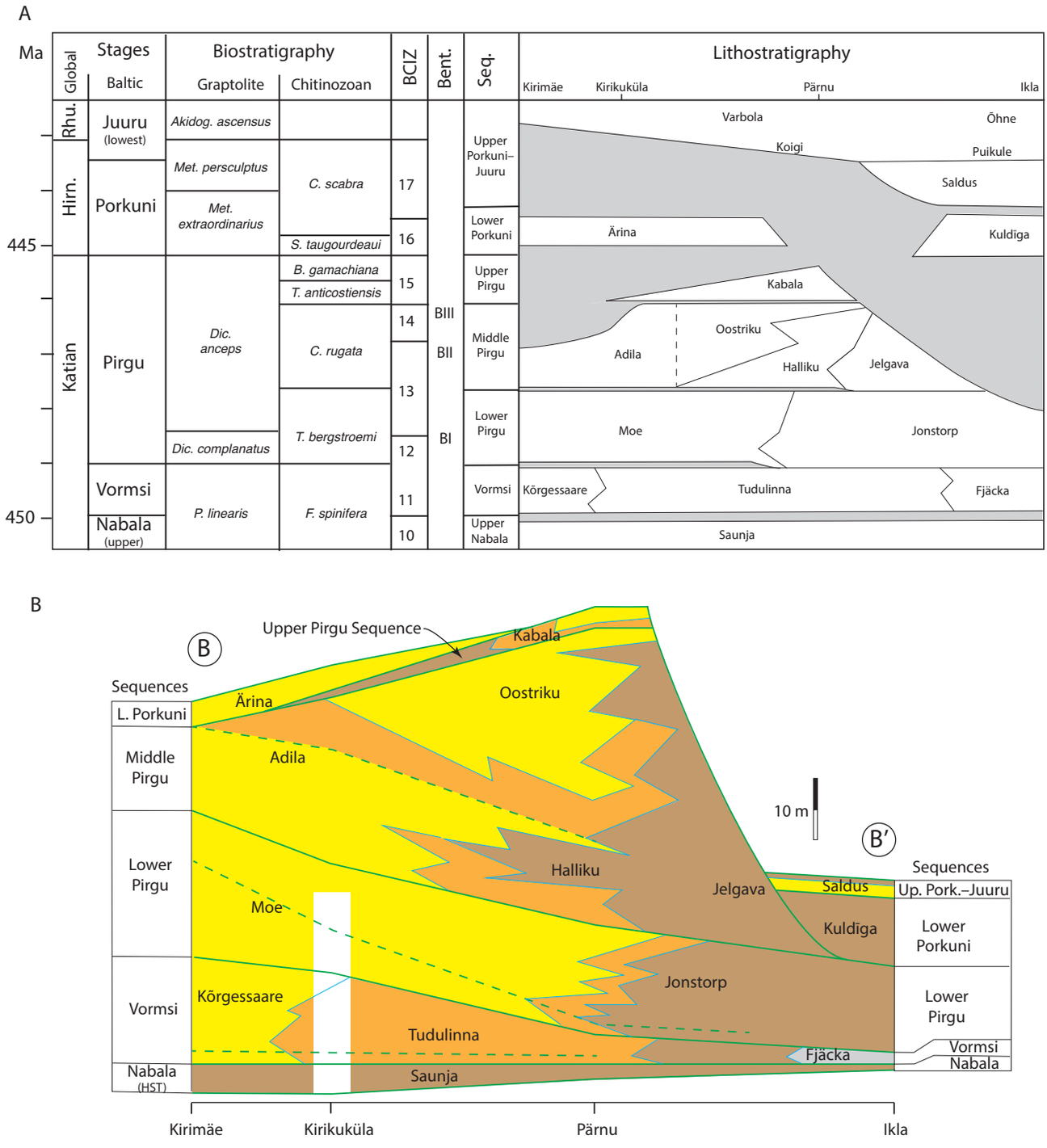

Fig. 5. Section B–B′ (Fig. 1B). **A** – chronostratigraphy; **B** – facies relations and sequence interpretations. See Fig. 4 for the key. The uncolored section of the Kirikuküla core represents missing core. Abbreviation: L. – Lower; for other abbreviations, see Figs 2 and 4.

units are in BCIZ 9, whereas the Saunja Fm forms the Saunja Carbon Isotope Excursion (BCIZ 10) (Ainsaar et al. 2010).

The Paekna and Mõntu Fms were not studied in detail in this study. They consist of packstones in the northwestern part of the study area and grade into mixed wackestones and mudstones toward the south. The overlying Saunja Fm varies in thickness between less than 5 and 20 m (Fig. 8A) across the study area, but thins to less than 1 m in northwestern Latvia (Calner et al. 2010) and is locally absent in the Aizpute core. The unit consists of the mud-supported facies (mudstone subfacies), except in the Pihla core, the most northwesterly location, where the mixed facies occurs; evidence of progradation is absent. The lower boundary is a marine flooding surface marked by a sharp contact with the underlying units. The upper boundary is a regional karst surface documented by Calner et al. (2010), who attributed some of the thickness variations to karst-related erosion. Seismic studies in the Baltic Sea west of the studied wells indicate that this horizon is also marked by erosional channels (Tuuling and Flodén 2000). The absence of the Saunja Fm in the Aizpute core is attributed to erosion along the sequence boundary.

The Paekna and Mõntu Fms are interpreted as shallow- and middle-ramp facies of the TST, overlain by a marine flooding surface. The deep-ramp facies of the Saunja Fm

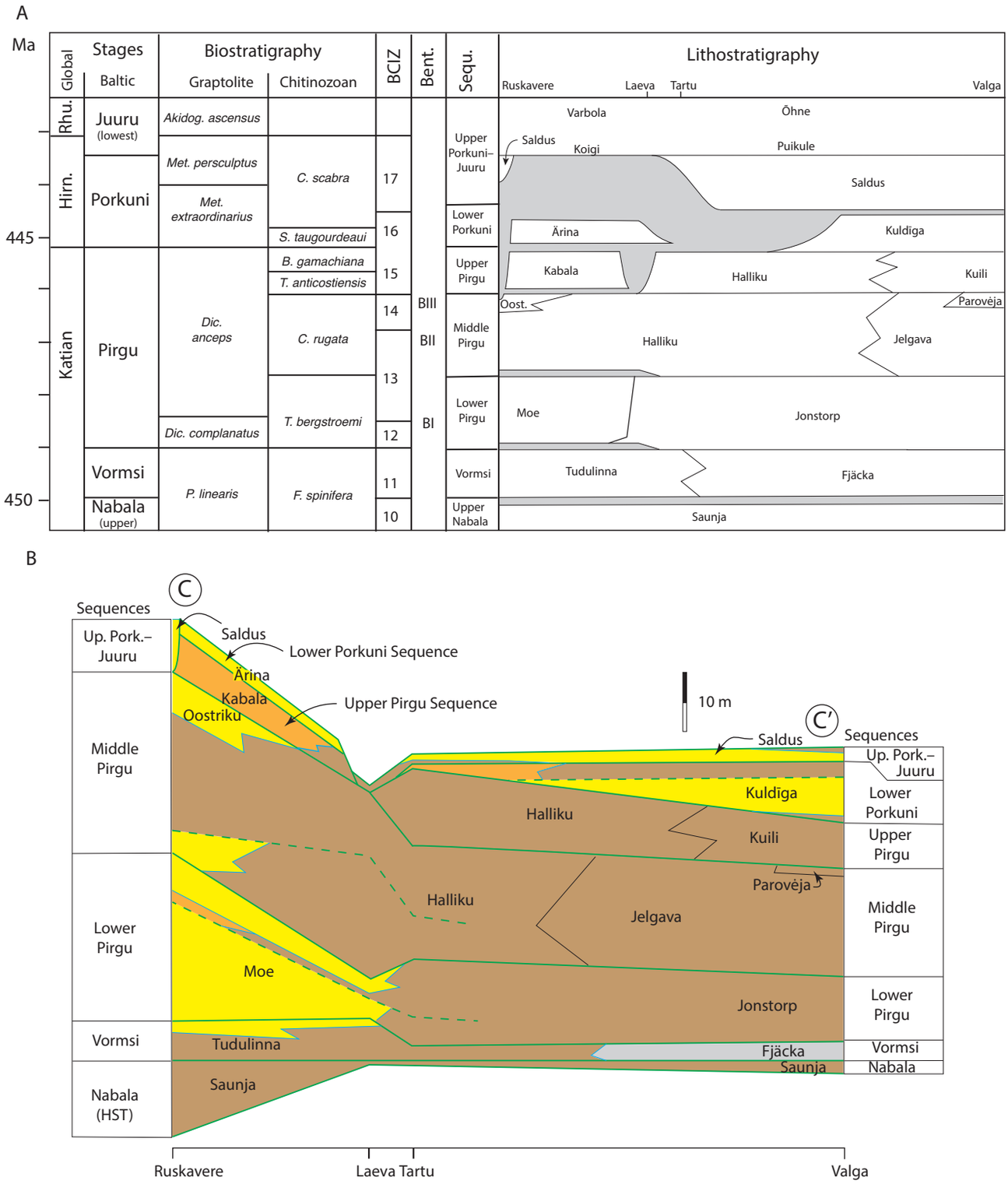

Fig. 6. Section C–C′ (Fig. 1B). **A** – chronostratigraphy; **B** – facies relations and sequence interpretations. See Fig. 4 for the key. Abbreviation: Oost. – Oostriku; for other abbreviations, see Figs 2, 4 and 5.

form the HST capped by the regional exposure surface. There is no evidence for highstand progradation within the study area.

Vormsi Sequence

The Vormsi Sequence consists of the time-equivalent Kõrgessaare, Tudulinna, and Fjäcka Fms. The sequence is in BCIZ 11 and the *F. spinifera* chitinozoan zone (including the *Acanthochitina barbata* chitinozoan subzone in its upper part).

Grain-supported facies and mixed facies comprise the updip Kõrgessaare Fm; mixed facies and mud-supported facies comprise the Tudulinna Fm; and the Fjäcka Fm consists of shale facies. The thickness of the sequence varies from less than 5 m in the basin to over 20 m in shallow-ramp areas (Fig. 8B). The facies and thickness patterns define a typical ramp-to-basin profile.

The basal boundary of the sequence is the regional karst surface above the Saunja Fm. In shallow-to-middle ramp set-

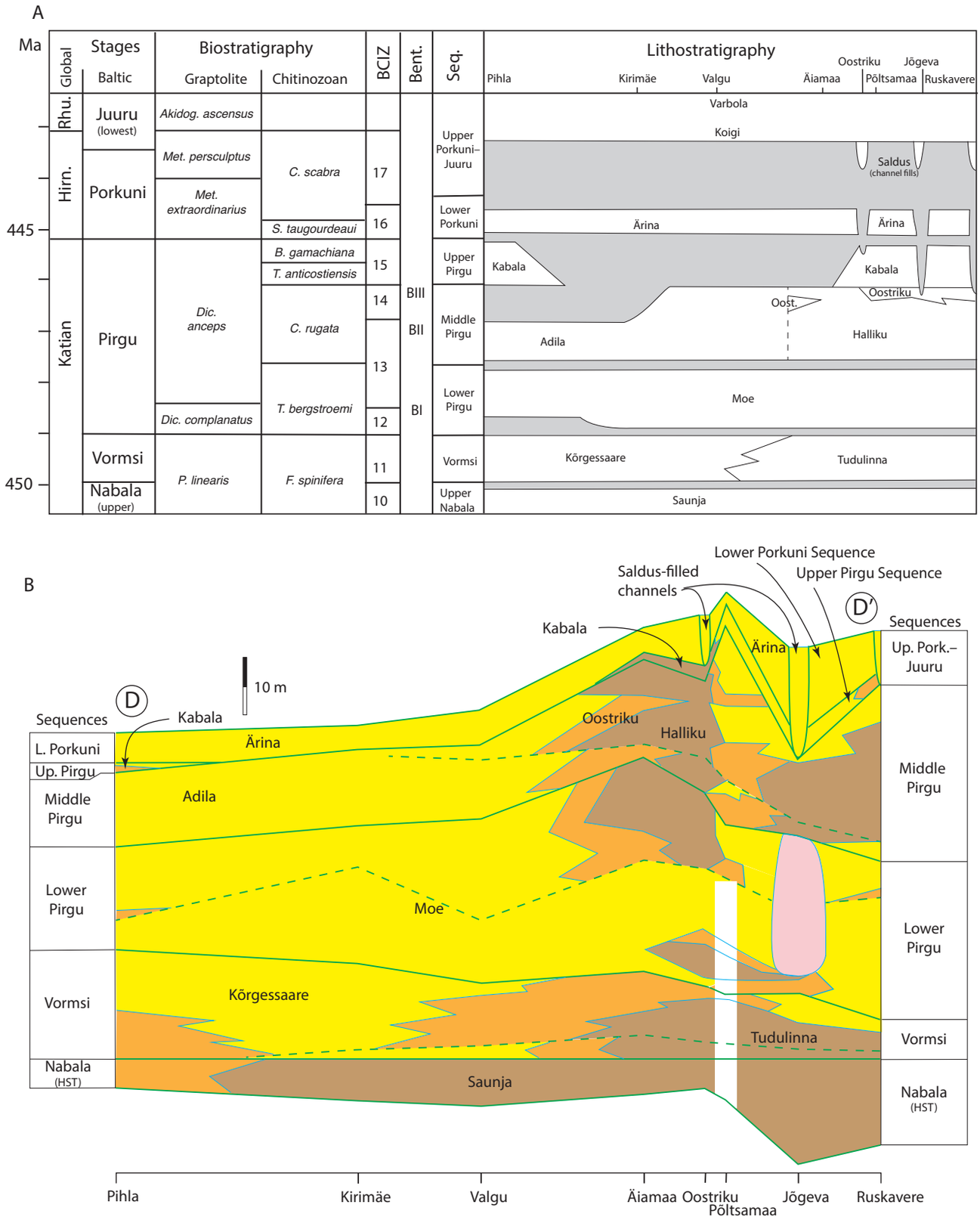

Fig. 7. Section D–D′ (Fig. 1B). **A** – chronostratigraphy; **B** – facies relations and sequence interpretations. See Fig. 4 for the key. The uncolored section of the Põltsamaa core represents missing core. For abbreviations, see Figs 2, 4 and 5.

tings, this surface is overlain by a thin (~2 m) shallowing-upward parasequence, which forms the TST, although it is absent in the northwest, indicating a subtle hiatus. A thick (10–13 m) shallowing-upward, prograding HST capped by grain-supported facies (shallow ramp) extends across the northern part of the study area. The upper boundary coincides with the stage boundary. Hints et al. (2007) attributed thickness variations in northern and central Estonia to erosion. The Vormsi RS is unusually thin in some outer-ramp cores (0.3 m in Ohesaare, 1.2 m in Kaugatuma), and the *Acanthochitina*

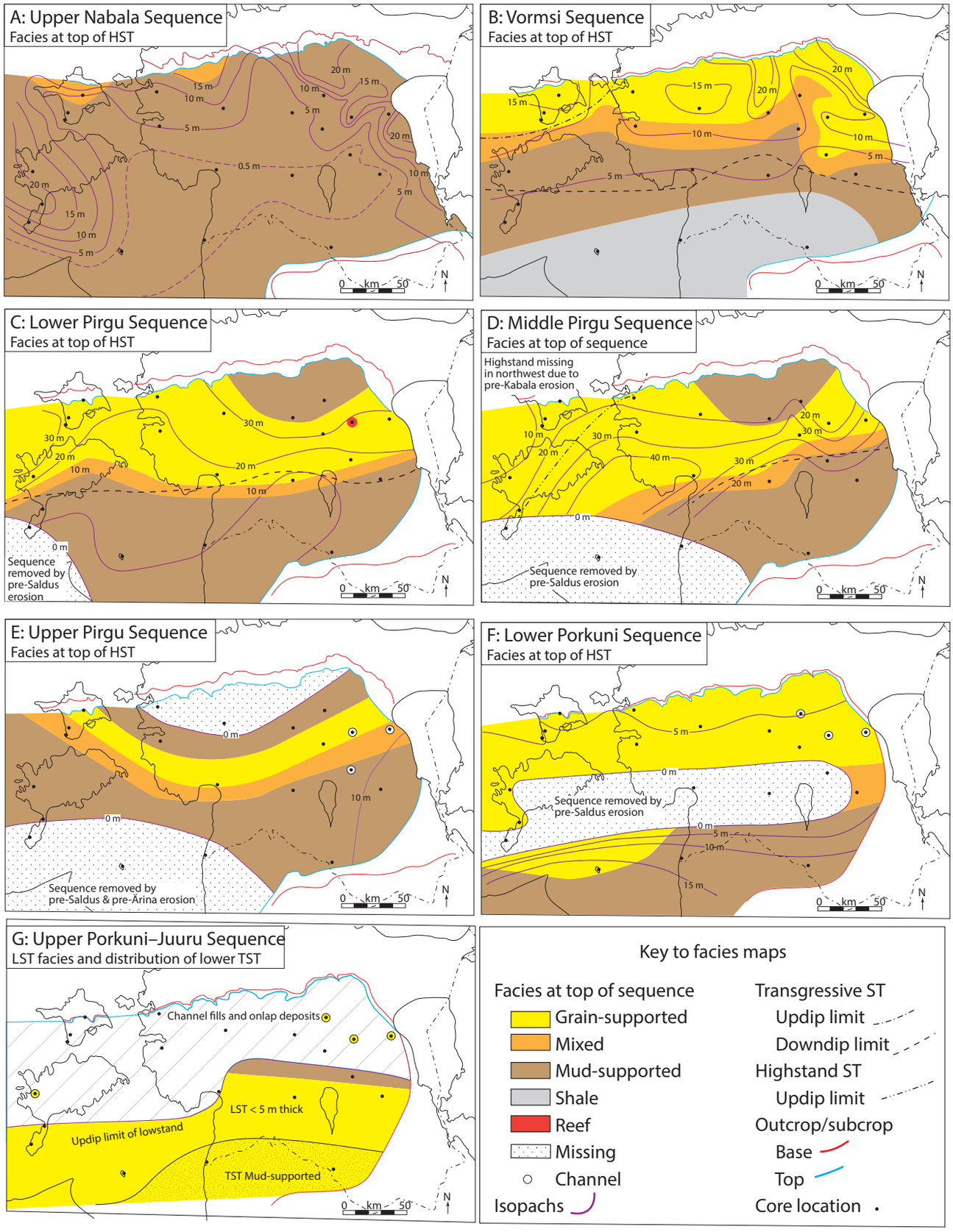

Fig. 8. Sequence isopach and facies maps. Facies at the top of the highstand systems tract (HST) except for the northwestern part of D. For abbreviations, see Fig. 3.

barbata chitinozoan subzone is missing in some southern cores (Kaugatuma, Ikla, and Viljandi; Nõlvak, unpublished data), indicating erosion along the upper boundary.

The Vormsi Sequence is bounded by erosional unconformities, and consists of a thin onlapping TST and a thick prograding HST. In contrast to the underlying Nabala Sequence, the full suite of ramp facies is present.

Lower Pirgu Sequence

The Lower Pirgu Sequence consists of the Moe and Jonstorp Fms, and is in the *Tanuchitina bergstroemi* chitinozoan biozone and BCIZ 12 and the lower part of BCIZ 13.

The Moe Fm consists of a shallowing-upward succession that consists of mixed facies (middle ramp) overlain by grain-supported facies (shallow ramp). The algal bioherm in the Jõgeva core formed in the middle ramp and extends upward into the shallow shelf, where it is capped by a karst surface (Perens 1995; Fig. 7). To the northeast, an area of mud-supported facies occurs, representing a lagoon north of shallow-ramp deposits (Fig. 8C). The Jonstorp Fm primarily consists of mud-supported (deep ramp) facies with some mixed (middle ramp) facies along its northern extent. In the Kaugatuma core, the lower part of the formation includes a stromatactis bioherm within the mixed facies (Fig. 4).

The base of the sequence is locally marked by erosion at the top of the Vormsi RS. The sequence is generally 20–30 m thick in shallow-to-middle ramp sections, and thins to less than 10 m in deep ramp settings (Fig. 8C). In the extreme southwest (Ohesaare), the sequence is missing due to pre-Saldus erosion. A TST consisting of a shallowing-upward parasequence is recognizable in the northern two-thirds of the area but cannot be differentiated in southern cores. The base of the HST is marked by a maximum flooding surface along which the Kaugatuma bioherm terminated. The overlying HST records the progradation of high-energy shallow ramp deposits and the development of a lagoon to the northeast.

Middle Pirgu Sequence

The Middle Pirgu Sequence consists of the Adila (excluding the Kabala Mb), Oostriku, Jelgava, and Parovėja Fms, and most of the Halliku Fm. The sequence is in the *Conochitina rugata* chitinozoan biozone and BCIZ 13 and 14.

Across northern Estonia, the base of the sequence consists of grain-supported (shallow ramp) facies (lower Adila Fm) capped by a flooding surface, which is overlain by mixed and mud-supported (middle and deep ramp) facies of the Halliku Fm. At the top of the sequence, grain-supported facies (Adila and Oostriku Fms) delineate up to four shallowing-upward packages (Pärnu core; Fig. 5); to the northeast, mud-supported facies delineate a lagoon. The upper part of the sequence (including all of BCIZ 14) is missing in northwestern cores (Figs 2 and 8D). South of the grain-supported belt, mixed and mud-supported facies (Halliku Fm) and argillaceous mud-supported facies (Jelgava Fm) record middle and deep ramp environments. The most basinal deposits are the argillaceous mudstones and marls of the Jelgava and Parovėja Fms (Valga and Aizpute cores).

The thickness of the Middle Pirgu Sequence ranges from 10 to over 40 m (Fig. 8D). The thickest accumulations are across the middle of the study area, along the southern edge of the shallow ramp deposits of the underlying Lower Pirgu Sequence. In the southwest, the area of missing section due to pre-Ärina and pre-Saldus erosion expanded to include the Ruhnu and Ikla core locations.

The sequence overlies a sharp surface marked by karst (Jõgeva core). In the north, the TST is dominated by high-energy shallow ramp facies that grades into deeper ramp facies to the south and southeast. The HST sits above a major flooding surface, but it is missing, presumably eroded, in western and northwestern cores, an area with a relatively thin section. In contrast, the Pärnu core has a thick section of multiple prograding ramp packages. This pattern of sediment accumulation resulted in a thick section in the west-central part of the study area (with a maximum exceeding 40 m).

Upper Pirgu Sequence

The Upper Pirgu Sequence consists of the Kabala Mb of the Adila Fm, part of the Halliku Fm, and the Kuili Fm. It falls in BCIZ 15 and includes the *Tanuchitina anticostiensis* and *Belonechitina gamachiana* chitinozoan biozones.

This sequence is a relatively thin (<10 m except to the southeast) package of argillaceous, mixed, and mud-supported facies that extends into shallow ramp settings (Figs 4, 5 and 8E). This is overlain by a grain-supported (shallow ramp) facies that separates an expanded lagoon (mud-supported facies) from the deep ramp settings toward the south (Halliku and Kuili Fms). The lower boundary is a flooding surface that overlies the eroded Lower Pirgu Sequence. The upper boundary is a sharp surface that marks the stage boundary above. The Upper Pirgu Sequence is missing in several northern mainland cores due to updip erosion or non-deposition (Kirimäe, Valgu), or erosion below pre-Saldus channels (Jõgeva, Ruskavere, Laeva; Perens 1995). The sequence is also missing in the southwest (Ikla, Ruhnu, Ohesaare) due to pre-Ärina erosion.

Systems tracts are difficult to identify in this thin package; it appears to be primarily an HST initiated by rapid flooding. The thickest section (Tartu core) indicates more accumulation in deep ramp settings to the southeast.

Lower Porkuni Sequence

The Lower Porkuni Sequence consists of the Ärina (except the Kamariku Mb) and Kuldiga Fms. The sequence sits in the *Spinachitina taugourdeaui* and lowest *Conochitina scabra* chitinozoan zones, and in BCIZ 16 and (probably) the lowest BCIZ 17.

A notable gap divides the sequence into a northern zone and a southern zone (Fig. 8F). In northern sections, the Ärina Fm is composed of 2–6 m of grain-supported facies and is divided into four interbedded members (below the Kamariku Mb) that include patch reefs and oolitic shoals (Hints et al. 2000). Southern sections consist of thicker (10–16 m) mud-supported facies (Kuldiga Fm); the lower part of one core (Valga) consists of grain-supported facies. A limited area of mixed

facies to the east (Tartu core) overlies the thickest section of the underlying sequence. Across both zones, quartz sand is a significant constituent (<15%) in some sections.

The sequence is bounded by erosional surfaces that are recorded by a widespread stratigraphic gap between the northern and southern zones, erosive fluvial channels, and influxes of quartz sand. The most extensive erosional surface occurs between the northern and southern zones based on lithostratigraphic and biostratigraphic data; in places, the entire Pirgu RS is absent (the Saldus Fm overlies a very thin Vormsi RS bed at Ohesaare). It appears to be a composite unconformity surface with truncation occurring below both the Lower and Upper Porkuni sequences (Figs 4–6). The stratigraphic gap is interpreted as the result of slumping and erosion along a margin steepened by the progradation of earlier ramps; the preserved mixed facies may be due to a lower slope to the east due to the thicker Upper Pirgu Sequence accumulation. In northern sections, the pre-Ärina surface truncates the Kabala Fm, which is thin or absent in some cores (Figs 7 and 8F). The upper sequence boundary is marked by numerous channels that cut into the Lower Porkuni, Upper Pirgu, and Middle Pirgu sequences (Perens 1995).

The two Porkuni sequences record the development of an open-shelf profile, which is attributed to the accumulation of a wedge of Vormsi and Pirgu ramp deposits (Figs 4 and 5).

Upper Porkuni–Juuru Sequence (LST and lower TST)

The Ordovician section contains the lower part of the Upper Porkuni–Juuru Sequence, including the Saldus Fm and the Kamariku Mb of the Ärina Fm. The Ordovician part of this sequence (LST and lower TST) is in the *Conochitina scabra* chitinozoan zone and in BCIZ 17.

The Porkuni part of this sequence consists of two components. The lower Saldus Fm in the basin and shelf channel fills consists of conglomerates and quartz-rich (up to 40–50%) rippled packstones. The upper Saldus Fm and Kamariku Mb are grain-supported facies with wavy ripples and normal marine fauna, whereas equivalent mud-supported facies (wackestones) occur in basinal areas (Fig. 8G).

The lower Saldus strata are interpreted as LST deposits that bypassed the exposed shelf (except for local channel fills) and accumulated in basinal areas. The TST is recorded in the shift to more normal marine deposits in the basin (Saldus Fm), shelf channel fills (Saldus Fm), and open-shelf (Kamariku Mb) settings. The full extent of the shelf deposits outside the channels is unclear because the Kamariku Mb is lithologically similar to the underlying Lower Porkuni Sequence beds; in the absence of typical basal Saldus Fm features (conglomerates and abundant quartz sand), paleontological and carbon isotope data are needed to identify the TST of this sequence (Ainsaar et al. 2015; Hints et al. 2023; Männik and Nõlvak 2023). The TST continues into the uppermost Ordovician beds of the lower Juuru RS in updip (Koigi Mb of the Varbola Fm) and downdip (Puikule Mb of the Õhne Fm) positions (Bauert et al. 2014; Ainsaar et al. 2015).

Discussion

Comparison to prior sequence interpretations

Our sequence interpretation is similar to prior East Baltic studies, although it differs from Nielsen (2004, 2011) in some details (see discussion in Simmons et al. 2020). The first detailed sequence interpretation of the East Baltic Ordovician by Dronov and Holmer (1999, 2002) included three sequences across the Vormsi, Pirgu, and Porkuni RSs. Subsequent work (Harris et al. 2004; Dronov et al. 2011) included finer subdivisions; the scheme presented here is similar (Fig. 2). The primary differences involve the interpretation of the Pirgu RS. (1) Harris et al. (2004) interpreted the Moe–Jonstorp section as consisting of two sequences; here the lower unit is interpreted as the transgressive systems tract, making the Lower Pirgu Sequence equivalent to Sequence XI of Dronov et al. (2011). (2) This paper follows Harris et al. (2004) in dividing the Adila–Halliku section into two sequences based on the facies, stratigraphic gaps (erosion below the Kabala Mb in the western wells), and the karst feature at the top of the reef mound in the Jõgeva core, splitting Sequence XII of Dronov et al. (2011) into the Middle and Upper Pirgu sequences.

Facies and sequences

Nabala, Vormsi, and Pirgu facies delineate a series of depositional sequences of shallow-to-middle ramp sections that thin basinward across deep ramp and basin settings. Porkuni facies record two thin open-shelf sequences. While each sequence has its unique features, some general patterns emerge. (1) While onlapping TSTs occur in most ramp sequences (Nabala to Middle Pirgu), thinner sequences lack clear TST accumulations. (2) HSTs have a more consistent facies pattern marked by one or more shallowing-upward packages in outer shelf sections with limited erosion (most notably, the Middle Pirgu Sequence in the Pärnu core). (3) Sequence boundaries are characterized by hiatuses detected by biostratigraphic and/or chronostratigraphic gaps, and by sedimentological features such as karst and incised channels. In some cases, ramp sequence boundaries are represented by facies offsets. (4) Pre-Porkuni-age algal reef mounds occur in middle ramp positions and may reach considerable thickness (25–50 m). In contrast, the high-diversity Porkuni-age reef fauna forms low-relief biostromes within shallow ramp grain-supported facies.

The shift in sequence boundary style from the Nabala–Pirgu ramp sequences to the Porkuni sequences occurs in response to higher-amplitude sea-level changes associated with Hirnantian glaciations on an open-shelf profile. Despite these differences, the sequences align with global eustatic records (Haq and Schutter 2006; Cooper and Sadler 2012).

Sequences and basin development

Variations in sequence architecture document the development of the north flank of the Livonian Basin. (1) The Nabala Sequence lacks significant lateral facies differentiation across the study area and is capped by a regional karst surface (Calner et al. 2010). (2) The Vormsi Sequence is marked by

a well-developed facies zonation from shallow ramp to deep basin. The onlapping TST and prograding HST indicate significant variations in lateral facies and depth, which resulted in thicker accumulations along the updip northern part of the study area. (3) The prograding ramps of the Lower and Middle Pirgu sequences built an updip sediment wedge with maximum accumulation in the Middle Pirgu Sequence across central Estonia. This led to the formation of a low-energy lagoon north of the high-energy deposits of the shallow ramp and a broadening of the shallow ramp. (4) The thin Upper Pirgu Sequence flooded over the shallow ramp but was truncated by a sharp exposure surface. (5) The Porkuni sequences record the development of an open shelf characterized by sequence boundaries marked by updip channels, stratigraphic hiatuses, and an LST at the base of the Upper Porkuni–Juuru Sequence.

Superimposed on the gradual accumulation of the sedimentary wedge, two subtle tectonic influences can be identified. The first relates to changes in ramp deposition between the Nabala and Vormsi sequences across the study area. The facies belts narrowed, deep basin shales appeared, and prograding HSTs developed. This change coincides with the widespread karst surface across Baltoscandia documented by Calner et al. (2010). This shift occurred at a time of changing tectonic geometries; Southwest Baltica (current orientation) was subducting under Avalonia during the oblique closure of the Tornquist Ocean (Winchester et al. 2002; Torsvik and Rehnström 2003; Cocks and Torsvik 2005). Mazur et al. (2017) indicated that the initial collision occurred at 450 Ma, the estimated date of the Nabala–Vormsi boundary. This suggests that the Nabala–Vormsi facies change was due to regional subsidence changes related to tectonics. A second tectonic signal emerges from the pattern of updip stratigraphic hiatuses. During most of the study interval, the accommodation minimum was toward the Fennoscandian Shield to the north. However, the Middle Pirgu HST is missing from the updip cores in the western and northwestern areas of Estonia, indicating that regional subsidence patterns were not uniform across the study area.

Conclusions

The main results of this study involve sequence architecture, stratigraphic gaps, and basin development.

1. The Nabala–Porkuni RSs can be divided into seven sequences (or partial sequences) based on the integration of facies patterns, stratigraphic gaps, and varied chronological data. Within these sequences, systems tract analyses provide insights into the internal architecture of the sequences and patterns of deposition.
2. The identification of stratigraphic gaps is critical to any sequence stratigraphic interpretation. While many gaps are widespread across the study area, others are more local. Thus, the duration and position of gaps had to be established in each core.
3. Nabala–Pirgu facies are a composite of carbonate ramp sequences with thin TSTs overlain by thicker prograding HSTs. These built a broad platform characterized by a landward lagoon. By Porkuni time, the ramp developed into an open shelf with sufficient relief, allowing local erosion and/or slumping along its basinward margin.
4. The sequence framework highlights the pattern of basin development that responded primarily to eustatic sea-level changes. Against this background, two subtle tectonic influences are detectable. The termination of the Nabala-age ramp by a regional karst surface and the narrowing of the profile may have been related to a plate-tectonic reconfiguration. In addition, updip hiatuses indicate that regional subsidence patterns varied through time.

Data availability statement

All data used in this study are contained within the article.

Acknowledgments

We wish to thank Jim Awe for his assistance in recording the core sections. The Geological Survey of Estonia, and the Department of Geology at Tallinn University of Technology and the Department of Geology at the University of Tartu provided access to and assistance with the cores. This research was supported by U.S. National Science Foundation grants EAR-9909286 (Harris) and EAR-9910198 (Sheehan), and Estonian Science Foundation grants 4574 (Ainsaar), 4674 (Hints), and PRG1701 (Ainsaar, Meidla, Männik). This is a contribution to the IGCP 735 Project "Rocks 'n' ROL (Filling knowledge gaps in the Early Palaeozoic Biodiversification)". We thank Patrick McLaughlin and an anonymous reviewer for their insightful comments and suggestions. The publication costs of this article were partially covered by the Estonian Academy of Sciences.

References

Ainsaar, L. and Meidla, T. 2001. Facies and stratigraphy of the middle Caradoc mixed siliclastic-carbonate sediments in eastern Baltoscandia. *Proceedings of the Estonian Academy of Sciences. Geology*, **50**(1), 5–23. https://doi.org/10.3176/geol.2001.1.02

Ainsaar, L., Kaljo, D., Martma, T., Meidla, T., Männik, P., Nõlvak, J. et al. 2010. Middle and Upper Ordovician carbon isotope chemostratigraphy in Baltoscandia: a correlation standard and clues to environmental history. *Palaeogeography, Palaeoclimatology, Palaeoecology*, **294**(3–4), 189–201. https://doi.org/10.1016/j.palaeo.2010.01.003

Ainsaar, L., Truumees, J. and Meidla, T. 2015. The position of the Ordovician–Silurian boundary in Estonia tested by high-resolution $\delta^{13}C$ chemostratigraphic correlation. In *Chemostratigraphy: Concepts, Techniques, and Applications* (Ramkumar, M., ed.). Elsevier, 395–412. https://doi.org/10.1016/B978-0-12-419968-2.00015-7

Bassett, M.G., Kaljo, D. and Teller, L. 1989. The Baltic region. In *A Global Standard for the Silurian System, Geological Series*, **9** (Holland, C. H. and Bassett, M. G., eds). National Museum of Wales, Cardiff, 158–170.

Bauert, H., Ainsaar, L., Põldsaar, K. and Sepp, S. 2014. $\delta^{13}C$ chemostratigraphy of the Middle and Upper Ordovician succession in the Tartu-453 drillcore, southern Estonia, and the significance of the HICE. *Estonian Journal of Earth Sciences*, **63**(4), 195–200. https://doi.org/10.3176/earth.2014.18

Burchette, T. P. and Wright, V. P. 1992. Carbonate ramp depositional systems. *Sedimentary Geology*, **79**(1–4), 3–57. https://doi.org/10.1016/0037-0738(92)90003-A

Calner, M., Lehnert, O. and Nõlvak, J. 2010. Palaeokarst evidence for widespread regression and subaerial exposure in the middle Katian (Upper Ordovician) of Baltoscandia: significance for global climate. *Palaeogeography, Palaeoclimatology, Palaeoecology*, **296**(3–4), 235–247. https://doi.org/10.1016/j.palaeo.2009.11.028

Cocks, L. R. M. and Torsvik, T. H. 2005. Baltica from the late Precambrian to mid-Palaeozoic times: the gain and loss of a terrane's identity. *Earth-Science Reviews*, **72**(1–2), 39–66. https://doi.org/10.1016/j.earscirev.2005.04.001

Cooper, R. A. and Sadler, P. M. 2012. The Ordovician period. In *The Geologic Time Scale 2012* (Gradstein, F. M., Ogg, J. G., Schmitz, M. D. and Ogg, G. M., eds). Elsevier, Amsterdam, 489–524.

Dronov, A. V. and Holmer, L. E. 1999. Depositional sequences in the Ordovician of Baltoscandia. *Acta Universitatis Carolinae. Geologica*, **43**(1–2), 133–136.

Dronov, A. V. and Holmer, L. E. 2002. Ordovician sea-level curve: a Baltoscandian view. In *Extended Abstracts: The Fifth Baltic Stratigraphic Conference "Basin Stratigraphy – Modern Methods and Problems", Vilnius, Lithuania, 22–27 September 2002* (Satkūnas, J. and Lazauskienė, J., eds). Geological Survey of Lithuania, Vilnius, 33–35.

Dronov, A. V., Ainsaar, L., Kaljo, D., Meidla, T., Saadre, T. and Einasto, R. 2011. Ordovician of Baltoscandia: facies, sequences and sea-level changes. In *Ordovician of the World. Cuadernos del Museo Geominero*, **14** (Gutiérrez-Marco, J. C., Rábano, I. and Garcia-Bellido, D., eds). Instituto Geológico y Minero de España, Madrid, 143–150.

Einasto, R. 1986. Main stages of development and facies models of the East Baltic Silurian pericontinental basin. In *Theory and Practice of Ecostratigraphy* (Kaljo, D. and Klaamann, E., eds). Valgus, Tallinn, 37–54.

Einasto, R. 1995. „Liivi keele" omapärast Baltika arenguloos. In *Liivimaa geoloogia* (Meidla, T., Jõeleht, A., Kalm, V. and Kirs, J., eds). University of Tartu, Tartu, 23–32.

Goldman, D., Sadler, P. M. and Leslie, S. A. 2020. The Ordovician Period. In *Geological Time Scale 2020* (Gradstein, F., Ogg, J. G., Scmitz, M. D. and Ogg, G. M., eds). Elsevier, Amsterdam, 631–964.

Goldman, D., Leslie, S. A., Liang, Y. and Bergström, S. M. 2023. Ordovician biostratigraphy: index fossils, biozones and correlation. In *A Global Synthesis of the Ordovician System: Part I, Geological Society London Special Publications*, **532** (Harper, D. A. T., Lefebvre, B., Percival, I. G. and Servais, T., eds). Geological Society, London, 31–62. https://doi.org/10.1144/sp532-2022-49

Haq, B. U. and Schutter, S. R. 2008, A chronology of Paleozoic sea-level changes. *Science*, **322**(5898), 64–68. https://doi.org/10.1126/science.1161648

Harris, M. T., Sheehan, P. M., Ainsaar, L. Hints, L., Männik, P., Nõlvak, J. et al. 2004. Upper Ordovician sequences of western Estonia. *Palaeogeography, Palaeoclimatology, Palaeoecology*, **210**(2–4), 135–148. https://doi.org/10.1016/j.palaeo.2004.02.045

Hints, L. 1990. Ordovician articulate brachiopods. In *An Excursion Guidebook: Field Meeting Estonia 1990* (Kaljo, D. and Nestor, H., eds). Estonian Academy of Sciences, Tallinn, 58–61.

Hints, L., Meidla, T. and Nõlvak, J. 1994. Ordovician Sequences of the East European Platform. *Geologija, Vilnius University*, **17**, 58–63.

Hints, L., Oraspõld, A. and Kaljo, D. 2000. Stratotype of the Porkuni Stage with comments on the Röa Member (uppermost Ordovician, Estonia). *Proceedings of the Estonian Academy of Sciences. Geology*, **49**(3), 177–199. https://doi.org/10.3176/geol.2000.3.02

Hints, L., Oraspõld, A. and Nõlvak, J. 2005. The Pirgu Regional Stage (Upper Ordovician) in the East Baltic: lithostratigraphy, biozonation, and correlation. *Proceedings of the Estonian Academy of Sciences. Geology*, **54**(4), 225–259. https://doi.org/10.3176/geol.2005.4.02

Hints, L., Hints, O., Nemliher, R. and Nõlvak, J. 2007. Hulterstad brachiopods and associated faunas in the Vormsi Stage (Upper Ordovician, Katian) of the Lelle core, central Estonia. *Estonian Journal of Earth Sciences*, **56**(3), 131–142. https://doi.org/10.3176/earth.2007.16

Hints, O., Martma, T., Männik, P., Nõlvak, J., Põldvere, A., Shen, Y. et al. 2014. New data on Ordovician stable isotope record and conodont biostratigraphy from the Viki reference drill core, Saaremaa Island, western Estonia. *GFF*, **136**, 100–104. https://doi.org/10.1080/11035897.2013.873989

Hints, O., Ainsaar, L., Lepland, A., Liiv, M., Männik, P., Meidla, T. et al. 2023. Paired carbon isotope chemostratigraphy across the Ordovician–Silurian boundary in central East Baltic: regional and global signatures. *Palaeogeography, Palaeoclimatology, Palaeoecology*, **624**, 111640. https://doi.org/10.1016/j.palaeo.2023.111640

Jaanusson, V. 1973. Aspects of carbonate sedimentation in the Ordovician of Baltoscandia. *Lethaia* **6**(1), 11–34. https://doi.org/10.1111/j.1502-3931.1973.tb00871.x

Jaanusson, V. 1976. Faunal dynamics in the Middle Ordovician (Viruan) of Balto-Scandia. In *The Ordovician System: Proceedings of a Palaeontological Association Symposium, Birmingham, September 1974* (Bassett, M. G., ed.). University of Wales Press and National Museum of Wales, Cardiff, 301–326.

James, N. P., Kendall, A. C. and Pufahl, P. K. 2010. Introduction to biological and chemical sedimentary facies models. In *Facies Models 4* (James, N. P. and Dalrymple, R. W., eds). Geological Association of Canada, 323–339.

Kaljo, D. 1990. An introduction to the geology of Estonia. In *Field Meeting Estonia 1990. An Excursion Guidebook* (Kaljo, D. and Nestor, H., eds). Estonian Academy of Sciences, Tallinn, 6–10.

Kiipli, E., Kallaste, T. and Kiipli, T. 2004. Metabentonites of the Pirgu Stage (Ashgill, Upper Ordovician) of the East Baltic. In *WOGOGOB-2004, 8th Meeting of the Working Group on the Ordovician Geology of Baltoscandia, 13–18 May 2004, Tallinn and Tartu, Estonia. Conference Materials, Abstracts and Field Guidebook* (Hints, O. and Ainsaar, L., eds). University of Tartu Press, Tartu, 1–52.

Kröger, B., Hints, L. and Lehnert, O. 2017. Ordovician reef and mound evolution: the Baltoscandian picture. *Geological Magazine*, **154**(4), 683–706. https://doi.org/10.1017/S0016756816000303

Männik, P. and Nõlvak, J. 2023. Boundary between the Porkuni and Juuru regional stages in the Neitla section, Estonia. *Estonian Journal of Earth Sciences*, **72**(1), 66–69. https://doi.org/10.3176/earth.2023.52

Männik, P. and Viira, V. 1990. Conodonts. In *Field Meeting Estonia 1990. An Excursion Guidebook* (Kaljo, D. and Nestor, H., eds). Estonian Academy of Sciences, Tallinn, 84–89.

Männil, R. 1976. Distribution of graptoloids in the Ordovician carbonate rocks of the East Baltic area. In *Graptolites and Stratigraphy* (Kaljo, D. L. and Koren, T. N., eds). Academy of Sciences of the Estonian S.S.R. and Institute of Geology, Tallinn, 105–118.

Männil, R. 1990. The Ordovician of Estonia. In *Field Meeting Estonia 1990. An Excursion Guidebook* (Kaljo, D. and Nestor, H., eds). Estonian Academy of Sciences, Tallinn, 11–20.

Männil, R. and Meidla, T. 1994. The Ordovician System of the East European Platform (Estonia, Latvia, Lithuania, Byelorussia, parts of Russia, the Ukraine and Moldova). In *The Ordovician System of the East European Platform and Tuva (Southeastern Russia)* (Webby, B. D., Ross, R. J., Jr. and Zhen, Y. Y., eds). International Union of Geological Sciences Publication, **28A**, Trondheim, and Geological Society of America, Denver, 1–52.

Mazur, S., Porębski, S. J., Kędzior, A., Paszkowski, M., Podhalańska, T. and Poprawa, P. 2017. Refined timing and kinematics for Baltica–Avalonia convergence based on the sedimentary record of a foreland basin. *Terra Nova* **30**(1), 8–16. https://doi.org/10.1111/ter.12302

Meidla, T. 1996. *Late Ordovician ostracodes of Estonia*. *Fossilia Baltica*, **2**. Institute of Geology, Tallinn, and University of Tartu Press, Tartu.

Meidla, T. and Sarv, L. 1990. Ostracodes. In *Field Meeting Estonia 1990. An Excursion Guidebook* (Kaljo, D. and Nestor, H., eds). Estonian Academy of Sciences, Tallinn, 68–71.

Meidla, T., Truuver, K., Tinn, O. and Ainsaar, L. 2020. Ostracods of the Ordovician–Silurian boundary beds: Jūrmala core (Latvia) and its implications for Baltic stratigraphy. *Estonian Journal of Earth Sciences*, **69**(4), 233–247. https://doi.org/10.3176/earth.2020.20

Meidla, T., Ainsaar, L. and Hints, O. 2024. The Ordovician System in Estonia. In *11th Baltic Stratigraphical Conference, 19–21 August 2024, Tartu and Abavere, Estonia. Abstracts and Field Guide* (Hints, O., Männik, P. and Toom, U., eds). Geological Society of Estonia, Tallinn, 54–59.

Nestor, H. 1990a. Some aspects of lithology of Ordovician and Silurian rocks. In *Field Meeting Estonia 1990. An Excursion Guidebook* (Kaljo, D. and Nestor, H., eds). Estonian Academy of Sciences, Tallinn, 27–32.

Nestor, H. 1990b. Basin development and facies models. In *Field Meeting Estonia 1990. An Excursion Guidebook* (Kaljo, D. and Nestor, H., eds). Estonian Academy of Sciences, Tallinn, 33–36.

Nestor, H. and Einasto, R. 1997. Ordovician and Silurian carbonate sedimentary basin. In *Geology and Mineral Resources of Estonia* (Raukas, A. and Teedumäe, A., eds). Estonian Academy Publishers, Tallinn, 192–204.

Nielsen, A. T. 2004. Ordovician sea level changes: a Baltoscandian perspective. In *The Great Ordovician Biodiversification Event* (Webby, B. D., Paris, F., Droser, M. L. and Percival, I. G., eds). Columbia University Press, New York, 84–93.

Nielsen, A. T. 2011. A re-calibrated revised sea-level curve for the Ordovician of Baltoscandia. In *Ordovician of the World. Cuadernos del Museo Geominero*, **14** (Gutiérrez-Marco, J. C., Rábano, I. and Garcia-Bellido, D., eds). Instituto Geológico y Minero de España, Madrid, 399–401.

Nõlvak, J. 1999. Ordovician chitinozoan biozonation of Baltoscandia. *Acta Universitatis Carolinae. Geologica*, **43**(1–2), 287– 290.

Nõlvak, J. and Grahn, Y. 1993. Ordovician chitinozoan zones from Baltoscandia. *Review of Palaeobotany and Palynology*, **79**(3–4), 245–269. https://doi.org/10.1016/0034-6667(93)90025-P

Perens, H. 1995. Ülemordoviitsiumist Põltsamaa-Jõgeva-Ruskavere joonel. In *Liivimaa geoloogia* (Meidla, T., Jõeleht, A., Kalm, V. and Kirs, J., eds). University of Tartu, Tartu, 45–50.

Raukas, A. and Teedumäe, A. 1997. *Geology and Mineral Resources of Estonia*. Estonian Academy Publishers, Tallinn.

Read, J. F. 1983. Carbonate platform facies models. *AAPG Bulletin*, **69**(1), 1–21. https://doi.org/10.1306/AD461B79-16F7-11D7-8645000102C1865D

Simmons, M. S., Miller, K. G., Ray, D. C., Davies, A., van Buchem, F. S. P. and Gréselle, B. 2020. Phanerozoic eustasy. In *Geologic Time Scale 2020* (Gradstein, F. M., Ogg, J. G., Schmitz, M. D. and Ogg, G. M., eds). Elsevier, Amsterdam, 357–400.

Torsvik, T. H. and Rehnström, E. F. 2003. The Tornquist Sea and Baltica–Avalonia docking. *Tectonophysics*, **362**(1–4), 67–82. https://doi.org/10.1016/S0040-1951(02)00631-5

Tuuling, I. and Flodén, T. 2000. Late Ordovician carbonate buildups and erosional features northeast of Gotland, northern Baltic Sea. *GFF*, **122**(2), 237–249. https://doi.org/10.1080/11035890001222237

Winchester, J. A., Pharaoh, T. C. and Verniers, J. 2002. Palaeozoic amalgamation of Central Europe: an introduction and synthesis of new results from recent geological and geophysical investigations. *Geological Society London Special Publications*, **201** (Winchester, J. A., Pharaoh, T. C. and Verniers, J., eds). Geological Society, London, 1–18. https://doi.org/10.1144/gsl.sp.2002.201.01.01

Zhang, A., Yang, C., Sahy, D., Condon, D. J. and Li, X.-H. 2026. New high-precision U–Pb zircon age constraints on the Sandbian stage of the Ordovician System from the Guanzhuang section in North China. *Palaeogeography, Palaeoclimatology, Palaeoecology*, **683**, 113468. https://doi.org/10.1016/j.palaeo.2025.113468

Eesti Ülem-Ordoviitsiumi faatsiesed, järjendstratigraafia ja basseini areng

Mark T. Harris, Leho Ainsaar, Linda Hints, Peep Männik, Tõnu Meidla, Jaak Nõlvak, Tory Schultz ja Peter M. Sheehan

Eesti aluspõhja Ülem-Ordoviitsiumi Nabala kuni Porkuni lademete (Ülem-Katy–Hirnanti) järjendstratigraafiline analüüs aitab selgitada paleobasseini karbonaatsete settekomplekside levikut ja settimise arengut, muutusi fauna ja süsiniku stabiilsete isotoopide koostises ning kivimkehi piiritlevaid settelünki. Eri tüüpi tunnuste integreerimine võimaldab eristada settebasseini arengus seitset etappi ehk sekventsi: (1) Nabala (Paekna ja Saunja kihistu), (2) Vormsi (Kõrgessaare, Tudulinna ja Fjäcka kihistu), (3) Alam-Pirgu (Moe ja Jonstorpi kihistu), (4) Kesk-Pirgu (suurem osa Adila ja Halliku kihistust, Jelgava ja Parovėja kihistu), (5) Ülem-Pirgu (Adila kihistu Kabala kihistik, osa Halliku kihistust), (6) Alam-Porkuni (suurem osa Ärina kihistust) ja (7) Ülem-Porkuni–Juuru sekvents (Ärina kihistu Kamariku kihistik ja Salduse kihistu, Koigi ja Puikule kihistik). Meretaseme sügavaim madalseis kajastub ainult kõige ülemises sekventsis. Sekventside transgressiivseid etappe iseloomustab vanuseliselt nooremate setendite levik ranniku suunas. Sekventside kõrgseisu kulg koosneb ühest või mitmest ülespoole madalduvast settetsüklist. Settejärjestused kajastavad nii madal- kui ka süvaveeliste faatsieste nihkumist basseini keskosa suunas, mis jätkus kuni Liivi basseini põhjaosa settimisruumi täitumiseni setetega Porkuni eal. Maailmamere taseme eustaatilised langused, mis olid peamised sekventsipiire markeerivate settelünkade tekitajad, olid suurima amplituudiga Hirnanti mandrijäätumise episoodi ajal Porkuni eal. Faatsieste sügavusliku diferentseerumise süvenemine Nabala ja Vormsi ea vahetusel langeb ajaliselt kokku Baltika ja Avaloonia mandrilaamade kollisiooni algusega.

Estonian Journal of Earth Sciences
2026, **75**, 1, 67–82

https://doi.org/10.3176/earth.2026.05

www.eap.ee/earthsciences
Estonian Academy Publishers

RESEARCH ARTICLE

Received 19 February 2025
Accepted 23 February 2026
Available online 20 April 2026

Keywords:
palaeosol, Frasnian, Baltic palaeobasin, carbon and oxygen isotopes, vertebrate fossils

Corresponding author:
Ģirts Stinkulis
girts.stinkulis@lu.lv

Citation:
Stinkulis, Ģ., Lukševičs, E., Pipira, D., Meire-Kārkle, M. and Martma, T. 2026. Dolocretes in the Amata Formation of Latvia as indicators of climate aridification during the Givetian–Frasnian transition. *Estonian Journal of Earth Sciences*, **75**(1), 67–82. https://doi.org/10.3176/earth.2026.05

Dolocretes in the Amata Formation of Latvia as indicators of climate aridification during the Givetian–Frasnian transition

Ģirts Stinkulis[a], Ervīns Lukševičs[a], Daiga Pipira[b], Marianna Meire-Kārkle[a] and Tõnu Martma[c]

[a] Department of Geology, Faculty of Science and Technology, University of Latvia, Jelgava Street 1, LV-1004 Riga, Latvia

[b] Latvian Environment, Geology and Meteorology Centre, Latgale Street 165, LV-1019 Riga, Latvia

[c] Department of Geology, Tallinn University of Technology, Ehitajate tee 5, 19086 Tallinn, Estonia

ABSTRACT

This study focuses on the description and interpretation of the origin of dolocretes and their siliciclastic host rocks in the upper part of the Amata Formation (Fm) in four exposures in Latvia. The dolocretes occur in at least four intervals. The composition and structure, as well as stable oxygen and carbon isotope data of the two upper dolocrete intervals, suggest that they developed in soils. The dolocretes correspond to an episode of climate change from warm, moist to drier and hotter conditions, which started in the Late Givetian and continued to the Early–Middle Frasnian. They formed during a short-lived sea-level fall, which took place after a longer sea-level rise trend. The diversity of vertebrate fossils decreases from the lower to the upper part of the Amata Fm, which is consistent with the sea-level fall and gradual climate change marked by the studied dolocretes in the upper part of the Amata Fm.

Introduction

The Amata Formation (Fm) of Latvia and Estonia corresponds to the lowermost part of the Frasnian (Fig. 1). In terms of lithologic composition, it belongs to the uppermost part of a dominantly siliciclastic succession representing the Lower Devonian to the lowermost Upper Devonian. The sites studied here are in the Main Devonian

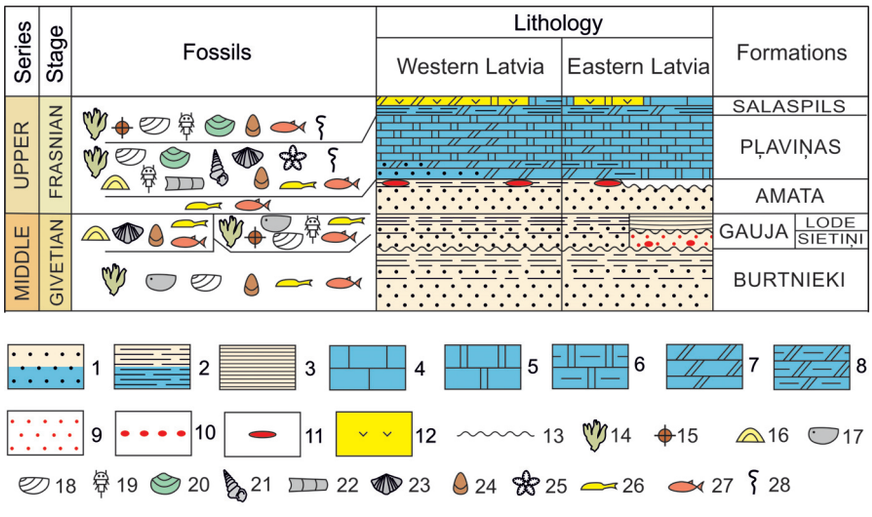

Fig. 1. Lithology and fossils of the Givetian and Lower–Middle Frasnian deposits in Latvia (modified from Lukševičs and Stinkulis 2018). 1 – sandstone, 2 – siltstone and clay, 3 – grey very fine clay, 4 – limestone, 5 – dolostone, 6 – clayey dolostone, 7 – dolomitic marl, 8 – clayey dolomitic marl, 9 – quartzose sandstone, 10 – quartz gravel and pebbles, 11 – dolocretes, 12 – gypsum rocks, 13 – unconformity surfaces, 14 – algae and plant macroremains, 15 – spores of algae, 16 – stromatopores, 17 – ostracods, 18 – conchostracans, 19 – eurypterids, 20 – bivalves, 21 – gastropods, 22 – cephalopods, 23 – articulate brachiopods, 24 – lingulate brachiopods, 25 – echinoderms (crinoids), 26 – agnathans, 27 – fishes, 28 – trace fossils.

Field (MDF), which covers the territory of the Baltic States and the Pskov, Leningrad, and Vologda oblasts of Russia. The western part of the MDF (WMDF) was a shallow epeiric basin in the southeastern part of the Euramerica continent (Lukševičs et al. 2012; Scotese 2014). The Amata Fm is composed of fine-grained sandstones and clayey deposits, and is considered as a transgressive unit (Kuršs 1992) and interpreted as tidally dominated estuarine deposits (Pontén and Plink-Björklund 2009).

Carbonate formations in the upper part of the Amata Fm of Latvia were noted (Kuršs et al. 1981a; Kuršs 1992), but the conditions of formation of carbonate nodules were usually not interpreted. However, such nodules were never reported from the Amata Fm of Estonia (Kleesment and Mark-Kurik 1997) or from the upper part of the Šventoji Fm of Lithuania (Narbutas 1981, 2004). Recently, such carbonate nodules and layer-like bodies interpreted as dolocretes were found at almost every site in Latvia where the upper part of the Amata Fm is exposed, suggesting that the dolomitic formations discussed here were probably formed over an area of hundreds to thousands of square kilometres. Dolocretes were documented in the western part of Latvia, the historical region of Kurzeme (Stinkulis and Spruženiece 2011; Fig. 2), and at several levels in the upper part of the Amata Fm in Vizuļi

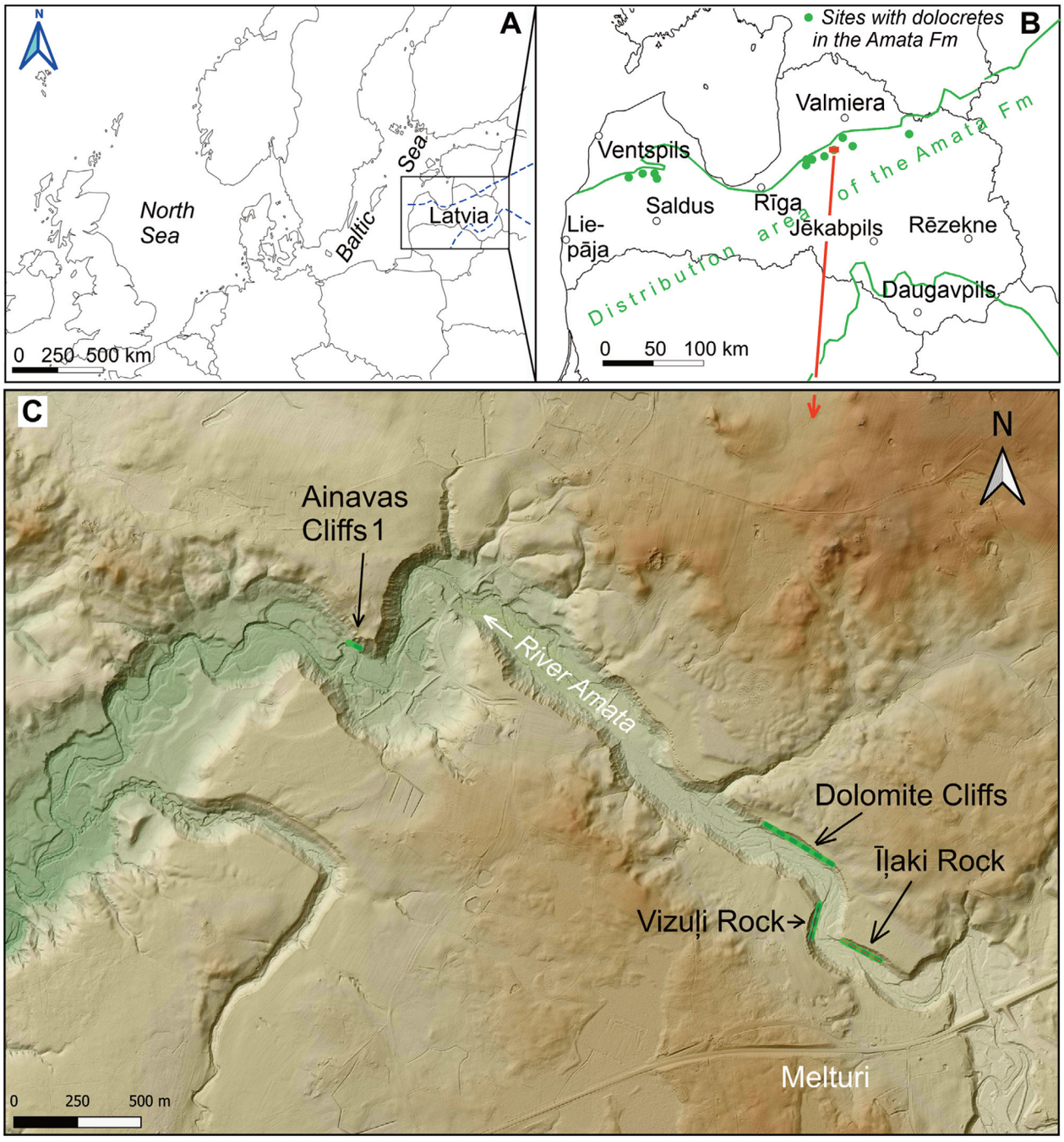

Fig. 2. Study area and sites. **A** – location of Latvia in northern Europe. The blue dashed line marks the distribution limit of the Upper Devonian deposits in the western part of the Main Devonian Field. **B** – location of the study area and sites with dolomite concretions in the upper part of the Amata Formation (contours from Eurostat). **C** – location of the study sites (LiDAR of Latvia; kartes.geo.lu.lv). Coordinates of the study sites: Īļaki Rock 57°13′29.2″ N, 25°13′33.4″ E; Vizuļi Rock 57°13′30.4″ N, 25°13′24.2″ E; Dolomite Cliffs 57°13′39.8″ N, 25°13′26.4″ E; Ainavas Cliffs 1 57°14′08.8″ N, 25°11′38.7″ E.

Rock (Pipira et al. 2015) in the historical region of Vidzeme. Detailed field and laboratory studies in the upper part of the Amata Fm in Vizuļi Rock allowed us to suggest that groundwater processes most likely influenced dolocrete formation in the lower part of the outcrop, while soil processes and subaerial exposure influenced the formation of massive and nodular dolocretes in two intervals in the upper part of the outcrop section (Pipira et al. 2015). The features of soil processes testify to a regressive development in the upper part of the Amata Fm. The general interpretation of the Amata Fm as tidally dominated estuarine deposits (Pontén and Plink-Björklund 2009) and the occurrence of dolocretes in the upper part of the formation (Pipira et al. 2015) make the situation at the end of the Amata time controversial, as to when and how the transgressive development turned into regressive development.

Dolocretes are carbonate crusts composed mainly of dolomite of groundwater-related or pedogenic origin. Calcretes or caliche, which consist mainly of calcium carbonate minerals, are the better known, more frequently documented, and more widespread analogues of dolocretes. However, both types of carbonate crust form near the Earth's surface due to the influence of phreatic (groundwater calcretes and dolocretes) or vadose (pedogenic calcretes and dolocretes) conditions, and the precipitation of authigenic calcium carbonate in the host rock (Wright and Tucker 2009). The identification of the origin of a carbonate crust – groundwater or pedogenic – is often not an easy task. Pedogenic calcretes can be identified by several features, mostly their pattern of vertical changes in the soil profile (Goudie 1973), as well as by abundant biogenic features (Wright and Tucker 2009). Groundwater calcretes are often of massive fabric. They lack internal horizons and biogenic features but have sharp boundaries (Wright and Tucker 2009).

Subsequent diagenetic processes may preserve the original mineral composition of the calcretes or transform them into dolocretes, e.g. due to fast precipitation of calcium carbonate, which causes a systematic decrease in the Ca/Mg ratio in groundwater and the progressive replacement of calcite by dolomite (Dixon 2010). Nowadays, calcretes usually form in arid to semiarid climates with a mean annual precipitation of less than 500−600 mm (Alonso-Zarza 2003). During the Pleistocene, dolocretes developed even as far from the equator as southern Australia (Dixon 2010), where the climate cycled rapidly between icehouse phases with cold, dry conditions and greenhouse phases with warmer and wetter conditions. The presence of calcretes and dolocretes indicates possible breaks in sedimentation and subaerial exposure over time; they are thus important indicators of certain palaeogeographic and palaeoclimatic conditions (Wright and Tucker 2009). However, the causes of dolocrete formation at the end of the Amata Regional Stage (RS) still remain poorly understood.

The composition of deposits within the WMDF changes from mainly sandy sediments of the Middle Devonian section, including the Gauja Fm, and quartz sands of the Sietiņi Fm, to gypsum-rich deposits of the Salaspils Fm (Fig. 1), obviously indicating a climate change from humid to arid. The dolocretes of the Amata Fm formed just before the basin-wide conversion from siliciclastic to carbonate deposition, and their study can help to understand the reasons for these changes. The aim of this study is the interpretation of the conditions of dolocrete formation and the sedimentary environment of their siliciclastic host rocks in the upper part of the Amata Fm. Data on the sea-level and global climate changes close to the Givetian–Frasnian boundary are also briefly discussed. The distribution of fossils in the Amata Fm is analysed as well. This study should allow the identification of the transgressive or regressive development trends during the formation of the deposits of the Amata Fm and the trends of climate changes during the same time.

Geological setting

The Amata Fm in Latvia and Estonia forms the upper unit in the Lower Devonian to lowermost Upper Devonian dominantly siliciclastic succession, cropping out in a relatively narrow belt known as the MDF, in the northwestern part of the East European Platform. This area of exposed Devonian deposits consists of two parts separated during the post-Visean denudation. The WMDF continues through Estonia, Latvia, Lithuania, the eastern part of the Baltic Sea floor, and the northern part of Belarus, which is sometimes referred to as the Devonian Baltic Basin (Pontén and Plink-Björklund 2009) or the Baltic Devonian Basin for convenience (Lukševičs et al. 2012). The eastern part corresponds to the territory of the Leningrad, Pskov, Novgorod, and Vologda regions of northwestern Russia (e.g. Lukševičs et al. 2018). The Devonian succession in the WMDF is represented by various siliciclastics, dolomites, limestones, gypsum rocks, and mixed-type deposits. There are distinct changes in the composition of deposits from the upper Givetian to the Lower–Middle Frasnian in the WMDF.

The deposits corresponding to the Gauja RS, upper Givetian, are represented by fine- to coarse-grained sandstones, as well as siltstones and clays (Kuršs et al. 1981c). Three formations correspond to the Gauja RS in Latvia (Fig. 1). The Gauja Fm (western and central part of the WMDF) is composed of quartz-feldspar sandstone, illite clays, and siltstones. The Sietiņi Fm (lower part of the Gauja RS in the northeastern part of the WMDF) is represented by white quartzose sandstones. High quartz content in the light mineral fraction, as well as dominance of zircon, tourmaline, and staurolite in the heavy transparent mineral fraction, indicates that the deposits were influenced by strong chemical weathering (Kuršs 1992). The Lode Fm (upper part of the Gauja RS in the northeastern part of the WMDF) is composed of clays and siltstones. The content of kaolinite is higher in the clayey deposits in comparison with other intervals of the Devonian siliciclastic succession of the WMDF, which also indicates the influence of continental chemical weathering (Kuršs 1992). The deposits of the Gauja RS formed in delta plain to delta slope settings (Pontén and Plink-Björklund 2007). Both the Gauja and Amata Fms of Latvia correspond to the undivided Šventoji Fm in Lithuania, which consists of sandstones, siltstones, and clays deposited in a lagoonal environment (Narbutas 2004).

The Amata Fm corresponds to the Amata RS, which in Latvia is attributed to the lowermost Frasnian, just above the

Table 1. Stratigraphy of the Givetian to Middle Frasnian in the Main Devonian Field (based on Narbutas 2004; Ivanov et al. 2012; Mark-Kurik and Põldvere 2012; Lukševičs and Stinkulis 2018; Lukševičs et al. 2018; Plax and Zaika 2020)

SYSTEM	SERIES	STAGES	Standard conodont zones	Regional placoderm zones	Regional stages	Formations, beds				Belarus	
						Latvia	Estonia	Lithuania	NW Russia	Regional stages	Formations
DEVONIAN	UPPER	FRASNIAN	*hassi*	*Bothriolepis traudscholdi*	DUBNIKI	Salaspils	Dubniki	Tatula	Dubniki	SARGAEVO	Vedrich
			punctata		PĻAVIŅAS	Pļaviņas	Chudovo	Kupiškis	Chudovo		Saria
			transitans	*Bothriolepis cellulosa*			Pskov	Suosa	Pskov		
							Snetnaya Gora	Jara	Snetnaya Gora		
			falsiovalis	*Bothriolepis prima – B.obrutschewi*	AMATA	Amata	Amata	Šventoji	Podsneto-gorskie	ZHELON	Degtya-revo / Zhelon
									Staritsa		
	MIDDLE	GIVETIAN	*disparilis*	*Asterolepis ornata*	GAUJA	Gauja / Lode / Sietiņi	Gauja		Oredezh	UBORT	Ubort
			hermanni-cristatus	*Watsonosteus*	BURTNIEKI	Burtnieki	Burtnieki	Butkūnai	Upper Luga	POLOTSK	Moroch
			varcus	*Asterolepis dellei*							Stolin

Givetian–Frasnian boundary (Lukševičs and Stinkulis 2018). Deposits corresponding to the Amata RS are widely distributed in the Baltic countries and the northwestern part of Russia. Several formations correspond to the Amata RS in the territory of the MDF (Table 1).

The overlying Pļaviņas Fm (Lower–Middle Frasnian) in Latvia is composed of dolomites, dolomitic marls, and clays (Fig. 1). Dolomite pseudomorphs after halite are present in dolomitic marls of the lower part of the Pļaviņas Fm (Sorokin 1981), indicating at least episodic development of a hypersaline environment. The dominant part of the formation is composed of pure dolostones, rather often containing stromatoporoid, gastropod, and brachiopod fossils. These deposits formed in a marine basin with normal salinity (Lukševičs et al. 2012).

The Pļaviņas Fm is followed by the Salaspils Fm (Middle Frasnian), represented by carbonate deposits, clays, and gypsum rocks (Fig. 1). The composition of sedimentary rocks varies significantly both in individual sections and across the distribution area. The gypsum-rich deposits likely accumulated in restricted hypersaline lagoons or bays, which developed among the parts of the basin with less saline water. The association of organisms is much poorer than in the Pļaviņas Fm (Sorokin 1981; Lukševičs et al. 2012). After the accumulation of deposits of the Salaspils Fm until the end of the Frasnian, the composition of the deposits changed several times from carbonate to sandy and clayey, and back. During the Famennian, the epicontinental basin retreated to the southwest, but the composition of the deposits changed several times from predominantly carbonate to mainly siliciclastic (Lukševičs et al. 2012).

The factors that influenced such repeated, considerable changes in the composition of deposits during the development of the WMDF basin have not been studied in detail. Nevertheless, the above-mentioned changes from sandy sediments of the Gauja Fm and quartz sands of the Sietiņi Fm to gypsum-rich deposits of the Salaspils Fm obviously indicate a climate change from more humid to arid. The dolocretes of the Amata Fm formed just before the basin-wide conversion from siliciclastic to carbonate deposition, and their study can help to understand the reasons for these changes.

Due to the lack of conodonts in the siliciclastic deposits of these formations and the impossibility of precisely correlating miospore and regional vertebrate zones with standard conodont zonation, the age of the Amata RS in the territory of the MDF is still controversial (Lukševičs et al. 2012, 2018). At least four versions of the position of the boundary between the Middle and Upper Devonian in the MDF have been proposed in the past: between the Burtnieki and Gauja RSs, between the Gauja and Amata RSs, within the Amata RS at the base of the Podsnetogorskie beds, and at the base of the Snetnaya Gora beds of the Pļaviņas RS (for a detailed discussion see Esin et al. 2000; Mark-Kurik and Põldvere 2012; Lukševičs et al. 2018).

In the most recent studies, the base of the Amata RS has been usually accepted as the boundary between the Middle and Upper Devonian. The deposits corresponding to the Amata RS – the Amata Fm in Latvia and Estonia, the upper part of the Šventoji Fm in Lithuania, the Zhelon beds and Degtyarevo Fm in Belarus, and the Staritsa and Podsnetogorskie beds in northwestern Russia, or at least their upper part – have most commonly been treated as the earliest Late Devonian in age (Kruchek et al. 2001; Lukševičs et al. 2012, 2018; Mark-Kurik and Põldvere 2012; Glinskiy and Mark-Kurik 2016; Plax and Zaika 2020).

All these lithostratigraphic units are characterised by a moderately diverse fossil fish assemblage corresponding to the *Bothriolepis prima* and *B. obrutschewi* vertebrate zones for the lower and upper parts of the Amata RS, respectively (Esin et al. 2000; Lukševičs et al. 2018). At least 21 vertebrate taxa were reported from the Amata RS (Esin et al. 2000), but only 18 of them were recorded in the Amata Fm in Latvia (Lyarskaya and Lukševičs 1992). Invertebrates have not been found in the deposits of the Amata Fm; there are only rare records of conchostracans in the upper part of the formation (Lyarskaya 1981).

All four sections described in this study are located on both banks of the River Amata downstream of the Melturi settlement and bridge, at a total distance of 2 km from each other (Fig. 2). This outcrop belt is likely the best exposure area for the Amata Fm in Latvia, especially its dolocrete-bearing upper part. Dolocrete samples from Īļaki Rock, Dolomīti Cliffs, and Ainavas Cliffs 1 were collected for sedimentological, mineralogical, and geochemical analyses, including the analysis of stable carbon and oxygen isotopes. The site Ainavas Cliffs 1 is named differently from another exposure known as Ainavas Cliffs, which is located 300 m to the northeast of Ainavas Cliffs 1. Dolocretes from Vizuļi Rock were analysed and interpreted in previous studies (Pipira et al. 2015), and these data are used here for comparison.

Materials and methods

Detailed logging of the Devonian succession was carried out for four outcrops along the River Amata downstream of the Melturi settlement and road bridge in northern Latvia (Fig. 2). During the field studies, the macrostructures, texture, and bedding of the Amata Fm deposits were studied and geological sections were compiled. Vizuļi Rock was documented by Daiga Pipira and Ģirts Stinkulis in 2013, Ainavas Cliffs 1 by Ginta Vasiļevska and Ģirts Stinkulis in 2016, and Īļaki Rock and Dolomīti Cliffs by Marianna Meire-Kārkle in 2017. The sedimentological logs were constructed for the upper part of the Amata Fm (5.2–7.9 m thick) and the lowermost part of the overlying Pļaviņas Fm. Lower portions of the Amata Fm were not documented, because the deposits do not contain notable dolomite nodules, veins, or other features of pedogenic or groundwater-related geological processes. The siliciclastic deposits of the Amata Fm in their whole thickness have been documented in detail by Pontén and Plink-Björklund (2009).

Vizuļi, Īļaki, and Dolomīti sections were sampled for further analysis of dolocretes in polished specimens, thin sections, and for geochemical investigation. Samples were taken from every part of the successions that contain dolomite concretions and veins. Due to the presence of metres-thick pure siliciclastic intervals and the irregular distribution of carbonates, the frequency of sampling varies considerably in the sections. Dolocretes were documented in polished slabs and thin sections (11 from Vizuļi, 13 from Dolomīti, and 24 from the Īļaki site) prepared at the Department of Geology, Faculty of Science and Technology (previously the Faculty of Geography and Earth Sciences), University of Latvia.

Stable carbon and oxygen isotope compositions ($\delta^{18}O$ and $\delta^{13}C$) were analysed in the dolomicritic material of dolocrete samples. The dolocrete material taken from the Īļaki (24 samples) and Dolomīti (13 samples) outcrops was analysed by Tõnu Martma at the Tallinn University of Technology. The dolocrete material from Vizuļi Rock (11 samples) was analysed at the University of Tartu. The weight of samples was 0.4–1.9 g. Sampling was performed on the surface of polished specimen slabs, with a drill designed for ceramic and glass drilling. Veins were mainly sampled, but some admixture of matrix material may have occurred. The material was taken from dolomicrite, possibly also from coarser-crystalline dolomite, but without admixture of clay or calcite. In both laboratories (Tallinn University of Technology and University of Tartu), the samples for stable carbon and oxygen isotope analyses were powdered to a fine silt size with a ceramic pestle and mortar and then treated with 99% phosphoric acid at 70 °C for 2 h in a GasBench II preparation line connected online to a Thermo Scientific Delta V Advantage continuous flow isotope ratio mass spectrometer.

At the Tallinn University of Technology, the samples were measured using three standards (for each GasBench row there were three standards and five samples): laboratory standard TLNC1 $\delta^{13}C = 2.2‰$, $\delta^{18}O = –9.11‰$; KH2 (DDR) $\delta^{13}C = 1.97‰$, $\delta^{18}O = –2.96‰$; NBS18 (IAEA) $\delta^{13}C = –5.01‰$, $\delta^{18}O = –23.0‰$. TLNC1 was calibrated using international IAEA standards: NBS19 $\delta^{13}C = 1.95‰$, $\delta^{18}O = –2.2‰$; LSVEC $\delta^{13}C = –46.6‰$, $\delta^{18}O = –26.47‰$; NBS18 $\delta^{13}C = –5.01‰$, $\delta^{18}O = –23.0‰$. At the University of Tartu, the measurements were performed according to IAEA standards: NBS19 $\delta^{13}C = 1.95‰$, $\delta^{18}O = –2.2‰$; LSVEC $\delta^{13}C = –46.6‰$, $\delta^{18}O = –26.47‰$; NBS18 $\delta^{13}C = –5.01‰$, $\delta^{18}O = –23.0‰$. Analytical precision (2σ) was 0.1‰. The results are expressed as per mil deviations relative to the Vienna Peedee Belemnite (VPDB) scale for oxygen and carbon. The reproducibility of replicate analyses was better than ± 0.1‰ for $\delta^{18}O$ and ± 0.1‰ for $\delta^{13}C$. In all cases, oxygen isotope values were corrected for dolomite acid–CO_2 fractionation; the factor $\alpha = 1.00913$ (Rosenbaum and Sheppard 1986).

The geological logging and the results of field and laboratory analyses of Vizuļi Rock have been partly published previously (Pipira et al. 2015). These data are also used for comparison and additional interpretations, which are provided in the present study.

Results

Siliciclastic deposits of the upper part of the Amata Formation

A general fining-upward trend occurs in the studied upper part of the Amata Fm. The lower part of the documented interval of the Amata Fm, 1.8–4.2 m thick, is composed of very fine-grained to fine-grained trough cross-bedded sandstones, with 0.l–0.3 m thick cross-beds (Fig. 3). The sandstones are light coloured, rich in an admixture of greenish-grey mica material. Trough cross-bedded sand accumulated in lingoid subaqueous dunes, which migrate in rapid traction currents (Pontén and Plink-Björklund 2007). More rarely, the

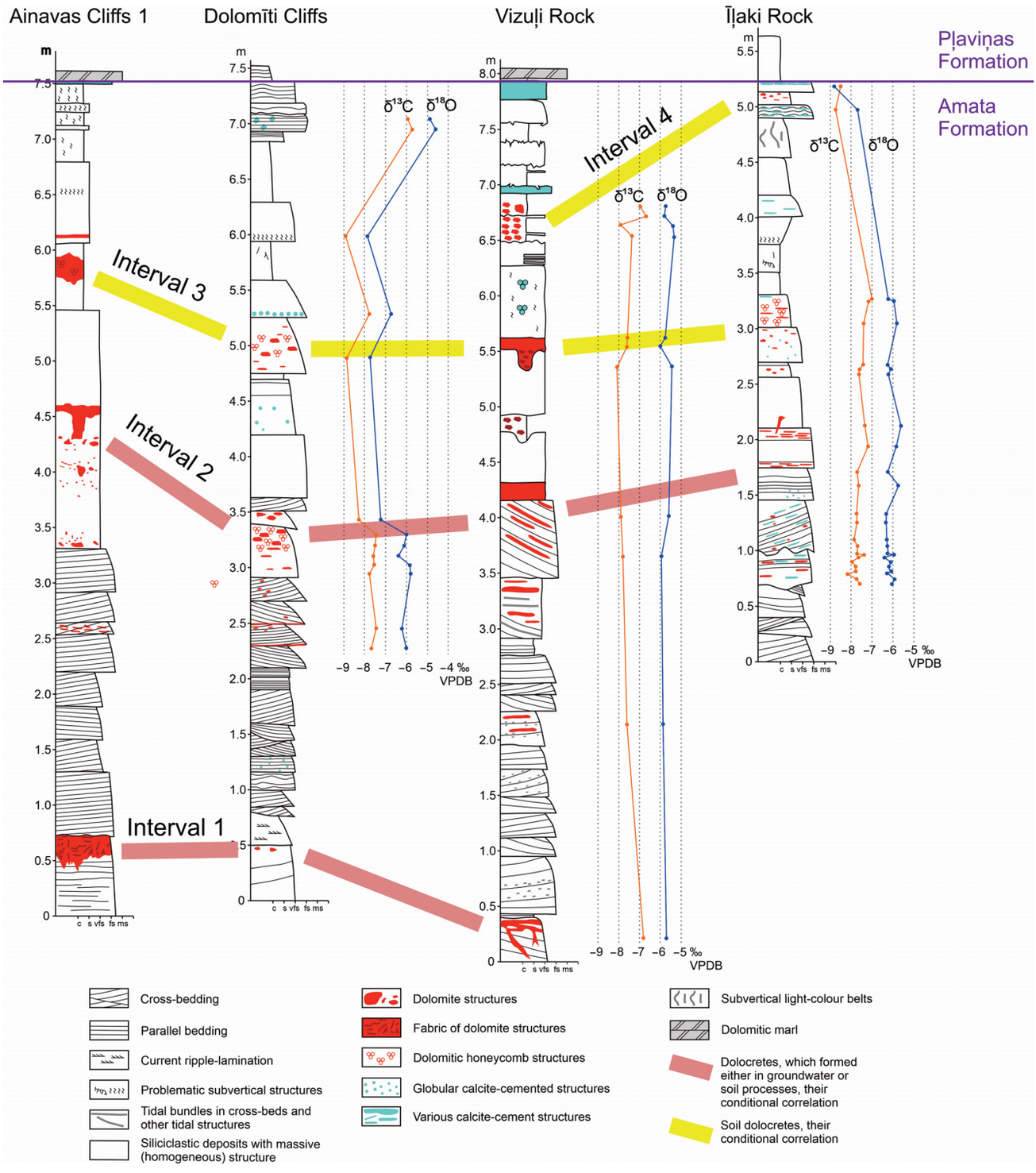

Fig. 3. Geological sections with stable isotope curves. They are approximately correlated according to lithological features. Abbreviations: c – clay, s – silt, vfs – very fine-grained sand, fs – fine-grained sand, ms – medium-grained sand, VPDB – Vienna Peedee Belemnite.

deposits are parallel-bedded, which indicates either the existence of low, flat subaqueous dunes, or lower energy settings.

The mica admixture allows to distinguish well-expressed tidal rhythmites (tidal bundles), which indicate the influence of tidal processes on sedimentation (Davis 2012). Greyish and greenish clay clasts are also present in the sandstone. In rare cases, the sandstone exhibits current ripple-lamination structures. Studies of complete successions of the Amata Fm indicate that such very fine-grained to fine-grained cross-bedded sandstones with tidal features are typical of this formation in general (e.g. Pontén and Plink-Björklund 2009; Stinkulis and Upeniece 2011).

Rather homogeneous, very fine-grained, more rarely fine-grained sandstones, with a few interlayers of clayey to silty material, follow in the next 1.5–2 m of this succession (Fig. 3). The siliciclastic material of the uppermost part of the Amata Fm, 1.5–2.1 m thick, is represented by an alternation

of claystones and siltstones with very fine-grained to fine-grained sandstones. The lack of sedimentary structures in the upper part of the Amata Fm complicates the interpretation of its sedimentary setting; however, the fining-upward trend of the siliciclastic deposits and the increasing importance of clayey material indicate a decrease in the energy of the environment. Tidal bundles or other structures indicating tidal processes were not found in the upper 4.5–5 m of the succession. The Amata Fm deposits do not contain any fossils in the outcrops studied, except for very rare fragmentary vertebrate bones (Fig. 4B), which are difficult to identify.

Succession of dolocretes and their peculiarities

Dolomitic nodules are rare in the lower part of the Amata Fm (Kuršs 1992), which was not examined in this study. In the upper part of the formation, 5.2–7.9 m thick, there are up to four well-expressed intervals of hard dolomite nodules and rather homogeneous, massive layer-like bodies (Fig. 3), which have been interpreted as dolocretes (Stinkulis and Spruženiece 2011; Pipira 2015). The dolocrete intervals can likely be correlated by their position in the geological section of the Amata Fm, lithological properties, and stable carbon isotope data. The main principles used in the tentative correlation were as follows:

1. Distance of dolocrete intervals from the well-expressed boundary between the Amata and Pļaviņas Fms;
2. Vertical distance of dolocrete intervals from each other;
3. Presence of a layer of siliciclastic deposits with problematic subvertical structures between the dolocrete intervals 3 and 4 (see below).

We would like to point out the existence of at least four dolocrete intervals in the documented sections. The lowermost carbonate-rich part of the documented successions (interval 1) is represented by nodular and vein dolocretes 7 m (Ainavas Cliffs 1) and 7.5 m (Vizuļi Rock) below the top of the formation (Fig. 3). The dolocrete nodules, more rarely subvertical and oblique veins, occur in very fine-grained to fine-grained sandstone. Dolomite nodules are almost absent in the next 2 m of the succession, then their content increases upwards until they form a distinct layer-like nodular to rather homogeneous body, mainly in very fine-grained to fine-grained sandstones 3–4 m below the top of the Amata Fm (interval 2). Nodules and their concentrations are present above this level, but the next considerable dolocrete (interval 3) is 1.7–2.5 m below the top of the Amata Fm. The interval is also represented by nodular to massive dolocrete, which occurs in clayey siltstone to fine-grained sandstone host rock (Figs 3 and 4A). Dolomite nodules are almost absent above this level in Ainavas Cliffs 1 and Dolomīti Cliffs, but one more nodular dolocrete formation (interval 4) occurs in clayey to silty deposits 0.2–1.2 m below the top of the Amata Fm in Vizuļi Rock and Īļaki Rock.

The maximum thickness of these dolomitic formations is 0.3 m for the massive layer-like dolocretes in Ainavas Cliffs 1 (intervals 1 and 2) and Vizuļi Rock (interval 3). Interval 2 in most of the studied outcrops (Ainavas Cliffs 1, Dolomīti, and Vizuļi sites) shows a gradual increase in dolomite abundance in a 1.2 m-thick part of the section. Siliciclastic deposits with separate dolomite nodules grade upwards into a massive, layer-like dolocrete formation.

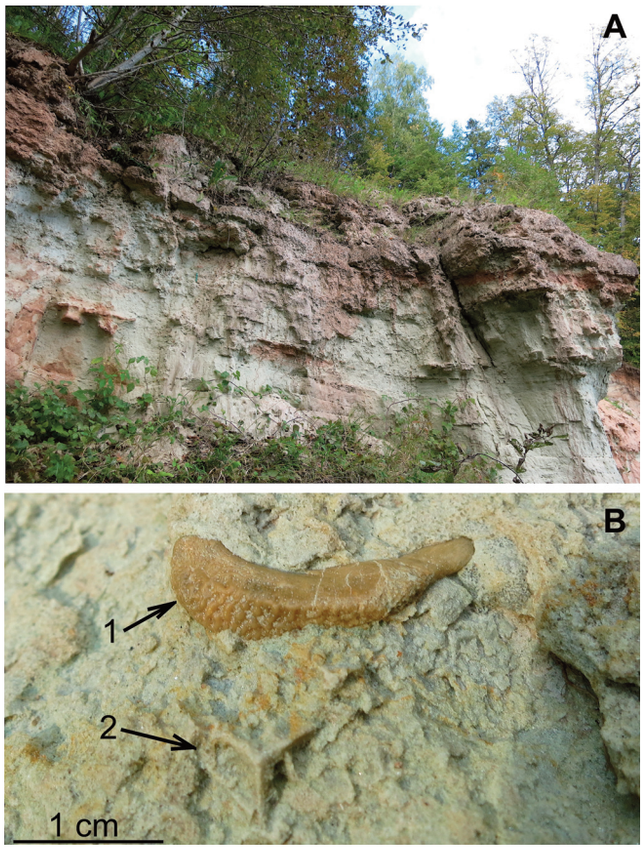

Fig. 4. Deposits of the upper part of the Amata Fm in Ainavas Cliffs 1. **A** – platy formations of dolocretes (mainly interval 3). **B** – vertebrate remains (1) and a dolomite pseudomorph after halite (2) in sandstones at the top of the Amata Fm, just below the dolomitic marls of the Pļaviņas Fm. Photos by Ģ. Stinkulis, September 2014.

A peculiar feature – a dolomite pseudomorph after halite – was found on the surface of the topmost sandstone layer of the Amata Fm in the Ainavas Cliffs 1 (Fig. 4B). Dolomite pseudomorphs after halite are rather typical of the lowermost part (the Koknese Member (Mb)) of the overlying Pļaviņas Fm (Sorokin 1981). The halite crystal remnant on the top surface of the Amata Fm indicates the existence of an arid or semiarid climate during that time.

In addition to dolomite as the main mineral of dolocretes, the Amata Fm contains quite abundant calcite admixture in the shape of globular and platy formations (Fig. 5). The calcite is usually related to porous, pure sandstones and has poikilotopic, as well as drusy, equant morphology. The size of calcite crystals changes from tens of millimetres to 2 × 3 cm. Its relationships with dolomite in thin sections allow the interpretation that crystallisation of calcite post-dated even the latest generation of dolomite (Stinkulis 1997). Based on carbon stable isotope and trace element analyses, the calcite is interpreted as having crystallised from groundwater of meteoric origin, most possibly related to palaeokarst events after the Devonian (Vernera and Stinkulis 2018). The calcite is not related to the formation of the dolocrete; therefore, we do not discuss its isotope data in this study.

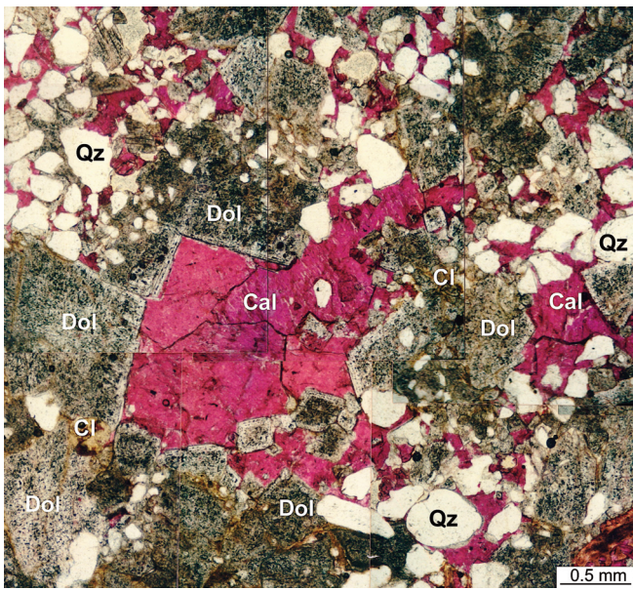

Fig. 5. Sandy and clayey dolocrete with secondary calcite. Dolomite (Dol) is associated with clayey material (Cl) and occurs as irregular, branched formations. This irregular distribution indicates that the carbonate material did not precipitate from basin water, but formed in already accumulated siliciclastic deposits. Calcite (Cal) is red due to staining of the thin section by alizarin-S solution. The distribution of calcite in sandstone pores among quartz (Qz) grains and in vugs of dolocrete indicates that it is the latest generation of carbonate minerals. Ī̧aki Rock, interval 3. Thin-section photomicrograph, parallel polarisers. The image was created by gluing together several printed photos. Photos and assemblage by Ģ. Stinkulis, March 1997.

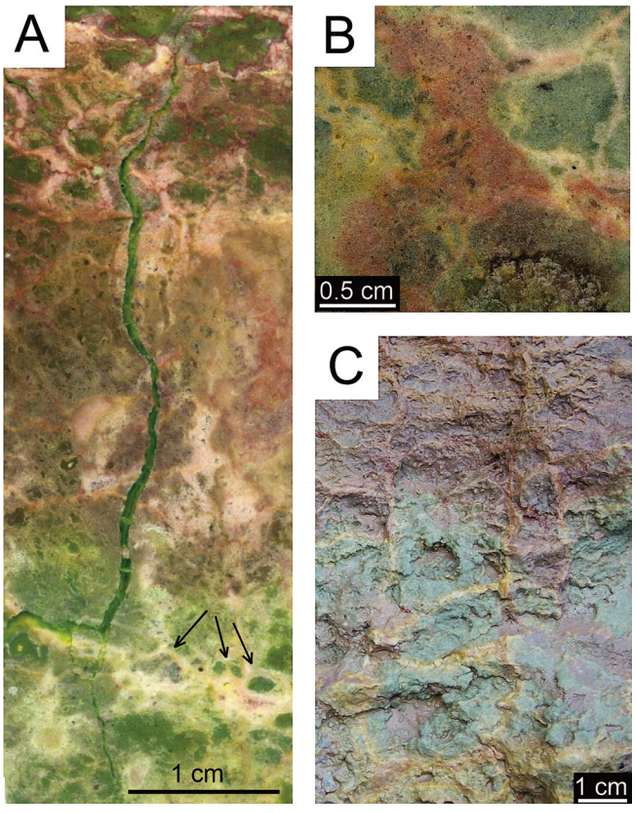

Fig. 6. Structures of dolocretes in polished specimens, under the reflected light microscope (A, B) and in outcrop (C). All samples are from Vizuļi Rock. **A** – irregular network of dolomite veins with a tendency towards a downward direction in massive dolocretes. Circumgranular cracks in the lower part of the figure are indicated by arrows. **B** – irregular dolomite veins and roundish honeycomb structures in massive dolocretes. **C** – honeycomb structures developed on the surface of a massive dolocrete layer. Radially branching dolomite veins are in the upper right corner of the photo. Photo A modified from Pipira et al. (2015); photos B and C by D. Pipira, January 2013.

Internal structure and texture of dolocretes

Studies of polished samples and thin sections supplement the descriptions and interpretations of dolocretes mentioned above. Under a microscope, it can be seen that dolomite is distributed as veins in the massive, layer-like dolocretes (Figs 6A–C and 7A–C). The matrix of massive, layer-like dolocrete bodies is looser than the veins and is represented by almost non-cemented to medium-cemented siliciclastic deposits. The matrix of the dolocretes depends on the host rock composition. In clay- and silt-dominated deposits, it is similar to non-carbonate clayey rocks, but sandstones contain irregularly, patchily distributed dolomite cement. Often the dolocrete matrix is of mixed clayey to sandy composition, and then the dolomite cement is mainly associated with the sand material.

The texture of the veins also depends on the siliciclastic host rock. In sandstones, they are not pure veins, but parts of the sandstone matrix with micritic or dense, equant, pore-filling to poikilotopic cement with crystal sizes up to 1 mm. In clayey and silty deposits, the veins are of pure dolomitic composition or contain irregularly distributed inclusions of the surrounding material. The dolomite is represented by micrite to crystals up to 0.4 mm in size. The dolomite veins are irregular, often radially branched (Fig. 6C), but they form a circumgranular pattern (Figs 6A, 7A, 9A, B). Boundaries between the veins and the matrix are quite sharp in clayey deposits (Fig. 7A), but rather gradual in sandy deposits (Fig. 7B).

Honeycomb structures are widespread in the dolocretes of the Amata Fm, especially in intervals 2 and 3 (Fig. 6B, C). The structures are formed by a network of dolomite veins, which are usually 1–2 mm wide. Bluish and greenish clayey material forms infillings ranging from several millimetres to 2 cm wide between the veins. The clayey fraction is dominated by illite with minor chlorite (Pipira et al. 2015); however, the origin of the colour has not been studied yet. This is probably related to the presence of Fe (II) oxides in the deposits, as discussed by Kuršs (1992).

The dolocrete intervals 3 and 4 are better developed and richer in indicative structures than intervals 1 and 2. Thus, dolocrete interval 3 in the Ainavas Cliffs 1 (Fig. 4A) and Vizuļi Rock shows the well-developed profile:

1. The nodular dolocretes in the lower part;
2. A massive dolocrete horizon in the upper part;
3. Honeycomb structures with poorly pronounced features of laminar (fine lamination) structures, as well as incipient laminar structures on the surface of the massive dolocrete.

Dolocrete interval 4 (nodular dolocrete) in Vizuļi Rock also demonstrates honeycomb structures. Microkarst pockets are recognised on the surface of a dolomite nodule (Fig. 7D).

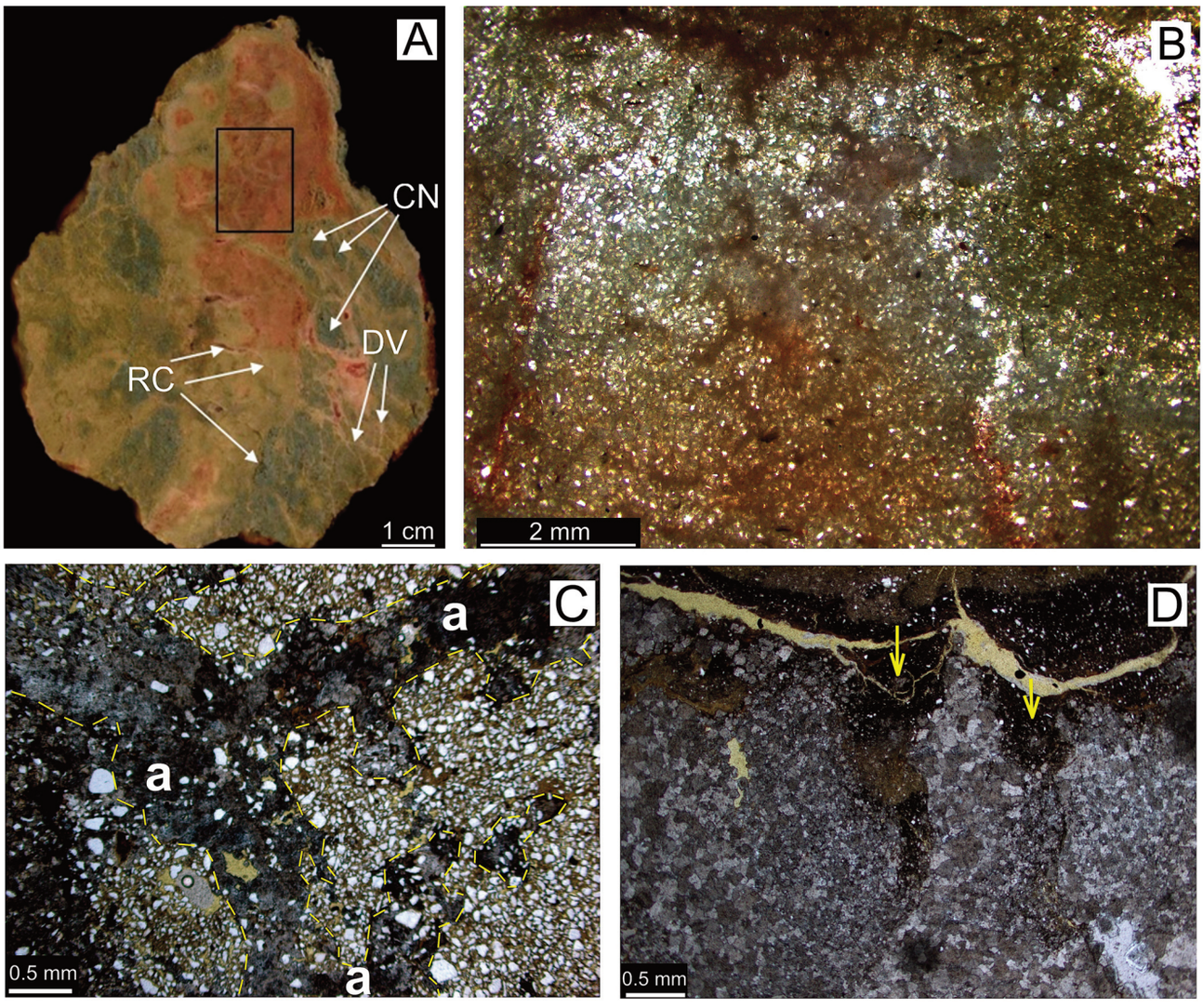

Fig. 7. Dolocrete microstructures in a polished specimen (A) and thin sections (B–D). **A** – relationships between dolomite and clay in dolocrete: DV – dolomite veins, CN – clay within the network of dolomite veins, RC – rounded, circumgranular veins. Īļaki Rock, interval 3. The rectangle shows the location of the thin section (B). **B** – thin, irregular, dolomicrite veins in the matrix of fine-grained sandstone with dolomite cement. Īļaki Rock, interval 3. Thin section, transmitted light, parallel polarisers. **C** – network of dolomite veins (a; marked with yellow dashed lines) within a fine sandy to clayey matrix. Massive dolocretes in Vizuļi Rock, interval 3. Thin section, transmitted light, parallel polarisers. **D** – microkarst features (indicated by arrows) on the upper surface of a dolomite nodule (nodular dolocretes) in Vizuļi Rock, interval 4. Thin section, transmitted light, parallel polarisers. Photos A and B by M. Meire-Kārkle, March 2018; photos C and D from Pipira et al. (2015).

These are V-shaped depressions in the dolomitic material, 0.5–1 mm wide and 1–2 mm long, which developed in dolomite and are filled with clayey material (Pipira et al. 2015).

Stable isotope data

The stable carbon isotope ($\delta^{13}C$) values for the studied dolocretes of the Amata Fm range from –8.9 to –5.7 ‰, and the stable oxygen isotope ($\delta^{18}O$) values range from –8.8 to –4.7 ‰ (Fig. 8). The most negative $\delta^{13}C$ values in the dolocretes of the Amata Fm are documented in the upper parts of intervals 3 (Dolomīti and Vizuļi outcrops) and 4 (Vizuļi and Īļaki outcrops). This is consistent with evidence of subaerial exposure found exactly in intervals 3 and 4 (Fig. 3). Moreover, the dolomite formations of these intervals are among the best-expressed, most massive ones. Conversely, the two most positive values of both $\delta^{13}C$ (–5.7 to –5.9 ‰) and $\delta^{18}O$ (–4.9 to –4.7 ‰) in the Dolomīti Cliffs correspond to the uppermost part of the section, but the dolomite concretions there are sparsely distributed.

Dolocrete $\delta^{18}O$ values in the documented sections are on average 1–1.5 ‰ higher (more positive) than $\delta^{13}C$ values. There is a general covariance between $\delta^{13}C$ and $\delta^{18}O$ (Fig. 8); Pearson's correlation coefficient is 0.76 (N = 49, P = 0.01) (Fig. 3).

Despite the overall trend, small positive excursions of oxygen values in several intervals are consistent with small negative excursions of carbon values. These trends occur in the following intervals in the studied logs: 2.6.–2.7 m and 2.9–3.0 m in Īļaki Rock, 2.5–3.0 m in the Dolomīti Cliffs, as well as 3.8–5.4 m and 6.5–6.7 m in Vizuļi Rock (Fig. 3). They correspond to the intervals of the sections where the siliciclastic deposits are enriched in dolomite concretions and veins, but not always to the upper parts of these intervals. These excursions, with a few exceptions, are only about 0.2–0.5 ‰,

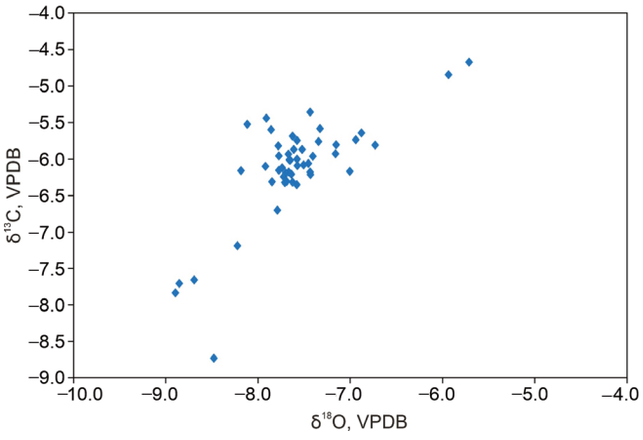

Fig. 8. Stable oxygen and carbon isotope diagram of dolomite from concretions, nodules, and platy formations of the Amata Formation in all studied sections. Abbreviation: VPDB – Vienna Peedee Belemnite.

which is close to the precision of the stable isotope analyses. Furthermore, the samples for the isotope analysis were taken from carbonate concretions, which are irregularly distributed in the geological section. Large intervals are composed of pure siliciclastic rocks. The results of oxygen isotope analyses may additionally be affected by dolomitisation and other diagenetic changes; thus, they should be rather interpreted with caution. This limits the reliability of the interpretations of isotope data, especially oxygen-isotope data, in this study.

Discussion

Influence of subaerial exposure and diagenetic changes suggested by stable isotope data

The negative stable carbon and oxygen isotope values for the studied dolocretes of the Amata Fm are typical of calcretes and dolocretes described in the literature (Kearsey et al. 2012; Rameil et al. 2012; Díaz-Hernández et al. 2013; Casado et al. 2014): $\delta^{13}C$ from –11 to 1‰ in calcretes and from –8 to 3‰ in dolocretes; $\delta^{18}O$ from –14 to –2‰ in calcretes and from –8 to 2‰ in dolocretes. As calcretes and dolocretes form from carbonates supplied either from soil or groundwater (Tucker and Wright 2009), their stable isotope values represent these environments.

The negative stable carbon isotope values indicate the presence of soil, because the decomposition products of plant material have a relatively high proportion of the light carbon isotope. This process could be accompanied by the influence of carbon from meteoric waters, which would also cause a decrease in the carbon isotope ratio. Both these features point to subaerial exposure processes (Díaz-Hernández et al. 2013; Casado et al. 2014). The most negative stable carbon isotope values, being lower than –8‰, in all studied sections of the Devonian Amata Fm occur near or at the dolocrete intervals 3 and 4 (Fig. 3), where the features of subaerial exposure were found, which support this suggestion.

The oxygen values for terrestrial carbonates, including those formed in soils and shallow groundwaters, usually are negative, because they form under the influence of meteoric waters (Sharp 2017). It corresponds well to the results of this study on the formation of dolomite concretions under the influence of surface processes.

In contrast to the carbon values, $\delta^{18}O$ values may show a positive trend near subaerial unconformity surfaces, because the ratio of $^{18}O/^{16}O$ there decreases due to evaporation. As a result, the oxygen isotope curves at unconformity surfaces reverse the carbon isotope values (Goldstein 1991). This, however, is not typical of calcretes, which form in non-carbonate substrates due to rapid downward migration of meteoric water, protecting the water from evaporation (Swart 2015). The influence of evaporation might help to explain the small positive excursions of oxygen values in several intervals of the Amata Fm, which correspond to small negative excursions of carbon values in relatively dolomite concretion-rich parts of the studied sections.

Diagenesis also lowers the $\delta^{18}O$ value (Swart 2015; Sharp 2017); therefore the explanation of the $\delta^{18}O$ values and their variation in the studied sections is more complicated to explain. Moreover, post-sedimentary processes can influence $\delta^{18}O$ values to a much larger degree than $\delta^{13}C$ values. This is related to differences in the sources of oxygen and carbon. Carbon can be supplied only from organic matter and CO_2, but oxygen is provided also by water molecules (Melezhik et al. 2004). This means that a much larger water/rock ratio is necessary to change the primary carbon isotope proportions than the oxygen isotope proportions. Thus, it is possible that the carbon values are better preserved than the oxygen values in the studied deposits of the Devonian Amata Fm.

The general trends of covariance of stable oxygen and carbon isotope values can be interpreted as linked to meteoric diagenetic fluids (Sharp 2017).

Origin of studied dolomite concretions, veins, and layer-like bodies

Layer-like horizons and nodules in the Amata Fm have in recent years been considered to be dolocretes, indicating subaerial conditions at the time of their formation (Stinkulis and Spruženiece 2011; Pipira et al. 2015). However, previous studies were either rather fragmented or focused on single exposures. This study allows us to discuss the genesis of dolomitic nodules and layer-like bodies along a rather long outcrop belt, taking into account the results of macro-sample and thin-section analysis, stable isotope data, and the tentative correlation of these dolomite formations.

In this study, the dolomite nodules and layer-like bodies in the Amata Fm are interpreted as dolocretes based on several facts. Dolomite is always distributed irregularly and never occurs as layers with definite boundaries, structures, and textures that could indicate primary sedimentation of the material. However, there are several intervals in the studied sites where hard, layer-like, platy bodies enriched in dolomite can be traced for at least 15 m (Fig. 4A), most possibly for kilometres, as indicated by the tentative correlation. Carbonate bodies with such structure and distribution are typical of both soil and groundwater calcretes and dolocretes (Alonso-Zarza and Wright 2010). It is important to note that such dolomite formations were recently found in almost every site in Latvia where the upper part of the Amata Fm is ex-

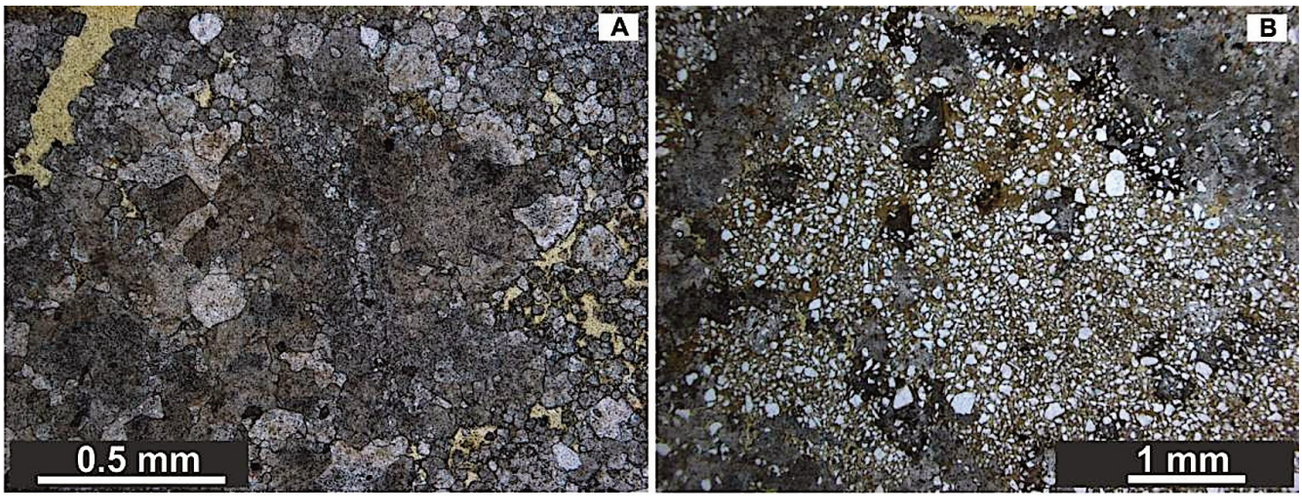

Fig. 9. Circumgranular cracks in dolocretes from Vizuļi Rock. **A** – circumgranular cracks partly filled with medium-crystalline dolomite cement in a matrix of clayey, impurity-rich dolomite. **B** – circumgranular cracks filled with pure dolomite surrounding sandy to clayey material. Some dolomite-filled cracks partly enter into the siliciclastic material. Vizuļi Rock, interval 3. Thin-section photomicrographs, transmitted light, parallel polarisers. Photos by D. Pipira, January 2013.

posed (Fig. 2) – in sites from the western to the eastern part of Latvia, at least 200 km apart from each other (Stinkulis and Spruženiece 2011; Pipira et al. 2015).

Macro-sample and thin-section studies allow us to distinguish such well-expressed and widespread features typical of calcretes and dolocretes as: 1) irregular, often subvertical, veiny distribution of dolomitic material with respect to siliciclastic material; 2) honeycomb structures. The development of veiny structures (Figs 6A–C and 7A–C) is a result of dissolution, repeated crystallisation, and cementation of mineral material (Machette 1985; Alonso-Zarza 2003; Zhou and Chafetz 2009; Alonso-Zarza and Wright, 2010). Irregular, often radially branched veins (Fig. 6C) indicate migration of carbonate solutions in radially developed desiccation cracks. The circumgranular pattern formed by veins in some places (Figs 6A, 7A, 9) is typical of calcretes and dolocretes of pedogenic (soil) origin (Theriault and Desrochers 1993; Zhou and Chafetz 2009).

The honeycomb structures are mentioned in many carbonate crust descriptions and classifications (e.g. Alonso-Zarza and Wright 2010; Pfeiffer et al. 2011; Pipira et al. 2023). They are not unequivocal indicators of groundwater or pedogenic carbonate formations; however, Goudie (1973) described honeycomb calcretes as a transitional form between nodular calcretes and hardpan calcrete in soil profiles.

The dolocrete interval 3 in the Ainavas Cliffs 1 (Fig. 4A) and Vizuļi Rock shows a profile characteristic of pedogenic dolocretes (Alonso-Zarza 2003). Furthermore, the combination of honeycomb and laminar structures present in interval 3 are characteristic of the upper part of carbonate-rich soil horizons (Alonso-Zarza 2003; Alonso-Zarza and Arenas 2004; Wright and Tucker 2009; Zhou and Chafetz 2009; Pfeiffer et al. 2011). The karsted dolomite surface (Fig. 7D) in the dolocrete interval 4 (Pipira et al. 2015) indicates that the deposits containing dolomite nodules were subaerially exposed and influenced by meteoric waters in the vadose zone (Calner et al. 2010), which also points to a soil horizon.

Further interpretation of the genesis of dolocretes is more problematic because similar carbonate formations, including nodules and massive bodies, can develop near the groundwater level and in soil (Alonso-Zarza and Wright 2010). There are also intermediate types ranging from more groundwater-controlled to more soil-water controlled variants (Chen 2002). Groundwater and soil (pedogenic) calcretes lacking specific structures such as laminar ones, pisoids, rhizoids, or karst phenomena are difficult to distinguish from one another. This is also the case for the dolocretes of intervals 1 and 2 in the studied sites. Dolomite concretions and horizons of massive to platy dolomitic material are present, which could have developed either in soil or near the capillary fringe zone due to fluctuations in the groundwater table (Wright and Tucker 2009).

A gradual increase in dolomite abundance and in the massiveness of dolocrete upwards in interval 2 in most of the study sites is indicative of pedogenic carbonate soil profiles (Wright and Tucker 2009); however, there is no further evidence of either groundwater or soil origin in intervals 1 and 2.

Thus, the dolocretes in intervals 1 and 2 could have formed both in groundwater and soil settings, but the dolocretes in intervals 3 and 4 developed in soils. The latter could also have been influenced by groundwater processes, but it is complicated to evaluate their role. These soil (pedogenic) dolocrete features indicate that during the late stage of accumulation of the siliciclastic materials of the Amata Fm at least two episodes of subaerial exposure occurred. It was not possible to provide a more detailed interpretation of the origin of the dolocretes in this study. We suppose that structures and textures indicative of the dolocrete formation mechanism could be partly obliterated by dolomitisation processes of precursor calcretes or by further diagenetic changes. A strong influence of multistage dolomitisation processes obliterating the fabrics of earlier formation stages of carbonate rocks has been suggested for the Pļaviņas Fm, which covers the Amata Fm (Kleesment et al. 2013).

Climate changes during the Givetian–Frasnian transition

The sedimentological logging, studies of polished specimens and thin sections, as well as data from stable carbon and oxygen isotope analyses, indicate the formation of dolocretes during several episodes throughout the accumulation of Amata Fm deposits. At least two episodes of subaerial exposure occurred before the end of the accumulation of Amata Fm deposits, as evidenced by the formation of soil dolocretes. This clearly marks the end of the transgressive phase characteristic of the Amata RS.

The observed decrease in grain size of siliciclastic deposits in the upper part of the geological section, which is noted in all studied sites, suggests a reduction in the energy of the sedimentary environment. Since the upper part of the section lacks well-preserved sedimentary structures – apart from problematic burrows – it is challenging to precisely interpret the sedimentary environment of the deposits containing dolocretes. However, no evidence has been found to contradict a regression at the end of the Amata Fm deposit accumulation time.

The decrease in grain size is likely due to a climate shift from wetter to drier conditions and a reduction in freshwater inflow, which also resulted in a decline in the overall hydrodynamic energy of rivers and their mouths.

Calcretes and dolocretes form in semiarid, more rarely in arid climates (Alonso-Zarza 2003). They are typical of monsoonal climate, as carbonate minerals accumulate in soils (fractures, root channels) during dry seasons, and remain fixed in the soil during moister conditions (Driese and Mora 2001). The appearance of the dolocretes in the upper part of the Amata Fm can also be considered an indication of climate change from moister to drier, more arid conditions at the beginning of the Frasnian, coinciding with a relatively short episode of sea-level fall. The same reason – climate change – likely initiated the overall transition from siliciclastic deposits with chemical weathering crust products (upper Givetian Gauja RS, Sietiņi and Lode Fms) to dolomites and gypsum-dominated deposits (Middle Frasnian Salaspils RS) in the WMDF. These longer-time changes likely led from a moist warm climate to a drier warm or even hot climate. The start of carbonate sedimentation in the Pļaviņas RS likely coincided with sea-level rise (Sandberg et al. 2002).

Changes in the fossil assemblages correspond reasonably well with changes in the geological sections and dominant deposit types. Fossil fishes from the Amata Fm of Latvia were previously described in detail only from a few localities, e.g. from the Pastmuiža site on the right bank of the River Daugava near Koknese (Klauenstein bei Kokenhusen in Gross 1942; Lyarskaya 1981), Ainavas Cliff near Kārļi (Karlsruhe in Gross 1942), and Ķūķi Cliff on the right bank of the River Gauja in the territory of the Gauja National Park (Lyarskaya 1981). The fossil-bearing beds at the Ainavas Cliff and Ķūķi Cliff are located in the lower part of the Amata Fm, whereas at the Pastmuiža site fossiliferous beds correspond to the middle part of the formation. Well-preserved but disarticulated vertebrate remains from the recently studied Zanderi Ravine near the town of Līgatne also come from the lowermost Amata Fm. The recently reported section of the Staritsa beds, cropping out on the left bank of the River Oredezh near the Borschovo village, Luga District, Leningrad Region, northwestern Russia, contains a moderately diverse vertebrate assemblage (13 taxa), plant remains, and trace fossils; this section is correlated with the lower part of the Amata Fm in Latvia (Lukševičs et al. 2018). As a result of this and previous studies (Stinkulis and Spruženiece 2011; Pipira et al. 2015), including five analysed sections, it seems that the upper part of the Amata Fm contains virtually no fossils, or only very few. This corresponds well with the distribution of dolocretes. The pattern of distribution of fossils within the Amata Fm resembles that in the sections of the Ketleri and Šķervelis Fms corresponding to the terminal Famennian. The Ketleri Fm, consisting mostly of sandy to clayey deposits accumulated in a tidal-influenced delta, yields a rather rich vertebrate assemblage, trace fossils of various invertebrates, rhizocretes, and macroscopic plant remains (Lukševičs et al. 2025), whereas the Šķervelis Fm, with strongly developed dolocretes in the same sandy to clayey host rocks, is practically fossil-free (Pipira et al. 2023).

The comparison of the fossil assemblages from stratigraphic units close to the Givetian–Frasnian boundary in Latvia demonstrates the decrease in fossil taxa diversity from the Burtnieki RS to the Amata RS, and an increase in the younger units (Table 2). The Amata Fm shows vertebrate diversity that is slightly larger than that of the Lode Fm,

Table 2. Number of fossil taxa reported from the Middle–Upper Devonian formations of Latvia (data from Kuršs et al. 1981a, b; Lyarskaya 1981; Lyarskaya and Lukševičs 1992; Kleesment and Mark-Kurik 1997; Ahlberg et al. 2000; Esin et al. 2000; Upeniece 2001; Jurina and Raskatova 2012; Mešķis 2013)

Regional stage	Number of fossil taxa			
	Vertebrates	Invertebrates	Other remains	Ichnotaxa (Mešķis 2013)
Salaspils	3	Lingulids, conchostracans, *Eurypterus lancmani*	*Chaetocladus*	Ichnofabrics
Pļaviņas	20	Stromatopores, *Aulopora*, rugose corals, conulariids, annelids, ostracods, conchostracans, 16 mollusc taxa, 19 brachiopod taxa, *Dactylocrinus*	Stromatolites (3 kinds), *Chaetocladus*	13 ichnotaxa
Amata	18	Conchostracans		
Gauja	21	Tabulate corals, stromatoporoids (3 taxa), brachiopods (3 taxa), platyhelminths, eurypterids, conchostracans, mysidaceans	*Prototaxites*, *Svalbardia banksii*, rhizocretes	
Burtnieki	24	Brachiopods, conchostracans, ostracods	Rhizocretes	

significantly larger than that of the Sietiņi Fm, but smaller than that of the Gauja Fm; however, the total diversity of organism fossils from the Gauja RS corresponding to three formations (Gauja, Lode, and Sietiņi Fms) is higher than that from the Amata RS. The overlying Pļaviņas Fm (and corresponding Pļaviņas RS) is characterised by 20 vertebrate taxa, which are unevenly distributed within the formation: 17 taxa in the lower, Koknese Mb; 13 taxa in the middle part, the Sēlija and Atzele Mbs; and only six taxa in the upper, Ape Mb (Lyarskaya and Lukševičs 1992). Besides vertebrates, a highly rich invertebrate assemblage, three different kinds of stromatolites, the green alga *Chaetocladus* (Sorokin 1981), and various trace fossils (Mešķis 2013) have been reported from the Pļaviņas Fm. The Salaspils Fm, composed of rocks of different composition, including clayey dolostone, dolostone, dolomitic marl, clay, gypsum, gypsum-dolomite, and various intermediate rocks, contains rather poorly preserved and usually difficult-to-determine fossils (Sorokin 1981; Lyarskaya and Lukševičs 1992; Mešķis 2013).

There are various hypotheses concerning climate changes and extinctions during the Devonian. For example, the so-called Devonian plant hypothesis (Algeo et al. 2001) postulates the influence of trees with deep root systems, and the first Middle Devonian forests on the acceleration of silicate weathering and/or organic carbon burial, resulting in several oceanic anoxic events, a decrease in atmospheric CO_2 levels, and global climate cooling during the Famennian and Carboniferous (Chen et al. 2021). However, this hypothesis does not explain the climate warming in the Givetian and Frasnian. Another hypothesis connects the cooling of the global climate close to the Frasnian–Famennian boundary with the first phase of the establishment of the Viluy traps in eastern Siberia (Ricci et al. 2013). However, the situation during the Givetian and around the Givetian–Frasnian boundary is not that clear. In accordance with the reconstruction of global palaeotemperatures for the Phanerozoic (Scotese 2015), global warming started close to the Emsian–Eifelian boundary, when the global mean annual temperature increased from 24 to about 26 °C, and the 'hothouse climate' conditions continued up to the Middle Frasnian. Recent reconstructions of seawater temperatures based on oxygen isotope ratios measured in marine calcitic and phosphatic fossils indicate a short but significant, 8–10 °C warming of the seawater during the interval around the Middle to Late Devonian transition (van Geldern et al. 2006; Joachimski et al. 2009; Chen et al. 2021). The main cause of the warming is still debated; it could be related to the injection of huge amounts of CO_2 that started about 390 Ma during the Acadian orogeny (Stewart and Ague 2018). If the above-mentioned climate reconstructions are correct, the climate warming coincided approximately with the early Eifelian Narva RS. It was earlier than the time of accumulation of deposits of the Gauja–Dubniki RSs.

Thus, the climate change from moister to drier from the Givetian to the Middle Frasnian has likely not been documented before outside the territory of the WMDF. Probably there are local reasons for the changing climate conditions. The climate could have been influenced by the Scandinavian Caledonides, which developed westwards from the WMDF and were oriented from north to south (Scotese 2014), perpendicular to the climate zones, thus influencing wind direction and moisture distribution. Hypothetically, the transition to a hotter climate from the Emsian–Eifelian to the Middle Frasnian (Scotese 2015) could have led to melting of the Scandinavian Caledonides' ice cap and cessation of freshwater inflow in the WMDF. This could also have influenced the change from siliciclastic to carbonate sedimentation.

Conclusions

Dolocretes in the upper part of the Amata Fm indicate at least two subaerial exposure episodes, which mark the transition from a longer sea-level rise trend to a short episode of sea-level fall in the WMDF during the Early Frasnian.

The dolocrete formation was an indicative episode of an overall period of climate change from warm, moist to drier and hotter conditions, which started in the Late Givetian (Gauja RS) and continued to the Early–Middle Frasnian (Dubniki RS). This climate change has likely not been documented before outside the WMDF and indicates locally different environmental conditions.

The geological succession of the Amata Fm with tidal features in its lower and middle parts, their absence in the upper part, the decrease in the abundance of fossils from the lower to the upper part of the formation, as well as the presence of dolocretes only in the upper part of the formation demonstrate a similar pattern to that of the Upper Famennian Ketleri and Šķervelis Fms. These features in the Ketleri and Šķervelis Fms were interpreted as the result of climate change and sea-level fall.

Data availability statement

Data for the stable isotope analyses are available in the Zenodo database: https://doi.org/10.5281/zenodo.19129793. All other data are included in this paper.

Acknowledgements

This study was partly financed by the grant of the Latvian Council of Science lzp-2018/2-0231 "Influence of tidal regime and climate on the Middle-Late Devonian biota in the epeiric Baltic palaeobasin". The authors are grateful to Dr. hab. Maciej Bojanowski and an anonymous reviewer for their valuable comments and recommendations. The publication costs of this article were partially covered by the Estonian Academy of Sciences.

References

Ahlberg, P. E., Lukševičs, E. and Mark-Kurik, E. 2000. A near-tetrapod from the Baltic Middle Devonian. *Palaeontology*, **43**(3), 533–548. https://doi.org/10.1111/j.0031-0239.2000.00138.x

Algeo, T. J., Scheckler, S. E. and Maynard, J. B. 2001. Effects of the Middle to Late Devonian spread of vascular land plants on weathering regimes, marine biotas and global climate. In *Plants Invade the Land. Evolutionary & Environmental Perspectives* (Gensel, P. G. and Edwards, D., eds). Columbia University Press, New York, 213–236.

Alonso-Zarza, A. M. 2003. Palaeoenvironmental significance of palustrine carbonates and calcretes in the geological record. *Earth-Science Reviews*, **60**(3–4), 261–298. https://doi.org/10.1016/S0012-8252(02)00106-X

Alonso-Zarza, A. M. and Arenas, C. 2004. Cenozoic calcretes from the Teruel Graben, Spain: microstructure, stable isotope geochemistry and environmental significance. *Sedimentary Geology*, **167**(1–2), 91–108. https://doi.org/10.1016/j.sedgeo.2004.02.001

Alonso-Zarza, A. M. and Wright, V. P. 2010. Palustrine carbonates. In *Carbonates in Continental Settings: Facies, Environments, and Processes. Developments in Sedimentology* (Alonso-Zarza, A. M. and Tanner, L. H., eds). Elsevier, Amsterdam, 103–131.

Calner, M., Lehnert, O. and Nõlvak, J. 2010. Palaeokarst evidence for widespread regression and subaerial exposure in the middle Katian (Upper Ordovician) of Baltoscandia: significance for global climate. *Palaeogeography, Palaeoclimatology, Palaeoecology*, **296**(3–4), 235–247. https://doi.org/10.1016/j.palaeo.2009.11.028

Casado, A. I., Alonso-Zarza, A. M. and La Iglesia, Á. 2014. Morphology and origin of dolomite in paleosols and lacustrine sequences. Examples from the Miocene of the Madrid Basin. *Sedimentary Geology*, **312**, 50–62. https://doi.org/10.1016/j.sedgeo.2014.07.005

Chen, X. Y. 2002. Classification systems. In *Calcrete: Characteristics, Distribution and Use in Mineral Exploration* (Chen, X. Y., Lintern, M. J. and Roach, I. C., eds). Cooperative Research Centre for Landscape Environments and Mineral Exploration, Australia, 16–22.

Chen, B., Ma, X., Mills, B. J. W., Qie, W., Joachimski, M. M., Shen, S. et al. 2021. Devonian paleoclimate and its drivers: a reassessment based on a new conodont $\delta^{18}O$ record from South China. *Earth-Science Reviews*, **222**, 103814. https://doi.org/10.1016/j.earscirev.2021.103814

Davis, R. A., Jr. 2012. Tidal signatures and their preservation potential in stratigraphic sequences. In *Principles of Tidal Sedimentology* (Davis, R. A., Jr. and Dalrymple, R. W., eds). Springer, 35–55.

Díaz-Hernández, J. L., Sánchez-Navas, A. and Reyes, E. 2013. Isotopic evidence for dolomite formation in soils. *Chemical Geology*, **347**, 20–33. https://doi.org/10.1016/j.chemgeo.2013.03.018

Dixon, J. C. 2010. Origin of calcrete and dolocrete in the carbonate mantle of St Vincent basin, southern South Australia. *Cadernos do Laboratorio Xeolóxico de Laxe*, **35**, 109–122.

Driese, S. G. and Mora, C. I. 2001. Diversification of Siluro-Devonian plant traces in paleosols and influence on estimates of paleoatmospheric CO_2 levels. In *Plants Invade the Land: Evolutionary and Environmental Perspectives* (Gensel, P. G. and Edwards, D., eds). Columbia University Press, New York, 237–253.

Esin, D., Ginter, M., Ivanov, A., Lebedev, O., Lukševičs, E., Avkhimovich, V. et al. 2000. Vertebrate correlation of the Upper Devonian and Lower Carboniferous on the East European Platform. *Courier Forschungsinstitut Senckenberg*, **223**, 341–359.

Eurostat. *Administrative units*, dataset from 2024. https://ec.europa.eu/eurostat/web/gisco/geodata/administrative-units (accessed 2024-09-18).

Glinskiy, V. N. and Mark-Kurik, E. 2016. Revision of *Psammosteus livonicus* Obruchev (Agnatha, Heterostraci) from the Devonian Amata Regional Stage of the NW of the East European Platform. *Estonian Journal of Earth Sciences*, **65**(1), 1–18. https://doi.org/10.3176/earth.2016.02

Goudie, A. S. 1973. *Duricrusts in Tropical and Subtropical Landscapes*. Claredon, Oxford.

Gross, W. 1942. Die Fischfaunen des baltischen Devons und ihre biostratigraphische Bedeutung. *Korrespondenzblatt des Naturforscher-Vereins zu Riga*, **64**, 373–436.

Ivanov, A., Stinkulis, G., Evdokimova, I. and Zhuravlev, A. 2012. *Опорные разрезы эйфельских-нижнефранских отложений востока Главного девонского поля (Key-Sections of the Eifelian–Lower Frasnian Deposits of the Eastern Part of the Main Devonian Field. Guidebook of the Field Trip)*. VSEGEI, St. Petersburg.

Joachimski, M. M., Breisig, S., Buggisch, W., Talent, J. A., Mawson, R., Gereke, M. et al. 2009. Devonian climate and reef evolution: insights from oxygen isotopes in apatite. *Earth and Planetary Science Letters*, **284**(3–4), 599–609. https://doi.org/10.1016/j.epsl.2009.05.028

Jurina, A. and Raskatova, M. 2012. New data on the Devonian plant and miospores from the Lode Formation, Latvia. *Acta Universitatis Latviensis, Earth and Environmental Sciences*, **783**, 46–56.

Kearsey, T., Twitchett, R. J. and Newell, A. J. 2012. The origin and significance of pedogenic dolomite from the Upper Permian of the South Urals of Russia. *Geological Magazine*, **149**(2), 291–307. https://doi.org/10.1017/S0016756811000926

Kleesment, A. and Mark-Kurik, E. 1997. Middle Devonian. In *Geology and Mineral Resources of Estonia* (Raukas, A. and Teedumäe, A., eds). Estonian Academy Publishers, Tallinn, 112–121.

Kruchek, S. A., Makhnach, A. S., Golubtsov, V. K. and Obukhovskaya, T. G. 2001. Девонская система (Devonian System). In *Геология Беларуси (Geology of Belarus)* (Makhnach, A. S., Garetsky, R. G. and Matveev, A. V., eds). Institute of Geology, National Academy of Sciences of Belarus, Minsk, 186–239.

Kuršs, V. M. 1992. *Девонское терригенное осадконакопление на Главном девонском поле (Devonian Terrigenous Deposition in the Main Devonian Field)*. Zinātne, Riga.

Kuršs, V., Viiding, H. and Mark-Kurik, E. 1981a. Аматская свита (Amata Formation). In *Девон и карбон Прибалтики (Devonian and Carboniferous of the Baltic Region)* (Sorokin, V. S., ed.). Zinātne, Riga, 157–167.

Kuršs, V., Viiding, H., Kajak, K. and Mark-Kurik, E. 1981b. Буртниекская свита (Burtnieki Formation). In *Девон и карбон Прибалтики (Devonian and Carboniferous of the Baltic Region)* (Sorokin, V., ed.). Zinātne, Riga, 129–141.

Kuršs, V., Viiding, H. and Mark-Kurik, E. 1981c. Гауйская свита (Gauja Formation). In *Девон и карбон Прибалтики (Devonian and Carboniferous of the Baltic Region)* (Sorokin, V., ed.). Zinātne, Riga, 146–157.

Lukševičs, E. and Stinkulis, Ģ. 2018. Nogulumiežu segas stratigrāfiskais iedalījums, uzbūve, sastāvs un reģionālās atšķirības (Stratigraphic subdivision, structure, composition and regional differences of sedimentary cover). In *Latvija: zeme, daba, tauta, valsts (Latvia: Land, Nature, People, State)* (Nikodemus, O., Kļaviņš, M., Krišjāne, Z. and Zelčs, V., eds). University of Latvia Press, Riga, 46–60.

Lukševičs, E., Stinkulis, Ģ., Mūrnieks, A. and Popovs, K. 2012. Geological evolution of the Baltic Artesian Basin. In *Highlights of Groundwater Research in the Baltic Artesian Basin* (Dēliņa, A., Kalvāns, A., Saks, T., Bethers, U. and Vircavs, V., eds). University of Latvia, Riga, 7–52.

Lukševičs, E., Stinkulis, Ģ., Ivanov, A. and Tirzmale, D. 2018. The Borschovo section of the Gauja and Amata regional stages (Leningrad Region, Russia): sedimentology and biostratigraphy. *Estonian Journal of Earth Sciences*, **67**(1), 21–32. https://doi.org/10.3176/earth.2018.01

Lukševičs, E., Stinkulis, Ģ., Alksnītis, V., Visotina, T. and Mešķis, S. 2025. The Upper Famennian Ketleri Formation of Latvia: new data on the fauna and flora from tide-dominated delta deposits in a seasonal climate. *Estonian Journal of Earth Sciences*, **74**(2), 160–171. https://doi.org/10.3176/earth.2025.11

Lyarskaya, L. 1981. *Панцирные рыбы девона Прибалтики: Asterolepididae (Baltic Devonian Placodermi: Asterolepididae)*. Zinātne, Riga.

Lyarskaya, L. and Lukševičs, E. 1992. Состав и распространение бесчелюстных и рыб в силурийских и девонских отложениях Латвии (Composition and distribution of agnathan and fish assemblages in the Silurian and Devonian deposits of Latvia).

In *Палеонтология и стратиграфия фанерозоя Латвии и Балтийского моря (Paleontology and Stratigraphy of the Phanerozoic of Latvia and the Baltic Sea)* (Sorokin V. S., ed.). Zinātne, Riga, 46–62.

Machette, M. N. 1985. Calcic soils of the southwestern United States. In *Soils and Quaternary Geology of the Southwestern United States* (Weide, D. L., ed.). Geological Society of America, **203**, 1–21.

Mark-Kurik, E. and Põldvere, A. 2012. Devonian stratigraphy in Estonia: current state and problems. *Estonian Journal of Earth Sciences*, **61**(1), 33–47. https://doi.org/10.3176/earth.2012.1.03

Melezhik, V. A., Fallick, A. E. and Grillo, S. M. 2004. Subaerial exposure surfaces in a Palaeoproterozoic ^{13}C-rich dolostone sequence from the Pechenga Greenstone Belt: palaeoenvironmental and isotopic implications for the 2330–2060 Ma global isotope excursion of $^{13}C/^{12}C$. *Precambrian Research*, **133**(1–2), 75–103. https://doi.org/10.1016/j.precamres.2004.03.011

Mešķis, S. 2013. *Pēdu fosiliju kompleksi Galvenā Devona lauka Franas stāva nogulumos* (*Trace fossil assemblages from the deposits of the Frasnian Stage of the Main Devonian field*). *Disertationes Geologicae Universitas Latviensis*, **26**. Doctoral thesis. University of Latvia, Riga.

Narbutas, V. 1981. Швянтойская свита (Šventoji Formation). In *Девон и карбон Прибалтики (Devonian and Carboniferous of the Baltic Region)* (Sorokin, V. S., ed.). Zinātne, Riga, 144–146.

Narbutas, V. 2004. Devonas ir karbonas (Devonian and Carboniferous). In *Lietuvos žemės gelmių raida ir ištekliai (Development and Resources of the Subsurface of Lithuania)* (Baltrūnas, V., ed.). Lithosphere, Vilnius, 233–247.

Pfeiffer, M., Le Roux, J. P., Solleiro-Rebolledo, E., Kemnitz, H., Sedov, S. and Seguel, O. 2011. Preservation of beach ridges due to pedogenic calcrete development in the Tongoy palaeobay, North-Central Chile. *Geomorphology,* **132**(3–4), 234–248. https://doi.org/10.1016/j.geomorph.2011.05.012

Pipira, D. 2015. *Features of subaerial exposure events and their formations in the Devonian succession in Latvia.* Summary of doctoral thesis. University of Latvia Press, Riga.

Pipira, D., Kostjukovs, J. and Stinkulis, Ģ. 2015. Mineral composition and morphology of dolocretes of the Devonian Burtnieki and Amata formations, Latvia. *Materials Science and Applied Chemistry*, **32**(1), 13–18.

Pipira, D., Ķeipāne, L., Stinkulis, Ģ., Vircava, I. and Martma, T. 2023. Dolocretes in the uppermost Famennian to Mississippian siliciclastic deposits (Šķervelis Formation, Latvia). *Estonian Journal of Earth Sciences*, **72**(2), 211–225. https://doi.org/10.3176/earth.2023.86

Plax, D. P. and Zaika, Yu. V. 2020. On the Zhelon deposits (Frasnian, Upper Devonian) of the Latvian Saddle in the basins of the Saryanka and Rositsa rivers (Belarus). *Geological and Mineralogical Resources*, **2**, 18–35.

Pontén, A. and Plink-Björklund, P. 2007. Depositional environments in an extensive tide-influenced delta plain, Middle Devonian Gauja Formation, Devonian Baltic Basin. *Sedimentology*, **54**(5), 969–1006. https://doi.org/10.1111/j.1365-3091.2007.00869.x

Pontén, A. and Plink-Björklund, P. 2009. Regressive to transgressive transits reflected in tidal bars, Middle Devonian Baltic Basin. *Sedimentary Geology*, **218**(1–4), 48–60. https://doi.org/10.1016/j.sedgeo.2009.04.003

Rameil, N., Immenhauser, A., Csoma, A. É. and Warrlich, G. 2012. Surfaces with a long history: the Aptian top Shu'aiba Formation unconformity, Sultanate of Oman. *Sedimentology*, **59**(1), 212–248. https://doi.org/10.1111/j.1365-3091.2011.01279.x

Ricci, J., Quidelleur, X., Pavlov, V., Orlov, S., Shatsillo, A. and Courtillot, V. 2013. New $^{40}Ar/^{39}Ar$ and K–Ar ages of the Viluy traps (eastern Siberia): further evidence for a relationship with the Frasnian–Famennian mass extinction. *Palaeogeography, Palaeoclimatology, Palaeoecology*, **386**, 531–540. https://doi.org/10.1016/j.palaeo.2013.06.020

Rosenbaum, J. and Sheppard, S. M. F. 1986. An isotopic study of siderites, dolomites and ankerites at high temperatures. *Geochimica et Cosmochimica Acta*, **50**(6), 1147–1150. https://doi.org/c10.1016/0016-7037(86)90396-0

Sandberg, C. A., Morrow, J. R. and Ziegler, W. 2002. Late Devonian sea-level changes, catastrophic events, and mass extinctions. In *Catastrophic Events and Mass Extinctions: Impacts and Beyond* (Koeberl, C. and MacLeod, K. G., eds). Geological Society of America, **356**, 473–487. https://doi.org/10.1130/0-8137-2356-6.473

Scotese, C. R. 2014. *Atlas of Devonian Paleogeographic Maps, Atlas for ArcGIS 4, The Late Paleozoic, Maps 65–72, Mollweide Projection*. PALEOMAP Project, Evanston, IL.

Scotese, C. R. 2015. *Phanerozoic Temperature Curve*. PALEOMAP Project, Evanston, IL.

Sorokin, V. 1981. Плявиньская свита (Pļaviņas Formation). In *Девон и карбон Прибалтики (Devonian and Carboniferous of the Baltic Region)* (Sorokin, V., ed.). Zinātne, Riga, 172–212.

Stewart, E. M. and Ague, J. J. 2018. Infiltration-driven metamorphism, New England, USA: regional CO_2 fluxes and implications for Devonian climate and extinctions. *Earth and Planetary Science Letters*, **489**, 123–134. https://doi.org/10.1016/j.epsl.2018.02.028

Stinkulis, Ģ. 1997. Karbonātu minerālu veidošanās devona Burtnieku-Amatas svītu klastiskajos iežos Latvijā (Origin of carbonate minerals in the siliciclastic deposits of the Devonian Burtnieki–Amata formations). *Latvijas Ģeoloģijas Vēstis*, **3**, 3–11.

Stinkulis, Ģ. and Spruženiece, L. 2011. Dolocretes as indicators of the subaerial exposure episodes in the Baltic Devonian palaeobasin. In *Eighth Baltic Stratigraphical Conference. Abstracts* (Lukševičs, E., Stinkulis, Ģ. and Vasiļkova, J., eds). University of Latvia, Riga, 62.

Stinkulis, Ģ. and Upeniece, I. 2011. Stop 3: sandstones of the Devonian Amata Formation in the cave Liepas Lielā ellīte. In *Eighth Baltic Stratigraphical Conference. Post-Conference Field Excursion Guidebook* (Stinkulis, Ģ. and Zelčs, V., eds). University of Latvia, Riga, 21–24.

Swart, P. K. 2015. The geochemistry of carbonate diagenesis: the past, present and future. *Sedimentology*, **62**(5), 1233–1304. https://doi.org/10.1111/sed.12205

Theriault, P. and Desrochers, A. 1993. Carboniferous calcretes in the Canadian Arctic. *Sedimentology*, **40**(3), 449–465. https://doi.org/10.1111/j.1365-3091.1993.tb01345.x

Upeniece, I. 2001. The unique fossil assemblage from the Lode Quarry (Upper Devonian, Latvia). *Fossil Record*, **4**(1), 101–119. https://doi.org/10.1002/mmng.20010040108

van Geldern, R., Joachimski, M. M., Day, J., Jansen, U., Alvarez, F., Yolkin, E. A. et al. 2006. Carbon, oxygen and strontium isotope records of Devonian brachiopod shell calcite. *Palaeogeography, Palaeoclimatology, Palaeoecology*, **240**(1–2), 47–67. https://doi.org/10.1016/j.palaeo.2006.03.045

Vernera, L. and Stinkulis, Ģ. 2018. Kalcīts augšējā devona Daugavas svītas dolomītos Latvijā (Calcite in dolomites of the Upper Devonian Daugava Formation in Latvia). In *Abstracts of the 76th International Conference of the University of Latvia. Geography. Geology. Environmental Science*. University of Latvia, Riga, 280–281.

Wright, V. P. and Tucker, M. E. 2009. Calcretes: an introduction. In *Calcretes*. IAS Reprint Series, Vol. 2 (Wright, V. P. and Tucker, M. E., eds). Blackwell, Oxford, 1–24. https://doi.org/10.1002/9781444304497.ch

Zhou, J. and Chafetz, H. S. 2009. Biogenic caliches in Texas: the role of organisms and effect of climate. *Sedimentary Geology*, **222**(3–4), 207–225. https://doi.org/10.1016/j.sedgeo.2009.09.003

Läti Amata kihistu dolokreedid kui Giveti–Frasnesi üleminekuaja ariidsema kliima indikaatorid

Ģirts Stinkulis, Ervīns Lukševičs, Daiga Pipira, Marianna Meire-Kārkle ja Tõnu Martma

Uuring keskendub nelja Läti paljandi dolokreetide ja nende terrigeensete peremeeskivimite päritolu kirjeldamisele ja tõlgendamisele Amata kihistu ülemises osas. Dolokreedid esinevad vähemalt neljas intervallis. Kahe ülemise dolokreedi intervalli koostis ja struktuur ning hapniku ja süsiniku stabiilsete isotoopide andmed viitavad sellele, et need tekkisid mullas. Dolokreedid vastavad kliimamuutuste episoodile soojast-niiskest kuivemaks-kuumemaks, mis algas hilis-Givetis ja jätkus kesk-Frasnesini. Need tekkisid pärast pikemat meretaseme tõusutrendi toimunud lühiajalise meretaseme languse ajal. Amata kihistus väheneb selgroogsete fossiilide mitmekesisus kihistu alumisest osast ülemise osani, mis on kooskõlas meretaseme languse ja järkjärgulise kliimamuutusega, mida näitavad ka Amata kihistu ülemises osas uuritud dolokreedid.

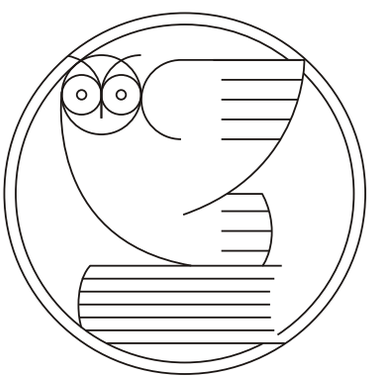

Estonian Academy Publishers
Kohtu 6, 10130 Tallinn, Estonia
Email: info@eap.ee
Subscription information available at
www.eap.ee/subscription
subscription@eap.ee

Estonian Journal of Earth Sciences 2026, 75/1

Contents

Estonian Journal of Earth Sciences 2026, 75/1

9 771736 472010